Structure and Casting Technology of Anodes in Copper Metallurgy

Dipl.-Ing. Christine Wenzl

Dissertation zur Erlangung des akademischen Grades eines Doktors der montanistischen Wissenschaften an der Montanuniversität Leoben

Leoben, September 2008

Eidesstattliche Erklärung

Ich erkläre an Eides statt, dass ich diese Arbeit selbstständig verfasst, andere als die angegebenen Quellen und Hilfsmittel nicht benutzt und mich auch sonst keiner unerlaubten Hilfsmittel bedient habe.

I declare in lieu of oath, that I wrote this thesis and performed the associated research myself, using only literature cited in this volume.

DI Christine Wenzl

Danksagung

Mit den folgenden Zeilen, möchte ich mich bei jenen Personen bedanken, die mir diese Arbeit ermöglicht und mich dabei unterstützt haben.

Ich bedanke mich ganz herzlich bei Herrn Ao.Univ.-Prof. Dipl.-Ing. Dr.mont. Helmut Antrekowitsch für die Möglichkeit diese Arbeit an der Nichteisenmetallurgie zu verfassen und für seine stete Unterstützung.
Ich bedanke mich auch bei Univ.-Prof. Dipl.-Ing. Dr.mont. Albert Kneißl, der sich als Zweitbegutachter meiner Arbeit zur Verfügung gestellt hat.

Des Weiteren möchte ich mich bei den Mitarbeitern der Nichteisenmetallurgie für die gute Zusammenarbeit bedanken, insbesondere bei der Werkstatt und Claudia Pelka. Danke auch an meine Bakkalaureatsstudentin Eva Raaber und die studentischen Mitarbeiter für die Unterstützung bei den zeitaufwändigen Probenvorbereitungen und Messungen.

Mein Dank gilt weiters Univ.-Prof. Dipl.-Phys. Dr.rer.nat. Andreas Ludwig, sowie Ao.Univ.-Prof. Dipl.-Ing. Dr.mont. Christian Bernhard und DI Sebastian Michelic für die Unterstützung bei der Simulation.

Ich bedanke mich auch bei Ing. Alois Lang, meiner Anlaufstelle bei allen elektro- und messtechnischen Problemen, sowie bei Siegfried Schider für seine Hilfsbereitschaft in allen metallographischen Fragen.

Mein besonderer Dank gilt meinen Betreuern von Seiten der METTOP GmbH, Dr. Andreas Filzwieser und Dr. Iris Filzwieser für die vielen anregenden Diskussionen und für die stete und engagierte Unterstützung und Betreuung, sowie die freundliche Aufnahme bei der METTOP.

Ein ganz großes Dankeschön an DI Robert Stibich und Dr. Josef Pesl für die Möglichkeit die Versuche bei der Montanwerke Brixlegg AG durchzuführen. Weiters möchte ich mich bei der Belegschaft der Schmelzhütte und des Labors der Montanwerke Brixlegg für die gute Zusammenarbeit und Unterstützung bedanken.

Zuletzt gilt mein Dank auch meiner Familie, Manuel und meinen Freunden, die immer an mich geglaubt haben und immer für mich da sind.

Abstract

Anode casting is the link between copper pyro- and hydrometallurgy. To achieve good electrorefining performance, the anodes must have a certain chemical and physical quality. The latter is directly linked with the anode casting process. The aims of anode casting—high output and long mould lifetimes—are not consistent with the objectives of electrorefining, which include uniform dissolution, minimum anode scrap, optimum current efficiency, and high cathode quality.

The elemental distribution and the grain size can be adjusted by altering the solidification conditions, for example change of cooling rate, thermal conductivity (i.e., material) of the anode moulds, and mould preheating. Faster cooling leads to finer grains and supersaturated solid solutions.

The anode cooling and solidification conditions were determined from mould temperature measurements. To investigate the influence of the casting process on solidification, cooling conditions, and anode quality, the process parameters mould material and mould wash were varied. The casting process at Montanwerke Brixlegg AG and the corresponding anode samples were investigated in detail to establish the reasons for different anode qualities and their effects on electrorefining.

The use of different mould materials and mould wash, as well as the different mould lifespan, resulted in significant differences in mould temperature and hence anode cooling conditions. However, these temperature variations did not seem to have an influence on chemical anode quality, but on physical quality.

The anodes, which were produced with barite as mould wash, showed a typical cast structure. Variations in structure were detected in the different anodes, namely across the anode thickness and over the anode area, which indicated different local cooling conditions. The cooling was found to be very important, not only regarding anode quality but also regarding mould life and casting rate.

As there were no differences across the anode thickness due to chemical quality, the inhomogeneous anodic dissolution behaviour might be caused to a great extent by structural differences across the anode thickness.

As dissolution occurs preferentially at the grain boundaries, the different solidification structures are reported to have different dissolution rates and tendency for passivation. Potential measurements demonstrated the different dissolution behaviours across the anode thickness.

A simulation of the anode casting process was carried out and a basic model for anode solidification developed by using the experimental temperature data. The basic model showed realistic results and can be used for the optimization of the casting system, the cooling arrangement, and the mould design.

Kurzfassung

Der Anodenguss ist die Schnittstelle von Pyro- und Hydrometallurgie in der Kupfererzeugung. Um gute Ergebnisse in der Raffinationselektrolyse zu erzielen, ist eine bestimmte chemische und physikalische Anodenqualität nötig, wobei letztere direkt vom Anodengießprozess bestimmt wird. Die Ziele des Anodengießens – hoher Durchsatz und lange Modellstandzeiten – stimmen nicht mit den Anforderungen der Raffinationselektrolyse überein, wie etwa gleichmäßige Auflösung, minimale Menge an Anodenresten, optimale Stromausbeute und gute Kathodenqualität.

Die Elementverteilung und die Korngröße können durch Veränderung der Erstarrungsbedingungen beeinflusst werden, etwa durch Änderung der Kühlrate, der thermischen Leitfähigkeit des Anodenmodells (z.B. Material) und der Modellvorwärmung. Eine schnellere Abkühlung führt beispielsweise zu feinerem Korn und übersättigten Mischkristallen.

Im Rahmen der Arbeit wurden die Abkühl- und Erstarrungsbedingungen der Anoden anhand der Modelltemperaturmessungen ermittelt. Um den Einfluss des Gießprozesses auf die Erstarrung, Abkühlbedingungen und Anodenqualität zu untersuchen, erfolgte eine Variation der Prozessparameter Modellmaterial und Schlichte. Der Gießprozess bei der Montanwerke Brixlegg AG und die entsprechenden Probeanoden wurden eingehend untersucht, um die Gründe für die unterschiedlichen Anodenqualitäten und deren Auswirkungen auf die Raffinationselektrolyse zu finden. Die Verwendung unterschiedlicher Modellmaterialen und Arten von Schlichte, sowie die verschiedene Einsatzdauer der Modelle zeigte deutliche Unterschiede bezüglich Modelltemperatur und folglich Abkühlbedingungen der Anode. Diese Temperaturunterschiede hatten allerdings keinen Einfluss auf die chemische, aber sehr wohl auf die physikalische Anodenqualität.

Die unter Verwendung von Barit als Schlichte erzeugten Anoden zeigten ein typisches Gussgefüge. Unterschiede in der Struktur, sowohl über die Anodendicke als auch –fläche, waren in den verschiedenen Anoden ersichtlich, was auf die wechselnden lokalen Abkühlbedingungen zurückzuführen ist. Die Kühlung erwies sich als sehr wichtiger Faktor, nicht nur für die Anodenqualität, sondern auch hinsichtlich Modellstandzeit und Gießrate.

Nachdem keine Unterschiede in der chemischen Qualität über die Anodendicke festgestellt wurden, scheint die ungleichmäßige anodische Auflösung zu einem großen Teil von den strukturellen Schwankungen zu kommen. Aufgrund der bevorzugten Auflösung an den Korngrenzen werden in der Literatur unterschiedliche Auflösungsgeschwindigkeiten und Passivierungsneigung für die verschiedenen Strukturen beschrieben. Die durchgeführten Potenzialmessungen zeigten dieses ungleichmäßige Auflösungsverhalten über die Anodendicke.

Unter Verwendung der experimentell ermittelten Temperaturdaten wurde eine Simulation des Anodengusses durchgeführt und ein Modell für die Erstarrung der Anode entwickelt. Dieses

zeigte sehr realistische Ergebnisse und kann für die Optimierung des Gießsystems, der Kühlung und der Modellgeometrie verwendet werden.

Contents

1. Introduction

Copper refining is necessary to remove impurities and achieve the required properties demanded by the customer. For high quality applications, the refining is performed in two steps: Firstly, anode copper is produced by fire refining in an anode furnace and cast into anodes. Secondly, these anodes are subjected to electrorefining. However, there are an increasing number of smelters that produce semi-finished products directly from fire-refined copper (FRHC copper), namely they do not perform anode casting and electrorefining using for example the process developed by the companies La Farga Lacambra and Continuus Properzi [1-4].

Anode casting, which is the link between copper pyro- and hydrometallurgy, has a significant influence on both the chemical and physical anode quality, and hence determines anodic dissolution and electrorefining operations. Anodes must have a certain physical and chemical quality in order to provide uniform anodic dissolution and meet the requirements of electrorefining, namely to achieve a high current efficiency, low energy consumption, low anode scrap levels, and low personnel input together with high cathode quality. Various anode properties can be influenced directly by the casting process, which is the interface between copper pyro- and hydrometallurgy. The aims of anode casting—high output and long mould lifetimes—are not consistent with good physical anode quality. The physical anode requirements to achieve a uniform dissolution behaviour include smooth surfaces, uniform weight and thickness, minimal edge effects, minimal distortion of the body and lugs, as well as a homogeneous structure. The overall chemical quality of the anode copper is the responsibility of fire refining operations; however the elemental distribution within the anodes, which should be as homogeneous as possible in order to provide uniform anodic dissolution, can be influenced by the casting process. The cooling rate, which determines the grain size and microstructure, has a significant impact on the elemental distribution. Hence it is vital to optimize the casting process, as the anode quality is decisive for electrorefining operations (e.g., output/efficiency and quality).

Optimization of electrorefining consists of two steps as illustrated in Figure 1. Firstly, an increase in current efficiency leads to a narrower current density distribution, as indicated by the transition from the broad blue curve to the narrow orange one. If this first step can be realized, then the second step of increasing the current density also becomes possible (green curve), for example by optimizing the anode quality and the casting process.

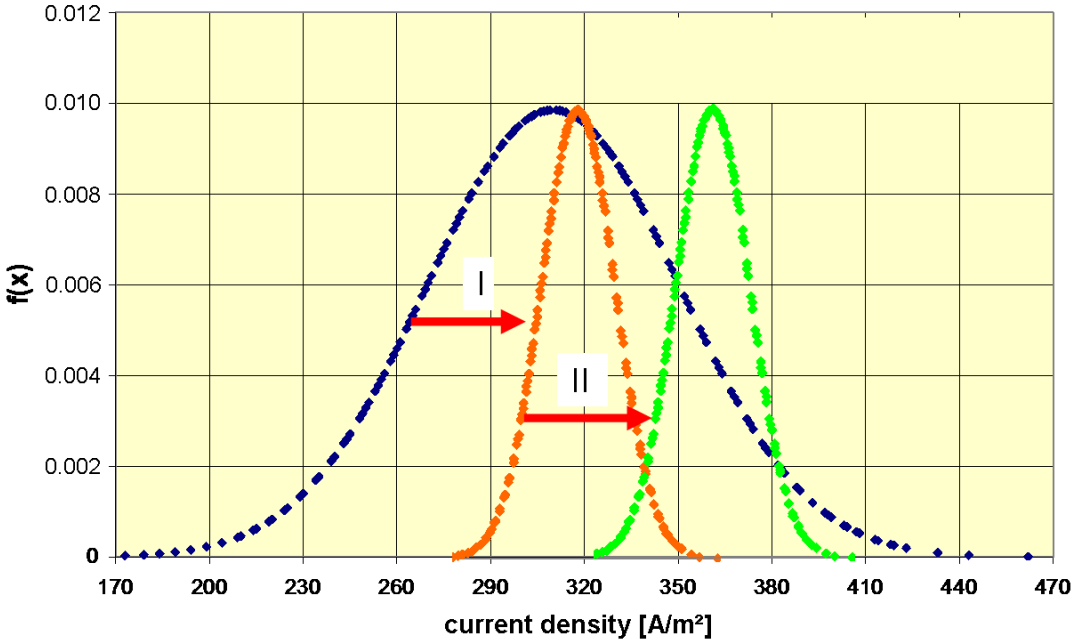

Figure 1: Optimization potential in electrorefining (Gaussian bell curve) [5]

The work described in this thesis was carried out in cooperation with METTOP GmbH (Leoben, Austria). Prior to this study, METTOP, in collaboration with Montanwerke Brixlegg AG (Brixlegg, Austria), developed a new electrolysis technology, termed the METTOP-BRX system, to increase current efficiency and/or current density. The principal component of this technology is the Parallel Flow Device (PFD), which enables parallel electrolyte flow and hence higher current densities (i.e., up to 450 A/m²) during electrorefining.

Studies carried out by METTOP in summer 2005 demonstrated that there are noticeable differences between anodic dissolution from the air and mould side, not only in the first cathodic crop but also in the second. This inhomogeneous anodic dissolution behaviour poses a limit to the application of high current densities in electrorefining. These findings led to a considerable interest in anode quality and how it can be influenced during casting, and hence to this work.

The aim of this work was to determine the optimum anode quality for electrorefining, so that higher current densities than those currently used (i.e., between 193 and 344 A/m² [6]) can be applied. In order to understand the influences on anode quality, a comprehensive literature and patent study was performed encompassing anode casting, as well as chemical and physical anode quality. The casting process at Montanwerke Brixlegg AG was studied and measurements (e.g., mould temperature, casting temperature, and cooling water) were performed at the plant. The influence of process parameters including the mould material, mould wash, period of use of the mould, and cooling were studied using temperature

measurements in the anode moulds. Potential measurements were also carried out in order to investigate the effects of the varying physical quality across the anode thickness on electrorefining. These experiments demonstrated that the dissolution behaviour was influenced by different structures and grain sizes. The results of this work indicated that uneven anodic dissolution is mainly caused by the physical quality, namely macro- and microstructure, as no significant variations in chemical composition across the anode thickness and area were detected.

A basic anode casting simulation model was developed using the experimental results, which can be used to design new anode moulds and predict the effects of a change in geometry, as well as for optimizing the cooling arrangement and casting system. This model enables anode cooling, solidification, and the resulting microstructure (DAS) to be predicted.

2. Fundamentals

In 2007, the total worldwide refined copper production amounted to 18,157 kt (global refinery capacity: 21,886 kt), comprising secondary copper production levels of 2,789 kt [7]. These refined production levels include both electrowon (SX-EW) and electrorefined copper (Figure 2). The division of production routes is depicted in Figure 3. The smelter production data in Figure 2 includes both primary (from concentrates) and secondary production (from scrap material) [8]. Refined copper production derived from mine production (i.e., either metallurgical treatment of concentrates or SX-EW) is referred to as primary copper production, since it is derived from a primary raw material source. In 2006, the refined copper production from SX-EW represented 16% of the total refined copper production, up from 11% ten years ago (Figure 4). Refined copper production from recycled scrap feed is classified as secondary copper production [7].

As previously mentioned, there are an increasing number of smelters that omit electrorefining and produce semi-finished products from FRHC copper. At present it is considered that there are some 250,000 t/y of scrap (93 to 94 wt.% Cu) converted into copper rod by the La Farga Lacambra/Continuus Properzi process. In 2008, seven plants will be put into operation in Russia, Iran, and China, so that the present production quantity will be almost doubled [9]. The trend for the use of copper including direct smelt scrap is shown in Figure 5.
However, this work deals with anode casting, namely the process route of electrorefining and upstream anode casting, whose importance can be seen in Figure 3 and Figure 4.

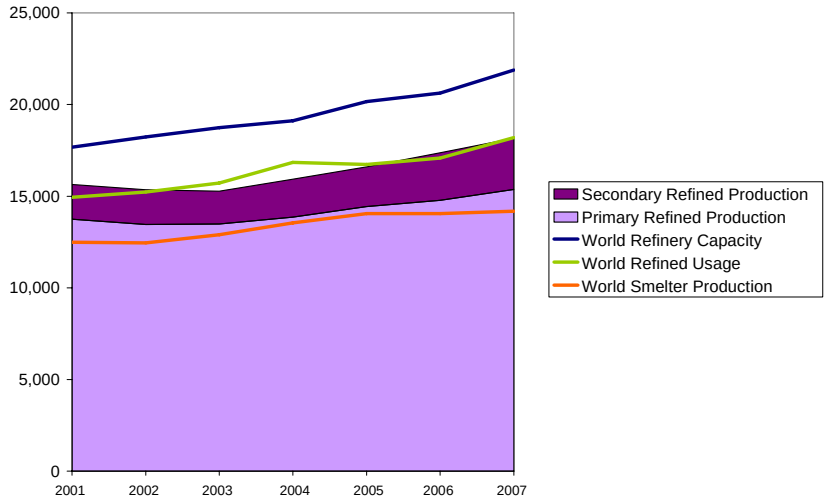

Figure 2: Copper production [kt] from 2001 to 2007 (with data from [7])

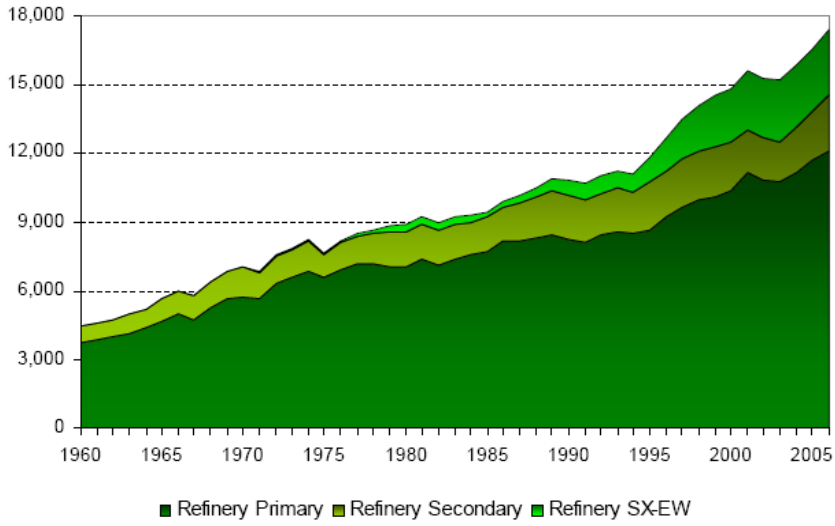

Figure 3: Refined copper production [kt] from 1960 to 2006 [10]

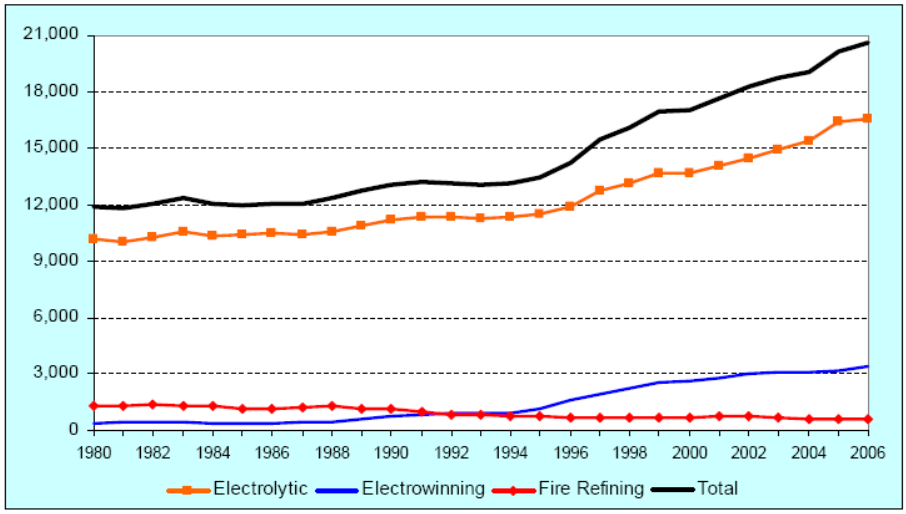

Figure 4: Trends in copper refining capacities [kt] from 1990 to 2006 [10]

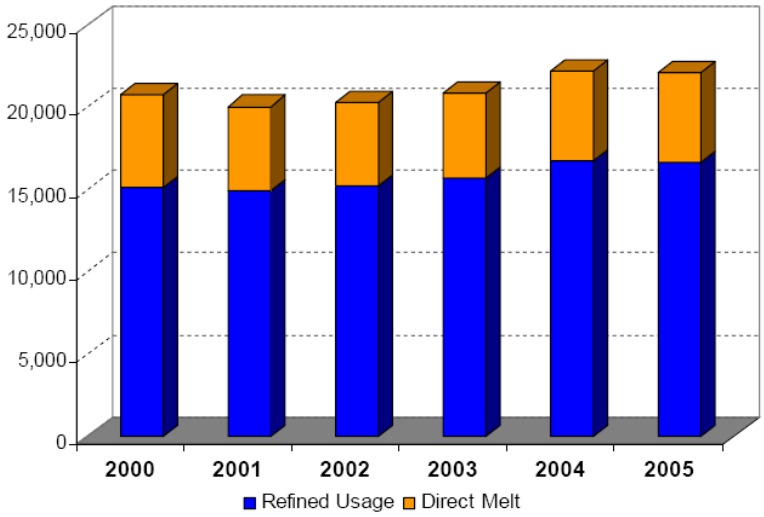

Figure 5: Total Cu use including direct melt scrap [kt] from 2000 to 2005 [7]

2.1 Anode Casting Process

As previously described, copper refining for high quality applications is performed in two steps: Firstly, anode copper is produced by fire refining in an anode furnace and cast into anodes. Secondly, these anodes are subjected to electrorefining. The anode casting process is of special importance as the quality of the anode is decisive for electrorefining operation (output/efficiency, quality).

Various anode properties can be influenced directly by the casting process. However, the anode quality is not only dependent on the casting technology used, but especially on proper process control. The anode weight should be as uniform as possible in order to produce a minimum amount of anode scrap, which has to be remelted, and ensure uniform current distribution (Section 2.3.2.2) [11]. Anode weight variation is mainly dependent on the weighing system accuracy (and hence its age) and on personnel. An accuracy of ± 1 [12, 13] to 3% [14] (± 1 kg [15]) for each anode has been reported

2.1.1 Casting Wheel

The most common technique is anode casting on casting wheels [16], although it is linked with the following disadvantages, especially regarding geometrical accuracy and surface quality [17-19]:

- Fluctuations in anode weight and thickness [17, 20]
- Various effects at the crystallization zone boundary (e.g., pore formation, oxide accumulation, and mould wash particles) [17, 20]
- Poor surface quality: "Inflamed" surface, very likely to have fins, warping, irregular surface due to gas discharge at the time of casting and other casting defects including oxide formation on the anode surfaces [17, 20]
- Numerous Cu_2O inclusions in the bulk of the anode [19]
- Different surface structures on air and mould side [18]
- Adhering mould wash, which may influence inclusions and is released during electrorefining [17, 19, 20]
- Potential finishing processes required

The casting defects can cause irregular electrode spacing, which can result in further defects including shorts, decreased current efficiency, and an uneven electrodeposition. The amount of anode scrap is high and non-uniform, which results in a higher remelting requirement and complicates automation [20].

Anode casting on a casting wheel is an automated process in so-called casting tables, where the moulds are shifted on a round casting table to the front of the casting trough [14]. The liquid copper flows from the anode furnace along a chute into the intermediate trough. From there, it is poured into the casting mould and then into horizontal copper moulds arranged on a casting wheel, which are coated with mould wash to prevent the anodes sticking. The solidification process is accelerated by water spray cooling on the mould underside and subsequently on the anode surfaces. Hence, the mechanical stability for take-off is achieved. After take-off the anodes are suspended from their lugs in a bosh tank and transported through the tank, where they cool down to about 100 °C. Then the anodes are withdrawn and stacked. Before the moulds are reused, they are coated with mould wash. The main parts of the casting wheel are the casting and batching unit, the cooling unit, the take-off system with cooling tank and stacker, the emergency take-off, and the coating unit [14, 20, 21].

Typically, the casting control system follows a preset optimum flow rate curve and a preset anode weight, and adjusts the tilting angle and pouring speed of the casting ladle. The optimized pouring rate reduces splashing and produces well formed lugs without fins or cups [22]. When pouring from the casting trough, the feeding is controlled by means of monitoring the trajectory and speed of the casting trough as well as its weight. For casting, the casting trough, which is equipped with weight sensors, is tilted so that the molten metal flows over the spout to the mould. The pouring is stopped when the weight of the casting trough is reduced by the target anode weight [14]. After filling one mould the wheel is turned to the next position. A gentle start and braking of the movement is very important to avoid liquid copper fluctuations and corresponding edge fins [20]. The flow of molten metal during pouring contains high levels of kinetic energy, which is directed to the bottom of the mould and to the melt already contained in the mould, and thus causes splashing and spilling. An additional negative effect of this kinetic energy is weighing distortions. Hence, it is important to minimize the pouring height. An even pouring process can either be achieved by slow pouring (which can make the casting step the bottleneck in the overall process) or by using specially shaped casting troughs. Lumppio [14] describes a casting trough with a spout, which comprises a curved pouring edge, a downwardly directed curved pouring surface, and a choking element for controlling the mass flow of the molten metal. This type of trough enables rapid casting but also reduces undulations of the molten metal in the casting trough, which improves weighing, as well as mould wear and mould wash consumption [14].

At the end of the casting process, the casting trough is normally left filled with metal, which solidifies there. The emptying of the casting trough would lead to lower maintenance operations, which otherwise often include the renewal of the entire trough lining [14]. Casting

wheels with different numbers of moulds and hence capacity are in use, but the use of larger casting wheels to achieve higher capacities only makes sense up to a certain size, as higher forces are required for acceleration and braking. The casting wheel at Montanwerke Brixlegg AG is illustrated in Figure 6.

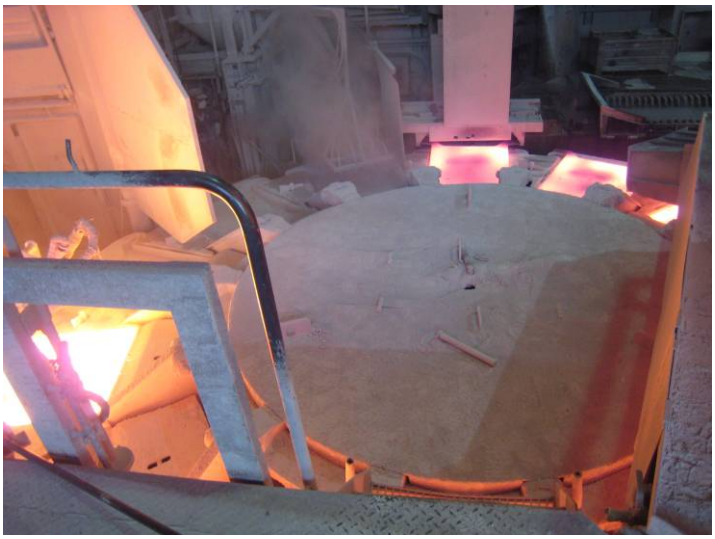

Figure 6: Casting wheel at Montanwerke Brixlegg AG

An alternative to one large casting wheel is the use of two smaller ones, on which anodes are cast alternately from one source that can be tilted sidewise (Figure 7). The benefits (compared to one large casting wheel) include [23]:

- Longer cycle times (increased time for solidification)
- Lower rotating speed
- Decreased acceleration and deceleration rates
- Less required space
- Smoother surface due to slower cooling
- Malfunction of one wheel does not result in a total production stop, but only in reduced output

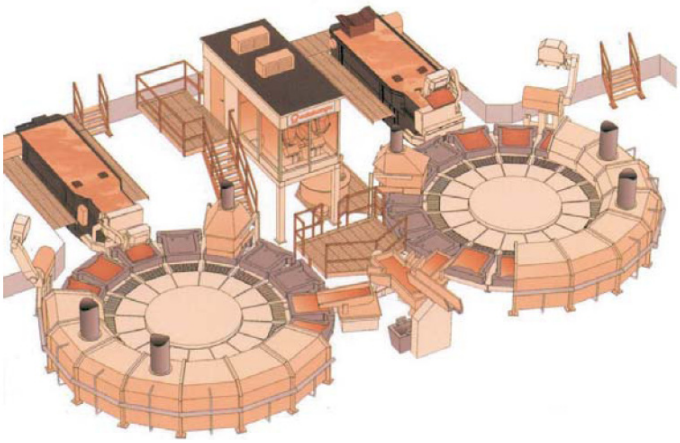

Figure 7: Schematic diagram of a twin-wheel [24]

Norddeutsche Affinerie AG (Hamburg, Germany) uses a 24-mould casting wheel with a production capacity of 80 t/h exceeding 450,000 t/a. The moulds are arranged in pairs, resulting in 12 positions in a cycle. In the first position, the moulds are filled with molten copper. The second position has no additional water cooling, and the anodes are only cooled by the ambient air. In the following four positions, water sprays (i.e., single fluid nozzles, process water) cool the moulds and the vapour is extracted. In all cooling positions the moulds are sprayed from underneath. Only in positions five and six the anodes are sprayed from the top since in the preceding positions radiation and convection cool the anode surfaces. In an emergency the anodes can be discharged manually at position seven. The automatic take-off is located at position eight and submerges the red-hot anodes into bosh tanks. A robot coats the moulds with barite suspension at position nine. The remaining positions are used for surface control [25].

2.1.1.1 Anode Moulds

Casting moulds are subjected to thermally induced stresses from molten copper and cooling water and probably side reactions with the anode copper and impurities. Hence, the main signs of wear are intercrystalline cracks and corrosion, as well as mould distortion [25]. Wear caused by the molten copper stream becomes apparent as furrowed surfaces, which result in wave-like concave cavities on the mould side of the anodes. Whilst this does not affect the cathode quality, it impedes extraction of the anode from the mould. Since the cracks are very deep, milling the surface of the mould is not possible due to problems in process automation [25]. Another sign of wear is distortion caused by thermal stress, which leads to convex anodes that locally shorten the distance to the cathode [25, 26].

The materials used for anode moulds are anode or cathode copper, however certain copper alloys (i.e., SE-copper (oxygen free phosphorus deoxidized with a low residual phosphorus content), SF-copper (oxygen free phosphorus deoxidized with a high residual phosphorus

content), OF-copper (oxygen free), or a copper alloy with up to 10% alloying elements including Ag, Cr, Zr, Mg, Zn, or Al [25, 26]) may be suitable. The chemical composition of the material used determines its thermal conductivity and therefore influences mould lifetime and anode solidification.

One parameter concerning mould durability is the copper heat conductivity, which is lowered by additives. The mould performance is improved by minimizing the oxygen level, as Cu_2O segregates along the grain boundaries and accelerates crack formation. If too high levels of P are used for deoxidation, the mould lifetime further decreases. In addition, the segregation of other alloy components limits the lifetime [25, 26].

The mould grain size, which depends on the manufacturing process, is decisive for mould wear and lifetime. The typical cause of mould replacement is either warping or cracking. Even moulds made of the purest copper suffer from cracks and distortion due to the coarse microstructure resulting from slow solidification, which promotes cracks along the grain boundary. A smaller grain size hinders crack elongation. Mould levelling is essential for producing anodes with a uniform thickness [22, 25, 26]. The mould lifetime also depends on the casting load, whereby lower casting rates result in longer lifetimes [25].

The higher conductivity of cathode copper moulds has some influence on the process, but statements regarding the correlation between mould material and mould lifetime are inconsistent. On the one hand, Hakakari and Pariani [21] did not find a significant increase in lifetime for the cathode copper moulds, but some (however not consistent) quality degradation in the lug area, as the softer cathode copper is damaged more easily than anode copper moulds. On the other hand, cathode copper moulds are said to have a longer lifetime and produce higher quality anodes than anode copper moulds [22]. However, the supposed benefits of cathode copper moulds regarding improved anode quality seem to outweigh the higher costs.

The quality of the moulds, which are usually cast by the smelters, varies with the quality of the copper used, the type of mould used, and the care and technique used to pour the mould [22]. The anode moulds are either produced by casting the metal in another mould with the contour of the anode or by inserting a cooled die with the desired anode contour into the molten metal [26]. The latter technique should improve the microstructure and hence prolong mould lifetime, however cavities beneath the surface may occur [25]. Cast anode moulds have certain disadvantages, such as coarse grains and internal stresses that result in a limited

lifetime. Furthermore, oxygen absorption during casting and high thermal stresses during solidification cannot be avoided [25]. Further disadvantages of cast anode moulds include [26]:

- Limited lifetime
- Internal stresses (due to thermal effects) that lead to crack formation
- Finishing required
- Deviations between individual anode moulds (non-uniform moulds): Oxygen uptake during casting and degassing during cooling lead to the formation of pores and oxides. This causes different thermal conductivities, which in turn promote crack formation and growth, and result in different mould lifetimes.
- Contour changes are associated with increased labour requirements
- Material defects that cause moulds with too large anode negatives can only be remedied by complex material additions

Continuous operational use is reported to have a stronger impact on mould lifetime than the temperature ranges, mould temperature variations, and tonnes of material cast. The moulds appear to require the same production parameters as anodes [21]:

- Good quality copper
- Proper control during processing
- Proper addition of mould dressing
- Good distribution of copper in the mould
- Mould design

A new anode mould manufacturing technique is milling the moulds out of continuously cast cakes with uniform material properties and sandblasting them for good mould wash adhesion. Alternatives to milling are other machining or forming operations, for example forging or extrusion. To overcome the disadvantages of the coarse microstructure due to slow solidification of the continuous cast cakes, which causes cracks and distortion even in moulds made of the purest copper, the blank should be forged (or extruded or rolled) before milling the mould in order to achieve a smaller grain size and hence hinder crack elongation. One of the advantages of this method is a prolonged mould lifetime (2,400 to 4,000 t compared to 300 [25] or 550 [27] to 2,200 t [25] with high variations for cast moulds) due to finer grains [25, 26]. Another advantage of milled moulds is that the anode shape can be changed easily without having to manufacture a new negative mould [25, 26].

2.1.1.2 Mould Wash

The mould wash enables quick release of the anode from the mould. It should not be cohesive to the anode, nor react with the Cu, and it must not interfere with the electrorefining

process. During electrorefining, the mould wash becomes part of the anode slime [22]. Adhering mould wash can lead to cathode contamination and dendrite formation during electrorefining [28]. The mould wash consists of a solid suspension in a liquid medium such as water. $BaSO_4$ is the most common material; other possibilities include alumina, a mix of $BaSO_4$ and alumina, clay, (synthetic) bone ash [21], chamotte mortar [17], graphite powder [22], TiO_2 [29], silica, bone black, ganister, lime or a combination thereof [29]. Suitable adhesives or binders are rosin, copal, gum arabic, glue or gelatine [29].

The liquid medium of the mould wash volatilizes because of the high anode mould temperatures (i.e., 90–540 °C), and a layer of the solid material is left behind on the mould surface [30]. The application of preheated mould wash (65–95 °C) was suggested in order to avoid thermal crack formation, which leads to bigger cracks that require a mould change [30]. There is limited information in the literature regarding mould wash properties (e.g., density 1.7 g/cm³ [31], solid fraction 27 wt.% [32]) or consumption (0.30 kg/t [12]).

2.1.1.3 Cooling

The solidification of casting wheel anodes is accelerated by water spray cooling of the moulds and—later—the anode surfaces themselves. Optimization of the spray nozzle layout and hence uniform cooling helps to minimize geometrical distortion [33]. At approximately 700–900 °C the anodes are released from the moulds by the push pins and extracted from the mould by an anode take-off device. However, anode extraction often causes distortion when the anodes adhere to the mould and the lugs may also be distorted. The take-off machine takes the hot anode to a bosh tank or water spray cooling chamber where the anode is cooled to 70–100 °C [22].

When anodes produced on casting wheels are cooled in bosh tanks, a certain amount of material falls off the anode, namely adhering particles like oxides or mould wash, which contaminate the cooling water. These materials accumulate at the bottom of the tank and have to be removed regularly. 1,000 t of anodes result in approximately 400 kg (approximately 1 m³) of these materials. Different systems for their collection and removal have been developed to avoid long standstills including [34]:

- Bags
- Separate basins
- Conveyors
- Mixing and holding in suspension (+ circulation)

The anode cooling and solidification process is very important since a rapid cooling (firstly in the mould and then in the water tank) is necessary in order to avoid the formation of surface oxide scales [35].

2.1.1.4 Thermal Anode Treatment

Thermal anode treatment at elevated temperatures (700–1,000 °C) in combination with slow cooling (approximately 200 °C/h from maximum T to approximately 500 °C and approximately 10 °C/h from 500 °C to 150 °C) can accelerate anodic dissolution due to the presence of CuO which forms due to Cu_2O oxidation and dissolves faster then Cu_2O. As the nature of the slimes is altered and the amount is decreased, the passivation time is prolonged for anodes with various oxygen and impurity levels [36, 37]. A similar thermal treatment under inert gas atmosphere, which can lead to a reduced tendency for passivation and improved electrorefining operations, is also described by Imamura [38].

Thermal treatment alone—namely without slow cooling—only slightly improves the dissolution behaviour. Slow cooling (20 °C or less per minute) should also result in impurity precipitation, segregation, and coalescing as well as a coarser Cu crystal structure. The coarse impurity particles, which accumulate along the grain boundaries, are less susceptible to dissolution in the electrolyte and fall more rapidly to the bottom of the cell. This enables the production of higher purity cathodes, as less impurities dissolve in the electrolyte [39].
A type of thermal treatment is reported to result in the following benefits [38]:

- Higher current density—higher output
- Applicable also for very impure anodes
- Lower cell voltages and lower anode slime levels result in lower energy consumption and reduced anode slime treatment costs
- Fewer shorts caused by passivation—better performance of the electrolysis and lower labour costs

The disadvantages of this treatment appear to be:

- Time and effort (time consuming processes: Slow cooling after removing the anodes from the casting wheel at 700–1,000 °C or standard casting process + reheating and slow cooling)
- No prolonged passivation times for anodes with high Ni and O
- Losses of valuable metals/complicated anode slime processing
- Slow dissolution

Because of these disadvantages, the thermal anode treatment is not used in industrial practice.

2.1.1.5 Preheating Anode Moulds

The majority of anode rejects are produced during the first round of anode pouring when the moulds are cold. When the moulds have reached 175–185 °C minimizing the number of rejects is then a matter of controlling the temperature of the cast copper (e.g., 1,190–1,205 °C, but sometimes even higher), proper calibration and maintenance of the casting system and casting wheel, proper maintenance and replacement of the anode moulds, as well as adjustment and maintenance of the anode take-off [22].

2.1.1.6 Atmosphere during Casting

The anode copper oxygen content is decreased by reduction in the anode furnace to achieve a final oxygen content after fire refining of 0.05–0.3 wt.% [40] (0.12–0.16 wt.% [12], 0.15 wt.% [15], 0.15–0.25 wt.% [41]). However, despite these efforts, during anode casting the oxygen content is subsequently increased. A rise in the oxygen content from 0.14–0.33 wt.% in the launder to 0.15–0.40 wt.% (0.25 wt.% [15]) in the anodes has been reported [42]. This oxygen uptake occurs especially due to liquid copper splashing and air entrainment beneath the liquid copper when pouring the liquid copper into the weighing and casting trough, as well as the anode mould. For electrorefining operations, it is important that the anode oxygen content is constant. Burners, which provide a reducing atmosphere, can avoid or minimize oxygen uptake during pouring and casting.

2.1.2 Continuous Anode Casting (Hazelett/CONTILANOD®)

Continuous anode casting started in the 1960s and has been subsequently developed and improved regarding anode design, cutting, and production capacity [43]. In the modern CONTILANOD® process, the anode copper is fed by a launder system to the casting furnace, which is a continuous holding furnace. From the casting furnace, the anode copper is transferred via the pipe-shaped outlet into the tundish, and then into the Hazelett twin-belt caster (Figure 8 and Figure 9). The metal is distributed evenly on the lower belt and into the moving caster mould. The wide casting spout ensures calm and non-turbulent flow into the mould area. The metal flow is regulated by an automatic level control system. The casting level, as well as the casting speed should be held constant. Two endless revolving steel casting belts, which are slightly tilted downwards, form the bottom and the top of the mould. They are supported by precise roller shafts to ensure perfectly flat anodes. Their backs are continuously cooled by high-speed water flow [11, 44-46].

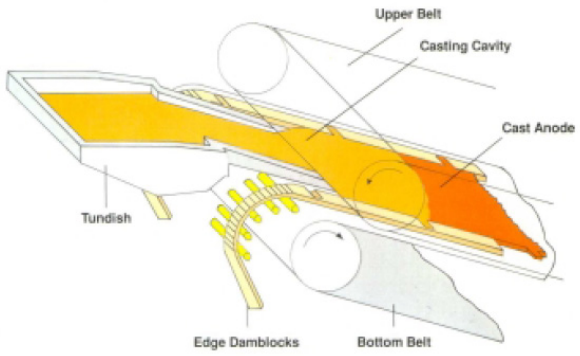

Figure 8: Metal flow into the casting machine [44]

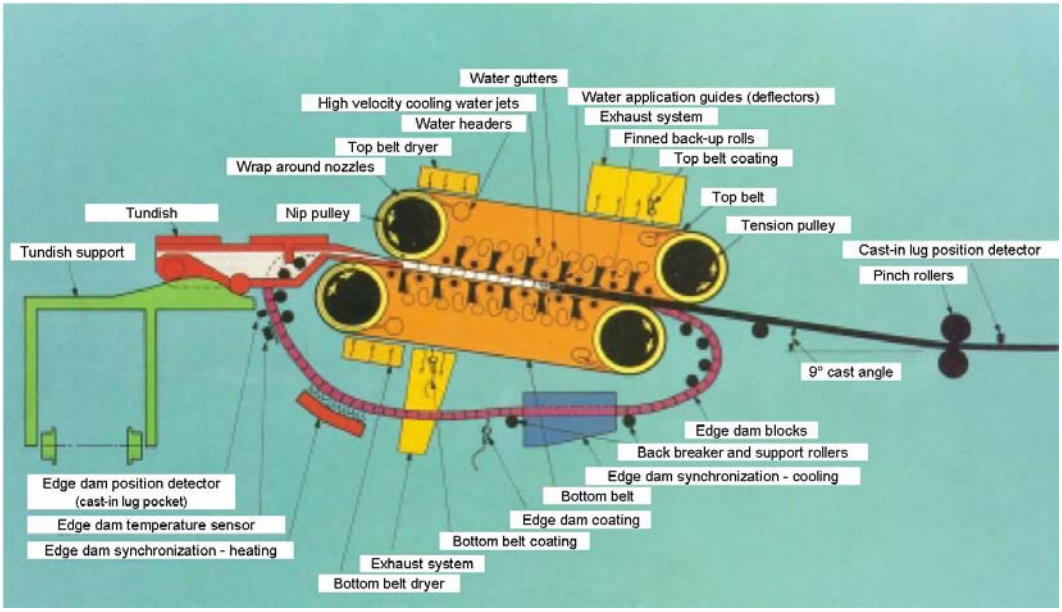

Figure 9: Schematic diagram of the Hazelett anode caster [44]

The layout of a modern CONTILANOD® line is illustrated in Figure 10.

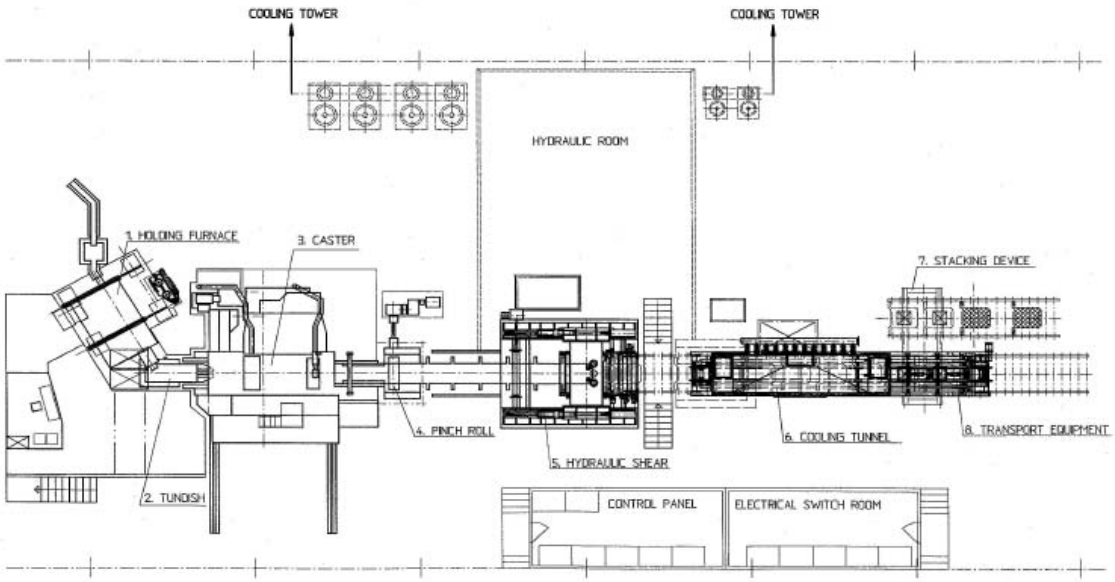

Figure 10: Schematic diagram of a CONTILANOD® line with hydraulic shear-system [44]

The mould sides are formed by two endless metallic dam blocks, whose height determines the anode thickness. Specially formed edge dam blocks with machined pockets for the anode lugs (Figure 11) are positioned periodically in the chain. The position of the anode lugs on the emerging slab is monitored continuously. The lug pocket blocks on both sides of the caster are synchronized by heating or cooling the dam blocks to regulate the distance between the single pocket blocks thermally [11, 44, 46]. The lugs are half the thickness of the anode and have a rake on the bottom surface, which provides a knife-edge contact on the anode centreline, and hence a maximum and equal current flow during electrorefining. The typical CONTILANOD® anode dimensions are detailed in Table 1 [44, 45].

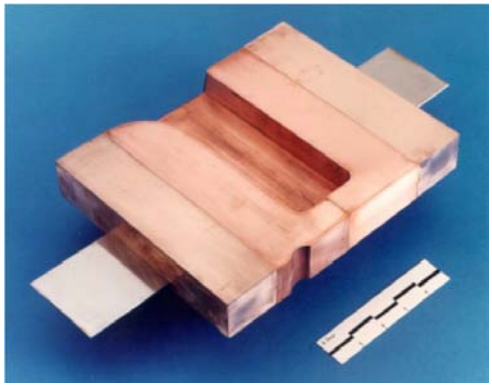

Figure 11: Edge dam block for anode lug casting [44]

Table 1: Typical CONTILANOD® anode dimensions [44]

Anode thickness	15–70 mm
Anode width	< 1,050 mm
Overall width (incl. lugs)	< 1,300 mm
Anode length	approx. 1,000 mm

The slab is cut after emerging from the caster by a hydraulic shear, which is moved along with the anode slab (Figure 12). In the cooling tunnel the anodes are cooled equally on both sides using spray nozzles, and subsequently stacked [11, 44, 46].

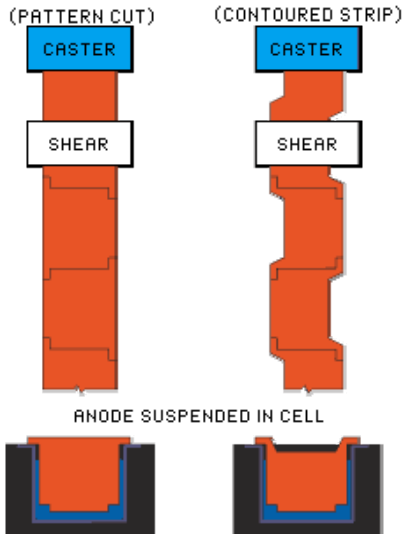

Figure 12: Cutting continuously cast anodes [45]

The continuous casting of copper anodes is not growing and only six refineries in the world have installed such a system, with only three currently in operation (i.e., operational: Gresik, Indonesia; Onahama, Japan; Kidd Creek, Canada; shut down: MKM, Germany; IMI, UK; now only toll refining casting wheel anodes: White Pine, USA) [16]. However, this casting system is reported to have various benefits [11, 16]:

- Less required space compared to production capacity—easier to maintain [20]
- Good anode quality: High density, fine and even structure, low porosity, smooth surface, and uniform anode thickness [11, 20, 45, 46]
- Better anode geometry, anode surface, and weight uniformity than the casting wheel process [11, 45]
- Uniform impurity distribution [11, 45, 46]
- Thin anode production [20]
- Higher casting rates [20]
- No additional straightening or machining [11, 46]

However, the statements regarding anode porosity are inconsistent. Whilst in certain cases it appeared that porosity was not a problem [11, 20, 46], a significant amount of segregated macroporosity in the anodes, presumably due to air entrainment (resulting from the turbulent and swirling liquid copper flow from the tundish to the belt caster), lubricant volatility, and [H] + [O] steam reaction was also reported [47]. The difference in quality between casting wheel technology and the CONTILANOD® process is dependent on process control: A well

controlled casting wheel process may produce anodes of the same quality as a poorly controlled CONTILANOD® process. The investment and operating costs are higher for the CONTILANOD® process. Leuprecht [11] reports that the slightly improved anode quality resulting from the CONTILANOD® process does not compensate for these additional costs through the cost reductions during the electrorefining process. The elemental distributions in CONTILANOD® anodes are detailed in Section 5.3.1.2.

The structures of two CONTILANOD® anodes from IMI (Walsall, UK) are illustrated in Figure 13. Anode A is a typical CONTILANOD® anode, whereas anode B has a structure similar to casting wheel anodes. The different anode cooling conditions are clearly visible from the micrographs: Anode A was solidified under regular process conditions, namely as described above. During anode B casting problems were reported with the cooling and excessive belt lubricant residue was present. Anode A showed a fine grain structure throughout but increased irregular microporosity in the upper half, which may have been due to the excessive presence of belt lubricant (silicone oil), which breaks down to CO_2, CO, H_2O, and SiO_2 on combustion. In contrast, anode B has nearly a cast structure with coarse columnar grains. These indicate slow cooling, namely insufficient cooling to promote nucleation of fine grains [44].

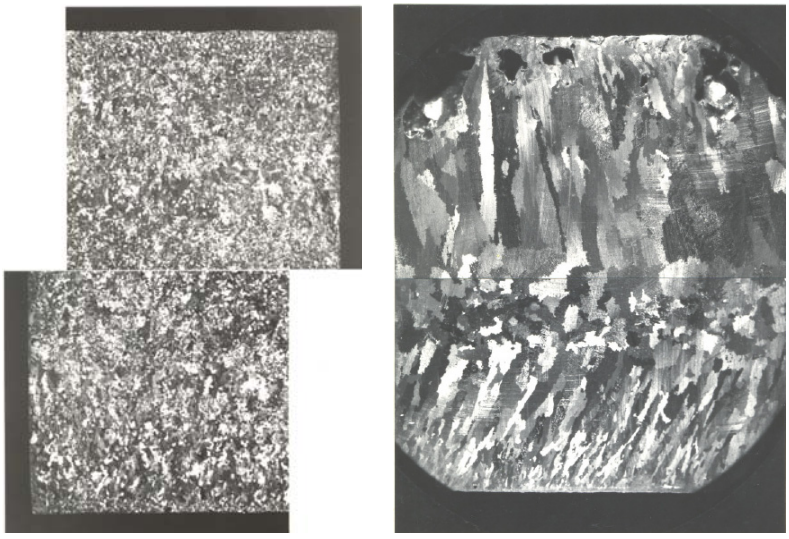

Figure 13: Macrostructure of the centre of CONTILANOD® anode A (left; 5 x) and B (right; 2.5 x) [44]

2.1.3 Vertical Moulds

Anode casting in vertical moulds has only been investigated on a laboratory scale [17, 18]. There are no reports regarding the industrial application, although vertical casting is reported to have some advantages compared to casting wheel anodes, for example more homogeneous cooling conditions and elemental distribution.

If a casting wheel were equipped with vertical moulds, the number of moulds could be increased, however a number of changes in the process would have to be made concerning for example the filling and cycle time, as well as mould wash application and anode take-off.
Anode casting in vertical moulds with (Figure 14) and without cooling on a laboratory scale (anodes: 100 x 80 x 10 mm) was investigated by Chernomurov et al. [17]. This technique should result in high geometrical accuracy, good surface quality, and high density as well as uniform elemental distribution over the entire ingot height. The Ni distribution in vertically cast anodes was reported to be almost constant over the casting height. Ni combines with oxygen and forms NiO, which concentrates close to the Cu_2O inclusions.

However, one disadvantage is the formation of shrink holes at the anode edges. Mould filling, density, and porosity distribution can be improved by preheating the moulds to approximately 200 °C.

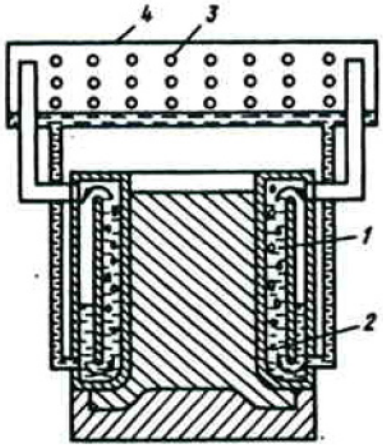

Figure 14: Vertical mould with condensation-gas cooling (1: Cooling jacket, 2: Intermediate heat transfer medium, 3: Cooled tube bank surfaces, 4: Condensation chamber) [17]

The mould is cooled using the warm tube principle. Each of the two detachable sections of the mould is equipped with a cooling jacket, which is partially filled with an intermediate heat transfer medium. The mould is cooled by boiling this intermediate heat-transfer agent followed by the condensation of the steam on the cooled surfaces of the tube bank in the condensation chamber. The steam releases heat in the condensation chamber during condensation of gaseous coolants (air). As a result, a closed cycle is achieved for the heat transfer through latent heat of evaporation of the intermediate coolant. Preheated air is returned to the furnace, contributing to reduced fuel consumption during the casting process.

Further investigations on anodes cast in a water cooled vertical mould were performed by Antrekowitsch et al [18]. The elemental distribution and hence dissolution behaviour during electrorefining was further improved by using magnetic stirring.

Due to the predominance of casting wheel technology in copper refineries, this work focuses on casting wheel anodes. Typical anode weights and properties for casting wheel and CONTILANOD® anodes are detailed in Table 2 and Table 3. In the following sections, the anode quality features, which are significantly influenced by the casting process, are described. A comparison of the elemental distribution in casting wheel and CONTILANOD® anodes is provided in Section 5.3.1.2.

Table 2: Casting wheel anodes [6]

Casting wheel anodes	Min	Max	Average
Anode length [mm]	800	1,333	972
Anode width [mm]	700	1,333	907
Anode thickness [mm]	32	60	44
Mass [kg]	220	435	334
Life [days]	14	28	21
Scrap [%]	10	26	16

Table 3: CONTILANOD® anodes [6]

CONTILANOD® anodes	Xstrata Copper Kidd Metallurgical Site Timmins, Canada	Mansfelder Kupfer und Messing GmbH Hettstedt, Germany 2003 data - shut down	P.T. Smelting Co. Gresik, Java, Indonesia	Onahama Smelting & Ref. Onahama, Japan	Average
Anode length [mm]	1,105	900	979	980	991
Anode width [mm]	960	950	930	960	950
Anode thickness [mm]	21.6	42	45	15	30.9
Mass [kg]	187	320	381	143	257.75
Life [days]	9	21	20	11	15.25
Scrap [%]	25	12-15	11.5~14.7	24	17

2.2 Anode Design

The general anode design is very similar in all refineries (Figure 15). However, as there is no standard design for anodes, there are slight differences between the individual refineries. It is important to have a proper mould design, namely the appropriate draft angles in the mould, and a design that does not create stresses in the anode that can cause cracking during cooling [21]. The anode mould cavity has the shape of the anode cross section and is somewhat deeper than the anode thickness [14].

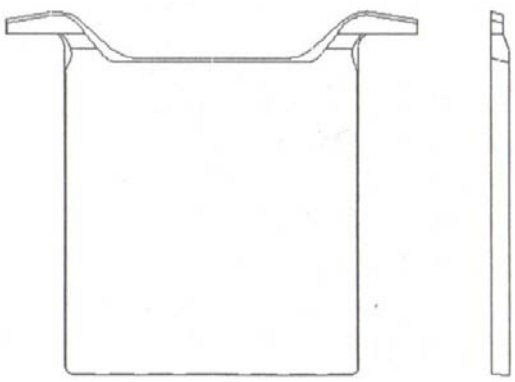

Figure 15: Anode geometry [11]

2.3 Anode Quality

As previously described, anode quality has a significant influence on electrorefining. The anode has to have a certain physical and chemical quality in order to meet the requirements for electrorefining, namely to achieve a high current efficiency, low energy consumption, low amount of anode scrap, and low effort together with high cathode quality [11]. A uniform anode weight and therefore thickness as well as smooth surfaces are essential for uniform anode spacing and hence dissolution. An even current distribution is assumed for the following statements regarding the effects on anodic behaviour during electrorefining, as variations in current density due to not perfectly vertical electrodes cause much more pronounced effects than other anode properties, for example the structure [28]. Anode preparation machines, which weigh, straighten, and mill the lugs, so that the anodes hang vertically in the cell and hence improve current distribution as well as enable higher current efficiencies at higher current densities, are becoming more prevalent [16].

The chemical quality criteria include a minimum content of harmful impurities, surface conditions of the anode body (especially the absence of passivating films), density, and the gas-saturation capacity [17, 22]. The chemical quality is mainly adjusted during fire refining, but it can be further influenced during the casting process. However, anode quality is not only dependent on the casting technology used, but especially on proper process control. Anode rejections are mainly based on visual inspections [21].

The structure and elemental distribution can be influenced by solidification conditions, for example the cooling rate and heat transfer, and these in turn by:

- Mould material (thermal conductivity)
- Mould wash
- Amount of cooling water
- Mould preheating
- Thermal treatment of anodes
- Liquid anode copper casting temperature

In the following sections the chemical and physical anode quality are discussed more in detail.

2.3.1 Chemical Anode Quality

The chemical anode quality is controlled during fire refining, but the distribution and form of the elements can be influenced by the casting process and cooling conditions. In addition, the level of non-metallic impurities including slag carry-over from the anode furnace, metal-

refractory interactions, and mould wash has to be taken into account. Not only the absolute impurity content is decisive for the chemical anode quality, but also the form and relative content. A uniform chemical anode quality is desirable in order to achieve anodes with a homogeneous dissolution behaviour and to assure optimum co-ordination with electro-refining.

Each electrorefining plant defines certain impurity limits. Not only the absolute content, but also the ratios of different impurities in relation to each other and their chemical forms are essential. The latter is not characterized by chemical analysis [11]. Two molar fraction ratios (MFR) are of special interest (Sections 2.3.1.3 and 2.3.1.8):

$$MFR\ I = \frac{As}{Sb + Bi} \qquad \text{Equation 1}$$

$$MFR\ II = \frac{Ag}{Se + Te} \qquad \text{Equation 2}$$

Depending on whether the anode copper is produced from primary or secondary sources, influences the accompanying elemental content. Typical primary and secondary copper anode compositions are given in the work of Robinson et al. [16] and Moats et al. [6], and are detailed in Table 4. The values in Table 4 also provide an orientation for the following explanations regarding “high” or “low” elemental content, which are frequently not clearly quantified in the literature.

Secondary copper anodes are generally rich in Sn, Pb, Ni, and Sb, but are notably deficient in Se, Te, and Ag. The behaviour of the impurities during electrorefining as well as the phases formed (depending on the relative amounts of the elements) are typically the same as for primary copper anodes, however the amounts of the phases differ. One obvious difference is the high Sn content in secondary copper anodes [48]. The chemical analysis is performed before casting [12].

Table 4: Chemical analysis of anodes [6]

Anodes	Primary			Secondary		
Analysis	**Min**	**Max**	**Average**	**Min**	**Max**	**Average**
Cu [wt.%]	98.00	99.80	99.29	98.70	98.95	98.82
Ag [ppm]	50	7,523	1,067	300	600	433
Au [ppm]	1	200	39	5	10	7
S [ppm]	1	100	29	20	25	23
Se [ppm]	30	1,250	420	30	50	40
Te [ppm]	0	650	103	10	50	30
As [ppm]	10	3,000	908	200	800	567
Sb [ppm]	1	1,300	195	400	1,300	833
Bi [ppm]	0	679	113	10	100	50
Pb [ppm]	4	3,120	895	50	3,500	2,017
Fe [ppm]	0	200	63	10	20	15
Ni [ppm]	13	27,584	1,561	4,500	5,000	4,667
O [ppm]	214	22,000	2,167	1,800	2,200	2,000

The chemical anode quality should be as uniform as possible in order to achieve anodes with a homogeneous dissolution behaviour and to assure optimum compatibility with electro-refining. This is especially difficult at secondary smelters, since the scrap composition tends to vary widely. Furthermore, the metal composition changes from the first to the last molten copper poured from the anode furnace, which results in a different dissolution behaviour and tendency for passivation. Gas purging can be used in the anode furnace to overcome these compositional variations within one batch [49]. Non-metallic impurities including slag carry-over from the anode furnace, metal-refractory interactions, and mould wash also have an influence on the chemical anode quality.

During solidification certain elements are enriched in the solid phase (e.g., Ni), whilst others are present in the melt (e.g., O, Sb, As, Sn, Pb) [50], depending on the value of their distribution coefficient, k, especially the effective distribution coefficient, k_{eff} (Section 2.3.1.11) [51]. This leads to either solid solutions ($k > 1$ [51]) or separate phases of various compositions in the solidified anode ($k < 1$ [51]). The mostly inhomogeneous distribution leads to different dissolution rates when in contact with the electrolyte [18]. During electrorefining, some impurities dissolve and concentrate in the electrolyte, whilst others are insoluble and accumulate in the anode slimes. These slimes contain significant metal levels (e.g., Cu, Au, Ag, Ni, Pb, As, Sb, Bi, Se, and Te) and hence undergo further processing for recovery. The mineralogy of the anodes has a direct influence on anode passivation, the formation of floating or suspended slimes, and the eventual recovery of valuable by-products [52].

Not only the overall anode composition should be uniform, but also the elemental distribution within the anode. The latter is strongly dependent on the casting process, as it is related to the grain boundary structure of the anode. The level of inclusion phases, for example selenides or oxides, is dependent on the element concentrations in the anode. Only Cu_2O

and NiO are formed by primary crystallization, the other phases are formed by secondary crystallization and therefore associated with crystallization-induced local accumulations [53]. The phases containing minor impurities including Sb, Sn, Pb, and Bi can be found as layers on the primary crystals or inhomogeneously distributed in the eutectic phase [18].

In the following sections the accompanying elements in anode copper are discussed more in detail.

2.3.1.1 Nickel

All the Ni is in solid solution when the anode contains < 0.3 wt.% Ni. Above this level NiO crystals are formed, whereby the amount of NiO is a function of the anode O content [52]. Forsen and Lilius [50] found that NiO occurs (due to supercooling of the melt) at a Ni content of 0.25 wt.%, when the O content is ≥ 0.3 wt.% [50]. In Ni-rich anodes, NiO, Cu-Sb-Ni oxide, and Cu-Sn-Ni oxide may be present [54].

Ni (like Ag) is distributed inhomogeneously in the Cu matrix, whereby the maximum concentration is 0.8 wt.% Ni at an average content of 0.4 wt.% [53]. The Ni content in secondary copper anodes may be as high as 0.5 wt.%, and sometimes even higher [55].
Ni has the following negative impacts on electrorefining [55]:

- NiO promotes passivation
- A high NiO content decreases Cu solubility (and therefore the Cu concentration) in the electrolyte
- Large amounts of Ni in the anode slimes
- High Ni concentrations in the electrolyte decrease its electrical conductivity
- Deteriorated dissolution behaviour, especially at a high Ni (1 wt.%) and O (0.6 wt.%) content [18]
- Higher Ni (and Pb) content in the anodes promote passivation

2.3.1.2 Arsenic

In high As anodes, at least 30% of the total As is in solid solution [52, 56]. It is enriched in the melt during solidification and is found along the phase boundaries in oxygen free copper anodes. At an As content of > 0.7 wt.% an intermetallic compound Cu_3As, which is more noble than copper, is formed due to nonequilibrium solidification and fast cooling, respectively [50, 57]. The anode As content (and the electrolyte bleed) controls the Sb content of the electrolyte [56], due to the kinetically faster oxidation of As^{3+} to As^{5+} compared to the oxidation of Sb^{3+} to Sb^{5+}, and hence the formation of floating slimes, which are formed by Sb^{5+}.

The As in solid solution is dissolved as As^{3+} ions during electrorefining. These ions produce an anode slime consisting mainly of Cu_3As and a minor amount of Cu powder. Depending on its structure, which in turn is linked to the As content, this slime hinders diffusion and promotes passivation. A decrease in As lowers the As/Sb ratio and (especially at As/Sb < 2) can lead to [42, 57-60]:.

- More shorts
- Decreased current efficiencies
- More apparent gas evolution
- Increased floating slimes (compounds of the type SbAs and BiAs (2 to 7 µm) [22, 60])
- Cathode top nodulation
- Slimes: Thinner, denser, less cracked, more tenacious, and more adherent during washing
- Anode passivation
- Decreased cathode surface quality

Claessens [61] found that anodes with a MFR I < 0.5 and a Pb content > 0.15 wt.% tend to passivate. As could prevent passivation induced by stable Cu_2O films, which form in acid depleted zones on the anode, by releasing hydrogen ions upon anode dissolution and therefore producing sufficient acid [58]:

$$[As]_{Cu} + 2H_2O \rightarrow HAsO_2 + 3H^+ + 3e^- \qquad \text{Equation 3}$$

A suitable molar ratio of As, Sb, and Bi, which can be adjusted by injecting AsO_3, helps to avoid floating slimes and enables higher current densities to be used without deteriorating the cathode quality despite other impurities being present [12].

2.3.1.3 Antimony

About one fifth of the total Sb in the anode occurs in solid solution [56]. A Sb content of 0.01 wt.% does not significantly change the electrochemical behaviour of the anodes, but causes a spheroidization of Cu_2O in the eutectic area along the phase boundaries. At a Sb content of > 0.05 wt.% and a Ni content > 0.25 wt.%, thin and flake-like inclusions (kupferglimmer) have been found at the grain boundaries [50].

A high MFR I (usually > 1) is beneficial for electrorefining operations, as a high As content prevents the oxidation of Sb^{3+} to Sb^{5+}, which is a main component of floating slimes [28, 59, 60, 62]. Hence, higher current densities are possible without deteriorating the cathode quality (despite other impurities being present).

2.3.1.4 Bismuth

The Bi content in the Cu matrix is usually below the minimum detection limit of 0.06 wt.% [52]. As Bi and Cu are nearly insoluble, thin Bi films, which are less noble than copper and cause cementation of Cu, are formed at the grain boundaries during the solidification process [50]. No observable impact of Bi on anode passivation has been detected, but it tends to co-deposit cathodically with Cu at a low Cu and high Bi content (> 0.22 g/l [58]) in the electrolyte [58-60].

2.3.1.5 Precious Metals

Au occurs in solid solution in the Cu matrix, however whilst no discrete Au phases were reported by Chen and Dutrizac [52], part of the Au may also be present in the Cu selenide inclusions. At least 85% of the total Ag in the anodes is found in the Cu matrix, presumably as a metastable solid solution [52, 56, 63], and traces are detected in Cu_2O and Cu_2Se [63]. Ag (like Ni) is distributed inhomogeneously in the Cu matrix, whereby the maximum difference in concentration is 0.5 wt.% (absolute; i.e., maximum 0.8 wt.% and minimum 0.3 wt.% Ag) at an average Ag content of 0.3 wt.%. Ni and Ag are distributed in an opposite manner, which can be explained by their different distribution coefficients (2 and 0.5, respectively) [53].

The Ag comes into contact with the electrolyte as the Cu is dissolved and forms fine, uniform particles on the anode surface (i.e., slime). Depending on the thickness of the slime layer passivation occurs at a critical value. Thereby, the dissolution potential of Ag is reached and dissolution as Ag^+ takes place [63-66]. The behaviour of Ag is not altered by the presence of Se, Pb, Sn, Sb, Ni, and As [63]. Ag is reported to promote passivation [42, 64-67].

2.3.1.6 Lead

Low concentrations of Pb occur in solid solution [56], but the major Pb carriers are the various oxide inclusions [42, 52]. It is sometimes concluded in commercial electrorefining operations that a high Pb content in the anode and Pb additions reduce the As, Sb, and Bi concentrations in the electrolyte due to oxide formation [56, 61]. Pb is believed to dissolve anodically along with the Cu and subsequently reprecipitate as $PbSO_4$ [68]. An increase in the Pb content facilitates anode passivation; however, when both Pb and O are present the anodes are less likely to passivate [36, 68].

2.3.1.7 Tin

In secondary copper anodes, Sn occurs mainly as SnO_2 and less frequently as Sn-Ni-Zn oxide and Sn-Ni-Zn-Fe oxide at the Cu grain boundaries. When the anode is rich in Ni and Sb, Sn is also found in Cu-Sn-Ni oxide (~ Cu_2NiSnO_5) and Cu-Sb-Ni oxide (kupferglimmer $Cu_3Ni_{2-x}SbO_{6-x}$ where x = 0.1 to 0.2). Only approximately 10% of the total Sn is found in solid

solution in the Cu [48]. The SnO_2, which contains minor amounts of Cu and traces of Fe, Ni, and Zn, is present both as euhedral "free" crystals and as a constituent of the complex grain boundary inclusions. The Sn-Ni-Zn oxide contains minor amounts of Fe and Cu, and traces of Sb [48]. In addition, Sn-CaO phases have been detected, where the CaO may be derived from slag carry-over [42]. Sn reacts with the electrolyte, forms H_2SnO_3, and precipitates as anode slime [22].

2.3.1.8 Selenium

The Se content in anode Cu ranges between 0.009 and 0.34 wt.%, however levels of > 0.1 wt.% are very rare. A higher Se content in the anode can lead to higher concentrations in the electrolyte and the cathode Cu [69]. 5 to 12% of the total Se is found in (metastable) solid solution due to rapid cooling [54]. In contrast, it has been reported [52, 63, 69] that all the Se is present as Cu_2(Se,Te), with some Ag replacing Cu and minor Te levels substituting Se [54]. The selenide phase invariably accounts for < 1 wt.% of the total Ag content and is the sole Te carrier in copper anodes. The presence of S in the selenide phase is uncommon [52]. Chen and Dutrizac [56] found some S in the selenide phase, as well as traces of Ag and Au [56].

The Cu_2(Se,Te) particles are always associated with Cu_2O and are frequently also intergrown with other oxide constituents [52, 54]. They are usually found at the copper grain boundaries and appear to have been rejected from the melt as the copper solidified [52, 54]. In many inclusions the selenide phase completely rims the oxide constituents [56]. Regarding MFR II, the relative amounts of Se, Te, and Ag are important. An excess of (Se+Te) with regard to Ag leads to the formation of Cu_2Se and Cu_2Te instead of Se/Te and Ag compounds. If there is too little Se and Te, the Ag is directly transferred to the cathode. The Cu selenide is transferred to the anode slime without dissolution [22, 63]. At higher Se levels a Cu_2O intermediate layer between the slime layer and the anode surface is formed [63]. Se has been found to promote passivation [67, 69].

2.3.1.9 Oxygen

A certain amount of oxygen is beneficial for casting flat anodes; however, for electrolysis a low O content is desirable [12]. The majority of the total O is concentrated at the free surface of the cast anodes. Cuprous oxide (Cu_2O) is the most abundant impurity in most Cu anodes. It is present either as free grains or as inclusions associated with Cu_2(Se,Te), NiO, and various Cu-Pb-As-Sb-Bi oxides [52, 54]. Elements other than Cu and O are not found in the Cu_2O-phase [53], although the cores of some particles may consist of possibly $CuFe_2O_4$ [52, 54]. The formation of Cu-O eutectics can be prevented by adding a Vb element (As, Sb, or Bi) at almost stochiometric levels for compound formation [70, 71].

The accompanying elements including Sb, As, Pb, and Sn accumulate in various oxide phases, which commonly occur in association with Cu_2O, $Cu_2(Se,Te)$, and kupferglimmer (Cu-Ni-Sb oxide). The most common are Cu-Pb oxide, Cu-Pb-As oxide, and Cu-Pb-As-Sb-Bi oxide, which sometimes contain minor amounts of Fe, Ni, and Ag [19, 52, 53, 56]. Cu-Sn-Ni oxide, Ni-Fe-Sn-Zn oxide, Ni-Sn-Zn oxide, $NiFe_2O_4$, Cu-Sb-Sn-Ni oxide, and kupferglimmer are not soluble under normal electrorefining conditions and have a very low electrical conductivity. Hence, they pass into the anode slimes without any changes or form floating slimes [48, 55].

Plekhanov et al. [72] attribute irregular anode dissolution to a high Cu_2O content and the nature of the distribution of the eutectic. A high O content was found to promote passivation due to increased amounts of Cu_2O, Cu powder, and NiO associated with the slimes as well as its impact on slime structure and porosity, and on As distribution within the slime layer [18, 55, 67]. The dissolution of Cu_2O inclusions leads to Cu^+ enrichment and a pH increase. Passivation is promoted if the Cu powder formed by the disproportionation reaction remains at the anode surface. If the Cu powder falls down it enhances convection in the vicinity of the anode surface and passivation is less likely to occur. If O is only present as PbO (i.e., at high Pb levels), it has no influence on passivation [68].

2.3.1.10 Sulphur

A low S content (45 ppm) is necessary to produce anodes that have no blisters, minimal "picture framing" and "road maps", and ensure efficient electrolytic refining [12].

2.3.1.11 Distribution Coefficient and Elemental Distribution

The levels of accompanying elements and their maximum solubility in Cu are detailed in Figure 16 [53]. The minimum and maximum concentrations of the accompanying elements in Cu can be determined theoretically if the distribution coefficients are known and if only binary interactions occur. The actual concentrations are given by geometrical and thermal conditions during crystallization, namely the developing microstructure; however, the predicted trends are valid in principle [53]. The different cooling conditions and solidification rates may lead to concentration variations over the anode thickness, which are reported especially for anodes cast on a casting wheel [17-19, 28].

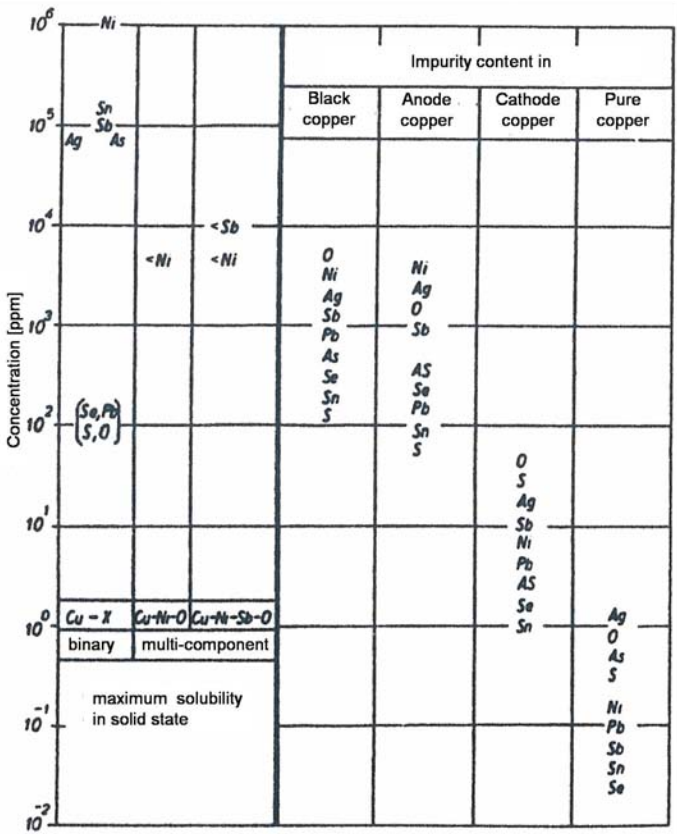

Figure 16: Maximum solubility (left) and levels (right) of accompanying elements in Cu [53]

In the case of a thermodynamic equilibrium the appearance of precipitations can be explained by phase diagrams; however, it must be noted that many of the multicomponent systems are not well defined [53]. There are two groups of impurities:

- High solubility in solid Cu (e.g., Ni, Sn, As, Ag, and Sb), whereby no precipitation occurs under equilibrium conditions
- Low solubility in solid Cu (e.g., Se, S, Pb, and O), whereby two-phase decomposition (precipitation during crystallization) takes place

However, the cooling conditions during anode casting and the fast solidification result in nonequilibrium conditions. Furthermore, the solubility in multicomponent systems with more complex interactions can be much lower than that in binary ones [53]: The solubility of Ni decreases from nearly 100% to values below 0.3 to 0.8% in the presence of O. NiO precipitations appear in anodes with high Ni levels. Kupferglimmer ($Cu_3Ni_{2-x}SbO_{6-x}$ where x = 0.1 to 0.2 [48]) is a multi-element compound, whose appearance is also linked with decreased solubilities in solid Cu. The solubility of Sb and Ni in this case is below 0.3 to 0.5%, but one premise for the formation of this phase is a defined Ni-Sb ratio. The tendency for the formation of kupferglimmer as a function of the Ni and O concentrations is illustrated in Figure 17, whereby the darker areas represent compositions which lead to larger quantities of kupferglimmer.

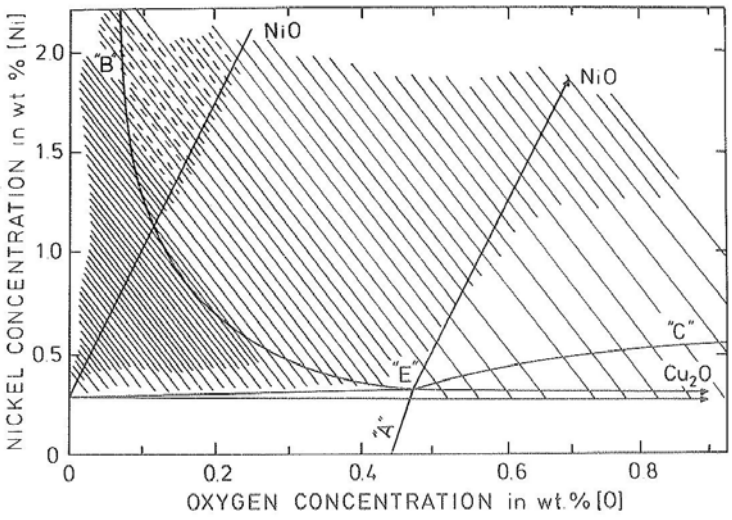

Figure 17: Potential areas of kupferglimmer formation [73]

The above statements have been confirmed by thermodynamic data of the compounds (Table 5). The relative stability of the compounds is described by a more negative enthalpy of formation and a high melting point and eutectic or peritectic temperature. Thus, under oxidizing conditions, Cu_2O, NiO, and the Sb-, Pb-, Sn- and As-oxides have a strong tendency to form separate phases. Under reducing conditions the formation of chalcogenides (Cu_2Se and Cu_2S) is most likely [53]. Further impurities including for example Bi could also be an important factor concerning precipitation [53].

Table 5: Thermodynamic data of compounds; 1: Formula, 2: Melting point [K], 3: Eutectic/ Peritectic temperature [K], 4: Enthalpy of formation [kJ/g atom], ~: No assured data available, -: No compound known [53]

	Se	S	O	Sn	Pb	As	Sb	Ag	Ni	
	Cu_2Se	Cu_2S	Cu_2O	Cu_3Sn		Cu_3As	Cu_3Sb			1
	1393	1402	1508			1103	960			2
Cu				~	-			-	-	
	1336	1340	1338			962	~			3
	- 22	- 27.3	- 55.8	- 7.5		- 26.8	- 2.6			4
	NiSe	NiS	NiO	Ni_3Sn		NiAs	NiSb			
	1253	1253	2233	1447		1243	1423			
Ni					-			-	-	S
	~	~	~	1433		~	~			
	- 37.4	- 47.1	- 120.3	- 25.7		- 35.9	- 41.8			
	Ag_2Se	Ag_2S	Ag_2O	Ag_3Sn			Ag_3Sb	SO_2	SeO_2	
	1170	1111	573	753			832	197	613	
Ag					-	~				O
	1113	1073	~	753			832	~	~	
	- 6.9	- 10.6	- 10.2	~			- 5.8	- 13.5	- 75	
	Sb_2Se_3	Sb_2S_3	SbO_3				SnO_2	SnS	SnSe	
	910	819	929				2203	1153	1133	
Sb				~	-	-				Sn
	803	793	~				~	~	913	
	- 25.5	- 41	- 143				- 193.4	- 55.8	- 47.3	
	As_2Se_3	As_2S_3	As_2O_3	SnAs			PbO	PbS	PbSe	
		580	586	878			1158	1383	1361	
As	~				-	-				Pb
		553	~	852			~	~	600	
	- 20.5	- 33.5	- 130.7	~			- 109.6	- 49.2	- 49.2	
							O	S	Se	

The distribution coefficient (k) describes the different elemental concentrations in the crystallized Cu (c_s) and the corresponding melt (c_L) during solidification. It is defined as [51]:

$$k = \frac{c_S}{c_L}$$ Equation 4

c_S Concentration in solid phase

c_L Concentration in liquid phase

During solidification, elements with $k > 1$ are preferentially accumulated in the solid, those with $k < 1$ are enriched in the liquid phase, which is known as segregation [51, 74]. The schematic liquidus and solidus lines in systems with $k < 1$ and $k > 1$ are depicted in Figure 18. The solute distribution ahead of the solid-liquid interface results in various growth

morphologies, which in turn determine the solute distribution in the solid and result in concentration differences over microscopic distances, interdendritic precipitates, and porosity [74]. As solutes can be transported by diffusion or convection (or both), the segregation pattern depends on the process involved. Mass transport via convection covers larger distances compared to that via diffusion and can hence result in macrosegregations. Microsegregation depends on solute diffusion in the liquid and solid and is related to the dendrite shape and size. Microsegregation also reveals the original microstructure of a solidified alloy, due to the differences in etching tendency of regions of varying local composition [74].

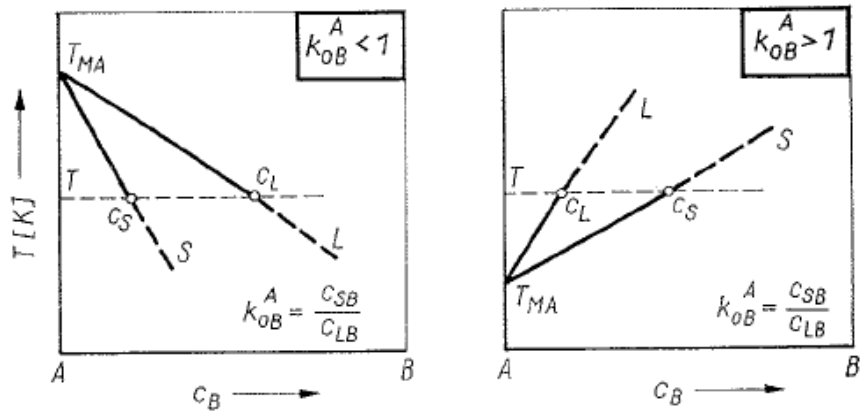

Figure 18: Liquidus (L) and solidus (S) lines in systems with $k < 1$ (left) and $k > 1$ (right) – schematic; T_{MA}: Melting temperature of element A, c_S: Concentration in solid phase, c_L: Concentration in liquid phase, k_{0B}^{A}: Equilibrium distribution coefficient of element B in element A [51]

The liquid and the solid phases are regarded as mixed phases. The distribution coefficient for a defined crystallization process is determined by:

- Thermodynamic properties of the main component and accompanying elements in the different phases (i.e., solid-liquid)
- Kinetics of the processes in the solid-liquid interface (e.g., phase boundary and crystallization front)
- Extent of mass transfer in the interface-near area by diffusion and convection
- Shape of solid-liquid interface

The equilibrium distribution coefficient, k_0, is only valid under equilibrium conditions, namely at a solidification rate $v \approx 0$. Under nonequilibrium conditions the elemental distribution is described by the kinetic distribution coefficient k_{kin} (including kinetics in the solid-liquid interface) and the effective distribution coefficient k_{eff} (including the influence of transport mechanisms in the interface-near area). Very high cooling rates result in distribution

coefficients approaching 1, namely a homogeneous distribution of the elements between the liquid and solid phases [51].

There are two extremes concerning the distribution coefficient [53]:

- Total equilibrium by diffusion in solid Cu: No single-phase decomposition, precipitation occurs at concentrations > maximum solubility
- No diffusion in solid Cu: Inhomogeneous distribution of accompanying elements (like directional solidification on macro-scale) and the formation of separate phases for elements with $k < 1$ in the final stage of crystallization

The practical conditions are somewhere between these extremes (Table 6). Elements with $k < 1$ (e.g., O, Sb, As, Sn, and Pb) have a tendency to form precipitates, even when their concentration is below the solubility limit. Especially Se, S, O, and Pb occur in an inhomogeneous distribution and separate phases. The elements Sn, Ag, Sb, and As concentrate in the last solidifying areas of the microstructure. Elements with $k < 1$ concentrate in the liquid phase and are found between the Cu grains, namely along the grain boundaries [53]. Elements with k > 1 are accumulated in the solid phase, namely the Cu grains, and form solid solutions with the Cu [51].

Table 6: Equilibrium distribution coefficients of impurities in Cu and examples of concentrations in anode copper; (1): Estimated value, (2): Calculated, (3): Literature data, (4): Experimentally determined, (5): In Cu matrix, (6): Not defined [53]

Element	Distribution coefficient		Concentration [ppm] average		maximum (5)		minimum (5)	
O	10^{-2}	(3)	10^{3}	(4)	10^{2}	(1)	10	(2)
S	10^{-2}	(3)	$8 \cdot 10^{1}$	(4)	10^{2}	(1)	$8 \cdot 10^{-1}$	(2)
Se	10^{-3}	(3)	$2 \cdot 10^{2}$	(4)	10^{2}	(1)	$2 \cdot 10^{-1}$	(2)
Ni	2	(3)	$4 \cdot 10^{3}$	(4)	$8 \cdot 10^{3}$	(2)	(6)	
Ag	0.5	(4)	$3 \cdot 10^{3}$	(4)	$8 \cdot 10^{4}$	(3)	$1.5 \cdot 10^{3}$	(2)
Sb	0.2	(4)	$9 \cdot 10^{2}$	(4)	10^{5}	(3)	$1.8 \cdot 10^{2}$	(2)
As	0.2	(3)	$5 \cdot 10^{2}$	(4)	$7.5 \cdot 10^{4}$	(3)	10^{2}	(2)
Pb	10^{-2}	(3)	$2 \cdot 10^{2}$	(4)	10^{2}	(1)	2	(2)
Sn	0.2	(3)	10^{2}	(4)	$1.6 \cdot 10^{5}$	(3)	$2 \cdot 10^{1}$	(2)

The accompanying elements in Cu can be divided into three groups [51]:

1. Elements that increase the liquidus temperature of Cu ($k_{0B}^{Cu} > 1$): Ni, Pd, and Pt have unlimited solubility, whilst Co, Nb, and Rh have limited solubility in Cu. Hence, the latter elements form peritectic systems with Cu.
2. Elements that lower the liquidus temperature of Cu ($k_{0B}^{Cu} < 1$): Mn and Au have unlimited solubility, whilst Li, B, Mg, Al, P, Ti, Cr, As, Y, Ag, Sb, Ce, Ho, and Th have

limited solubility in eutectic systems. The systems with Be, Si, Zn, Ga, Ge, Cd, In, and Sn form peritectics.

3. Elements with a very low solubility in Cu ($k_{0B}^{Cu} << 1$): O, S, Ca, Se, Sr, Re, Ba, La, Pr, Yb, Tl, Pb, U, Bi, and Pu

The anode microstructure is not in an equilibrium state. This leads to the formation of regions (i.e., components of the microstructure, but within one phase) with different electrochemical properties, which result in locally different dissolution behaviours [18, 53]. The nonequilibrium state is described by constitutional undercooling and oversaturation of the melt, which are the driving forces for phase transformations and determine the value of k_{kin} [51]. Phase transformations consist of two processes, which can both be rate-determining: The processes at the phase boundary (i.e., actual transformation) and the transfer processes in the different phases. The crystallization rate during metal solidification is generally determined by heat transfer. Mass transfer is important regarding the accumulation of elements, which are not built into the solid phase ($k_0 < 1$), in front of the phase boundary as well as a lack of elements which preferentially go into the solid phase ($k_0 > 1$) [51]. The deviation of k_{kin} from k_0 and its dependence on undercooling and oversaturation is determined to a great extent by atomic processes during solidification. If many nuclei for crystal growth are present in the melt and the undercooling is small, the value of k_{kin} is almost equal to k_0. This is not the case if the undercooling is large. If the cooling rate is high enough or the temperature gradient is decreased, dendritic growth occurs due to constitutional undercooling [51].

2.3.1.12 Influence of the Casting Process on Chemical Anode Quality

The anode chemical quality requirements can be summarized as follows:

- For optimum electrorefining operations, the anodes should have a homogeneous chemical composition, so that the electrolysis can be adjusted properly for effective operation. Gas purging in the anode furnace is recommended for a uniform chemical composition within one charge.
- The elemental distribution within one anode is important for homogeneous dissolution.
- The accompanying elements in the anode should form soluble compounds with the copper or solid solutions, as insoluble compounds lead to high levels of Cu in the anode slimes or the formation of passivating layers on the anode surface.

The elemental distribution (and the grain size) can be adjusted by altering the solidification conditions, for example changing the cooling rate, thermal conductivity (i.e., material) of the

anode moulds, and preheating the moulds. During rapid cooling, the effective distribution coefficient for all elements approaches 1 ($k_{eff} \rightarrow 1$) as no equilibrium is reached. When in equilibrium, the elemental distribution is described by the equilibrium distribution coefficient k_0: Depending on its value, the elements are either enriched in the liquid ($k_0 < 1$) or in the solid ($k_0 > 1$) phase. Hence, with rapid cooling no elemental distribution takes place as the elements are not enriched in one of the phases. Faster cooling leads to finer grains and supersaturated solid solutions.

The level of non-metallic inclusions may be reduced by minimizing slag carry-over from the anode furnace, metal-refractory interactions, as well as oxygen uptake during liquid metal pouring, for example using burners that provide a reducing atmosphere. The optimization of mould wash (i.e., composition and amount) is also important as adhering mould wash can cause the formation of buds and dendrites. Preheating the anode moulds may be a suitable means to reduce the number of rejects.

The following effects are related to the accompanying elements in the anode copper, and hence the chemical anode quality:

- Enhanced passivation: Ag, Se, Ni + O, Se, O, low As levels, presence of Pb without sufficient O for oxide formation
- Dendrite formation: Low As content
- Decreased cathode quality: Sb, Bi, (Ag, Se), low As content
- Poor electrical conductivity of electrolyte: Ni
- Altered anode slime properties: Ni; As, Se, (Sn), O, and oxides

These effects can be minimized either by low impurity levels and suitable relative amounts of the elements in the anode copper, which is mainly the task of fire refining, or by the appropriate chemical form of the elements and the elemental distribution, which can be influenced by the casting process and the cooling conditions.

2.3.2 Physical Anode Quality

To achieve uniform anodic dissolution during electrorefining, the anode has to have certain physical properties. To satisfy the requirements of the electrolysis the anodes must provide uniform dissolution, close anode spacing, reduced tankhouse cell loading time, minimum anode scrap, optimum current efficiency, and high quality cathode production. Hence, the anodes require smooth surfaces, a uniform weight and thickness, minimal edge effects, as well as minimal distortion of the body and the lugs [17, 22, 35]. The aims of anode casting—high output and long mould lifetimes—are not consistent with good physical anode quality [11]. The

physical anode quality—anode surface, geometry, and weight, as well as structure—is very important for electrorefining operations. In contrast to chemical quality, which is determined by fire-refining operations, the physical characteristics can be influenced by the anode casting process. Smooth anode surfaces as well as uniform anode weight and thickness are dependent on proper control of the casting process and the weighing system. Independent of the technology used, proper control of the casting process is vital to produce high quality anodes of uniform weight that are free from casting defects.

Anodes cast on a casting wheel are reported to have certain disadvantages, especially regarding geometrical accuracy and surface quality [17-20], which can lead to irregular electrode spacing, and hence result in further defects including shorts, decreased current efficiency, and uneven electrodeposition. These effects due to not perfectly vertical anodes are much more pronounced than those resulting from other anode properties, for example microstructure [28]. The effects of uneven anode surfaces, which lead to variations in current density, are described in the work of Filzwieser [28].

2.3.2.1 Physical Quality Control

Some physical anode quality features, which can be controlled, are [12]:

- Anode weight
- Anode verticality
- Anode lug requirements (i.e., thickness, cracking and fissures)
- Anode body thickness control
- Lug indent distance
- Anode body and lug fissure control
- Anode "picture framing" and "road map" control
- Anode mould wash (i.e., preparation, application, excess mould wash, and anode slime)
- Bridge contact distance
- "End-to-end" lug distance

Also improvements regarding the casting control system, anode lifting system, uniform mould wash, and better mould cooling are reported to increase the physical anode quality [31].

2.3.2.2 Anode Weight

The anode weight should be as uniform as possible and only show small deviations from the preset value. However, sufficiently stable anode scrap is required for automation and this is calculated on the basis of lighter anodes [11]. The larger the anode weight deviation, the higher the anode scrap level that cannot be used and has to be remelted [11]. Weight

constancy also has an effect on the uniformity of current distribution. Heavier anodes are thicker than lighter ones, resulting in narrower electrode spacing and hence higher current densities at the beginning of the cathodic crop [11].

A maximum anode weight is desirable for a minimal amount of anode scrap and minimal handling requirements. This can normally only be achieved through a variation of the anode thickness within certain limits, which depend on the maximum crane loads, current density, slime levels, and flow conditions in the cell. Narrow anode spacing is also linked to a smaller voltage drop in the electrolyte and therefore lower energy consumption. However, reduced electrode spacing is not possible when high levels of anode slime are produced, because of the danger of slime particle entrapment in the cathodes [11].

2.3.2.3 Anode Geometry

The anode geometry has to suit the cathode dimensions. The cathodes should overlap the anodes by approximately 20–35 mm, in order to produce even cathodic deposits. This overlap is dependent on current density, anode thickness, electrode spacing, and flow conditions in the cell. When the overlap is too small it can cause the formation of bulges at the cathode edges, which deteriorates the cathode quality (especially at the lower end). The higher pressure on the sides can lead to the destruction of the permanent cathode side strips. A too big overlap leads to thin cathode borders and the cathodes become porous in these regions. This causes incomplete stripping, as well as the danger of anode slime entrapment and hence poorer cathode quality [11].

A constant anode thickness over the entire anode (i.e., the region submerged in the electrolyte) is also very important. An irregular thickness leads to shifts in current density, which cause problems with cathodic deposition. If the lower end of the anode is thicker than the upper region (i.e., pear-shaped) the anode may tear off at the electrolyte level at the end of the anodic crop. This results in cell damage, higher anode scrap levels, a negative influence on current density distribution in the cell, shorts, and additional effort when emptying the cell [11].

To ensure stable hanging of the anodes in the cell, the anode length has to be selected in accordance with the lug position, so that the upper part of the anode is above electrolyte level. In addition, the upper part and the lugs must not be too large, as this amount of material is not used during electrorefining. Therefore, a compromise between sufficient stability and minimum anode scrap has to be found [11].

2.3.2.4 Anode Surface

For optimum electrorefining the anode surface should be smooth and free of non-copper inclusions or adhesions. The most common casting defects (air side) and their causes are detailed in Table 7 [11].

Table 7: Casting defects and their causes [11]

Casting defect	Cause
Road maps, picture framing, and edge fins	Jerky casting wheel movement Improper mould wash application Improper mould temperature Non-uniform mould casting
Bumps	Improper mould temperature Damp mould wash Sulphur in copper Unfavourable cooling conditions
Water blisters	Too early start of direct anode cooling

Uneven surfaces on the mould side are mainly caused by mould wear. These defects are multiple and can appear for example as bulges, fins, pikes, and grooves. Adhering mould wash on the anode surface can decrease the electrical conductivity and lead to non-active surface areas, which cause shifts in the current density. Refractory inclusions, originating from trough or launder, cause the same problems [11].

During pouring of the liquid copper into the moulds, the molten metal must not be splashed towards the outside of the cavity, spilt, nor moved, to avoid the melt rising up to the cavity edges and solidifying as edge fins. Hence, on the one hand the surface must remain undisturbed, and on the other hand minimum pouring times are desired [14]. The anode surface quality may also be improved to a certain extent by optimizing the casting trough design, as its shape influences the direction and quantity of the kinetic energy in the molten metal [14].

2.3.2.5 Anode Solidification and Structure

The anode structure is linked to the elemental distribution and determines the anode dissolution behaviour. Horizontal anode casting causes different surface structures (air and mould side), which affect electrode polarization [18]. The solidification areas detected in the anodes correspond to the general solidification structure in castings (Figure 19). Solidification involves the formation of curved solid-liquid interfaces (leading to capillarity effects) and microscopic heat flow, as well as solute in the case of alloys [74]. The deviations from equilibrium conditions (e.g., undercooling and oversaturation) are the driving force for phase transformation, which comprises two processes, actual transformation and transport

mechanisms, which can both be rate-determining. The crystallization rate is mainly determined by heat conduction [51].

During metal and alloy solidification, crystallization is mainly determined by the nuclei and these in turn by the degree of undercooling. Higher undercooling causes an increase in the number of nuclei and hence also a higher crystallization rate. The direction of the temperature drop influences the crystal growth, where the crystal axes align with the direction of heat flux. Higher cooling rates result in finer grains, whilst lower cooling rates generate coarse and mostly columnar crystals. Porosity is also linked with the solidification structure [75].

At the beginning of solidification, solid nuclei are formed close to the mould. For a short time, they grow and form the outer equiaxed zone. Then, those crystals in the outer equiaxed zone, which can grow in an opposite direction to the heat flux (e.g., in cubic metals: Columnar grains having one axis close to the heat flux) advance more rapidly and overgrow other crystals, which have a less favourable orientation. This leads to the formation of the columnar zone. The inner equiaxed zone results from detached dendrite branches, which tend to take up an equiaxed shape because their latent heat of solidification is derived radially through the undercooled melt. The transition of columnar to equiaxed growth occurs when the melt has lost its superheat, becoming slightly undercooled, and detached dendrite branches form a barrier ahead of the columnar zone, and is highly dependent on the degree of convection in the liquid and hence the casting process [74]. Equiaxed growth continues until the dendrites, which grow freely in the melt, impinge on one another [74]. In a pure metal, these dendrites are not visible after solidification, but only the points of their impingements (i.e., grain boundaries). In alloys the dendritic structure remains visible after etching due to local composition differences (e.g., microsegregations) [74]. Nuclei growth is limited by [74]:

- Kinetics of atom attachment to the interface
- Capillarity
- Heat and mass diffusion

The relative importance of these factors is determined by the material and solidification conditions [74].

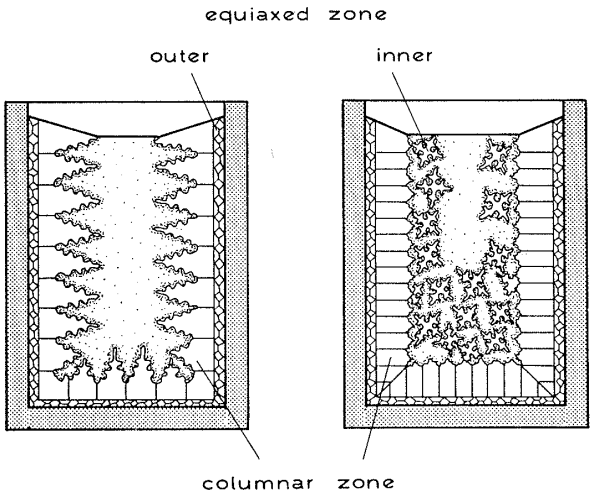

Figure 19: Solidification structures in castings [74]

The morphology depends upon [74]:

- Alloy composition
- Temperature gradient (*G*)
- Growth rate (*V*)

The cooling rate $\dot{T}$ is given by [74]:

$$\dot{T} = -GV \qquad \text{Equation 5}$$

$\dot{T}$ Cooling rate [K/s]

G Temperature gradient [K/m]

V Growth rate [m/s]

When the heat flow is in the opposite direction to the crystal growth, namely directional or columnar solidification, the rate of the isotherm advance constrains the dendrites to grow at a given velocity (i.e., constrained growth). The grain boundaries are parallel to the primary dendrite axes (i.e., trunks) and are continuous along the length of the solid. Most of the dendrites are arranged parallel to each other, and a characteristic trunk spacing, λ_1, can be defined. Many trunks together make up one grain (Figure 20) [74].

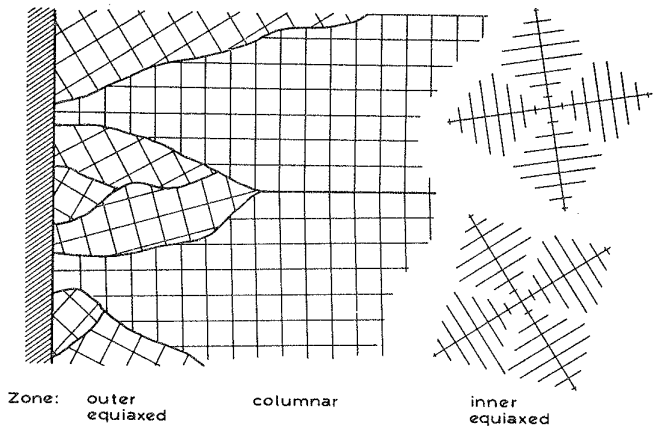

Figure 20: Formation of columnar and equiaxed dendritic microstructures [74]

During equiaxed solidification, where the heat flows from the crystal into the melt, the dendrites can grow freely and as rapidly as the imposed undercooling permits. They grow until they impinge on one another and the grain boundaries form a continuous network throughout the solid. Each dendrite forms a grain and the primary (i.e., dendrite trunk) spacing, λ_1, usually equals the grain diameter [74]. For both columnar and equiaxed dendrites, a secondary (i.e., dendrite arm) spacing, λ_2, can be defined [74] (Figure 21). The value of λ_1 in the solidified microstructure is the same as that during growth, but λ_2 undergoes a ripening process and increases enormously due to the long contact time between the highly-curved, branched structure and the melt. λ_2 is proportional to the cube root of time and hence gives an indication of the local solidification conditions [74]:

$$\lambda_2 = Bt_f^{\,n} \qquad \text{Equation 6}$$

λ_2 Secondary dendrite arm spacing [µm]

B,n Constants

t_f Local freezing time [s]

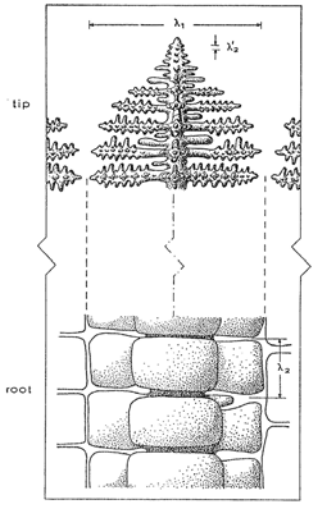

Figure 21: Growing dendrite tip und dendrite root in a columnar structure [74]

The effect of the cooling rate on the size and shape of crystals in a solid solution alloy is depicted in Figure 22, where the arrow indicates an increased cooling rate. Higher solute levels also result in finer grains [76].

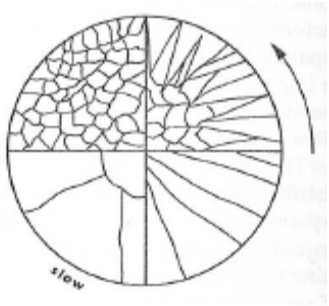

Figure 22: Schematic diagram of the cooling rate effect on crystal size and shape in a solid solution alloy [76]

The various microstructures, which are produced when the imposed temperature gradient *G* or growth rate *V* are varied, are illustrated in Figure 23. The cooling rate ($G \cdot V$) controls the size of the microstructures formed and moving from the lower left to the upper right in Figure 23 leads to a refinement of the structure, for example λ_2, for a given morphology. In addition, the ratio *G/V* determines the morphology and moving from the lower right to the upper left of Figure 23 leads to changes in morphology (i.e., planar to cellular to dendritic). Hence, fine or coarse dendrites can be produced when *G* and *V* can be altered independently, for example in directional solidification (“D.S.” in Figure 23). However, in conventional casting *G* and *V* are interrelated via the heat flux and the thermal properties of the metal, so that only the conditions close to the arrow in Figure 23 can be exploited [74].

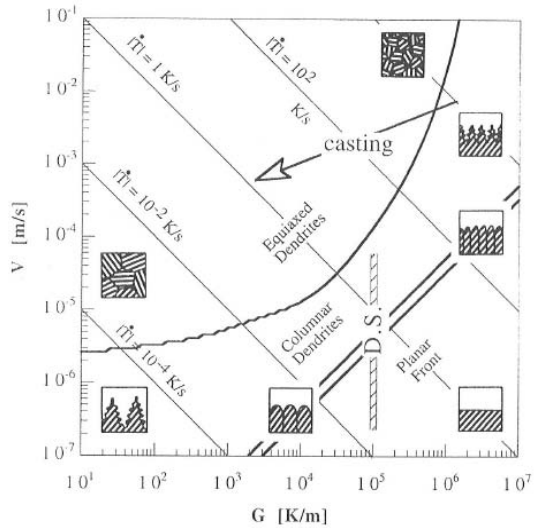

Figure 23: Schematic summary of single-phase solidification morphologies

The main cast structure characteristics (Figure 24) are [77]:

- Columnar zone extension (x_{st})
- Average crystal diameter in the inner zone (d)
- Average columnar crystal diameter (d_{st})
- Secondary dendrite arm spacing (d_M) (not visible in Figure 24)

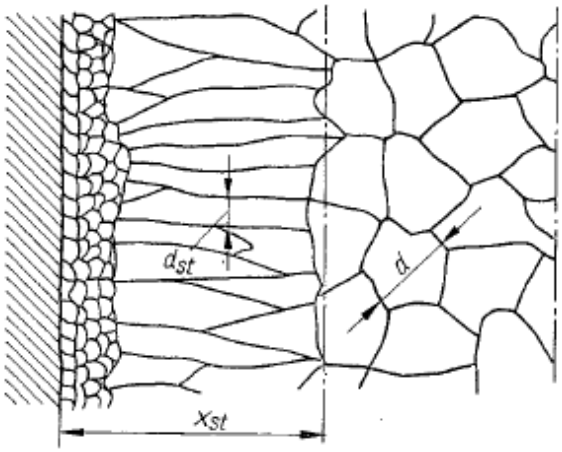

Figure 24: Casting zones [77]

The interrelations between these factors (e.g., x_{st} and d) were investigated for some metals and alloys, for example steel, aluminium, and different aluminium alloys. The correlations between x_{st} and d, d_{st} and d, as well as d_M and d can be used qualitatively for other metals and alloys [77]. The columnar zone can be minimized by a reduced melt overheating, namely a low casting temperature [77]. The creation of a crystal from the melt always leads to a local composition change. The difference in composition at the growing interface can be described by the distribution coefficient (Section 2.3.1.11).

The microstructure of casting wheel anodes shows significant variations across the anode thickness. Due to the different cooling conditions, the following zones are found (Figure 25) [18, 42, 78]:

- Mould side: Thin zone with fine grains (approximately 1 to 2 mm; blue lines in Figure 25)
- Towards centre: Columnar crystals, up to 5 mm long (area 3)
- Centre: Last solidified part with high amount of nucleation seeds—fine globulitic structure (area 2)
- Air side: Solidified in contact with the atmosphere (air), usually cooled with a spray of hot water—equiaxed and coarse grained (area 1)

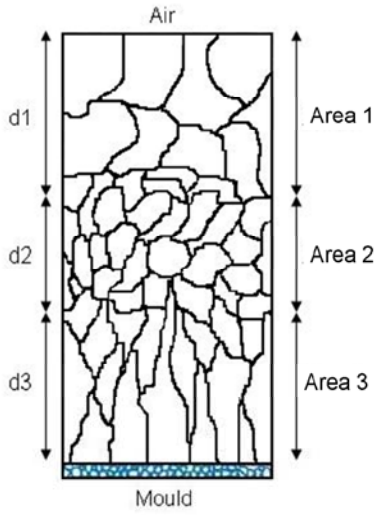

Figure 25: Schematic diagram of the zones and structures in a casting wheel anode across the thickness [18, 42, 78]

The macrostructure of all casting wheel anodes is similar because of the similar casting methods. They differ only in size, thickness, and composition [78]. Commercial anodes of smaller dimensions have a smaller grain size in areas 1 and 3. This may be due to a shorter solidification time, which does not allow larger grain growth. There is no dimension-related tendency in area 2. This area results from constitutional undercooling of the melt. As the level of impurities is similar, so is the grain size [78].

The structure of the anode, which is linked to the elemental distribution and dependent on both thermodynamic and kinetic parameters, has an influence on the dissolution behaviour [18]. The solidification type is of special importance in secondary metallurgy as—due to varying scrap compositions—the impurity levels are much higher and hence have a greater influence on the electrochemical behaviour of the anodes. During solidification some elements are enriched in the solid phase (e.g., Ni), and others in the melt (e.g., As, Sb, and

Bi). This leads to either solid solutions or separate phases of various compositions in the solidified anode. The mostly inhomogeneous distribution leads to different dissolution rates when in contact with the electrolyte [18].

The dissolution rates and the energy requirement for dissolution, as well as the tendency for passivation are different for the described areas [78]. As—due to the lower (crystallization) overvoltage—electrochemical dissolution occurs preferentially at the Cu grain boundaries, the grain size distribution has an influence on anodic dissolution: Anodes with finer grains dissolve more rapidly at a given current density because of their higher grain boundary content [18]. Areas having a larger grain size require higher potentials for the onset of passivation. The dissolution starts at the grain boundaries and is always more intense around impurities or inclusions. Hence, larger grain sizes reduce the susceptibility to passivation, as they present fewer surfaces where impurities are located. Therefore, the impurity contribution to the formation of a passive layer on the anode surface is smaller. However, anodes with finer grains are more susceptible to passivation, so that—regarding passivation—a uniform, relatively coarse, equiaxed structure is desirable [78]. Industrial practice has shown that finer grains demonstrate an improved (electrochemical) dissolution behaviour.

For plating processes anodes with a fine, uniform grain structure are desirable; however, anodes for plating are much purer than those for electrorefining [79]. As anodes with globulitic structures are less susceptible to passivation, the dissolution behaviour of anodes can be improved by magnetic stirring, which minimizes the dendritic zone and results in a smoother transition zone between the dendritic and inner globulitic zone [18, 80]. Gumowska [68] did not detect any influence of grain size on the passivation behaviour, whereas Ahan et al. [81] found that anodes with a larger dendrite arm spacing (DAS) exhibited superior passivation properties such as a longer time to passivation and a higher critical current density.

Due to their different dissolution behaviours, the anodic structures (as well as anode-cathode spacing) would require different cathodic crops. An optimum schedule when using constant current density would be as follows: In the first shorter period, the anodes are thick and the structural differences between air and mould side are significant (dissolution of areas 1 and 3). As the irregular outer areas of the anode are dissolved, anodic dissolution improves (dissolution of area 2), which results in a longer second period. This is followed by another shorter third period, which deals with irregular shaped, possibly porous and perforated anodes, and causes irregular current densities, and therefore irregular dissolution (which leads to Cu losses to the anode slime) and deposition. The cathodes produced from the

anode air side have a rougher surface (e.g., dendrites and buds). This effect is more pronounced in the first cathodic crop, as the outer, more irregular regions of the anode are dissolved [82].

2.3.2.6 Influence of the Casting Process on Physical Anode Quality

The anode requirements regarding physical quality can be summarized as follows:

- Independent of the technology used, proper control of the casting process is vital to produce high quality anodes with a uniform weight that are free from casting defects.
- As dissolution occurs preferentially at grain boundaries, anodes with a fine globulitic/equiaxed structure, and hence a lower (crystallization) overvoltage, have a higher electrochemical dissolution rate at a given current density than those with coarse grains.
- Coarser globulitic/equiaxed grains are less susceptible to passivation.
- The grain size and the elemental distribution can be adjusted by altering the solidification conditions, for example a change of cooling rate, anode mould thermal conductivity (i.e., material), and mould preheating. Faster cooling results in finer grains and supersaturated solid solutions. The grain boundary structure is also linked to the elemental distribution, as the value of the distribution coefficient is determined by the cooling rate.

The optimization of mould wash (e.g., composition and amount) is important as adhering mould wash can cause the formation of buds and dendrites. Preheating anode moulds may be a suitable means to reduce the number of rejects. It is established that the cooling rate determines the structure: High cooling rates lead to fine grains, whereas slow cooling results in a coarse microstructure. Therefore, as a fine structure is reported to result in a better dissolution behaviour [18, 79, 83], rapid cooling would appear preferable.
This requires:

- High thermal conductivity of the mould material
- High amounts of cooling water
- Minimum liquid copper casting temperature

Problems that have to be considered are the thermal shock resistance of the mould material, the cooling water supply, and temperature-dependent properties of liquid copper, as well as the fact that fine grained anodes are reported to have a higher tendency for passivation.

2.3.3 Differences in Quality Between the Air Side and Mould Side

In casting wheel anodes, one side solidifies in contact with the mould (mould side), whereas the other side has air contact (air side). The following characteristics of the air side (compared to the mould side) are reported [42]:

- Higher impurity content (e.g., Ni, Sn, and O)
- Higher oxidic surface portion
- Continuous NiO layer in high Ni anodes and circular NiO arrangements in low Ni anodes
- Higher Cu_2O content (i.e., Cu_2O network)
- Lower electrical conductivity
- Denser slimes
- Poor dissolution and higher tendency for passivation

Adhering barite on the mould side can cause varying barite levels in the anode slimes. However, the results of previous investigations, which also compared anodes from different copper smelters, regarding the impurity content were not consistent [82, 84].

Spray cooling is used in anode casting to cool the anode surface on both the air side as well as the mould bottom. As described, both the chemical and physical anode quality can be influenced by the cooling conditions; therefore spray cooling is described in the following section.

2.4 Spray Cooling

Spray impingement has the capability to remove large amounts of energy at low temperatures through the latent heat of evaporation. Heat transfer rates much higher than those when using pool boiling are possible with sprays since the vapour removal from the surface is more efficient [85]. The heat transferred due to the impact of a spray onto a surface depends on the liquid thermo-physical properties and on the surface temperature, as well as on the size, velocity, and mass flux of the impinging droplets [85]. When a drop of liquid impacts onto a hot solid surface it may splash, rebound, or remain on the surface. Heat is transferred from the solid to the liquid phase, so that the mean temperature of the droplet increases. Then it boils and evaporates [86, 87].

The surface temperature has a significant influence on the spray cooling efficiency, as a stable vapour layer is formed if the surface temperature is sufficiently high (Figure 26), which protects the surface from direct contact with the coolant and hence causes a low cooling intensity (Leidenfrost effect). The stability of this vapour layer is coupled with the surface

temperature. When the temperature decreases and the vapour layer collapses, the cooling increases immediately and can be 10-fold higher than in the high temperature region [86-90].

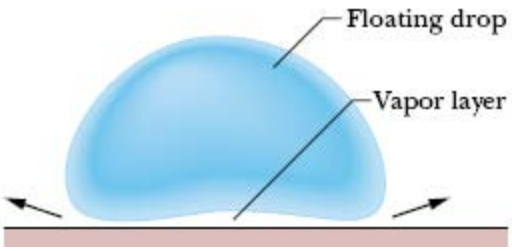

Figure 26: Leidenfrost drop in cross section [89]

Due to the poor heat transfer of the vapour film, the evaporation rate is low and the heat transfer reaches a local minimum and the evaporation lifetime of the droplet a maximum. The Leidenfrost point is the surface temperature at which the total evaporation time of a droplet on the surface is the longest [86, 87]. Based on the evaporation lifetime of a droplet and heat transfer coefficient (HTC), four different evaporation regimes are defined (Figure 27):

- Film evaporation
- Nucleate boiling
- Transition boiling
- Film boiling

The critical heat flux (CHF) and the Leidenfrost phenomenon (LFP) associated with the local maximum and local minimum in the boiling curves (Figure 27) are usually used to describe the different heat transfer regimes [85, 87]. In the so-called steady film boiling regime the HTC is a function of the water mass flux density. Below a specific temperature T_L, the HTC shows a significant dependence on temperature. Generally, the HTC is a complex function of the surface temperature, the water mass flow density, and the surface condition [91]. The HTC, α, is defined through the following relation, which is most applicable for situations with a constant HTC (i.e., independent of T_S) [91]:

$$q = \alpha \cdot (T_S - T_W) \qquad \text{Equation 7}$$

q Heat flow density to the surface [W/m²]

T_W Water temperature [K]

T_S (Local) Surface temperature [K]

α HTC [W/m²K]

Water spray cooling of a surface, which has a temperature of 1,000 °C, starts in the range of stable film boiling (Figure 27). An increase of water mass flux density V_S leads to faster

cooling. More rapid cooling (i.e., unstable film boiling) begins at a temperature of approximately 400 to 500 °C (depending on V_S), when the Leidenfrost temperature has been reached. The HTC in the range of stable film boiling (i.e., above ΔT = 600 K) is assumed to be independent of the surface temperature, but a decrease in HTC even in the stable film boiling regime is reported for high spray water densities. Stable adhesive scale surface layers need to grow thicker than 250 µm in order to influence the local HTC. In the lower ΔT (i.e., unstable film boiling) regime, scale layers can significantly influence the apparent HTC [91].

In a poly-dispersed spray, the most important parameter determining these regimes is the surface temperature, but also other parameters including successive impacts of droplets on top of others, collision of droplet films during spreading, and lamella interaction affecting the crown development in neighbouring splashing droplets may be important for the effect of the impingement and the wall heat transfer. For multiple-intermittent sprays, the heat transfer regimes depend on the injection conditions, such as pressure, duration, and frequency [85].

The Leidenfrost effect and temperature, are dependent on factors including the liquid properties (e.g., impurity levels), droplet properties (e.g., size), and surface properties (e.g., roughness and temperature) [85-88, 92, 93]. Hence, values ranging from 225 °C [87] to 1,200 [88] °C or 1,300 °C [88] are found in the literature. The water used for industrial spray cooling usually contains dissolved gases or ionic solids from the piping system or the processing environment. It has been found that even slight variations in water quality affect the heat treatment result, namely spray cooling. Dissolved salts increase the Leidenfrost temperature (i.e., a higher surface temperature is necessary to initiate the Leidenfrost transition) [89, 92], whereas a higher amount of dissolved gases decreases the Leidenfrost temperature [92]. Additionally, salt deposition gradually decreases the surface roughness and raises the Leidenfrost temperature [92].

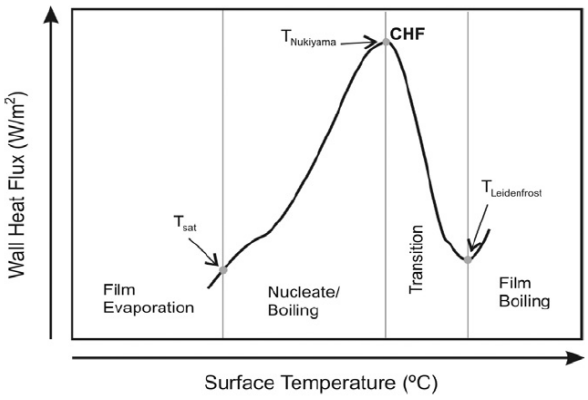

Figure 27: Typical boiling curve and heat transfer regimes [85]

Oxide layers influence the HTC during water spray cooling, namely they form a resistance to heat transfer. Lower and particularly non-uniform cooling can lead to structure inhomogeneities, tensions, and finally cracks [91]. An even surface coverage by the spray nozzles is important. Therefore, the spraying distance has to be taken into account, as the HTC is a function of this parameter. Hence, a minimum distance is desirable, which is not always possible due to practical limitations [94]. With regard to a uniform coolant distribution, it has to be considered that the circular pattern of full cone nozzles creates overlapping zones [94]. A higher impact density for a given flow rate and pressure is possible (i.e., with flat-spray nozzles) when narrow spray angles instead of wide angles are used, so that the dwell time of the coolant is diminished, which determines the resulting heat transfer [94].

Higher water pressure increases the HTC, but does not enhance cooling. Increasing the water pressure is only effective up to 7 to 10 bar (Figure 28), as above 10 bar there is only a minimal gain in the heat transfer, but significantly higher costs are incurred for the equipment [94].

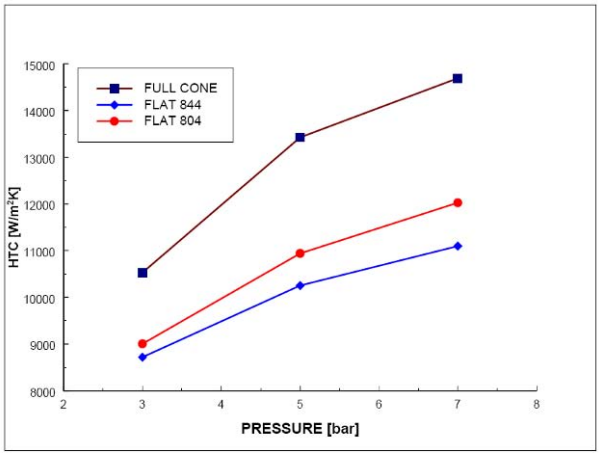

Figure 28: Average HTC for full cone and flat jet nozzles (surface temperature 340 °C, 18.03 l/min water, 5 bar) [95]

A new generation of nozzles enables control of the cooling intensity by setting a combination of water and air pressures. These mist nozzles (i.e., two-phase) use water and compressed air to produce fine droplets. The main cooling effect is caused by evaporation. The major advantage of these nozzles is their wide range of controllability, as the cooling intensity can be varied by setting the air and water pressures. Most systems with water-only nozzles or constant air pressure do not ensure constant cooling [88]. Although the spray cooling intensity [$lm^{-2}s^{-1}$] is often used to estimate the cooling intensity, heat transfer tests have showed no explicit link between the coolant flow and cooling intensity. The same nozzle can produce different cooling intensities for the same water flow, as the heat transfer is not only determined by the water flow, but is also influenced by droplet size and velocity. These can

be varied by changing the air flow [88]. The Leidenfrost temperature increases with an increase in water pressure. The sensitivity to pressure differs with the nozzle diameter. For a 7 mm-nozzle the Leidenfrost temperature varies from 600 to 1,200 °C with varying water pressure. However, there is no known numerical or analytical method for determining the Leidenfrost temperature theoretically from the spray parameters [88].

The Leidenfrost effect, namely the vapour barrier between the hot surface and the coolant, results in a very low heat transfer. Adding additional water only results in more steam; hence, air and radiation would be more efficient at removing heat [94].

The distribution of the HTC for a nozzle is depicted in Figure 29. It can be seen that for stationary casting conditions, namely a stationary surface, the peak is narrow and symmetrical. Surface movement, like in continuous casting, leads to a more asymmetrical distribution due to water flow on the surface and different vapour forming conditions in front and behind the impinging jet [88]. It is evident, that cooling is non-uniform along the spray width [88]. Spray heights and nozzle spacing must be determined correctly in the overlapping spray areas. However, ensuring uniform water distribution along the surface does not guarantee cooling uniformity [88]. Droplet size and velocity, impact angle, and water impingement density are all significant, and the situation is complicated by different boiling regimes below and above the Leidenfrost temperature [88].

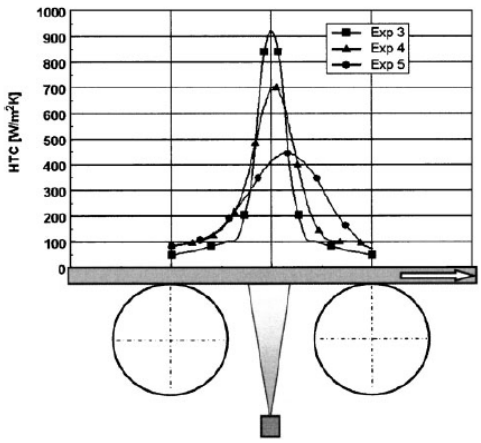

Figure 29: Influence of casting velocity on heat transfer (Exp. 3: Stationary, Exp. 4: 2 m/min, Exp. 5: 5 m/min) [88]

One possibility to avoid the Leidenfrost effect and hence achieve homogeneous cooling on the air side is the use of atomized spray cooling [96] or intermittent spraying [85]. The use of atomized spray cooling, where water is atomized to a fine spray by compressed air and the formation of the vapour layer is avoided, also results in a significant lower water consumption (i.e., approximately one-quarter of the amount for traditional spray cooling) [96]. The vapour

layer, which causes the Leidenfrost effect, collapses when the surface reaches a temperature < T_{Leid}. When the surface is then wetted again, a much higher (10-fold [88]) HTC occurs. The non-uniform film breakdown—firstly at the edges and lastly in the middle—causes inhomogeneous surface cooling conditions. Surface roughness and edges, for example, also cause the vapour layer to collapse; hence an inhomogeneous cooling occurs over the surface. For atomized water spray cooling, the water is atomized to a fine spray using compressed air. Only single droplets touch the surface. During deformation of the droplets heat transfer by conduction and partial evaporation takes place. Then the droplets rebound and are removed by the air. Hence, no closed vapour film forms. The HTC of water spray cooling is dependent on impingement density and HTCs as high as 10,000 W/m²K can be achieved, namely significantly higher values than with traditional spray cooling. Other advantages of atomized spray cooling are the possibility of locally defined heat transfer profiles and the lower cooling water consumption: For a HTC of 1,000 W/m²K with traditional spray cooling 8 kg/m²s are necessary, in contrast to only 1.8 kg/m²s with atomized spray cooling, namely one-quarter the amount compared with traditional spray cooling [96].

Different coolants are used in cooling and quenching. A key difference between quenching in a liquid and quenching in a gas lies in the different mechanisms involved in their heat transfer characteristics [97].

Most liquids (Figure 30, left) such as water or oil have distinct boiling points, and thus different heat transfer mechanisms (and rates) at various temperature stages. For example oil has three distinct heat transfer phases: (1) Vapour blanket or film boiling, (2) nucleate or bubble boiling, and (3) convection, (Figure 27) [97]. For gaseous media (Figure 30, right) heat transfer only takes place by convection [97].

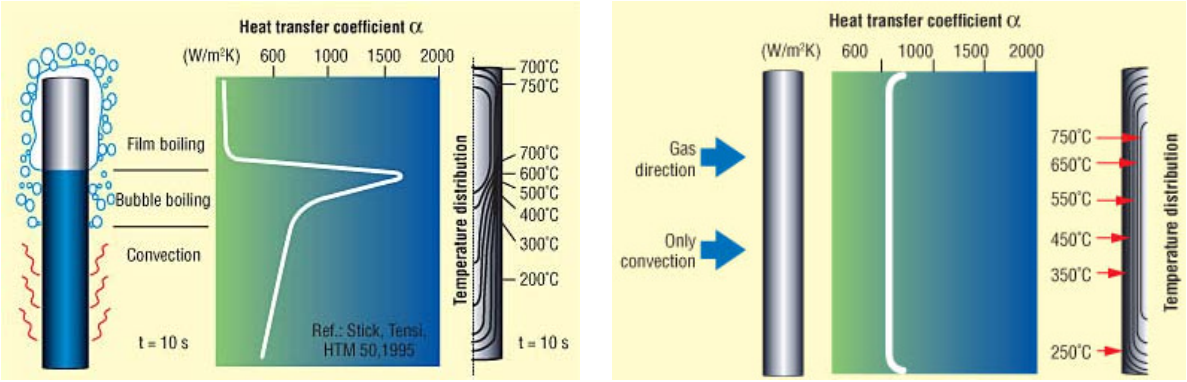

Figure 30: Heat transfer in liquid quenching (left) and gas quenching (right) [97]

Liquid quenchants such as water, polymers, or oil have the characteristic that during their nucleate boiling phase, extremely high HTCs can be achieved, which are not possible with gas quenching (Figure 31). However, with the breakdown of the vapour phase at the onset of

boiling, the so-called Leidenfrost phenomenon occurs. This results in a non-uniform heat transfer rate, and hence temperature differentials. Gas quenching avoids the Leidenfrost phenomena and therefore has the inherent capability to produce smaller temperature differences during quenching, and thus lower dimensional variations [97].

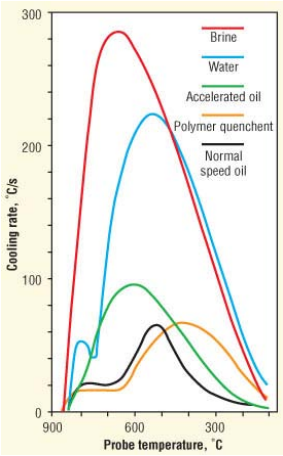

Figure 31: Heat transfer coefficient in liquid quenchants [97]

Although the maximum quenching ability may be described by the instantaneous value of the HTC, the average HTC (Table 8) provides a better relative comparison of the various quenching media since it represents the value of the HTC over the entire cooling range (i.e., from the start to the end of quenching) [97]. The magnitude of the HTC is influenced by many parameters, such as geometry, flow rate, flow condition, and fluid type. The flow conditions can be categorized as [98]:

- Laminar or turbulent
- Entry length, fully developed, or both
- Internal or external flow
- Natural convection, forced convection, jet impingement, boiling, or spray

Figure 32 details HTCs for different liquids and heat transfer modes.

Table 8: Average HTC values [W/m²K] [97]

Quench media	Average value	Instantaneous value
Brine or caustic	3,500–4,500	> 15,000
Water	3,000–3,900	> 12,000
Oil, highly agitated	2,000–2,500	4,000–6,000
Polymer	1,500–2,000	3,000–4,500
Oil, agitated	1,500–1,750	3,000–4,500
Oil, still	1,000–1,500	
Gas, high pressure	300–1,000	1,000–2,000
Salt	400 – 500	
Air	100 – 300	

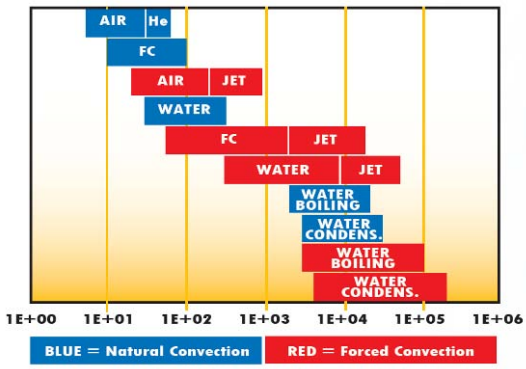

Figure 32: HTCs [W/m²K] for some common liquids and different modes [98]

The previous chapters addressed anode production and quality. In the following sections, anode dissolution during electrorefining is described.

2.5 Anodic Dissolution during Electrorefining

The anodic process consists of anodic dissolution, anion discharging, or the simultaneous progression of these two reactions. During electrorefining, namely anodic dissolution, cations are formed. The anode is not dissolved completely, but a certain residual component (i.e., anode scrap) remains. The amount of anode scrap increases with a higher anode oxygen content and a more porous anodic structure. This incomplete dissolution deteriorates the contact and hence increases the electrical resistance. The process is further complicated by the fact, that Cu forms two ions with different valencies and that metals, which form such ions with different valencies, act like an alloy of metals with different potentials during anodic polarization[35]. The anodes in electrorefining are Cu alloys with low levels of accompanying elements. At low current densities especially the elements with the lowest potential are transferred into solution, at higher current densities those with more electropositive potential are dissolved [35].

There are three groups of anode impurities [35]:

1. Elements less noble than Cu (e.g., Co, Ni, Zn, and Fe): These elements are almost totally dissolved, namely transferred to the electrolyte. They are not deposited cathodically, but may contaminate the cathodes through electrolyte inclusions or insufficient cathode washing. As these elements may produce negative effects during electrolysis, electrolyte cleaning is necessary.
2. Elements more noble than Cu (e.g., Au, Ag, Se, and Te), metals insoluble in H_2SO_4 (e.g., Sn and Pb), and weakly electrochemical active Cu compounds (e.g., Cu_2Te, Cu_2Se, Cu_2S, and Cu_2O): These impurities are almost completely transferred to the anode slime.
3. Impurities with a potential similar to Cu (e.g., As, Bi, and Sb): These impurities are the most disruptive, as they are dissolved and may be co-deposited under certain conditions. If As is present in the electrolyte together with Bi and Sb, floating slimes can be formed ($Bi_2O_3 \cdot As_2O_5$ and $SbAsO_4$), which contaminate the cathode.

The behaviour of the anode components is mainly determined by the chemical and phase composition of the anode as well as by the electrolyte composition and the hydrodynamics at the electrode surface. Additional influences come from secondary reactions of dissolved substances in the electrolyte near the anode and with components of the anode slime [99, 100]. In multicomponent anodes, like the anodes in copper electrorefining, the behaviour of the anode components is determined by the electrode potential, the anode chemical composition and phases, electrolyte composition, as well as the hydrodynamics at the electrode surface [100].

The main influences on anode process progression during electrorefining are summarized in Table 9.

Table 9: Main influences on anode processes [99]

Input Parameters		Evolving Parameters		Output Parameters	
I 1	Anode	E 1	Physical	O 1	Electrolyte
I 1.1	Metallic impurity concentrations	E 1.1	pH of electrolyte	O 1.1	Initial composition change
I 1.2	Non-metallic impurity concentrations	E 1.2	Electrolyte conductibility	O 1.2	Electrolyte impurities
I 1.3	Phase composition	E 1.3	Electrolyte density	O 1.3	Solid fraction in electrolyte
I 1.4	Component activities	E 1.4	Electrolyte viscosity	O 1.4	Colloid-dispersed substances in electrolyte
I 1.5	Surface quality	E 1.5	Electrolyte surface tension	O 2	Anode
I 1.6	Electrode shape and arrangement (stationary, non-stationary)	E 1.6	Ion-transport velocity (convection, migration, diffusion)	O 2.1	Anode scrap mass
I 1.7	Electrode dimensions	E 1.7	Concentration gradient of ions in anode-near electrolyte	O 3	Anode slime
I 1.8	Electrode mass	E 1.8	Layer-thickness and consistency of anode slime	O 3.1	Anode slime amount and composition of
I 2	Electrolyte	E 2	Electrochemical-energetics	O 4	Energetics
I 2.1	Initial composition	E 2.1	Anodic polarization	O 4.1	Anodic current efficiency
I 2.2	Addition (inhibitor) concentrations	E 2.2	Ion activities	O 5	Cathode
I 2.3	O_2 concentration	E 2.3	Anode passivation	O 5.1	Cathode composition
I 2.4	Flow direction and volume	E 3	Electrochemical-chemical		
I 2.5	Temperature	E 3.1	Base metal and impurity electrochemical dissolution behaviours		
I 3	Electrode load	E 3.2	Progress of dissolved substance secondary reactions (solvation, hydrolysis, complexation, salification)		
I 3.1	Anodic current density	E 3.3	Anode slime formation due to disproportionation		
I 4	Time effect	E 3.4	Anode slime formation due to dissolved substance reactions with anode material and metal ions		
I 4.1	Experimental duration	E 3.5	Dissolved metal ion reactions with anode slime components		
		E 3.6	Dissolved metal ion valence change		
		E 3.7	Adsorption processes on anode and anode slime		

The anodic dissolution behaviour is influenced by the anode purity and composition, the physical structure, the physical-chemical condition of the surface, as well as the electrolyte composition and purity [100]. Hence, not only the chemical, but also the physical quality of the anode is decisive for the dissolution behaviour. According to the literature, the different structures across the anode thickness have different dissolution rates and tendencies for passivation [18, 78, 79, 83]. Furthermore, a correlation between dissolution and dendrite arm spacing (DAS) has been described [81]. The dissolution rates and also the necessary energy for dissolution are different for each of the anode areas. The dendritic region has the strongest tendency for passivation [78]. Areas having a larger grain size require higher potentials for the onset of passivation. The dissolution starts at the grain boundaries and is always more intense around impurities or inclusions. Hence, larger grain sizes reduce the susceptibility to passivation, as they present fewer surfaces where impurities are located. Therefore, the contribution of the impurities to the formation of a passive layer on the anode surface is smaller [39].

The dissolution of a cast anode with a dendritic structure starts at a certain potential. At first the components with a higher surface energy are dissolved. Smaller crystals, which have a higher surface energy, have the highest dissolution rates. Due to the dissolution of the smaller crystals the connection between the coarser remaining crystals is broken and these are transferred to the anode slime. The preferred dissolution of crystal edges and tips also leads to a smoothing of the anode surface. The more homogeneous the structure and geometric the form of the anode, the more homogeneous the dissolution and the lower the losses to the anode slime [100].

The appearance of an overvoltage is typical for anodic dissolution, whereby the current density-potential curves obey Tafel's equation. At soluble anodes a potential, which the metal assumes in equilibrium with the solution of its ions at the corresponding concentration, is established at low current densities. Increasing current density leads to a concentration overvoltage due to insufficient ion transport and hence ion enrichment near the anode [100]. Copper is dissolved anodically as Cu^{+} and Cu^{2+}, respectively. According to the standard electrode potentials E_H^0 [V], it is obvious that it is transferred into the solution mainly as Cu^{2+} [100]:

$$Cu \leftrightarrow Cu^{+} + e^{-} \quad E = +0.51V$$ Equation 8

$$Cu \leftrightarrow Cu^{2+} + 2e^{-} \quad E = +0.34\,V$$ Equation 9

$$Cu^{+} \leftrightarrow Cu^{2+} + e^{-} \quad E = +0.17\,V$$ Equation 10

During the anodic polarization of a copper electrode in an electrolyte containing H_2SO_4 and $CuSO_4$ Equation 10 with the most electronegative potential should occur, but, however, due to the lack of Cu^+ ions Equation 9 is favoured. Even Equation 8 is possible when the Cu/Cu^+ potential approaches that of Cu/Cu^{2+} at low Cu^+ concentrations [99]. The concentration relationships are determined by Equation 11 and its corresponding electrode potential [100]:

$$Cu + Cu^{2+} \leftrightarrow 2Cu^{+} \qquad \text{Equation 11}$$

In addition to the special effects of inhomogeneous anodic dissolution due to passivation of single anode areas, also a general inhomogeneity of the anodic and cathodic process occurs [35]. During electrorefining—even if the anodes are perfectly vertical—the electrical field lines are unevenly distributed in the electrolyte volume, depending on the ohmic resistance of the electrolyte (i.e., due to an uneven $CuSO_4$ distribution). Especially at the edges a higher density of field lines occurs, and hence also a more pronounced dissolution in these areas. A further reason for uneven anodic dissolution is the presence of inclusions with poor conductivity or solubility (e.g., Cu_2O, Cu_2S, Cu_2Te, and Cu_2Se). Hence, rapid dissolution, and consequently the formation of holes, occurs in certain areas [35].

The principle of anodic dissolution is illustrated in Figure 33. The anodes for electrorefining are multicomponent alloys. Only if the contained metals are completely insoluble the anodic dissolution takes place according to the electrochemical series, namely with a more electropositive character. More frequently the components form solid solutions (e.g., Cu-Ag, Cu-Sb, Pb-Bi, and Pb-Sb) or intermetallic compounds (e.g., Cu-Sb and Cu-Se at high Sb- and Se-levels, respectively), which cause the establishment of a composition-dependent electrode potential that differs from that of the pure metals. A certain electrode polarization causes a combined dissolution of the components. In multicomponent alloys, firstly a selective dissolution of the electrochemically least noble phase occurs, followed by the more noble phases at higher polarization [99].

If single impurities are soluble in the base metal and form single-phase solid solutions or intermetallic compounds with it, their primary anodic co-dissolution cannot be avoided, even when they are electrochemically nobler. If an accompanying element is distributed amongst multiple phases, only the least noble phase is dissolved selectively at low polarizations, and the nobler phase remains undissolved and builds up an anode slime (i.e., skeleton) [99].

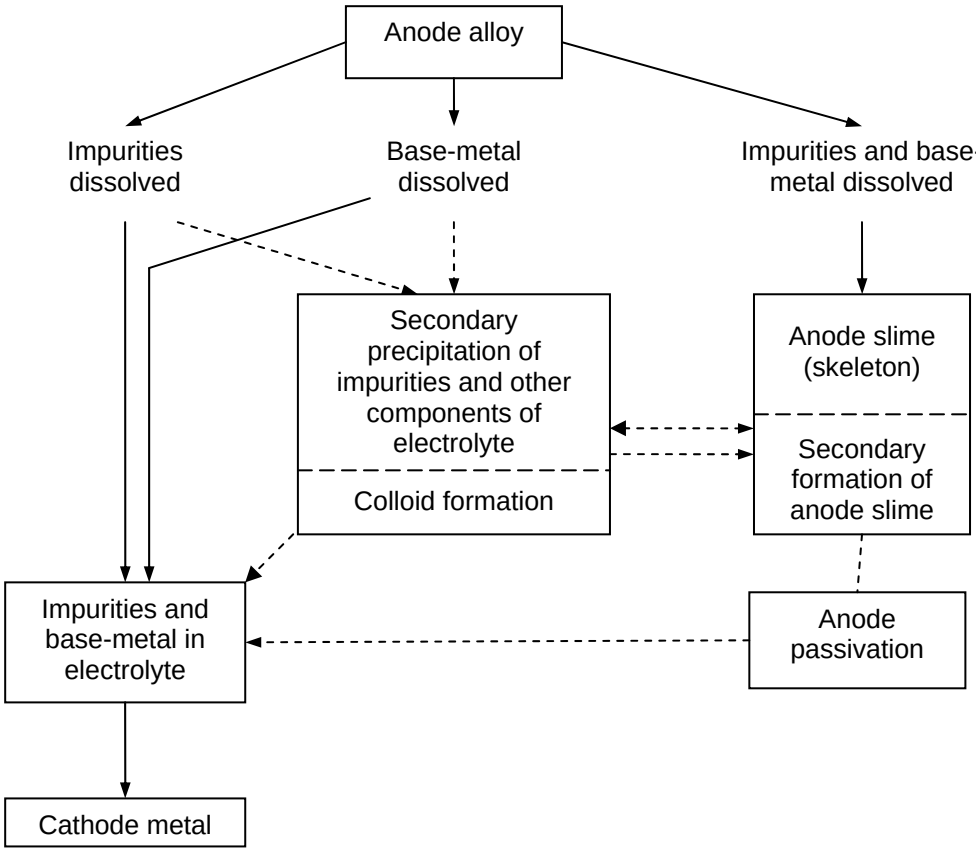

Figure 33: Dissolution of anode alloy during copper electrorefining [99]

2.5.1 Passivity of Metals

The anodic reactions during electrolysis often lead to the formation of surface layers. The state of passivity of a metallic surface is reached when the current density increases with increasing overvoltage, but then suddenly drops after reaching a certain value of polarization (Figure 34) [100, 101]. The electrode potential, where the maximum current density i_{max} is reached and the sudden drop in current density occurs, is called the Flade potential, U_F (or E_F). The passive state may be caused by [100, 102]:

- Pore-free layer of solid salt or oxide
- Complete coverage with chemisorbed oxygen

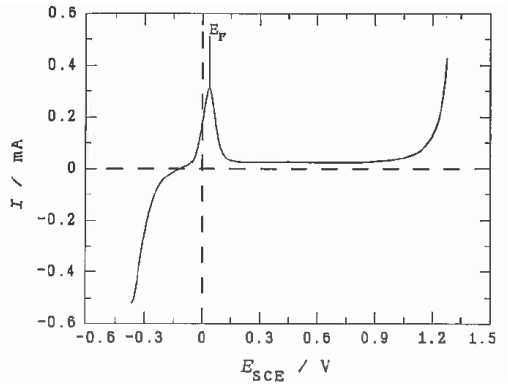

Figure 34: Current-potential curve of metal dissolution with formation of a passive layer (E_F: Flade potential) [101]

When passivation occurs, the anodic dissolution nearly stops and only a low current, which is called corrosion current density, i_K (or i_R), remains, which compensates the chemical dissolution by the electrolyte in the stationary state. A further increase of overvoltage may activate a new potential defining process, for example the anodic formation of gaseous oxygen, which results in another current density increase [100, 102, 103]. The passive layer can be removed by reversing the polarity. The process of passivation can also be suspended by contacting the surface with a less noble metal. This is also the cause of electrochemical corrosion, where a galvanic element is formed at the contacting surface. The nobler element is the cathode, and the hydrogen produced there reduces the passivating oxide layer, so that the metal returns to the active state. The less noble metal is dissolved and its hydrogen overvoltage relieved anodically [103].

Mechanical passivity means that a visible or detectable surface layer is found on the surface, whereby no surface alterations are visible for chemical passivity. A special type of chemical passivity is electrochemical passivity, which is caused by anodic polarization and also does not show visible alterations [104]. The passivity properties of a metal are dependent on the given conditions. Chemical or electrochemical treatment do not strongly influence the properties of copper, but passivation occurs in the anodes, whereby also their chemical composition is decisive [35]. If the anodes contain not only the usual elements but also PGM, passivity occurs at current densities of > 200 A/m². Also high levels of Sn and Pb in the anodes, as well as a high concentration of $NiSO_4$ in the electrolyte promote passivation [35].

The passive state of an anode is characterized by the formation of a dense surface layer, which hinders further electrochemical dissolution of the components. It can be detected by a sudden increase of anode polarization (and therefore terminal voltage) at galvanostatic loads and a substantial drop of current density under potentiostatic operating conditions. The causes of passivation are the deposition of electrochemically noble metals, layers of metal

salts or oxides, and covering of the anode surface with chemisorbed oxygen. Most of the precipitates result from the formation of redox-systems or exceeding the solubility product [99]. There are four characteristic regions associated with passivation [105, 106]:

1. Active dissolution—a slow increase in potential
2. Prepassivation—initial potential oscillations
3. Passivation onset—a sharp increase in potential at passivation time and a nearly linear increase in potential thereafter
4. Passivation—irregular and continuous potential oscillations

Bounoughaz et al. [67] detected three characteristic regions: (1) active dissolution, (2) dissolution and precipitation, and (3) a current plateau. The behaviour of pure Cu and anode Cu is similar at low current densities (191 mA/cm²), but significantly different at high current densities (382 mA/cm²), where the anode passivates rapidly (i.e., a sharp increase in potential) [106]. Hence, current density has an influence on anode passivation. If the anodic film formed is not a conductor, the potential of the coating increases until a new electrode process commences, for example the dissolution of the metal in a higher valency state, the discharge of anions (i.e., oxygen evolution), or the formation of a new film possessing different characteristics (i.e., passivation). This is indicated by a rise in potential [106]. The formation of a film, which is an ionic conductor, results in an almost linear potential increase as the layer continues to grow [106]. An electronically conducting film enables ion discharge from the electrolyte at the interface [106]. The passivation time can be described as [68]:

$$\log\left(1-\frac{i_{pr}}{i_A}\right)=b+a\cdot t_p \qquad \text{Equation 12}$$

i_{pr} Permissible current density [A/m²]

i_A Anodic current density [A/m²]

t_p Passivation time [s]

a,b Coefficients

Different causes for passivation, namely different types of layers, are mentioned in the literature [106, 107], for example $CuSO_4 \cdot 5H_2O$ layers, $PbSO_4$, NiO, and Cu_2O surface films, Ag deposits, deposits of various Se compounds, CuCl, and $PbSO_4$. Although several mechanisms have been suggested, the precise cause of anode passivation has not been established and no single mechanism has been accepted. Passivation may depend on the properties of the surface slimes to a large degree (i.e., a diffusion barrier) [106].

2.5.2 Polarization and Overvoltage

The potential of an electrode, E_H, is a measurable relative value with respect to the standard hydrogen electrode (SHE), whose potential is 0 V by definition [100]. The equilibrium value under standard conditions termed the standard electrode potential, E_H^0. The Galvani potential of an electrode, which is defined as the difference between the mean electrical potentials of the two electrode phases (e.g., metal and electrolyte), cannot be measured and is an absolute value [100]:

$${}^{I}g^{II} = \eta^{I} - \eta^{II} \qquad \text{Equation 13}$$

If the electrochemical reaction, which occurs at an anode, is in equilibrium (e.g., $Me^{\pm 0} \leftrightarrow Me^{z+} + z \cdot e^{-}$), this Galvani-potential is termed the equilibrium Galvani potential [100]:

$${}^{I}g^{II} = g_{gl} \qquad \text{Equation 14}$$

If the electrochemical reaction of an electrode without current load is not in equilibrium, this Galvani potential is termed the rest Galvani potential [100]:

$${}^{I}g^{II} = g_0 \qquad \text{Equation 15}$$

If the electrochemical reaction of an electrode takes place under standard conditions, namely at a metal ion activity of 1, a pressure of 1 atm, and a temperature of 25 °C, this Galvani potential is termed the standard Galvani potential [100]:

$${}^{I}g^{II} = g^0 \qquad \text{Equation 16}$$

The polarization η of an electrode is the difference between the Galvani potential without (g_0) and with (g_I) current load [100]:

$$\eta = \Delta g_I = g_I - g_0 \qquad \text{Equation 17}$$

The electromagnetic force (EMF) is the potential, measured between the electrodes without an external electric load. All EMFs opposed to the external applied voltage are encompassed by the term galvanic polarization. There are reversible and irreversible types of polarization: The concentration polarization, which consists of diffusion and reaction polarization, is reversible, and transition and resistance polarization are irreversible. Reversible polarization types can be overcome during electrolysis by applying externally their counter EMF, irreversible polarizations require a higher counter voltage (i.e., potential), which is defined as overvoltage [103]. The anodic polarization leads to a shift towards more electropositive values, the cathodic polarization towards more electronegative values. The overvoltage is a special case of polarization, where the rest Galvani potential equals the equilibrium Galvani potential [100]:

$$\eta = \Delta g_l = g_l - g_{gl}$$ Equation 18

The appearance of a polarization and overvoltage, is caused by the inhibited progress of an electrochemical reaction under current load. As the total reaction consists of various subprocesses, also the overvoltage consists of multiple parts, which are due to the special inhibition of these single parts. Hence, the following basic types of overvoltage are distinguished [100, 103]:

- Transition overvoltage (η_D)
- Diffusion overvoltage (η_d)
- Reaction overvoltage (η_R)
- Crystallization overvoltage (η_K)

The total overvoltage can be written as [100]:

$$\eta = \eta_D + \eta_d + \eta_R + \eta_K$$ Equation 19

The value of the overvoltage is dependent on temperature, electrode material, type and concentration of the ions to be deposited, current density, and surface properties of the electrodes. Increasing temperature leads to lower overvoltage. Smoother electrode surfaces increase the overvoltage, whereas rougher surfaces increase the effective surface and hence decrease the current density and the overvoltage [103].

The open circuit potential of an electrode, namely the potential without current load, can be determined by measuring the potential against the SHE (i.e., counter electrode) with high impedance. The potential of a working electrode under current load cannot be determined in this way, as with the current load also on the SHE an overvoltage occurs. Hence, the potential under current load is determined by introducing a third electrode without current flow (i.e., reference electrode). The difference between the potential under current load and the open circuit potential is the overvoltage of the working electrode. In order to minimize the error due to the ohmic voltage drop in the electrolyte, a glass capillary, the so-called Haber-Luggin capillary, is used, which is positioned close to the surface of the measurement electrode [102].

2.5.3 Copper Electrolysis

Small amounts of chlorides (i.e., 8–260 g/t cathode [6]) promote electrodeposition in fine crystalline form and minimize anodic passivation, whilst higher chloride levels lead to brittle, chloride-containing cathodic depositions. A smooth deposition is achieved by adding colloids, including gelatine, glue, and thiourea (e.g., glue: 35–306 g/t cathode, thiourea: 25–136 g/t cathode, and Avitone A: 0–42 g/t cathode [6]). The temperature should be in the range of 55–

65 °C in order to avoid coarse crystalline deposition. Higher temperatures decrease electrolyte resistance, but increase evaporation and heat losses from the cell. Fe ions cause current losses as they are oxidized anodically and reduced again cathodically [108].

The cell voltage is determined by the ohmic resistance of the cell and a developing concentration polarization, and can be increased by passivation effects. A higher concentration of Cu^{2+} decreases the resistance, but promotes the formation of Cu^{+} and metallic Cu. Decreased electrode spacing increases the possibility of shorts. Anodic passivation is promoted by high current density, as well as a high concentration of H_2SO_4 and Cu. The concentration polarization near the electrodes can be decreased by high electrolyte flow, whereby the maximum flow is limited by the settling of the anode slime, or applying periodic current reversal [108]. The use of high current densities is limited by certain problems [108]:

- Increased concentration polarization
- Even current distribution between electrode groups and single electrodes
- Increased anodic passivation
- Increased cathodic inclusions of anode slime
- Deteriorated current efficiency

These problems can be overcome by the following measures [108]:

- Higher electrolyte velocity and temperature
- Vibrating electrodes
- Ultrasonic application
- Wider electrode spacing
- Alteration of stationary current flow by
    - Pulsing direct current
    - Periodic current reversal
    - Direct current with superimposed alternating current

The actual current densities used in electrorefining are much lower than the theoretically feasible maximum current density, because of rough electrodeposits resulting in higher Au and Ag losses and a higher tendency for anode passivation at higher current densities [38]. To avoid anode passivation, the following measures may be taken [38]:

- Lower current density
- Higher electrolyte temperature
- Higher electrolyte circulation
- Suitable electrolyte composition with type and amount of organic additives

In addition, thermal anode treatment (Section 2.1.1.4) is reported to reduce the tendency for passivation, even when impurity levels in the anode are high [38].

In summary, it can be stated that anodic dissolution, namely electrorefining operations, is dependent on anode quality, which in turns is determined to a large extent by the casting process.

The chemical quality of an anode is defined by the absolute and relative impurity levels, the phases present, as well as the distribution of the elements and phases across the anode thickness and area. In order to ensure steady conditions for electrorefining, batch-wise variations in the anode copper composition and hence the anodes should be avoided.

Regarding physical quality, not only the surface quality, weight, and geometric accuracy have to be considered, but also structure. The solidification rate, which affects both the physical (i.e., structure) and chemical (i.e., elemental distribution and phases formed) quality, can be adjusted by the cooling conditions, namely the casting process parameters, mould material, mould temperature, mould wash, casting temperature, and cooling. A homogeneous chemical and physical quality is necessary to achieve homogeneous anodic dissolution during electrorefining.

The experimental investigations, which were carried out on the basis of this literature study, examined the dependencies between casting process, anode quality, and dissolution behaviour. The casting process at Montanwerke Brixlegg AG was investigated, and a variation of process parameters (i.e., mould material, mould wash, and period of use of the mould) was carried out. The corresponding anodes were analysed regarding the chemical and physical quality, in order to evaluate the effects of the process parameters. The dissolution behaviour of the anode samples with different chemical and physical qualities was studied by potential measurements. Furthermore, a model for the simulation of anode casting was developed in order to examine the influence of variations in cooling conditions on anode solidification. This model can also be used for microstructure predictions, mould geometry optimization, as well as casting system and cooling arrangement design.

3. Objective

Previous studies, which were carried out by METTOP demonstrated that anode quality significantly affects electrorefining operations, especially at high current densities, which can be applied when using the new METTOP-BRX-Technology in the tankhouse. It was found that there are dissolution differences between the air and mould side of the anode, and hence production of the corresponding cathodes, not only in the first cathodic crop, which would be consistent with the literature regarding variations in chemical quality in the outer anode areas, but also in the second cathodic crop, where the anode quality is considered to be homogeneous.

This work described in the following chapters was performed in order to establish the causes for these observations. A variation of anode quality across the anode thickness was assumed, and hence appropriate investigations were carried out, regarding the causes, namely the casting process and its effects on the anodic dissolution behaviour. The aim of this work was to determine the optimum anode quality for electrorefining at high current densities.

As previously discussed, the investigations were initiated on a macroscale, namely the casting process in general, and then progressed into more and more detail, namely the chemical and physical anode quality, as well as anodic dissolution behaviour. The actual experiments, namely varying the cooling conditions, were accompanied by and compared with casting process simulations. The developed model can be used to predict anode solidification and also the effects of mould design or cooling arrangement changes, which are currently determined by trial and error.

4. Experimental Investigations

The work was divided in the following sections:

1. Determination of the chemical and physical anode quality
    a. Chemical analysis across the anode thickness and area
    b. Investigation of the structure and grain size
2. Determination of present cooling conditions
    a. Investigation of the casting process (i.e., cooling water, mould material, and mould wash)
    b. Temperature measurements in anode moulds
3. Modelling of anode casting
    a. Heat transfer modelling
    b. Solidification modelling
    c. Correlation with potential measurements

By establishing the optimum cooling rate, namely how to produce the desired anode quality theoretically, the next step is the practical implementation and adjustment of water spray cooling.

4.1 Casting Process at Montanwerke Brixlegg AG

The casting process at Montanwerke Brixlegg AG was investigated in detail on 15 casting days to determine the anode production conditions.

4.1.1 Cooling Water

The temperature and amount of cooling water used for anode spray cooling were measured on multiple days.

4.1.2 Casting Temperature

The casting temperature was measured on multiple days using pyrometer and thermocouple lances.

4.1.3 Variation of Process Parameters

A variation of mould material and design (i.e., anode Cu, cathode Cu, and cooling ribs), as well as mould wash (i.e., barite and carbon black) was carried out in order to study the influence of these process parameters on mould temperatures and hence the anode solidification conditions. In addition, the influence of the period of use of the mould, namely the number of casting days that the mould has been in use, was investigated.

4.2 Mould Temperature Measurements

To measure the temperature in the anode moulds and determine the anode cooling and solidifications conditions a temperature measurement system was installed in the anode moulds. The temperatures were measured at different depths and at different positions to record the temperature variation across the thickness and investigate the evenness of mould heating and cooling. Therefore, the moulds were drilled to defined depths and equipped with thermocouples. These were fixed with screws to ensure a direct contact with the mould and hence a correct temperature measurement.

Two measurement setups were used. The first setup (used only on 17–19.10.2006 and 7–8.11.2006) enabled the simultaneous measurement in two moulds with eight measurement points, namely 140 and 100 mm deep at four positions (i.e., top, side, centre, and bottom). The second setup included four different depths, namely surface, 50, 100, and 140 mm, at the aforementioned four positions. In between the different series of measurements the measurement system was removed from the mould. To avoid effects due to limescale, which forms at the bottom of the mould due to the contact with the cooling water, the thermocouple holes were drilled out, namely cleaned of limescale, before the measurement system was reinstalled.

Some of the original positions for the measurement points, which were planned according to technical drawings, could not be realized as they coincided with the position of the two supporting rings and the ejector pins. Hence, the holes were drilled after the mould had been mounted and the exact positions were determined after removal of the mould. The planned and actual positions of the measurements are depicted in Figure 35.

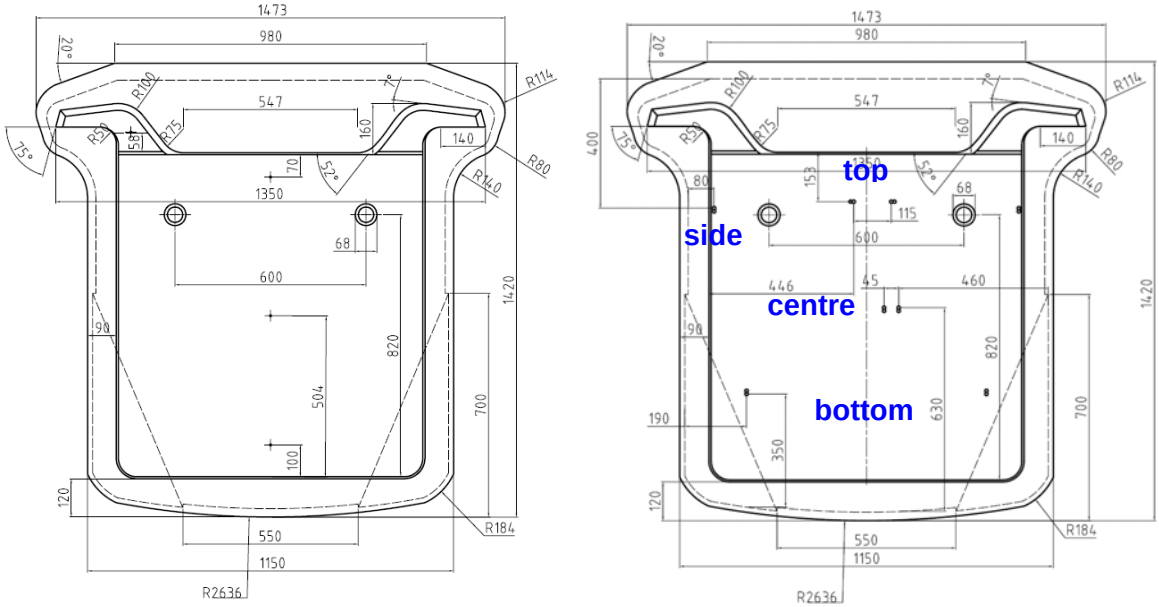

Figure 35: Positions for temperature measurements—planned (left) and actual (right)

All the measurements performed and samples taken are detailed in Table 10. Samples were not taken on every measurement day, but when changes in the process parameters should have resulted in differences in the cooling conditions and hence anode quality. The first measurements (17–20.10.2006) were done to establish the functionality of the measurement system and investigate the general temperature behaviour as well as the temperature differences between subsequent casting days and during one casting day. The results of the temperature measurements are discussed in Section 5.2.

Table 10: Conducted measurements

Date	Anode no.	Mould material	Mould wash	Comments
19.06.2006	A	Anode Cu	Barite	No temperature measurements
17.10.2006	-	Anode Cu (new) Cathode Cu (new)	Barite	4 measurement positions at 2 depths (i.e., 100/140 mm); 2 moulds
18.10.2006	-	Anode Cu Cathode Cu	Barite	4 measurement positions at 2 depths (i.e., 100/140 mm); 2 moulds
19.10.2006	-	Anode Cu Cathode Cu	Barite	4 measurement positions at 2 depths (i.e., 100/140 mm); 2 moulds
20.10.2006	-	Anode Cu Cathode Cu	Barite	4 measurement positions at 2 depths (i.e., 100/140 mm); 2 moulds
07.11.2006	B C	Anode Cu Cathode Cu	Barite	4 measurement positions at 2 depths (i.e., 100/140 mm); 2 moulds
08.11.2006	-	Anode Cu Cathode Cu	Barite	4 measurement positions at 2 depths (i.e., 100/140 mm); 2 moulds
28.11.2006	D	Anode Cu (new)	Barite	4 measurement positions at 4 depths (i.e., 0/50/100/140 mm); 1 mould
29.11.2006	E	Anode Cu	Carbon black	4 measurement positions at 4 depths (i.e., 0/50/100/140 mm); 1 mould
30.11.2006	F	Cathode Cu	Barite	4 measurement positions at 2 depths (i.e., 100/140 mm); 1 mould
27.02.2007	G	Anode Cu (new) Cooling ribs 1	Barite	4 measurement positions at 4 depths (i.e., 0/50/100/140 mm); 1 mould
28.02.2007	-	Anode Cu (new) Cooling ribs 2	Barite	4 measurement positions at 4 depths (i.e., 0/50/100/140 mm); 1 mould
01.03.2007	-	Anode Cu (new) Cooling ribs 3	Barite	4 measurement positions at 4 depths (i.e., 0/50/100/140 mm); 1 mould
13.03.2007	-	Anode Cu Cooling ribs 1	Barite	4 measurement positions at 4 depths (i.e., 0/50/100/140 mm); 1 mould
10.05.2007	H	Cathode Cu (new)	Barite	4 measurement positions at 4 depths (i.e., 0/50/100/140 mm); 1 mould
11.05.2007	-	Cathode Cu	Barite	4 measurement positions at 4 depths (i.e., 0/50/100/140 mm); 1 mould
07.12.2007	I	Cathode Cu	Barite	4 measurement positions at 4 depths (i.e., 0/50/100/140 mm); 1 mould

The measurement system was planned in collaboration with LANG electronic (Leoben, Austria), and a measuring program was developed. The program is based on the LabVIEW software (National Instruments, USA) and enables the temperatures to be displayed as numerical values, graphically, and in tables during the measurement. All measured values including the time points are saved as a table and can be read using Excel. The measuring interval is 1 s, markers for start and end of casting can be set.

The thermocouple selection (i.e., type, model, plug, and wiring) was made according to the application requirement. The following points had to be considered:

- Temperature range
- Measurement accuracy
- Spray water
- Easy replacement of the single parts

The measurement system consisted of the following components:

- 16 mantle thermocouples type K (140 and 230 mm—8 pieces each)
- Thermocouple compensating line type K (80 m)
- 16 plugs type K
- 2 Bluetooth adapters
- 2 ICP modules
- Interface converter
- Power supply unit
- Laptop with measurement software

The thermocouples were linked to the measurement modules and the interface converter, which were mounted on a rail, via plugs and a thermocouple compensating line. The data transmission from the measurement modules to the laptop measurement software was performed via Bluetooth. This enabled the laptop to be positioned in an area protected from heat and dust (i.e., the casting wheel control stand). Those parts of the measurement system, which were installed on the casting wheel (i.e., measurement modules, interface converter, and power supply), were protected from the harsh environmental conditions by an insulated plastic box, which was transparent to the Bluetooth signal transmission. The power supply on the rotating casting wheel was provided by a slip ring. The measurement setup at Montanwerke Brixlegg AG and a schematic overview are depicted in Figure 36 and Figure 37.

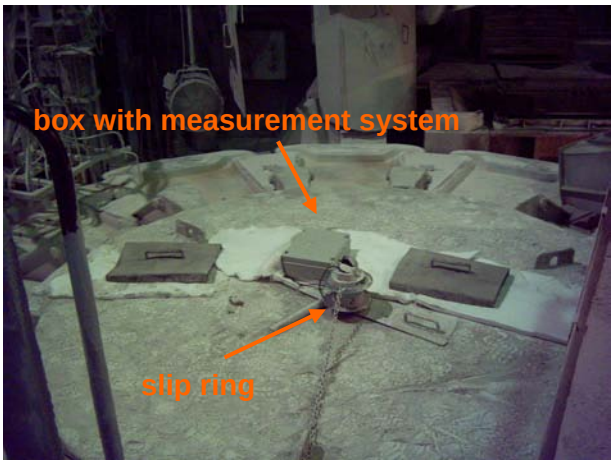

Figure 36: Measurement setup on the casting wheel at Montanwerke Brixlegg AG

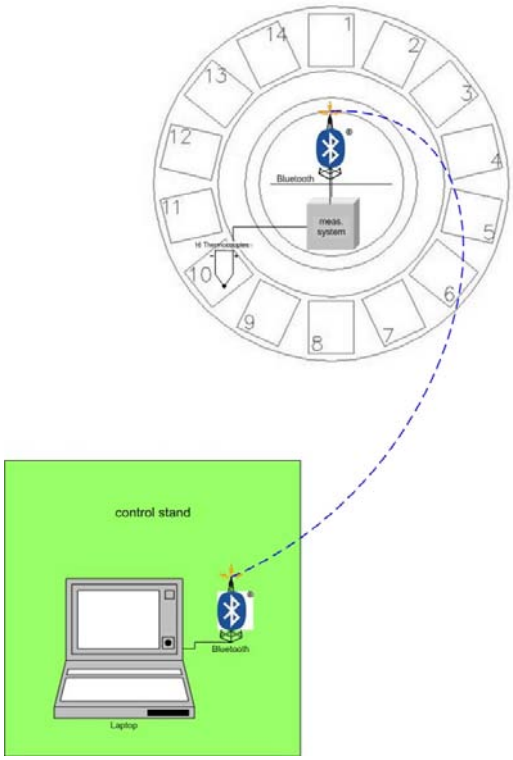

Figure 37: Measurement system—schematic overview

4.3 Chemical Analysis

The batch chemical analysis is performed routinely at the chemical laboratory at Montanwerke Brixlegg AG. A sample of liquid copper is taken, solidified, and analysed by spark emission spectroscopy (at least 3 measurements per sample). Each batch is analysed 2–3 times during fire refining and casting:

- After oxidation: sample "OxidCu"
- After reduction: sample "AnodCu"
- Final sample, taken in the last third of the casting process: sample "EP" (“Endprobe”)

The analysis of the sample "EP" is not performed for every batch.

To study the variation of anode copper composition during the casting process and hence within one batch, samples were taken every hour during casting. The results of these investigations are presented in Section 5.3.1.1.

Samples were cut from anodes, which were cast in the moulds where the temperature measurement system was installed, to investigate the elemental distribution within one anode (Section 5.3). These samples were subsequently cut into slices across the anode thickness to study the elemental distribution from the air- to the mould side (Figure 38). For the analysis of the air and mould side, the uneven surface had to be removed, as flat surfaces are required for spark emission spectroscopy. This was performed with minimum material loss. The results of chemical variation across the anode thickness are discussed in Section 5.3.1.2.

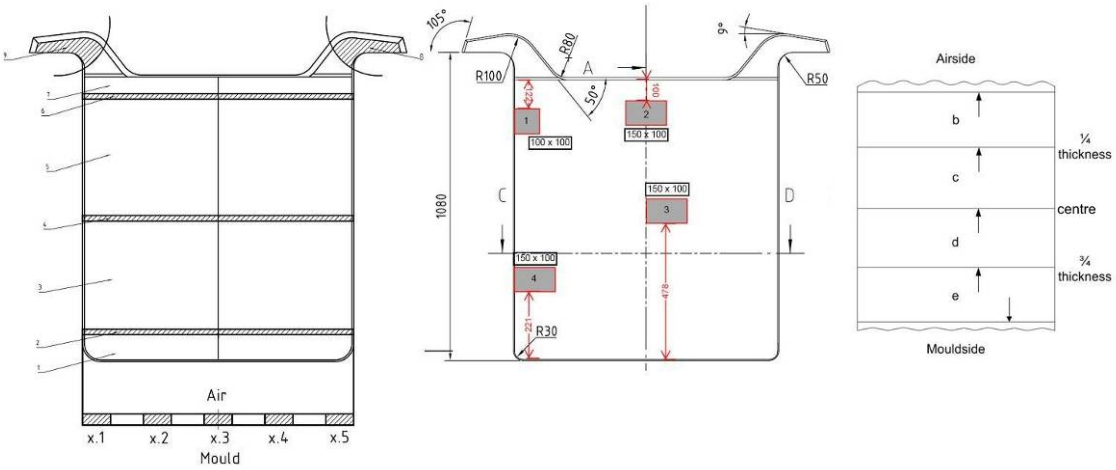

Figure 38: Anode samples (grey shading) from anode A (left) and anodes B–I (centre), slices from shaded regions (right)

The elemental distribution was examined by spark emission spectroscopy (minimum 3 measurements per slice) and quantitative scanning electron microscopy (SEM). SEM with EDX analyser was also used for inclusion analysis (i.e., distribution and type), and the results are discussed in Section 5.3.2.

4.4 Physical Analysis

Metallographic investigations were performed on the samples cut from the anodes to study the physical quality, namely structural variations, across the anode thickness. The samples (Section 4.3) were ground (up to 1200 grit), polished, and etched. Adequate etching methods for the anode copper micro- and macrostructure were selected according to the literature [42,

[80, 109] and inquiries. The use of ammoniumpersulfate solution at different concentrations (i.e., 5 wt.% $(NH_4)_2S_2O_8$ for microstructure and 25 wt.% $(NH_4)_2S_2O_8$ for macrostructure) led to good results. The grain sizes and secondary dendrite arm spacing (DAS) were measured with the Clemex Nikon image analysis software (Clemex Technologies Inc., Canada). The results of the metallographic investigations are discussed in Section 5.4. The grain sizes and DAS given are mean values calculated from 20 grain and 50 DAS measurements, respectively.

4.5 Dissolution Behaviour/Potential Measurements

The potential measurements investigated the differences in anodic dissolution behaviour between the different solidification areas across the anode thickness (due to the variations in physical quality, grain size, and structure). The results are presented as current density-potential curves (Section 5.5). From these plots, a maximum current density and the corresponding potential (Flade potential) and anode polarization could be determined. With these values, the anodic dissolution behaviour was quantified.

The samples (Samples A–E from anode C, G, and I) were cut, so that the different solidification zones across the anode thickness could be investigated. The anodic samples were 1 cm² (10 x 10 mm). The samples were embedded in a synthetic resin, contacted with an insulated copper wire, ground (240, 600, and 1200 grit), and cleaned before starting the measurement. The polarization scans were performed at a scan rate of 0.1 mV/s. In order to keep the experimental conditions and the distances between the electrodes constant, a sample holder made of Teflon was used (Figure 39). The distance between anode and cathode was maintained at 2 cm, as described for similar experiments [80, 110, 111], the distance between anode and Luggin capillary was kept minimal, but sufficiently large enough that no direct contact occurred. The space between the sample holder and the bottom of the beaker enabled magnetic stirring. Before starting the anodic scan the open circuit potential (OCP) was measured for 5 minutes, which was sufficient since the OCP reached a constant value within this time.

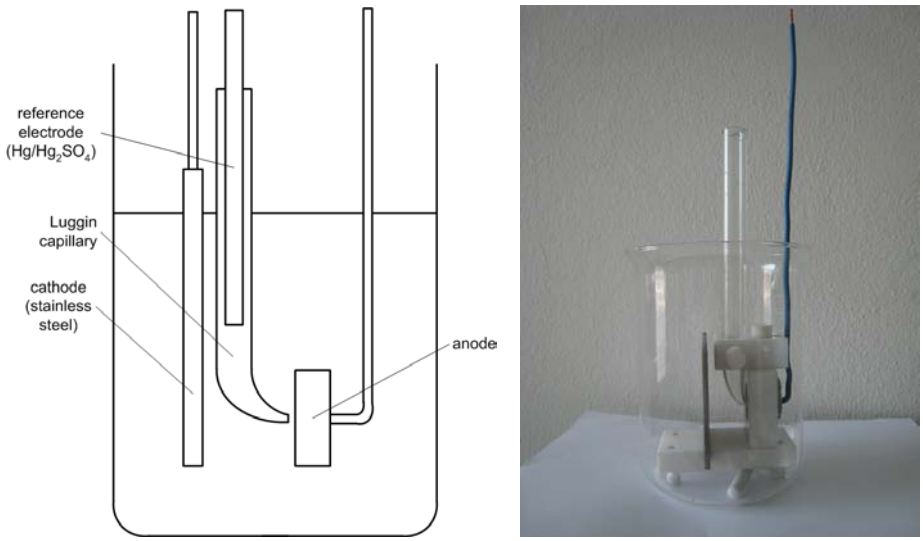

Figure 39: Experimental setup for potential measurements

A $Hg/Hg_2SO_4/SO_4^{2-}$ electrode was used as the reference electrode. The process at this electrode is [102]:

$$Hg_2SO_4 + 2e^- \leftrightarrow 2Hg + SO_4^{2-} \qquad \text{Equation 20}$$

The potential of this electrode with saturated K_2SO_4 solution was 650 mV_{SHE}, where SHE is the standard hydrogen electrode [102]. The cathodic area, namely the counter electrode area, should be maximal, as electrolyte reactions also occur there. A higher current density at the counter electrode leads to an increase in potential—up to water decomposition. Also the counter electrode material, namely the use of cathode copper or stainless steel, is decisive, as the different materials lead to a different polarization of the electrode. For example platinised surfaces have a lower overvoltage for many reactions and hence cause a lower electrode polarization. As a rule, the area of the counter electrode should be so large that the current density remains below 10 mA/cm² [112].

In similar experiments, maximum anodic currents as high as approximately 450 mA occurred. As this current also has to go through the cathode, a cathodic area of approximately 45 cm² is necessary to keep the current density below the limit of 10 mA/cm². The cathode area in the experiments was 2 x 70 x 105 mm ² (= 2 x 73.5 cm² = 147 cm²). Hence, effects due to cathodic deposition should have been avoided.

The electrolyte composition (Table 11) was selected close to the composition at Montanwerke Brixlegg AG. The experiments were carried out with an electrolyte volume of 700 ml (= 800 ml - volume of sample holder) at 65 °C. Magnetic stirring was used.

Table 11: Electrolyte composition

50	g/l	Cu
20	g/l	Ni
175	g/l	H_2SO_4

Each experiment was repeated twice for reproducibility. The potential measurements were carried out with a Jaissle (IPS) potentiostat/galvanostat type PGU 10V-1A-E (IPS, Germany). The measuring accuracy of the potentiostat/galvanostat was ± 0.5%.

The samples to investigate the influence of the different structures were cut from the anode samples 4.3.2 (anode A), C-3, G-3, and I-3 (Figure 40). The samples are described in Table 12. The measured surfaces correspond to the orange areas and lines in Figure 40. As the fine equiaxed zone close to the mould (sample E) was not very visible in all samples and this area was also too thin for repeated measurements (as a certain thickness of the sample was consumed during the measurement, the columnar zone was reached), only samples A to D were investigated from anodes G and I.

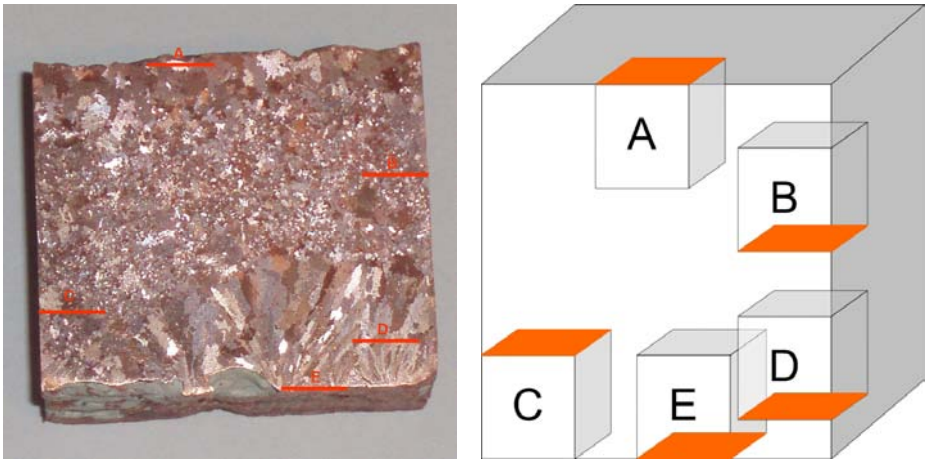

Figure 40: Macrostructure (left) and position of samples for potential measurements (right) of anode sample C-3

Table 12: Samples of anode samples C-3, G-3, and I-3

Sample	Zone
A	Air side (outer equiaxed)
B	Air-centre
C	Mould-centre
D	Mould side (columnar)
E (only anode C)	Mould side (fine outer equiaxed)

5. Results

The casting process at Montanwerke Brixlegg AG and the corresponding anode samples were investigated in detail to determine the causes for different anode qualities and the effects on electrorefining. The investigated anodes and the corresponding process conditions are listed in Table 13.

Table 13: Investigated anodes

Anode	Mould material	Mould wash	Comments
A	Anode Cu	Barite	Standard anode
B C	Anode Cu Cathode Cu	Barite	13th casting day
D	Anode Cu (new)	Barite	1st casting day
E	Anode Cu	Carbon black	2nd casting day
F	Cathode Cu	Barite	30th casting day
G	Anode Cu (new) cooling ribs 1	Barite	1st casting day
H	Cathode Cu (new)	Barite	1st casting day
I	Cathode Cu (new)	Barite	2nd casting day

5.1 Casting Process at Montanwerke Brixlegg AG

The anode furnace at Montanwerke Brixlegg AG has a capacity of 300 t. The additional scrap charging during casting, which can also influence the chemical analysis, results in up to 360 t of anode copper per charge. The duration of the casting process is approximately 6 hours. An overview of the casting process and the 14-mould casting wheel at Montanwerke Brixlegg AG is provided in Figure 41 and Figure 42.

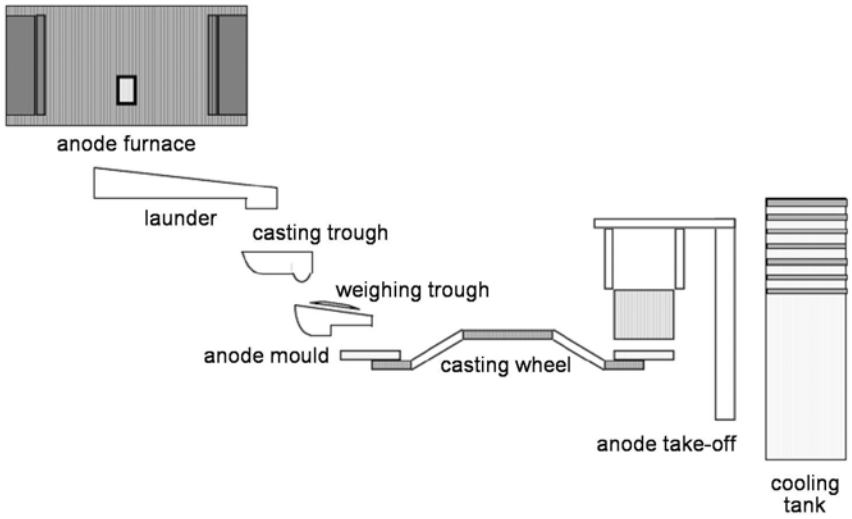

Figure 41: Anode casting at Montanwerke Brixlegg AG

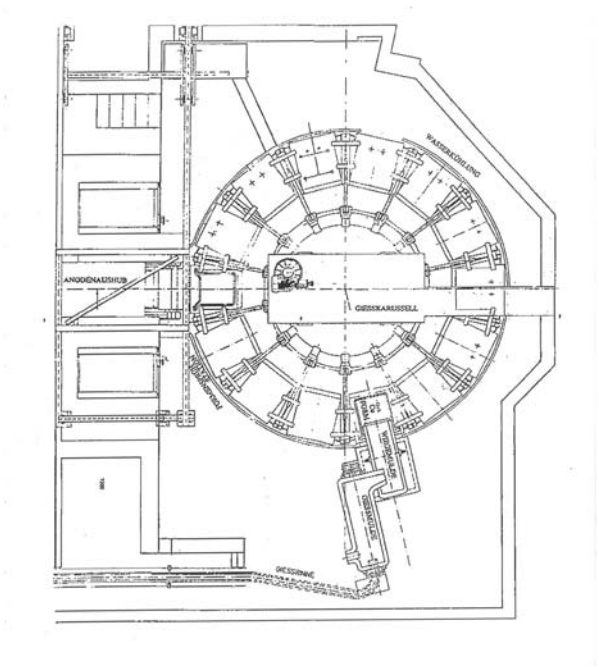

Figure 42: Casting wheel at Montanwerke Brixlegg AG

The nominal anode weight was set at 289 kg and since autumn 2007 at 290 kg. The deviation from the nominal anode weight over 15 casting days is depicted in Figure 43. As can be seen from the narrow curve, the casting process is very precisely controlled and hence the anode weight is very uniform. The casting velocity is approximately 50 t/h (since the changes in summer 2007 even slightly higher). Especially at the start of the casting process rejects are produced, namely the first 3–4 anodes are too heavy (> 10 kg above nominal value). Anodes with a weight deviation of more than 6–7 kg from the nominal weight are rejected.

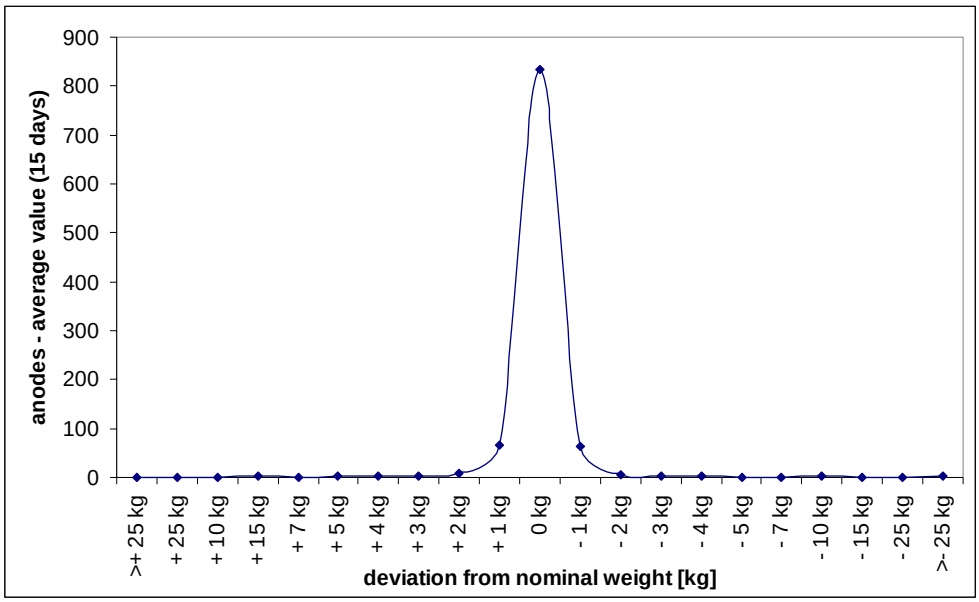

Figure 43: Average anode weight distribution (15 casting days)

The casting process is weight controlled (i.e., scales). Casting one anode takes 15 s, during which the casting velocity varies from slowly at the start, increasing to approximately 50 kg/s, and then slowing down. Turning the casting wheel from one position to the next takes 6 s. If necessary, the operator can manually vary the casting velocity. The filling level of the weighing trough is also considered, and hence the casting process is adjusted to its condition (e.g., condition of the refractories and crusts). The nominal anode weight can only be altered by using a corresponding access code to the casting control software.

The weighing trough is heated by a burner to avoid the formation of needle-like solidified copper, which would interfere with the weighing system. Additional burners, which are used as required, are directed at the anode surface and keep the copper liquid a little longer, so that the gases, which result from gassing of mould wash that has entered cracks in the mould, can escape from the liquid copper.

Typically, the anode moulds are produced from anode copper and cast at Montanwerke Brixlegg AG, whereby a negative model of the mould is used and a core is inserted for the future anode volume. Usually, one mould per day is changed. The moulds are not preheated before anode casting. Hence, the first anodes produced do not meet the quality requirements and are instantly recycled to the anode furnace.

Barite is used as the mould wash. The barite powder is delivered in big bags containing 1,000 kg each. One big bag is sufficient for 1.5–2 batches. The mould wash is prepared with drinking water, as water from the creek or recycling water cannot be used for this application. The mould wash is applied to the moulds automatically by 18 nozzles (Figure 44). A constant mould wash density should be ensured by density measurements, however these are not carried out regularly at the plant. The nominal mould wash density at Montanwerke Brixlegg AG is 1.3 kg/l, with the actual values ranging between 1.25 and 1.40 kg/l. After the automatic application, additional mould wash is applied manually to the lugs, around the push pins, and the sprue area. The mould wash for the following casting day is applied at the end of the casting process. The hot moulds are sprayed with mould wash, so that it burns-in the moulds. The amount of mould wash is judged visually by the workers.

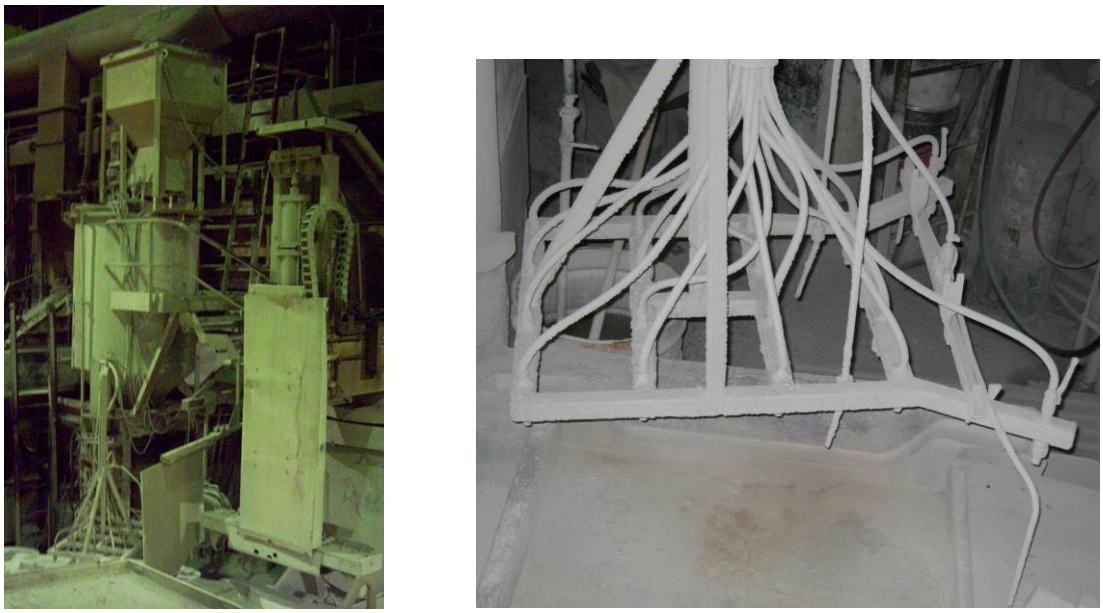

Figure 44: Automatic mould wash application

The anodes are cooled with water (spray cooling and cooling tank)—normally, recycled water from the anode furnace and only in exceptional cases, namely when the cooling effect is too low, with fresh water from the nearby creek. Due to the small casting wheel the water cooling starts very quickly after mould filling. The water spray cooling of the mould bottom underside starts three positions after filling (No. 8 in Figure 45) and ends two positions before take-off (No. 3 in Figure 45). At each position, two nozzles (Figure 46) are installed (except No. 3 in Figure 45, where 4 nozzles are located). After a solid surface has formed on the air side, it is water cooled at two positions with 4 nozzles (Figure 46). The used water runs off on the floor beside the casting wheel. The amount of cooling water used is not measured, but adjusted from experience. The water pressure is 5 bar.

In summer 2007, the bottom cooling arrangement was altered, as the investigations and measurements during this work had shown some optimization potential: Since then the cooling with 4 nozzles at each position starts at the first position after filling (No.10 in Figure 45) and ends at the automatic application of mould wash (No. 14 in Figure 45). The mounting of the moulds was also altered, so that only the outer supporting ring and a holder are used and not two concentric supporting rings (i.e., inner and outer). Before summer 2007 only a small portion of the mould underside was accessible for cooling due to the two supporting rings. However, due to the new mould mounting design, this area was increased.

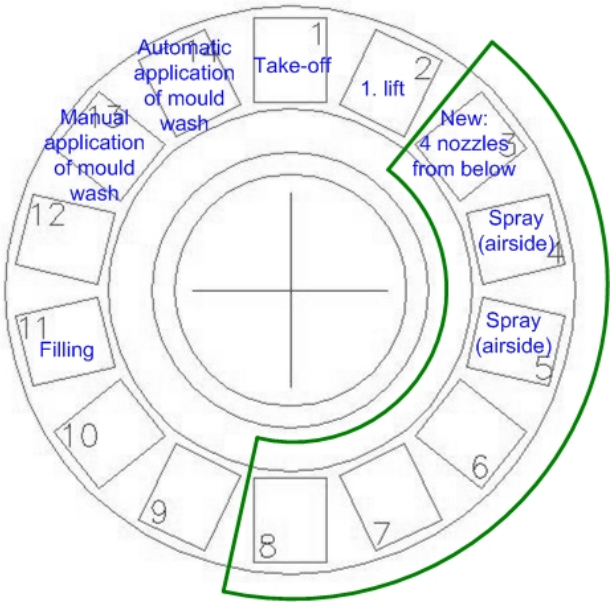

Figure 45: Casting wheel positions

Figure 46: Water spray cooling on the air side (left) and the mould bottom (right)

Problems due to nozzles blocking occur very often. It is important that the nozzles are clear and have sharp edges, so that the spray pattern and direction do not alter uncontrollably and the cooling effect is decreased. Nozzle blocking could be minimized by adequate water purification and filtration. The nozzle spray cones should overlap by ⅓–¼, as the amount of water applied decreases from the centre to the edge of the cone.

5.1.1 Cooling Water

The temperature and amount of the cooling water was measured on several days. Certain variations in temperature were detected (Figure 47 and Table 14), whereas the amount stayed relatively constant. With the cooling system changes in summer 2007, the cooling water consumption increased.

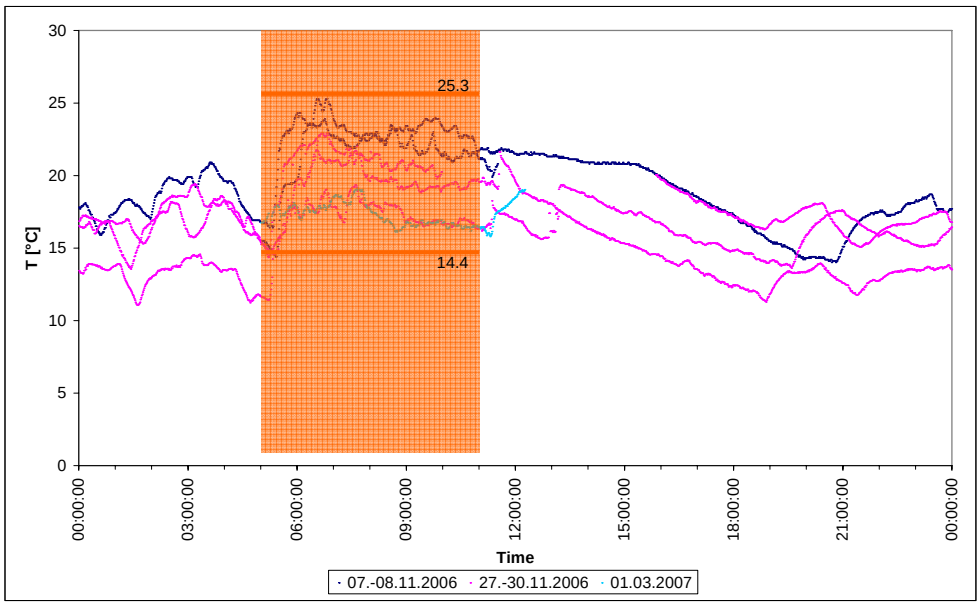

Figure 47: Cooling water temperature (shaded region marks the time of anode casting)

Table 14: Mean water temperatures and standard deviation during casting

Date	Mean value-casting [°C]	StDev casting
07.11.2006	22.35	2.24
08.11.2006	21.89	1.64
28.11.2006	19.32	1.63
29.11.2006	17.02	1.48
30.11.2006	20.69	1.46
01.03.2007	17.20	0.77

The water temperature changes over time can be explained by the fact that water recycled from cooling the anode furnace is used. However, only small fluctuations in temperature were registered during casting. Calculations of the heat transfer coefficient (HTC) for heat removal by spray cooling demonstrated that it did not vary significantly for water temperatures between 15 and 25 °C and remained in a feasible range for water spray cooling.

The amount of cooling water could not be recorded continuously, but was read and noted several times, approximately every 30 min, during casting. The flow of cooling water remained relatively constant at approximately 67 m³/h (new cooling arrangement: approximately 88 m³/h). This amount included two supply lines for the mould bottoms cooling (approximately 33 m³/h each) and one for spray cooling on the air side (approximately 1 m³/h). A variation and increase in the amount of cooling water is limited by the removal of used water and the pump.

Before the anode take-off a certain amount of cooling water remaining on the surface of the anode was visible. This is an indication of the Leidenfrost effect occurring, which leads to a

decreased cooling effect, as the heat transfer decreases significantly due to the formation of an insulating vapour layer between the hot surface and the cooling water droplets (Section 2.4) [85-87, 89, 90, 97].

However, the amount of remaining water on the anode surface was different from one casting day to another. This could have been due to different anode surface temperatures (due to different casting temperatures and/or anode cooling) or variations in the quality and amount of water used for spray cooling on the air side.

On the same casting day, the moulds with carbon black had larger amounts of remaining water than the moulds with barite (Figure 48). This can be explained by a higher heat flux to the mould due to the carbon black, which resulted in higher mould temperatures (Section 5.2.2) as well as lower anode temperatures, and hence less evaporation of the cooling water on the anode surface.

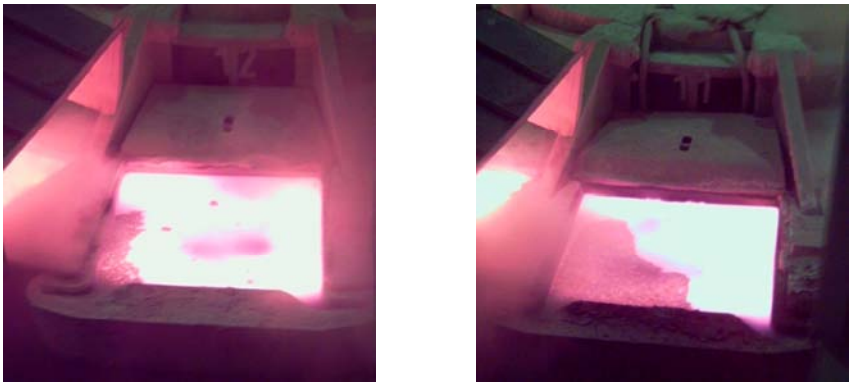

Figure 48: Remaining water on the anode surface with different mould washes (left: barite, right: carbon black)

5.1.2 Casting Temperature

The casting temperature of the liquid copper is not measured regularly or continuously at Montanwerke Brixlegg AG, but only judged visually. For the occasional measurements, which are carried out by the shift foreman, a pyrometer (ULTIMAX UX-20; IRCON, USA) is used. However, the accuracy of the measurements with the pyrometer is highly dependent on proper adjustment of the emissivity, ε, which is different for metallic copper and oxidized surfaces. In the pyrometer user manual, the following values for the emissivity are detailed:

- Planar unoxidized surfaces:
    - Cu: 0.10–0.20
    - Brass: 0.15–0.30
    - Bronze: 0.20–0.40

- Smooth oxidized surfaces:
    - Cu: 0.40–0.80
    - Brass: 0.50–0.80
    - Bronze: 0.50–0.80

Hence, incorrect readings occur if the emissivity of the measured spot is different from that it is adjusted against. In addition, dust and steam clouds influence the measurement. More accurate results were achieved using a thermocouple lance immerged in the liquid copper. However, a more effective method would be continuous infrared temperature measurement.

To detect the temperature loss during casting, the temperature was measured in the casting and weighing trough. These measurements were performed 3 times per casting day (i.e., start, middle, and end). The temperature trends varied from one casting day to the other, namely an increase with casting duration was observed as well as a relatively constant casting temperature. However, a temperature loss of approximately 20–40 °C occurred from the weighing trough to the casting mould, whereby this temperature difference decreased with casting duration.

Typical casting temperature measurements are detailed in Table 15. Multiple values in Table 15 are missing, as these temperatures could not be measured exactly with the pyrometer because of partly oxidized surfaces. The measuring error provided by the manufacturer for the respective methods used is low (i.e., thermocouples: ± 2.5 °C and pyrometer: ± 0.5% of reading), but as mentioned, the pyrometer measurement results are highly dependent on the settings and the actual measured surface (oxidized/non-oxidized), so that the results of the thermocouple measurements are more reliable.

The increase in casting temperature on certain days might have also caused the temperature increase in the moulds, which was detected in several measurements (Section 5.2). The differences in casting temperature and its influence on mould temperature also limited the comparability of the temperatures measured on different casting days, as not only the variation of process parameters but also differences in casting temperature have to be considered. However, due to technical issues the casting temperature was not routinely recorded during the course of the experiments.

Table 15: Typical casting temperatures (Py (0.15): Pyrometer (ε = 0.15), ThC: Thermocouple)

T [°C]	Time	Location			Method
Date		Launder	Casting trough	Weighing trough	
22.02.2007	Start of casting	1210			Py (0.15)
	Middle of casting	1182			Py (0.15)
	End of casting	1225			Py (0.15)
23.02.2007	Start of casting	1177			Py (0.15)
	Middle of casting	1183			Py (0.15)
	End of casting	1165			Py (0.15)
26.02.2007	Start of casting	1198			Py (0.15)
27.02.2007	Start of casting	1203			Py (0.15)
28.02.2007	Start of casting	1208			Py (0.15)
05.12.2007	09:30	1151	1141	1125	ThC
	09:30	1145			Py (0.15)
	11:45	1197			Py (0.15)
		1200			Py (0.15)
		1195			Py (0.15)
06.12.2007	05:30		1161	1122	ThC
	09:15		1167	1143	ThC
	09:20	1130 ± 3	1200 ± 10	1135 ± 5	Py (0.15)
	11:00		1166	1144	ThC
07.12.2007	05:40		1136	1105	ThC
	08:40		1172	1154	ThC
	11:00		1187	1168	ThC

5.1.3 Variation of Process Parameters

The variation of the process parameters (e.g., mould material, mould wash, and period of use of the mould) resulted in different mould temperatures and hence anode cooling conditions (Section 5.2). Besides these controlled parameters, some the following uncontrolled influences were determined that caused general quality variations between the anodes produced from one batch and within one anode:

- Casting temperature fluctuations
- Different mould wash densities
- Inhomogeneous mould wash application
- Different period of use of the mould/wear (e.g., cracks and limescale)
- Different mould material (i.e., anode copper batch from which the mould is cast)

5.2 Mould Temperature Measurements

In the following section, typical mould temperature curves are presented and discussed. The wave-like form of the curve represents the mould filling and anode take-off (Figure 49). Interruptions in the casting process, for example due to mould casting or problems with anode take-off, are also visible from the temperature curves. The sample anodes (i.e., anodes A–I) for the investigations were always taken 3 hours after the start of casting, namely in the middle of the casting process, to avoid temperature instabilities due to mould casting and initial heating-up of the moulds.

A typical temperature curve is depicted in Figure 49. In this figure, the temperatures measured simultaneously at the measurement points in the centre of the anode mould are presented, as the most homogeneous conditions were found there due to the absence of influences from the edges. Each peak represents the casting of one anode. The temperature difference between minimum and maximum temperature was approximately 70, 20, 10, and 60 °C for the measurements at a depth of 140, 100, 50 mm and on the surface, respectively. At the start of the casting process, the heating-up of the moulds from ambient temperature was visible. After approximately 1 h (or approximately 14 anodes), a steady temperature behaviour was reached in the mould. The mould casting, which interrupted the casting process, resulted in a short temperature drop, but the steady temperature conditions were re-established within 1 or 2 cycles, namely 1 or 2 anodes cast in the mould. A similar temperature decrease was caused by sticking anodes and corresponding problems with take-off, which led to a standstill of the casting wheel until the anode was removed manually, and hence a certain temperature loss from the mould occurred.

The temperature differences between the single cycles may have been caused by inhomogeneous mould wash application. Differences in water spray cooling should not have occurred during one casting day, as the cooling water was switched on at the beginning of the casting or after a few cycles and the amount of cooling water was not altered during casting. One exception was the complete turning-off of the water spray cooling when the mould temperatures were too low so that the mould wash did not dry before the mould was filled again.

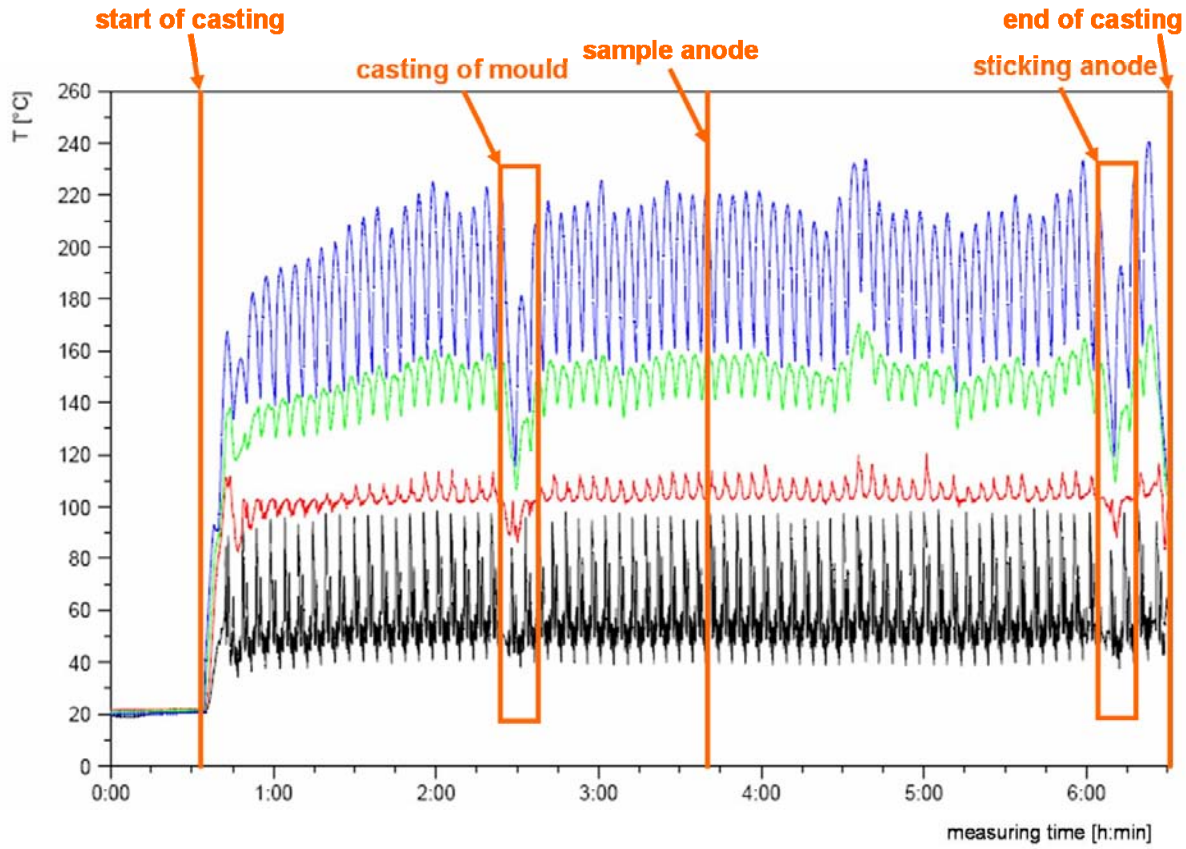

Figure 49: Typical temperature curve over the duration of the casting process—measurement points in the mould centre (blue: 140 mm, green: 100 mm, red: 50 mm, and black: surface)

As the casting temperature tended to increase towards the end of the casting process on certain casting days (Section 5.1.2), the increase in mould temperature can also be explained by the higher copper temperature. However, this increase did not occur on every casting day, and was also dependent on furnace operations (Figure 50).

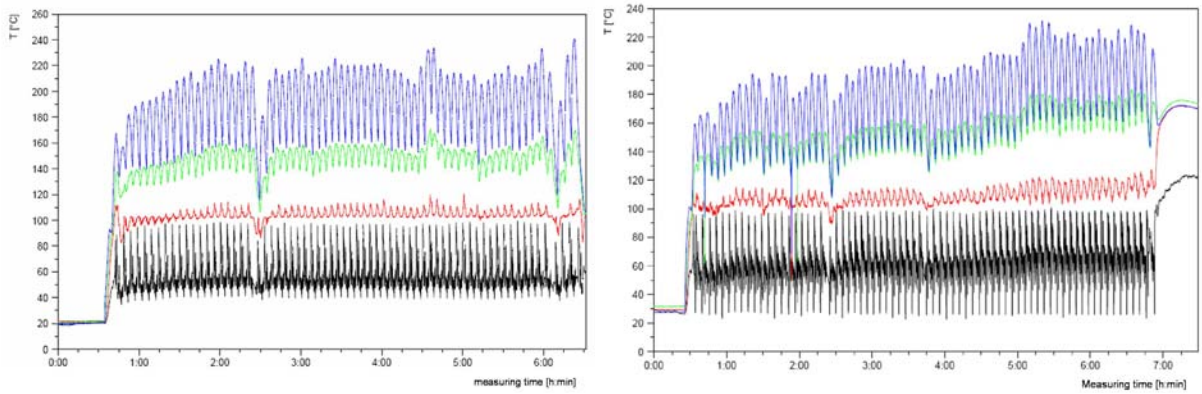

Figure 50: Comparison of temperature curves on different casting days—measurement points in the mould centre (blue: 140 mm, green: 100 mm, red: 50 mm, and black: surface; left: constant temperature conditions, right: increasing temperatures with casting duration)

The temperature variations over anode area are depicted in Figure 51. To improve data comparison, the upper (i.e., maximum temperatures) and lower (i.e., minimum temperatures) envelope curves are depicted, namely the range of temperature variations. The highest variations occurred for the surface temperature (top: approximately 40 °C, side: 70–80 °C, bottom: 50 °C, and centre: 60 °C) due to the direct contact between the mould and the cooling water. It is evident from these different temperature differences that the spray cooling was not homogeneous across the mould underside.

The 140 mm deep measurements showed similar fluctuations (top: 40 °C, side: 25–30 °C, bottom: 50 °C, and centre: 60 °C). As these measurement points were only 90 mm away from the mould curvature and hence the liquid copper, there were distinctive effects due to mould filling and anode take-off. The differences in temperature variations, namely smaller variations on the side and higher ones at the bottom and the centre, indicate different cooling in these areas. The temperatures and also the fluctuations on the side were lower. This could have been due to an influence from the edges of the mould. A similar situation may have occurred at the top, as these measurement points were also relatively close to the edge of the mould.

The smallest variations were found for the 50 and 100 mm deep measurements (approximately 20 and 30 °C, respectively), as there was a certain distance from the bottom cooling as well as the liquid copper, and the temperatures in this region of the mould were more homogeneous and did not change as much as in the outer areas.

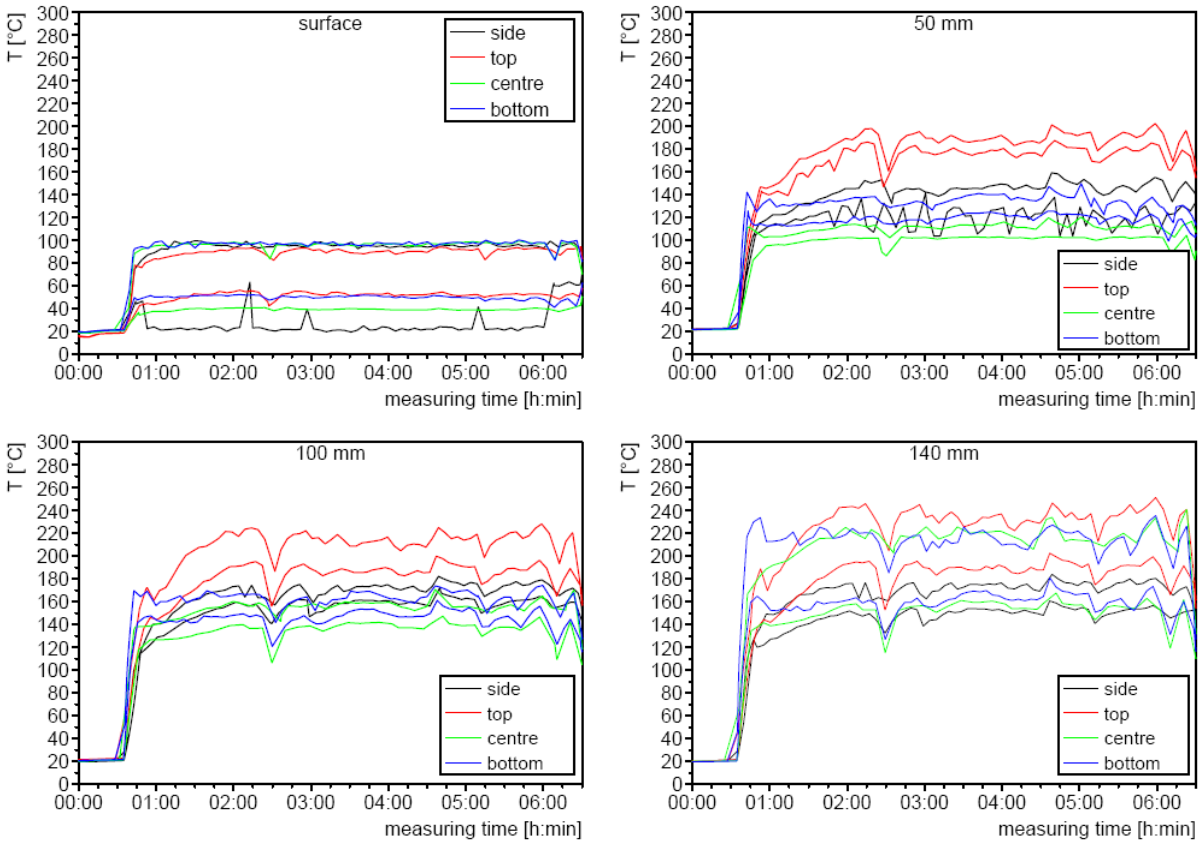

Figure 51: Temperatures over anode area (new anode copper mould)—envelope curves

The temperature variations and the mean temperatures at the different positions and depths on the casting days of anode B–I are listed in Table 16 and Table 17.

Table 16: Mean mould temperature differences for different positions and depths on the casting days of anodes B–I (-: not measured, *: measurement failure)

Mean Δ T [°C]		**Anodes**							
Depth	**Position**	**B**	**C**	**D**	**E**	**F**	**G**	**H**	**I**
0	Side	-	-	75	80	-	60	30	60
0	Top	-	-	40	50	-	40	40	50
0	Centre	-	-	60	55	-	60	75	60
0	Bottom	-	-	45	45	-	55	70	50
50	Side	-	-	25	70	-	30	10	25
50	Top	-	-	10	25	-	30	20	45
50	Centre	-	-	10	20	-	15	15	20
50	Bottom	-	-	16	20	-	15	20	10
100	Side	10	10	13	20	10	15	15	25
100	Top	15	65	30	40	10	25	15	30
100	Centre	20	25	20	20	20	30	20	40
100	Bottom	20	20	15	20	20	30	10	20
140	Side	20	20	20	20	20	20	15	25
140	Top	50	15	45	50	30	*	*	40
140	Centre	30	45	60	60	40	55	60	55
140	Bottom	40	45	50	80	30	45	35	40

Table 17: Mean mould temperatures for different positions and depths on the casting days of anodes B–I (-: not measured, *: measurement failure)

Mean T [°C]		Anodes							
Depth	**Position**	**B**	**C**	**D**	**E**	**F**	**G**	**H**	**I**
0	Side	-	-	70	84	-	75	78	66
0	Top	-	-	71	74	-	72	59	62
0	Centre	-	-	60	69	-	53	64	64
0	Bottom	-	-	69	78	-	66	61	63
50	Side	-	-	136	161	-	131	137	130
50	Top	-	-	182	229	-	148	161	135
50	Centre	-	-	105	114	-	106	109	116
50	Bottom	-	-	127	149	-	133	120	102
100	Side	170	175	163	210	215	146	159	142
100	Top	225	143	202	244	232	181	183	160
100	Centre	184	186	149	176	201	144	154	155
100	Bottom	200	196	156	192	219	174	146	135
140	Side	202	177	164	215	217	165	174	148
140	Top	255	191	214	266	244	*	*	192
140	Centre	220	215	193	222	228	174	180	191
140	Bottom	222	232	193	233	225	185	174	169

The temperature differences between subsequent days with similar casting temperatures were not larger than the temperature fluctuations within one casting day (Figure 52).

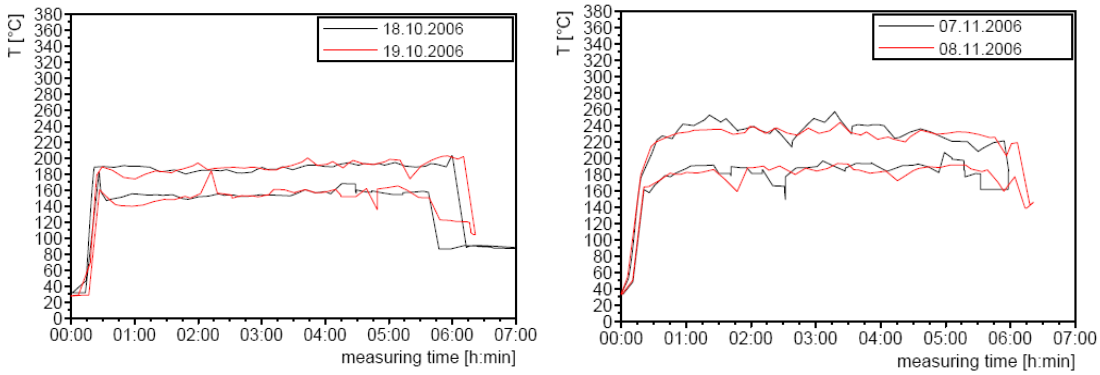

Figure 52: Temperature curves of subsequent casting days in same mould (centre, 140 mm)

The time between mould filling and reaction of the temperature measurement, namely temperature increase, at the position "top 140 mm" was measured several times and was approximately 34 s. According to the manufacturer's information, the response time of the thermocouple, namely the time required to detect 50 and 90% of the difference of a temperature change, was < 2.5 and < 5.9 s in water (0.2 m/s), respectively.

In December 2007 an additional continuous, infrared surface temperature measurement (Figure 53) was installed, which measures the side surface temperature of the mould after the cooling positions (i.e., position No. 3 in Figure 45). The temperatures detected with the

infrared system before the start of casting and during the first cycles, where no water cooling was applied, showed good agreement with the surface measurements recorded with the measurement system, namely approximately 25 °C for ambient temperature and approximately 100 °C in the first cycles. After starting the water cooling, the surface temperature on the bottom of the mould (maximum approximately 100 °C) was approximately 70 °C lower than the temperature on the side (approximately 170 °C ± 30 °C, depending on the individual mould).

Figure 53: Infrared mould surface temperature measurement

5.2.1 Influence of Mould Material and Mould Design

Due to the different material properties, for example thermal conductivity, the solidification and cooling conditions can be influenced by the mould material. Geometric changes of the mould also affect the cooling conditions due to different amounts of surface exposed to the cooling and hence different heat transfer. In the future, optimization of the geometry should be carried out by simulation, namely using the developed model (Chapter 6) instead of by trial and error.

Improvements regarding material and design of the mould should not only influence the anode cooling conditions, but also decrease the tendency for crack formation in the mould especially due to thermal shock and hence increase the mould life. The areas most likely to be damaged are the sprue area and around the push pins (Figure 54). The tendency for crack formation is also linked to the oxygen content of the copper used to cast the mould (Section 2.1.1.1).

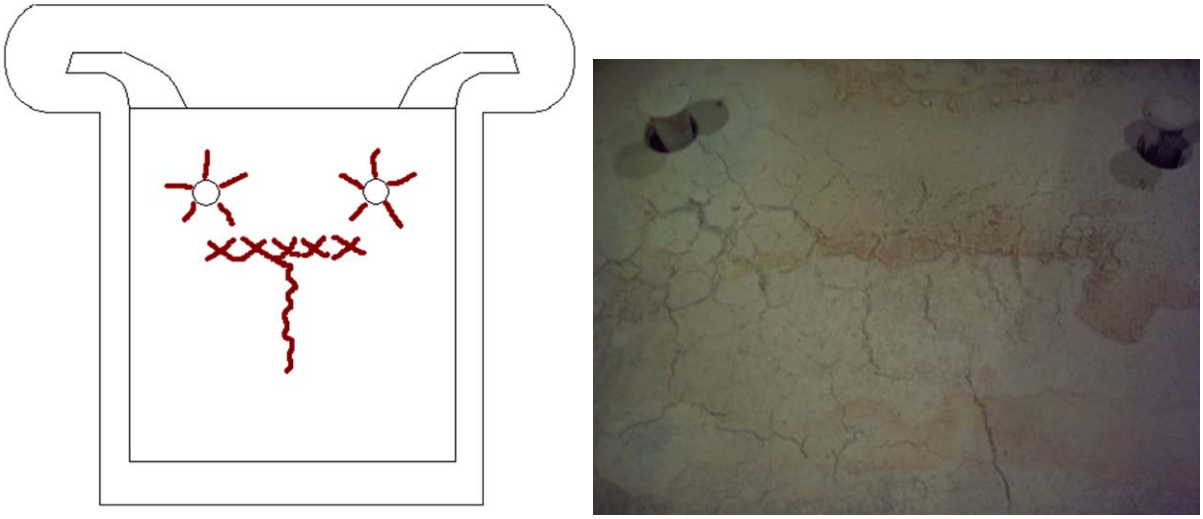

Figure 54: Crack formation in an anode mould—left: schematic, right: mould at the end of life

In general, the temperature differences between different depths was smaller in the moulds manufactured from cathode copper than in the anode copper moulds, namely approximately 60 °C and approximately 25 °C between the measurements at 140 and 100 mm deep in the anode copper and cathode copper moulds, respectively (Figure 55). This indicated a better, more homogeneous heating of the cathode copper mould, which may also be the reason for the delayed crack formation and finally the longer mould life compared to the anode copper mould. As the moulds were measured simultaneously, namely on the same casting day, an influence due to different casting temperatures on different days could be excluded. Higher temperatures and larger temperature variations between mould filling and take-off were visible for the anode copper mould compared to the cathode copper mould. The lower temperature of the latter can be explained by the higher thermal conductivity, which also led to a higher cooling effect.

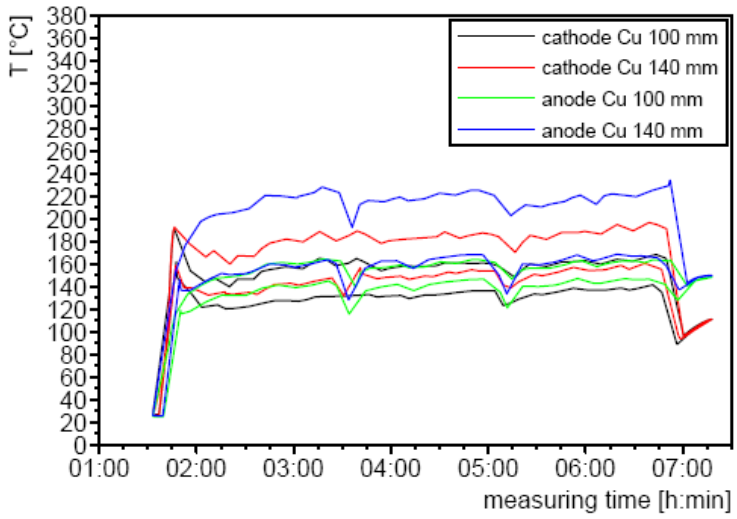

Figure 55: Temperatures in new anode and new cathode copper moulds on the same casting day (centre, 140 mm)

However, there were specific differences in chemical quality and hence also in material properties between the different anode copper moulds, depending on the batch from which they were cast. Former investigations and also in-service results have shown that the chemical composition has an influence on both the mould life and the mould temperature [113].

The trend that cathode copper moulds stay cooler during casting was confirmed by the infrared mould surface temperature measurements on two different casting days with 1 cathode copper and 13 anode copper moulds in the casting wheel (Figure 56). The light blue and pink bars and plateaus of the curves in Figure 56 indicate the measurement of the mould surface temperature, namely the time when the mould was in the measuring position. The time span between the bars, namely the narrow peaks between the plateaus, represents the time in which the wheel was turned to the next position. The position of the cathode copper moulds was marked during the measurements, so that each temperature plateau of the curve could be associated with a specific mould.

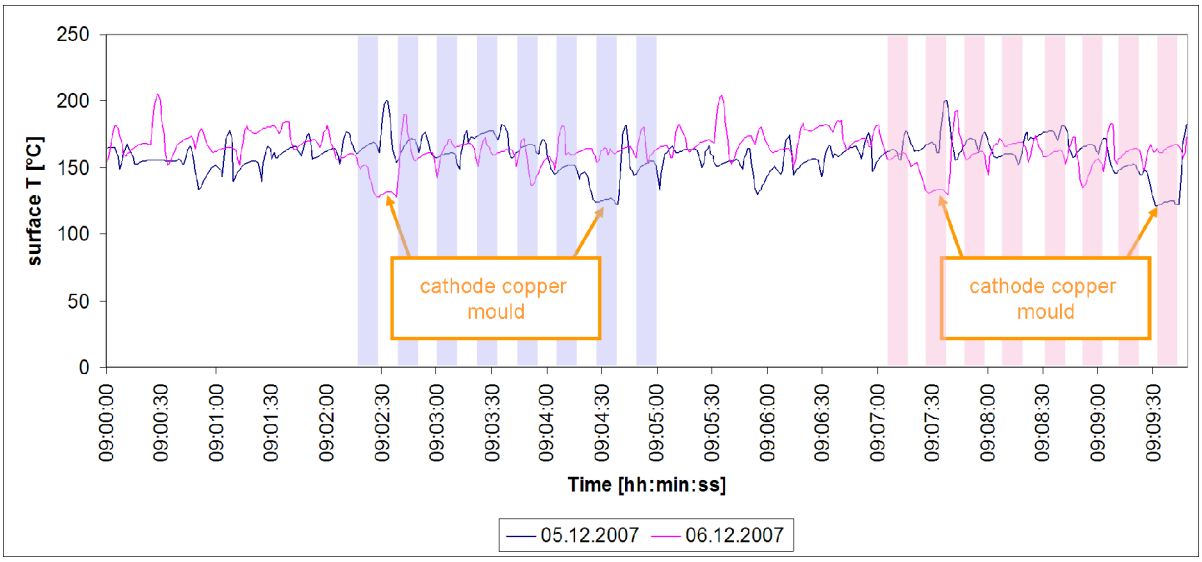

Figure 56: Surface temperature of moulds on two different casting days for a casting wheel comprising 1 cathode copper and 13 anode copper moulds

Another possibility to influence the anode cooling and solidification conditions is the use of moulds with cooling ribs across the bottom, which result in a larger cooling area. Three different types of cooling ribs were tested in moulds made of anode copper (Table 18, Figure 57, and Figure 58).

Table 18: Moulds with cooling ribs

Mould	Type of cooling ribs	Mould life [casting days]
Mould 1	5 deep longitudinal indentations	26
Mould 2	Diagonal grooves	7
Mould 3	Round indentations	22

Figure 57: Cooling ribs of mould 1, 2, and 3

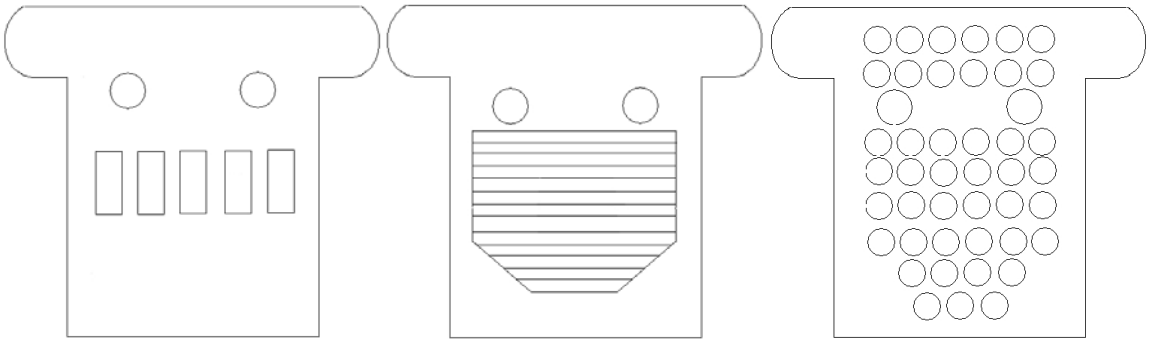

Figure 58: Schematic diagram of the cooling rib design of mould 1, 2, and 3

The temperatures measured in these moulds are shown in Figure 59 and it is evident that the temperatures in mould 1 (black curve) were the lowest. The peak near the middle of the measuring time resulted from a complete turning-off of the water cooling, as the mould temperature was so low that the mould wash did not dry before the next mould filling. Subsequently, the temperatures were only a little higher; however this small temperature increase was sufficient to avoid water deflagration and assure safe casting conditions.

The temperatures in mould 2 (red curves) and 3 (green curves) were not lower than in normal anode copper moulds (blue curves). However, after the trials with these moulds, the mould type 2 was set as standard mould design at Montanwerke Brixlegg AG since it is the most appropriate design for bulk manufacture. The mould life of mould 2 detailed in Table 18 is unrepresentative of this design as according to information from Montanwerke Brixlegg AG other moulds of this type have a longer mould life.

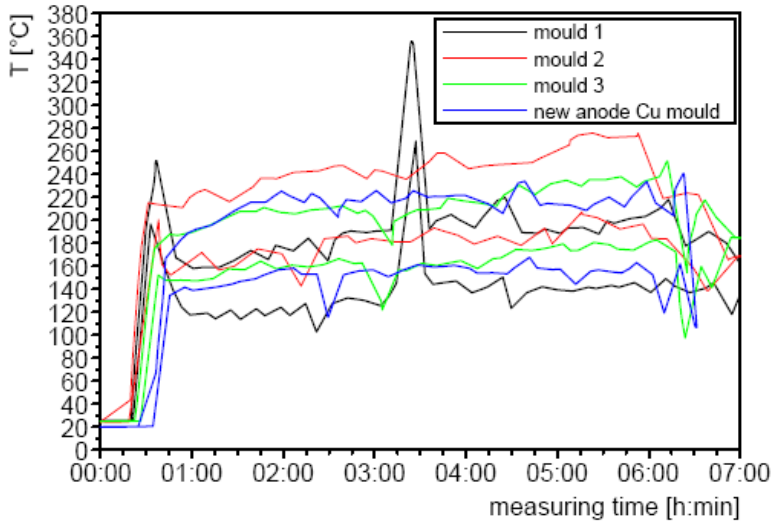

Figure 59: Comparison of moulds with cooling ribs—anode copper mould (centre, 140 mm)

5.2.2 Influence of Mould Wash

The trials with carbon black as a mould wash were performed in collaboration with Linde Gas (Stadl-Paura, Austria). These experiments were carried out to provide data for investigating the effect of higher mould temperatures and altered cooling conditions on anode quality.

The temperatures were compared to those of the previous day (i.e., first casting day of the mould) and to those of new anode copper moulds on other casting days. The carbon black was applied by means of an acetylene burner (Figure 60) and resulted in significantly higher mould temperatures (Figure 61) due to a higher heat flux into the mould. Hence, it had the same effect as mould preheating. The higher temperatures lead to a smaller temperature gradient that had a significant effect regarding the solidification structure and dissolution behaviour (Section 5.4 and 5.5).

One advantage of using carbon black instead of barite is that there are no adhering barite particles on the anode and hence no barite transferred to the tankhouse. However, the trials showed that barite has to be applied to the areas around the push pins, as barite acts as a sealing for the slit between the push pins and the mould, so that no copper can enter at this point and cause anode sticking.

Figure 60: Acetylene burner (left) and trials (right)

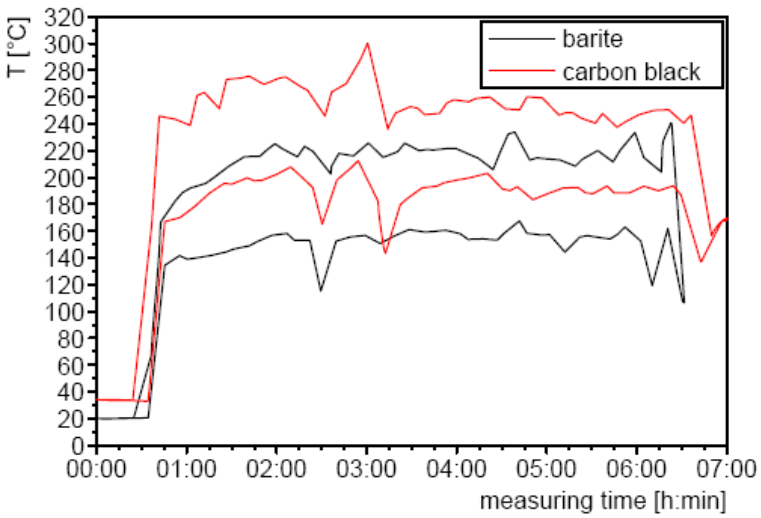

Figure 61: Effect of mould wash (centre, 140 mm)

5.2.3 Influence of Period of Use of the Mould

An increase in mould temperature with period of use of the mould was found (Figure 62). This may have resulted from the build-up of an insulating limescale on the underside of the mould bottom (Figure 63) due to the precipitation from the cooling water. The temperature differences between the 13th and 30th casting day were in the range of the observed casting temperature differences, but the increase by approximately 80 °C between the 1st and 30th casting day could not be explained by a variation in casting temperature.

In general, the mould life at Montanwerke Brixlegg AG varies significantly due to the different time span until crack formation occurs in the mould curvature, especially in the sprue area and around the push pins. The average lifespan of the cathode copper mould was higher than that of the anode copper mould (35 vs. 27 days).

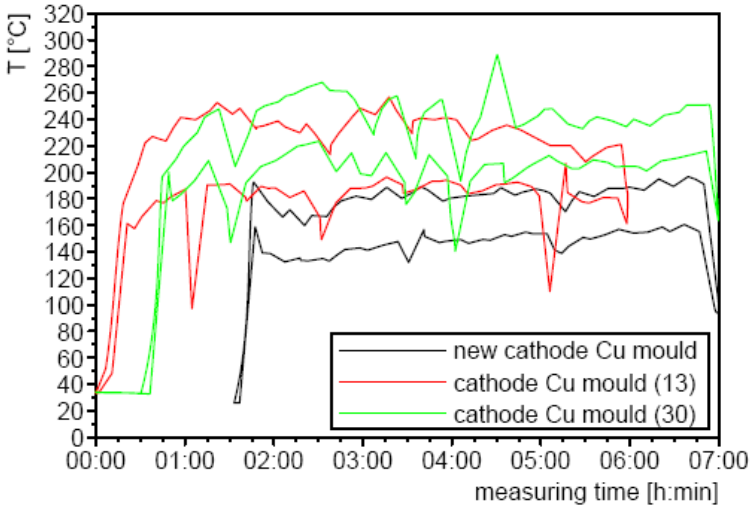

Figure 62: Influence of period of use of the mould (centre, 140 mm)

Figure 63: Anode copper mould—left: new mould, right: after 27 casting days—limescale on the bottom underside

5.2.4 Influence of Casting Temperature

The measurements of the casting temperature variations during one casting day indicated an influence on mould temperature, as described above (Section 5.1.2). The variation in casting temperature was as high as approximately 40 °C during one casting day, especially when the casting temperature was relatively low in the beginning, but normally a temperature variation of ± 10–15 °C was detected (measurements with thermocouples). However, these were only punctual measurements. A continuous measurement of the casting temperature would provide more information about the casting temperature trends and a better correlation with the mould temperatures.

5.2.5 Influence of New Cooling Arrangement at Montanwerke Brixlegg AG

The new cooling arrangement (i.e., more positions and modified nozzle number—Section 5.1) caused higher water consumption, as previously described. However, no significant differences in mould temperatures were detected (Figure 64). This cannot be explained by a higher casting temperature on the days where the measurements with the new cooling system were performed, as the casting temperature on these days was not extraordinary high (Section 5.1.2). The measurements points on the surface indicated a better coverage of the mould bottom by the spray cooling, as the temperature of the mould surface remained cooler and more homogeneous.

These measurement results are contradictory to personnel observations that the intense mould cooling led to problems with the drying of the mould wash before filling because of the low mould temperatures and also to the simulation results (Section 6.2).

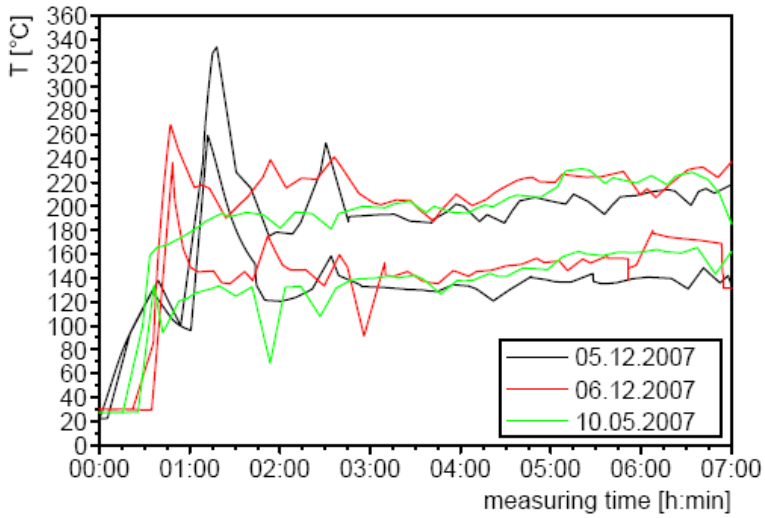

Figure 64: New cathode copper moulds (01.05.2007: old cooling arrangement, 05./06.12.2007: new cooling arrangement) (centre, 140 mm)

The anode samples, which were taken from the anode moulds where the measurement system was installed so that their cooling conditions were known, where analysed regarding their chemical and physical quality, in order to establish, if and to what extent the different cooling conditions had an effect on the anode quality.

5.3 Chemical Analysis of the Anodes

The chemical analysis across the anode thickness and anode area, as well as the type and distribution of inclusions were found to be relatively homogeneous. This might be due to the relatively fast anode cooling at Montanwerke Brixlegg AG. The use of gas purging in the anode furnace should also ensure a constant copper composition within one batch.

5.3.1 Elemental Concentrations

The batch analysis (sample "AnodCu") of all investigated anodes, where temperature measurements were also performed, is provided in Table 19. The maximum and minimum values are highlighted in orange and blue, respectively.

Table 19: Batch analysis of all investigated anodes

Anode	[wt.%]								[ppm]				
	Cu	Ag	O	Ni	Pb	Sn	As	Sb	Fe	Zn	Bi	Te	Se
A	98.90	0.050	0.22	0.57	0.16	0.04	0.01	0.03	18	25	17	17	13
B, C	99.01	0.034	0.15	0.47	0.13	0.06	0.02	0.02	50	88	12	26	12
D	99.18	0.030	0.04	0.45	0.12	0.05	0.01	0.02	32	50	24	30	13
E	99.20	0.028	0.11	0.39	0.10	0.03	0.01	0.03	18	26	20	30	13
F	99.27	0.029	0.06	0.39	0.09	0.02	0.01	0.03	25	45	41	32	13
G	99.08	0.043	0.04	0.53	0.11	0.06	0.01	0.02	49	131	15	10	10
H	99.41	0.036	0.05	0.23	0.10	0.03	0.01	0.02	20	165	15	18	12
I	99.01	0.029	0.06	0.41	0.30	0.04	0.01	0.03	22	102	15	12	12

In general, deviations between the batch analysis and spark spectroscopy measurements of the anode samples were found (Figure 65). The analysis of the slices also showed higher values for the Cu concentration, but the relative differences for Cu were only in the range of - 0.03 to - 0.3 wt.%, and hence not shown in Figure 65.

The measurement error of spark emission spectroscopy is dependent on proper calibration. The measuring device at the Montanwerke Brixlegg AG laboratory, where the analyses for this work were carried out, is calibrated regularly to provide the required accuracy for the smelter and foundry batch analysis.

The deviations, which have also been described in previous investigations at Montanwerke Brixlegg AG [84], could be explained by the method used for the chemical analysis. Both the batch analysis and the analysis of the slices were performed with spark emission spectroscopy. However, this method that uses an average value of all measurements is susceptible to inclusions. Hence the analysis is also dependent on the number of measurements per sample. However, as all the samples from Montanwerke Brixlegg AG were measured with the same equipment, the results are comparable. Another reason for the deviation between batch and sample analysis could be a change in copper composition between the batch analysis, which is taken directly from the furnace, and removal of sample anode, for example due to additional charging or inhomogeneities due to non-perfect bath mixing. The time point at which the batch sample was analysed was not the exact point at which the sample anode was cast.

However, the copper composition over the casting duration was relatively constant on the days when anode samples were taken (Section 5.3.1.1).

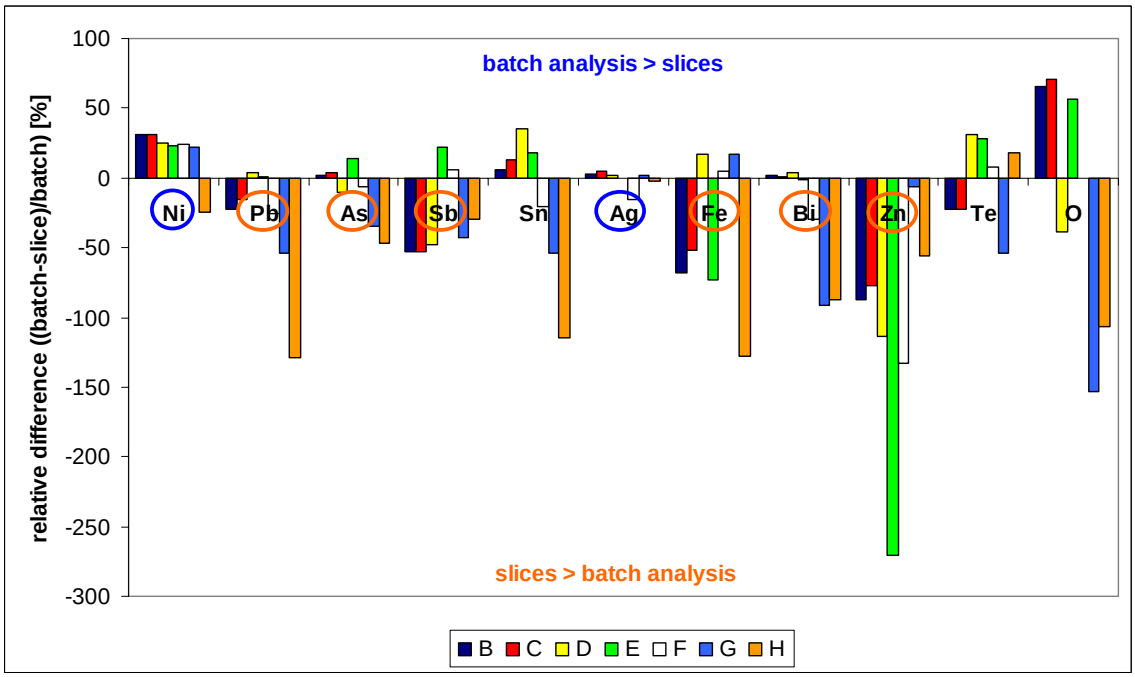

Figure 65: Differences between batch and slice analyses

The use of carbon black as mould wash, which produced a more homogeneous and to a greater extent globulitic structure (Section 5.4) also resulted in an even more homogeneous elemental distribution across the anode area and thickness (Section 5.3.1.2 and 5.3.1.3)

5.3.1.1 Chemical Composition during Casting

The chemical composition of the anode copper during casting was analysed every hour to investigate compositional variations within one batch (Figure 66). The implementation of gas purging in the anode furnace ensures a constant anode copper composition during casting. The reported varying metal composition (e.g., Pb and Ni content variations of up to 30% and 20%, respectively [42]) between the first and last amounts of molten copper poured from the anode furnace was not found.

Compared to data before the implementation of gas purging a significant improvement in chemical quality during the casting process, namely within one batch, has been seen. The variation of analysis especially decreased for Ni, Sn, Zn, and Fe within the batches as the gas purging improves melt homogenization. The variation expressed as the average of the absolute relative deviation of batches without and with gas purging was for Sn: 94% → 26%, Zn: 145% → 51%, and Fe: 116% → 41%. Thus the variation has been decreased by a factor of 3 to 4 [41].

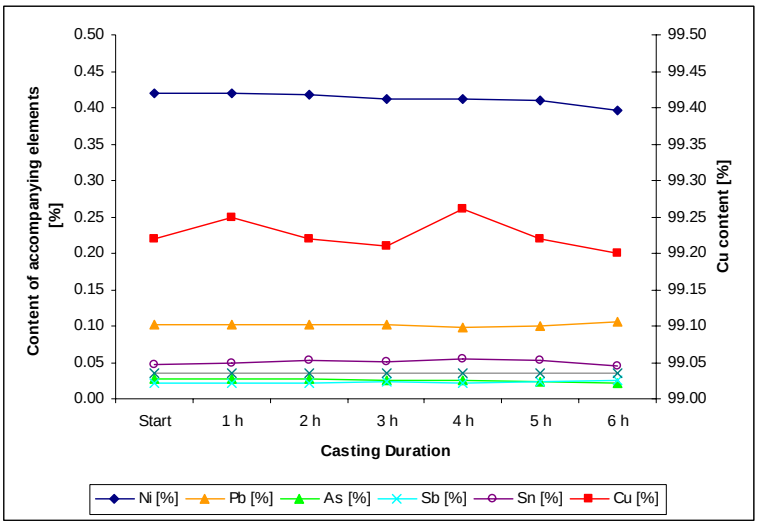

Figure 66: Variation of chemical composition during casting

5.3.1.2 Chemical Composition across the Anode Thickness

The elemental distribution across the anode thickness for different cooling conditions is depicted in Figure 67–Figure 70. As no definitive inhomogeneities were found over anode area (Section 5.3.1.3), the results for the anode centre are presented. The dotted lines represent the average analysis of the anode sample, and the solid lines the mean value of the chemical analysis of each slice. The standard deviation of the measured values is also indicated. It can be seen that the variation of the elemental concentration is in the range of the standard deviation. Contrary to the literature [17, 18, 28, 51, 53], which describe a significantly uneven elemental distribution due to the different distribution coefficients of the elements, a relatively homogeneous composition across the anode thickness was detected, independent of the mould material used. This could be due to the generally rapid anode cooling at Montanwerke Brixlegg AG. It has to be noted, that the very surface of the air side could not be measured by spark emission spectroscopy. As described in Section 5.3.2 and 5.4.2, a thin oxide layer (approximately 100–1,000 µm) was detected on the air side. As the thickness of this layer was smaller than the surface unevenness of the air side, this area had to be removed for the spark emission spectroscopy measurements, which require a flat surface.

A general difficulty is measuring the oxygen content. An analysis by LECO (LECO, Mönchengladbach, Germany) requires drilling chips out of the sample, which can cause a certain degree of oxidation. Hence, the oxygen content was also measured by spark emission spectroscopy. As all the samples from Montanwerke Brixlegg AG were measured with the same equipment, the results are comparable. The oxygen content detailed in the following sections is the total oxygen content, namely it includes both dissolved oxygen and oxygen in the form of oxides. As each slice was analysed by multiple sparks, those, which

were located directly at an oxidic inclusion could be clearly identified by high oxygen levels (visible in Figure 70—¼ thickness).

The use of carbon black as mould wash (Figure 68) resulted in even smaller deviations in the chemical composition across the anode thickness. No definite trend for the general behaviour of the different elements was found. This agrees with the inconsistent results of former investigations, which also compared anodes from different copper smelters [82, 84].

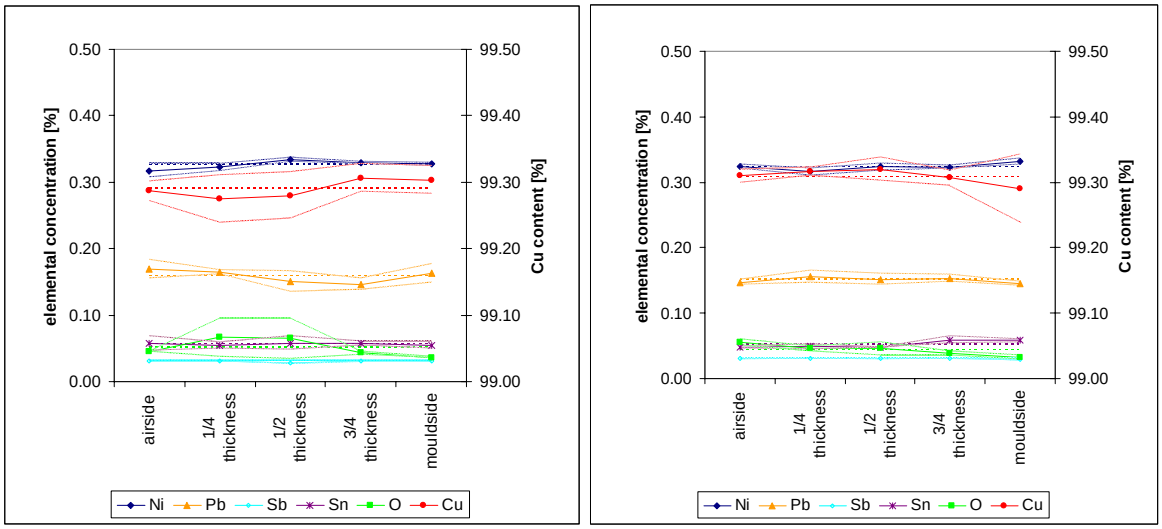

Figure 67: Elemental distribution across the anode thickness in anode B (left) and C (right)

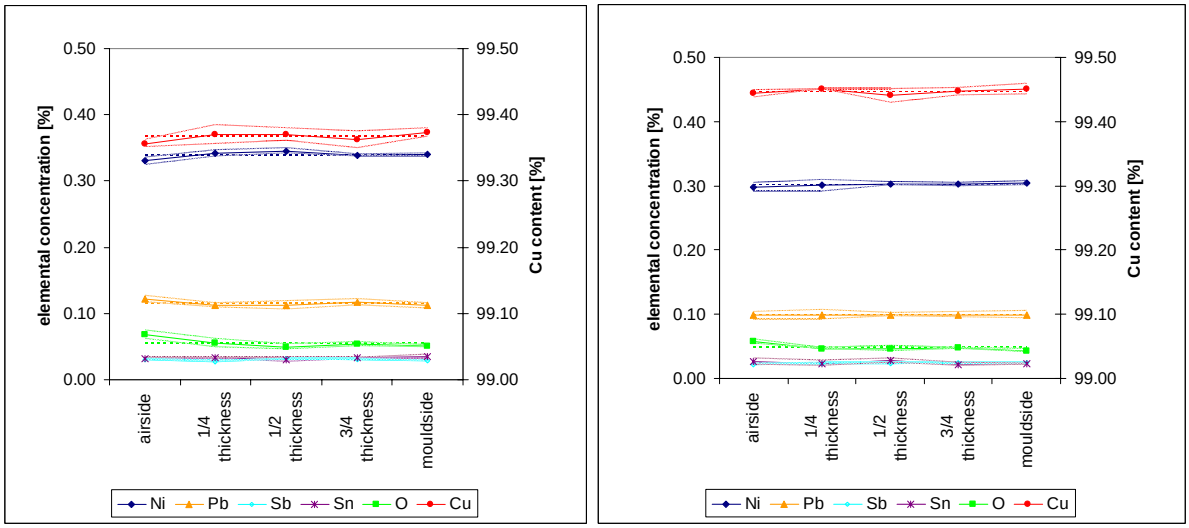

Figure 68: Elemental distribution across the anode thickness in anode D (left) and E (right)

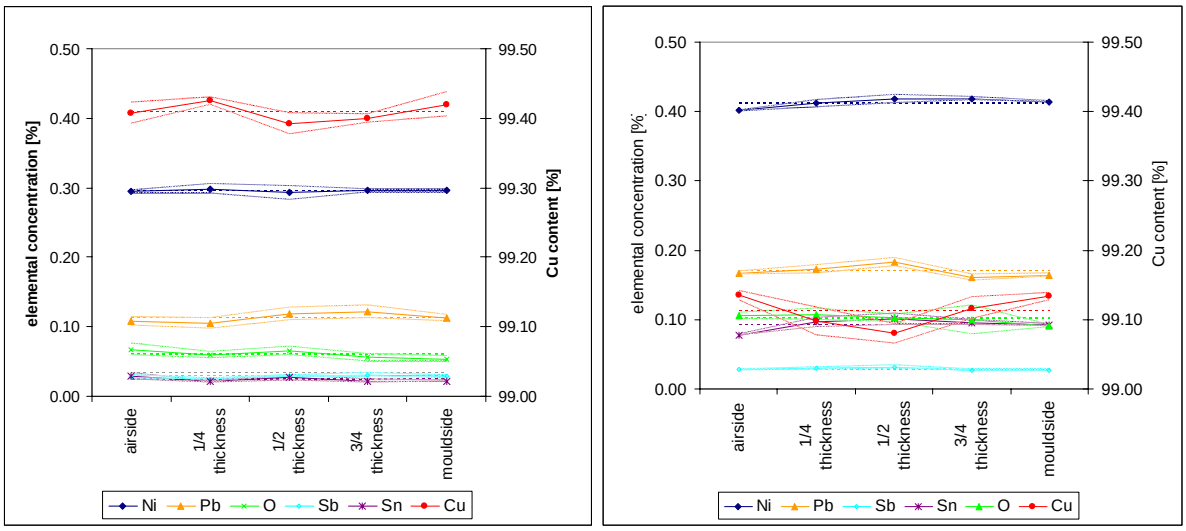

Figure 69: Elemental distribution across the anode thickness in anode F (left) and G (right)

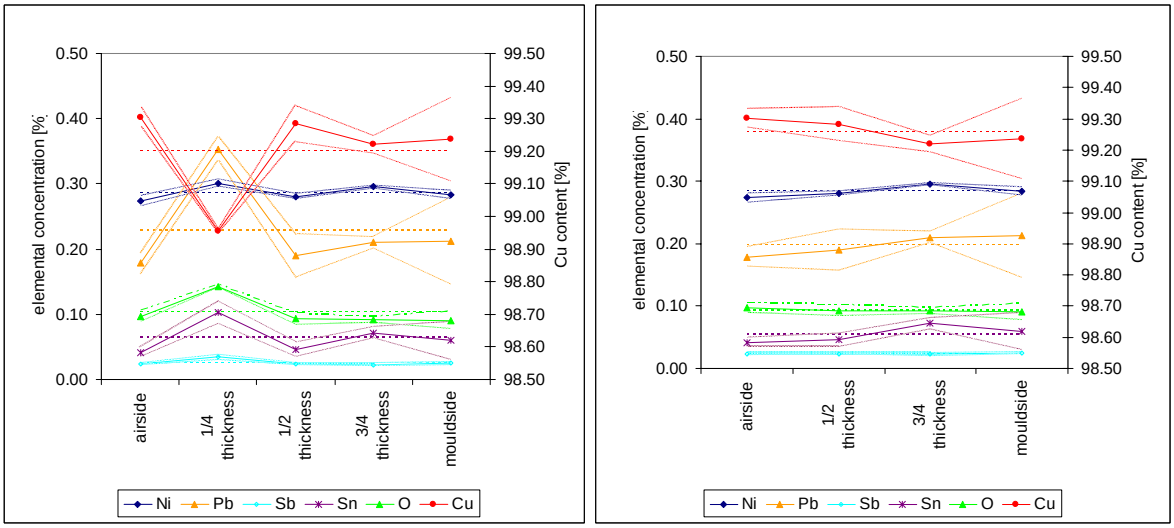

Figure 70: Elemental distribution across the anode thickness in anode H (left) and H without measurement at ¼ thickness (right)

When compared with CONTILANOD® anodes the investigated anodes were relatively homogeneous, as described in the following sections. A quantitative overview of the elemental distributions is provided at the end of this section. Elemental distributions in CONTILANOD® anodes (measurement points are depicted in Figure 71) from the Gresik smelter, Indonesia, are shown in Figure 72–Figure 74.

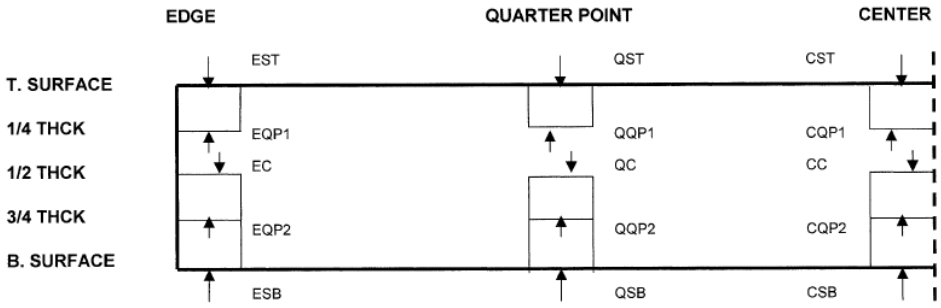

Figure 71: Anode samples from CONTILANOD® anode [44, 114]

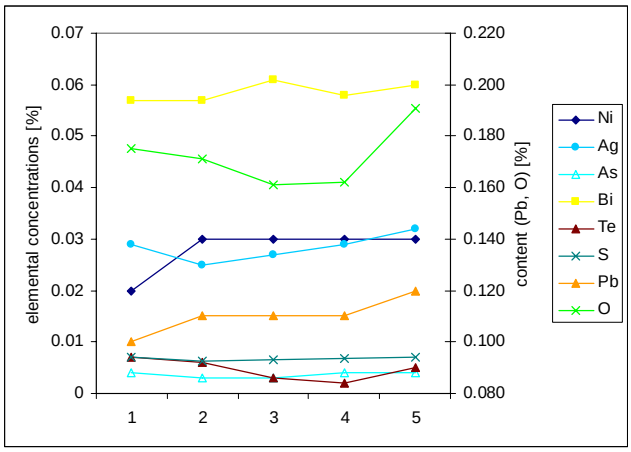

Figure 72: Elemental distribution in CONTILANOD® anode—edge [44, 114]

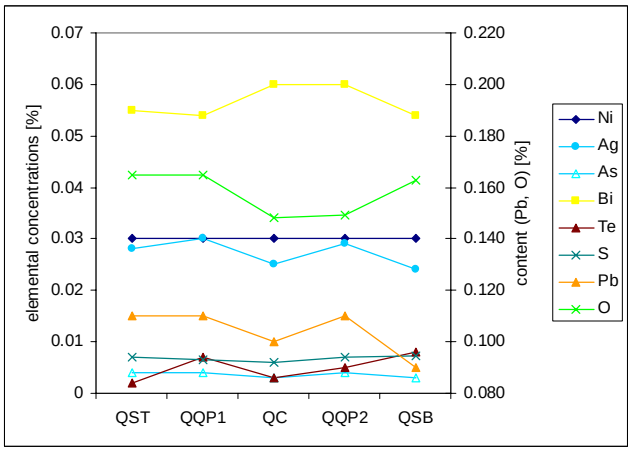

Figure 73: Elemental distribution in CONTILANOD® anode—quarter point [44, 114]

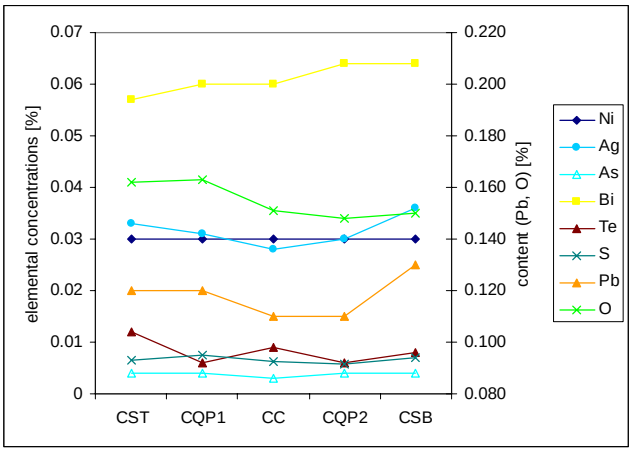

Figure 74: Elemental distribution in CONTILANOD® anode—centre [44, 114]

The elemental distributions in two other CONTILANOD® anodes (A and B) from IMI, UK, are depicted in Figure 75 and Figure 76. Both CONTILANOD® anodes were described as showing no significant segregation across the anode thickness, namely from top (sample 1-T) to bottom (sample 6-B), in the corresponding report, which also stated that the possible pattern of segregation visible in the graphical representations that seems similar for all elements may still be regarded as not significant as far as cathode quality is concerned. Anode A is a typical CONTILANOD® anode as described in the literature with a fine globulitic structure, whereas anode B has a cast structure (Section 2.1.2) [44]. It can be seen that a cast structure does not imply an uneven elemental distribution. A comparison of the elemental distribution in these two CONTILANOD® anodes between the edge and centre is provided in Figure 77 and Figure 78.

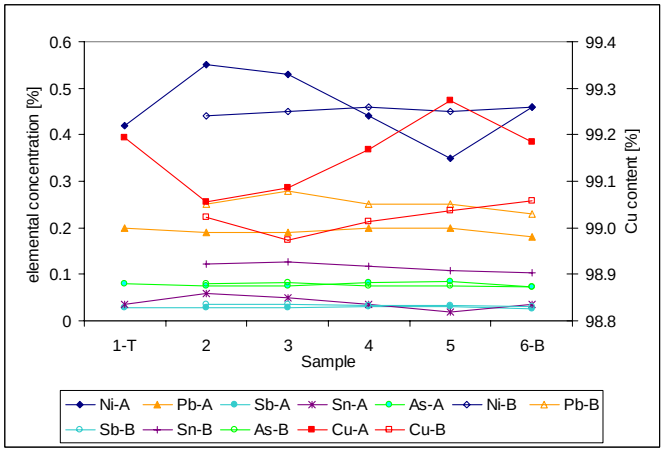

Figure 75: Elemental distribution across the anode thickness in the centre of the CONTILANOD® anodes (A and B) (values from [44])

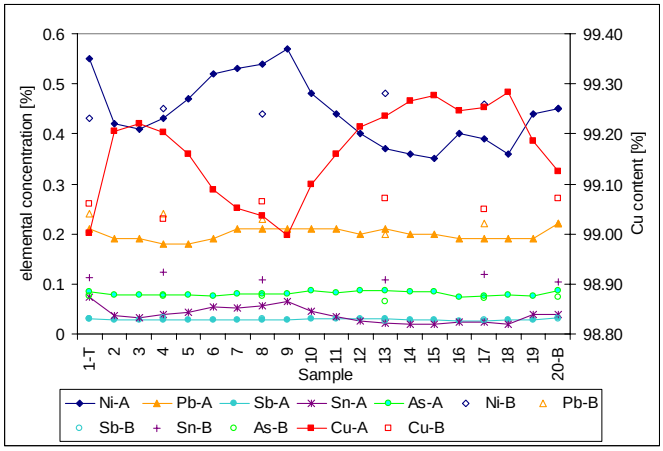

Figure 76: Elemental distribution across the anode thickness at the edge of the CONTILANOD® anodes (A and B) (values from [44])

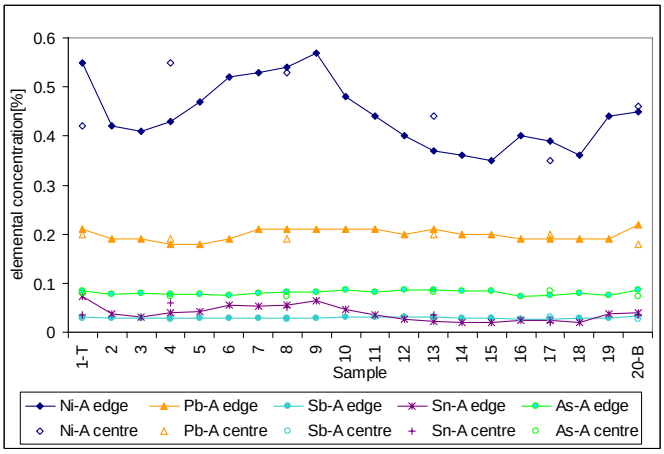

Figure 77: Comparison of elemental concentrations at the centre and edge of CONTILANOD® anode A (values from [44])

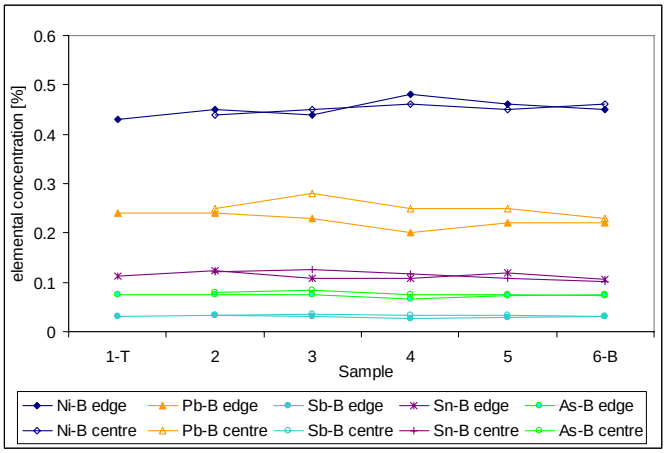

Figure 78: Comparison of elemental concentrations at the centre and edge of CONTILANOD® anode B (values from [44])

The absolute differences in elemental concentrations between the highest and lowest levels measured across the anode thickness are provided in Table 20. The maxima are highlighted

in orange. It can be seen that the analysed samples from the Brixlegg casting wheel anodes do not show higher variations than CONTILANOD® anodes.

Table 20: Absolute differences in elemental concentration across the anode thickness

Absolute difference (max-min)	[wt.%]								[ppm]				
Anode	**Cu**	**Ag**	**O**	**Ni**	**Pb**	**Sn**	**As**	**Sb**	**Fe**	**Zn**	**Bi**	**Te**	**Se**
B	0.032	0.005	0.030	0.016	0.022	0.003	0.004	0.003	20	49	3	10	2
C	0.030	0.003	0.023	0.016	0.011	0.012	0.002	0.002	27	38	1	6	1
D	0.017	0.002	0.018	0.015	0.010	0.004	0.001	0.004	3	21	4	2	0
E	0.010	0.001	0.014	0.005	0.001	0.006	0.000	0.002	9	20	2	3	1
F	0.033	0.002	0.014	0.005	0.016	0.008	0.002	0.006	4	21	15	4	1
G	0.055	0.002	0.017	0.017	0.022	0.023	0.001	0.004	6	17	4	1	1
H	0.083	0.003	0.006	0.022	0.034	0.030	0.004	0.002	10	99	3	1	0
CONTIL-ANOD®	-	0.008	0.015	0.000	0.020	0.001	0.001	0.002	30	0	70	60	-
CONTIL-ANOD® A	0.220	0.003	-	0.200	0.020	0.040	0.012	0.004	0	80	10	0	8
CONTIL-ANOD® B	0.084	0.003	-	0.020	0.050	0.024	0.011	0.006	10	30	0	0	9

5.3.1.3 Chemical Composition over the Anode Area

Contrary to statements in the literature [63], no significant differences in chemical composition were detected over the anode area either (Figure 79). In addition, CONTILANOD® anodes (Section 5.3.1.2) do not show higher homogeneity than the investigated anodes. As previously mentioned, measurement on the air side was not performed directly on the surface, but some mm below, as flat surfaces are required for spark emission spectroscopy analysis.

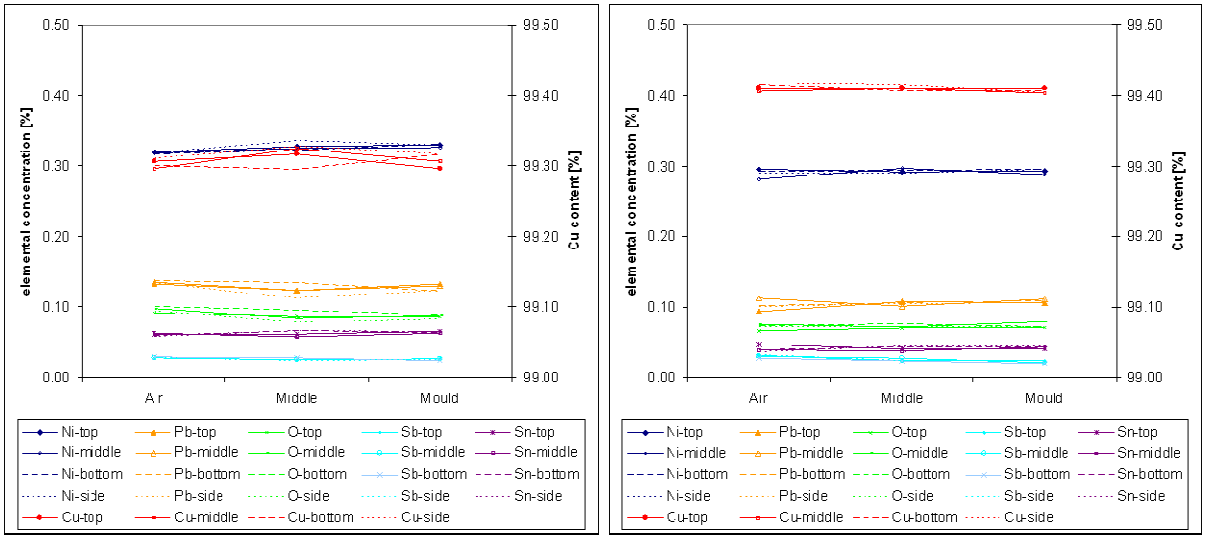

Figure 79: Elemental distribution over the anode area in anode D (left) and E (right)

As no significant differences in elemental concentrations were found across the anode thickness and area, the samples were investigated more closely by scanning electron microscopy (SEM) to determine if there were differences regarding the phases present and their distribution, which could cause inhomogeneous anodic dissolution behaviour.

5.3.2 Analysis of Inclusions

The phases detected were generally the same on the air and mould side and agreed very well with previous studies [19, 48, 50, 52, 53, 80, 107, 115-117]. A closer analysis revealed that the grey regions in Figure 80 and the light areas in Figure 81–Figure 83, consisted of pure Cu (i.e., primary Cu dendrites), which comprised the majority of the structure. A eutectic phase (Cu-Cu_2O) was found between the Cu dendrites. The oxidic particles of this phase, which have also been described as dark spherical particles in the literature [42, 50, 52, 80, 115] (Figure 80 and Figure 81), did not only consist of Cu and O, but also contained a certain amount of other accompanying elements (i.e., Ni, Pb, Sn), as described by Chen et al. [19, 42, 52]. On the air side, the Cu_2O particles also occurred in an elongated form next to the surface of the anode (Figure 82).

A higher oxide content on the air side compared to the mould side was clearly visible from the oxide layer on the surface and the higher levels of interdendritic phases in Figure 83. The Cu_2O particles were often partially rimmed with PbO (Figure 82). Pb was only detected as PbO, often also containing some Sb, as a separate phase, or a rim of Cu_2O or other complex oxides.

Ni was present mainly as NiO and in complex oxides, especially on the air side. The oxide layer on the surface, resulting from the contact with air during the casting process, and also the NiO layer on the air side are clearly visible in Figure 82 and Figure 83. Sn was found as an oxide in the form of needles or angular crystals, whereby the needles have often nucleated heterogeneously on other oxidic phases.

Ag was only found in solid solution in the Cu—no separate Ag containing phases were detected. This agreed with the literature [52, 56, 63]. Sb and As were found as various oxides, for example Cu-Pb-As oxide and Cu-As-Sb-Pb oxide. As was expected from the anode analysis and the literature concerning area of existence (Sb levels > 0.05 wt.% and Ni levels > 0.25 wt.% [50]), no kupferglimmer was detected.

Besides these relatively small spherical particles (some µm) some larger "inclusions" were also found, which appeared to be gas trapped during solidification. Various oxides, containing Sn, Zn, Ni, As, Sb, Pb and Fe had formed in these areas (Figure 84). These pores

were also visible without a microscope on both the ground and polished samples. They appeared as black spots under the microscope.

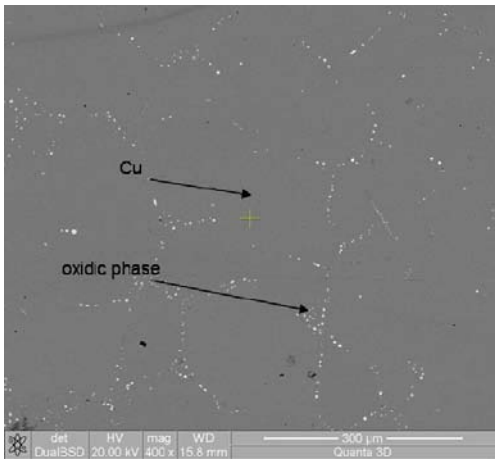

Figure 80: SEM micrograph of anode sample—phase distribution on the air side

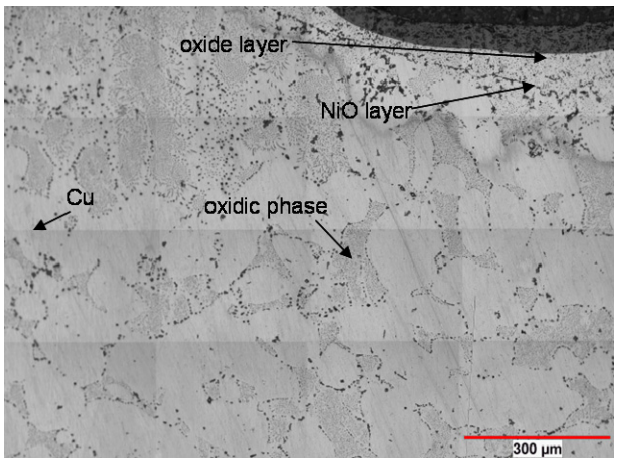

Figure 81: Phase distribution on the air side

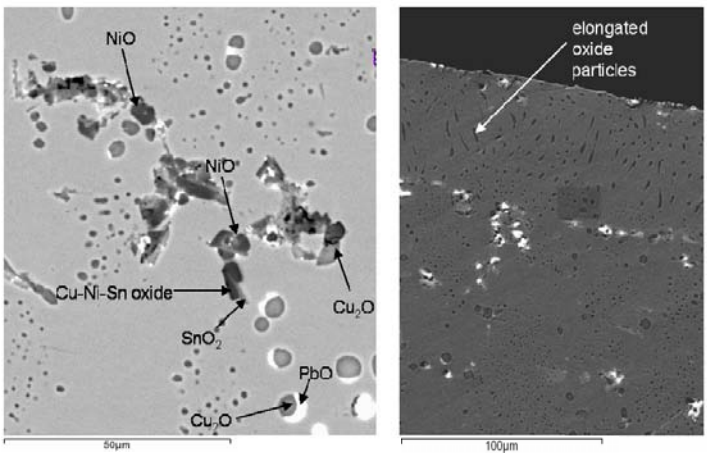

Figure 82: Interdendritic phases (air side)

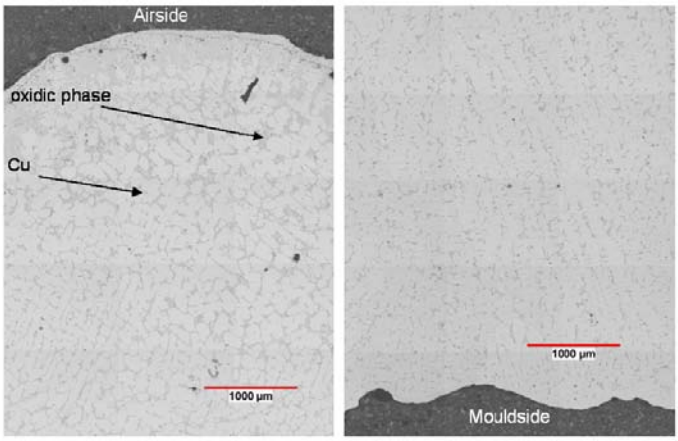

Figure 83: Air side (left) and mould side (right)—structure and phase distribution

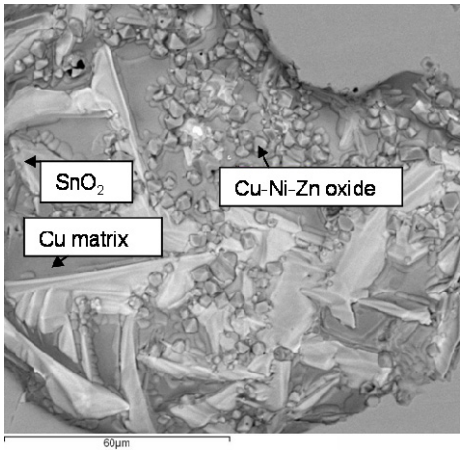

Figure 84: Higher magnification of a pore

Regarding the inclusions, no significant differences between the air and mould side were detected, except the oxide layer on the air side. As the significant differences in anodic dissolution behaviour and hence performance during electrorefining, especially during the second cathodic crop, cannot be explained by variations in chemical quality across the anode thickness, they must result from variations in physical anode quality, namely the structure and grain size.

5.4 Physical Analysis of the Anodes

The different solidification structures (i.e., columnar and equiaxed regions), as well as the grain size variation across the anode thickness were clearly visible in the anode samples (Section 5.4.1). The macrostructure (columnar and equiaxed areas) varied over the anode area, which indicated different local solidification and cooling conditions. The typical cast structure described in the literature [18, 42, 78] was present in all the anode samples where barite was used as mould wash, namely anodes A–D and F–H. However, unlike the other investigated anodes, anode E had a relatively homogeneous and globulitic structure. This

may have been caused by a smaller temperature gradient due to the higher mould temperatures when using carbon black.

The anodic microstructure consisted of Cu dendrites and an interdendritic oxide phase containing various accompanying elements, including Ni, Pb, Sn, As, and Sb. The phase type and distribution did not vary significantly across the anode thickness. Variations in secondary dendrite arm spacing (DAS) indicated different solidification conditions at the air and mould side (Section 5.4.2). A certain variation in the anode sample thickness was detected over the anode area (Figure 85), which indicated a non-perfectly vertically mounted mould.

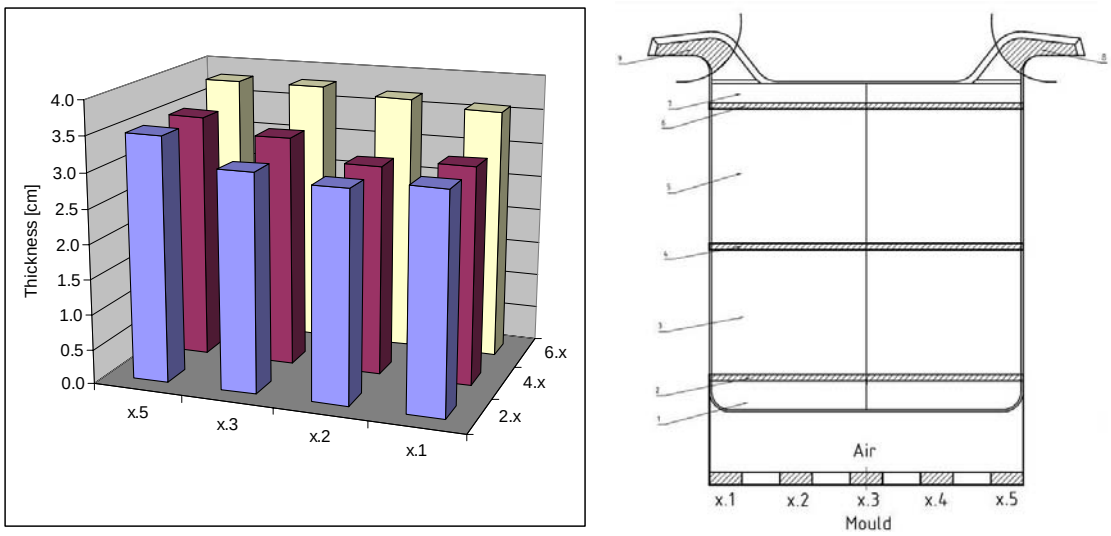

Figure 85: Variation in anode thickness over anode area

5.4.1 Macrostructure of the Anodes

The different solidification structures across the anode thickness resulted from the inhomogeneous cooling conditions at the air and mould side. As expected from the solidification theory, coarse grains with a size of several mm were found on the air side. The outer equiaxed zone on the mould side was very thin. In most samples, a columnar zone with crystals up to approximately 10 mm long was present.

In some of the investigated anodes, also the inner equiaxed region (area 2) showed a certain variation in grain size and was hence divided into "area 2-air" and "area 2-mould" for the investigations (Figure 86 and Table 21).

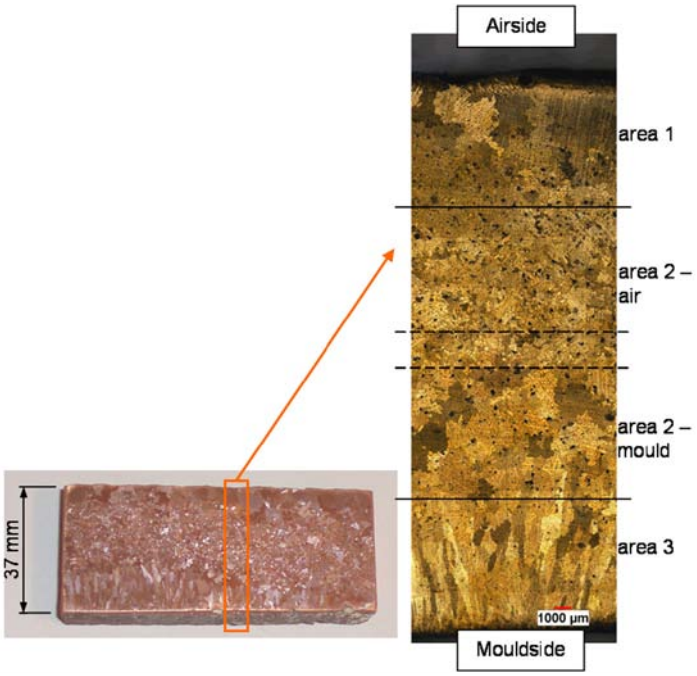

Figure 86: Macrostructure across the anode thickness (anode D-3)

Table 21: Grain sizes and corresponding standard deviations across the anode thickness (anode D-3)

Area	Average grain size [µm]	Standard deviation [µm]
1	2240	656
2-air	534	185
2-mould	1127	537
3	2719	1229

Anode B and C were from the same batch, but were produced in moulds made of different materials. The structures of the anodes from different mould materials did not show significant differences (Figure 87), although cathode copper has a higher thermal conductivity than anode copper. As there are no data concerning thermal conductivity of anode copper available in the literature, but thermal and electrical conductivity are linked, measurements of electrical conductivity were performed (Table 22).

At room temperature, the Wiedemann-Franz-Lorenz law, which states that the ratio of thermal conductivity (λ [W/mK]) and the product of electrical conductivity (κ [$(\Omega m)^{-1}$]) and absolute temperature (T [K]) has a constant value, is approximately valid for all metals:

$$\frac{\lambda}{\kappa \cdot T} = 2.45 \cdot 10^{-8} \left[\frac{V^2}{K^2}\right] \qquad \text{Equation 21}$$

Using this formula, approximate values for the thermal conductivity can be calculated from the measured values of electrical conductivity. Alloying elements result in a tremendous

decrease in thermal conductivity in most metals, especially at low temperatures (i.e., below room temperature) [118].

The measured electrical conductivity of the cathode copper was consistent with the literature [40, 118]. The calculated cathode copper thermal conductivity showed a certain deviation (5%) from the value in the literature (401 W/mK) [40, 118]. The electrical and thermal conductivity of anode copper were approximately 62–69% of the cathode copper values. Even though these calculations were only approximations, there was a significant difference in electrical and thermal conductivity between the anode and cathode copper, which should also result in different cooling conditions during anode casting.

Table 22: Electrical and thermal conductivity of anode and cathode copper mould at room temperature (25 °C)

Material	Measured electrical conductivity [MS/m]	Calculated thermal conductivity [W/mK]
Cathode copper	58	423.5
Anode copper	36–40	262.8–292

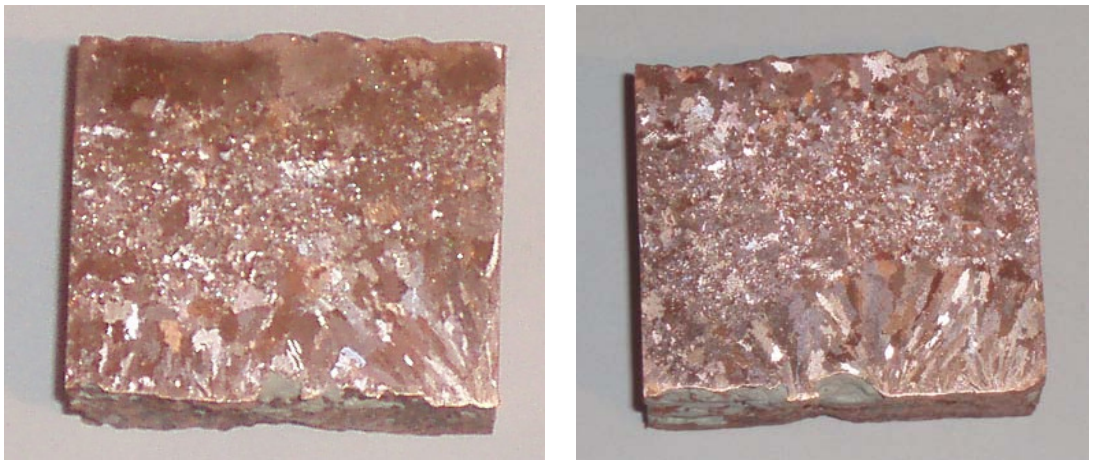

Figure 87: Structural variations under different cooling conditions (mould material)—anode B (anode copper mould, left) and C (cathode copper mould, right)

The structural differences between anodes from anode copper and cathode copper moulds due to the different thermal conductivity should be most pronounced at the beginning of the anode mould life, as no insulating limescale is present at that time. However, the moulds had already been used for 12 casting days when samples B and C were taken. Hence, an insulating limescale had already built-up on the mould bottom underside, where the cooling water impinges, and this could have decreased the heat conductivity of the cathode copper mould. This insulating layer was clearly visible when the mould was removed from the casting wheel. The samples from anode B and C had very similar structures (Figure 87), but the latter—as well as the sample from anode F—showed a finer grain size on the air side.

Anode F was taken from a cathode copper mould on the 30th casting day. As would be expected from the temperature curves (Section 5.2.3), which showed higher mould temperatures with increasing period of use of the mould—and hence a smaller temperature gradient—this anode had a structure which approached that of anode E (cast with carbon black mould wash) (Figure 88). The insulating effect of the limescale was also evident from the rise in temperature in the anode mould. After 13 casting days (anode C), the average temperature in the mould had risen by approximately 25 °C, and after 30 casting days (anode F) by approximately 50 °C.

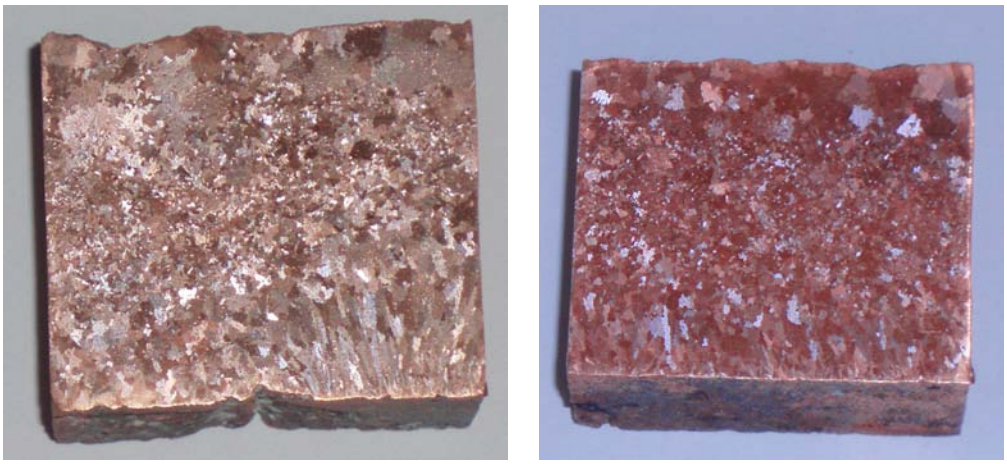

Figure 88: Structural variations under different cooling conditions (mould wash)—anode F (barite, left) and E (carbon black, right)

The use of carbon black instead of barite resulted in even higher temperatures in the mould, which had the same effect as mould preheating and caused a smaller temperature gradient. This in turn resulted in a generally more homogeneous structure across the anode thickness. As in the samples from cathode copper moulds (C and F), the air side showed a relatively fine grain size. The columnar zone in anode E was not as clearly visible as in anode D, and was also thinner. However, in the edge areas (that were not covered by the burner but had to be covered with carbon black manually, and hence seemed to be cooler) a pronounced columnar structure was also detected (Figure 89). These columnar edge regions, which were also detected in other anodes, were less pronounced in anode F.

Figure 89: Outer area of anode E (carbon black, left) and F (barite, right)

Anode H, which was cast in a new cathode copper mould (Figure 90), had a pronounced columnar zone on the mould side that extended through approximately 1/3 of the anode thickness. This indicated fast cooling on the mould side, due to the high thermal conductivity of cathode copper and the corresponding lower temperatures compared to the anode copper moulds. However, the cooling was not sufficiently rapid to induce equiaxed solidification as seen in anodes produced using the CONTILANOD® process. The columnar zone in anode D, which was cast in a new anode copper mould, was thinner (Figure 91) than in anode H, which suggested slower cooling in the anode copper mould. Furthermore, in these anodes the inhomogeneous grain size in the central area was visible.

Approximately half way down the length of sample H no columnar crystals were found on the mould side, but only equiaxed grains. As the material properties of the cathode copper should have been homogeneous within the mould, this local difference in cooling conditions might have been caused by inhomogeneous mould wash application or an uneven mould surface, whereby the latter was indicated by the irregular anode surface at this location.

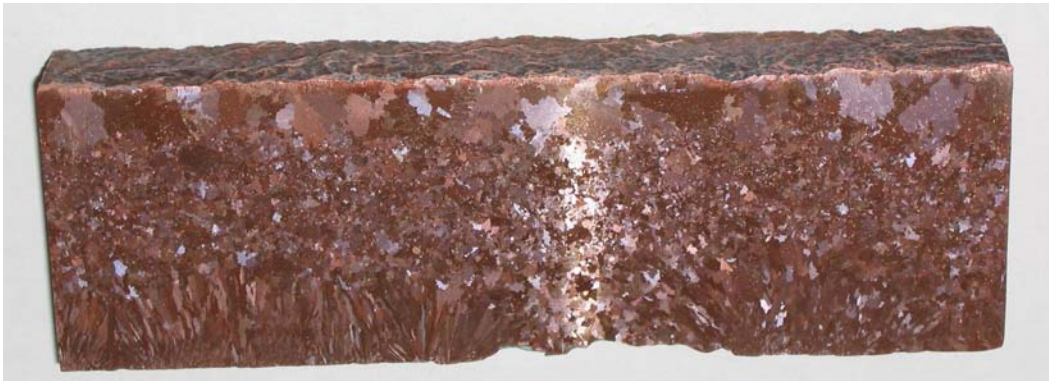

Figure 90: Macrostructure of anode H (new cathode copper mould)

Figure 91: Macrostructure of anode D (new anode copper mould)

An even higher cooling than in the cathode copper mould, as indicated by the temperature curves, was achieved using cooling ribs on the mould bottom. Anode G showed a wide columnar zone (left side of Figure 92) that indicated even faster cooling on the mould side than when using cathode copper moulds. However, it is evident from Figure 92 that the structure across the anode thickness varied within small distances over anode area. The columnar crystals on the right side of Figure 92, which are notably smaller than on the left side of the sample (total length of the sample: approximately 100 mm) indicate significant variations of the solidification conditions in the mould.

Figure 92: Macrostructure of anode G (mould with cooling ribs, type 1)

The new cooling arrangement at Montanwerke Brixlegg AG did not result in a significant change in the macrostructure, as indicated by the temperature measurements, which showed similar cooling conditions as the old cooling arrangement. The macrostructure of anode I, which was cast with the new cooling arrangement, is shown in Figure 93. However, the microstructure was changed significantly by the new cooling conditions (Section 5.4.2).

Figure 93: Macrostructure of anode I (new cathode copper mould, new cooling arrangement)

As described above, an inhomogeneous structure was not only found across the anode thickness, but also over the anode area. This indicated local differences in solidification and cooling conditions. On the mould side, these differences may have resulted for example from uneven mould temperatures due to uneven mould wash application, cracks in the curvature, a different impact of the spray cooling, and inhomogeneities in the mould materials. Bath movement due to pouring the liquid copper into the mould and movement of the casting wheel when the copper is still liquid also influences the solidification structure, as detached dendrite arms act as additional nuclei.

The inhomogeneous structure over anode area on the air side indicated inhomogeneous numbers of nuclei on the air side. The finest grain size on the air side was detected in the middle of the anode, namely in sample 4.3 and 4.2 (anode A) (Figure 94). The anodes are cooled in air in the first positions after pouring. A solid layer has to have formed when the water-cooling starts in order to avoid an uneven anode surface. Hence, the grain size directly on the air side should only be dependent on the number of nuclei present, as the whole surface solidifies in contact with ambient air.

The inhomogeneous grain size close to the air side indicated varying cooling conditions, possibly due to the water spray nozzle arrangement and the occurrence of the Leidenfrost-effect, which deteriorates the effect of water cooling because of the formation of an insulating water vapour layer between the copper and the cooling water.

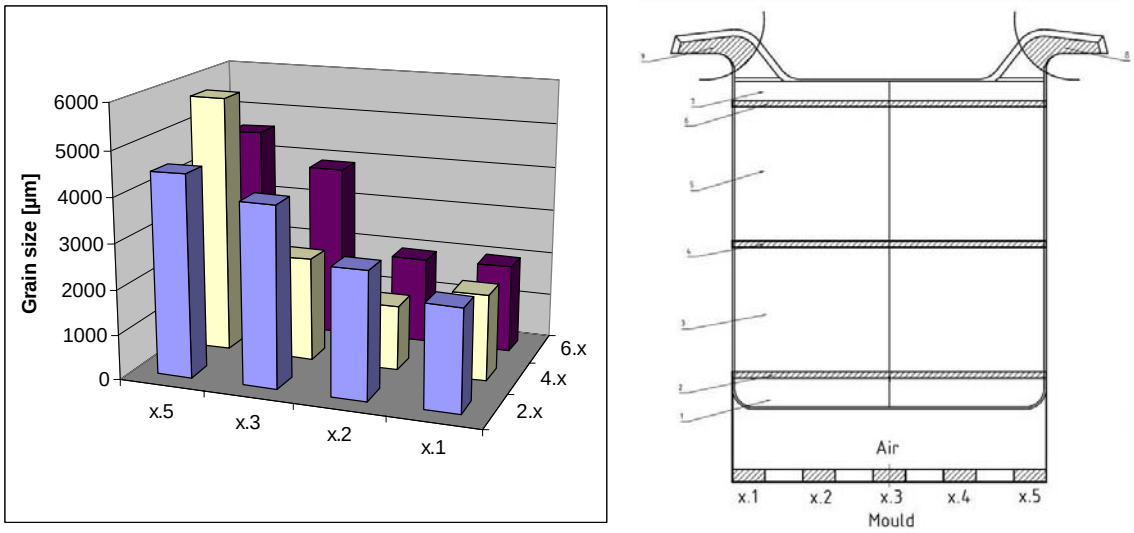

Figure 94: Variation of grain size on air side over anode area (anode A)

The structure variations over the anode area are illustrated in Figure 95. The extent of the different structures across the anode thickness is dependent on the cooling conditions, namely the progression of solidification from the mould and air side. The thickness of the different areas in all investigated anode samples is detailed in Figure 96. The structures showed significant variations over the anode area, which should result in inhomogeneous dissolution behaviour during electrorefining.

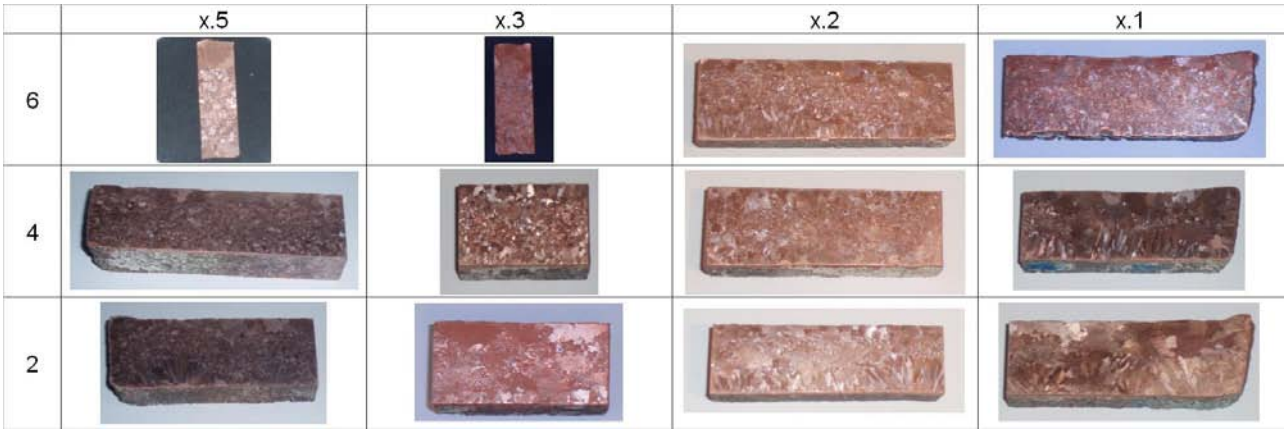

Figure 95: Macrostructure over anode area (anode A)

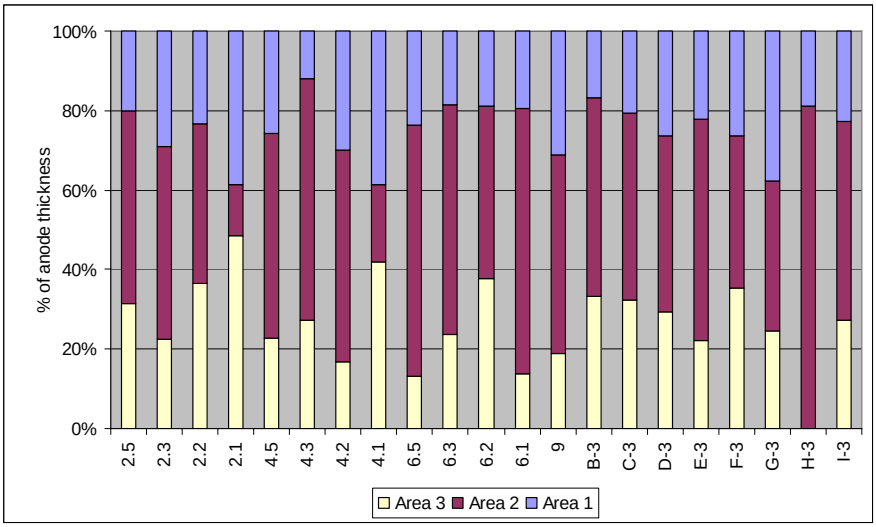

Figure 96: Distribution of anodic structures over anode thickness (Area 1: Columnar zone; Area 2: Inner equiaxed zone; Area 3: Outer equiaxed zone)

In some locations, the columnar zone totally disappeared and an almost equiaxed zone was detected instead on the mould side (e.g., samples 2.3, 4.3, 4.5, 6.1, and 6.5). These samples also showed a larger fine equiaxed area in the centre of the anode. In some samples, the columnar crystals on the mould side were not arranged in a parallel manner, but fan-shaped columnar crystals were visible (e.g., sample 2.5, Figure 97).

Figure 97: Fan-shaped columnar crystals in sample 2.5 (anode A)

The grain size in the inner area is determined by the amount of impurities present, which act as nuclei. Further causes for different local solidification and cooling conditions within one anode mould may be inhomogeneities regarding the mould, mould wash, and movement of the liquid copper due to pouring and movement of the casting wheel. The uneven surfaces (i.e., cracks) in the mould surface result in inhomogeneous mould cooling conditions. As the mould wash is not only applied automatically, but also corrected manually, the actual amount of mould wash and hence the heat transfer through the mould varies not only between different anodes, but also over the anode area, as additional mould wash is applied to certain areas, where the mould is highly stressed or cracks are already present. The liquid copper

bath movement in the mould comes from pouring the liquid copper into the mould and also from movement of the casting wheel when the copper is still liquid. This may cause a certain bath stirring and hence temperature distribution within the solidifying anode, as well as a detachment of dendrite arms, which then act as additional nuclei for solidification. These effects are in general similar to magnetic stirring, where a bath movement is applied in order to achieve a finer, equiaxed structure. The variation in grain size in the central area and on the mould side over the anode area is depicted in Figure 98. This indicates locally different solidification conditions.

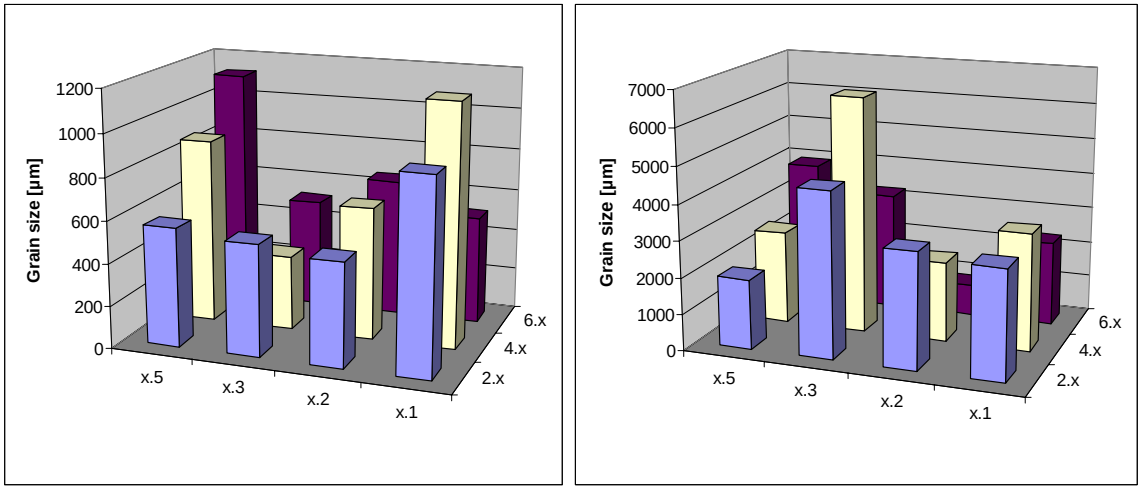

Figure 98: Grain size variation in the central area (left) and on the mould side (right) over the anode area

The grain size variation in the samples from the same position in the different anodes, namely from the middle, is depicted in Figure 99. The varying grain sizes at other positions are presented in Figure 100–Figure 102. The differences in grain size on the air side could not only be caused by the cooling nozzle arrangement, as the samples were taken from the same position.

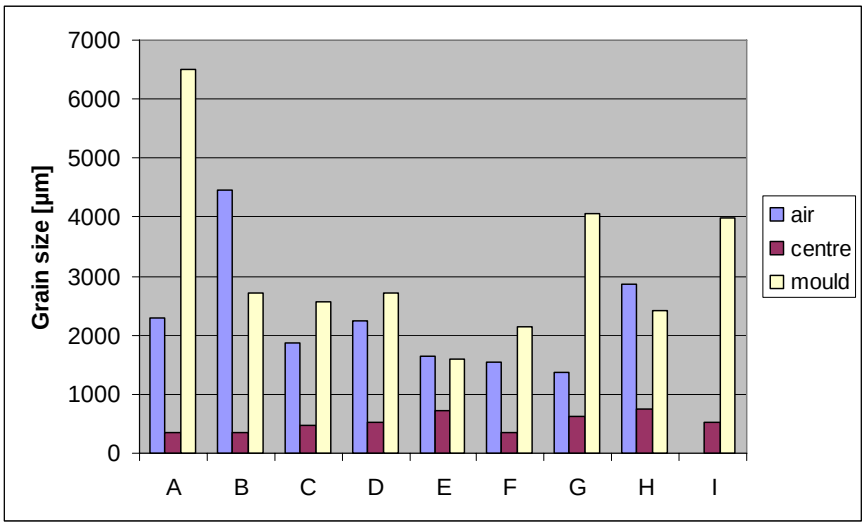

Figure 99: Grain size of different anodic areas in samples from the anode centre

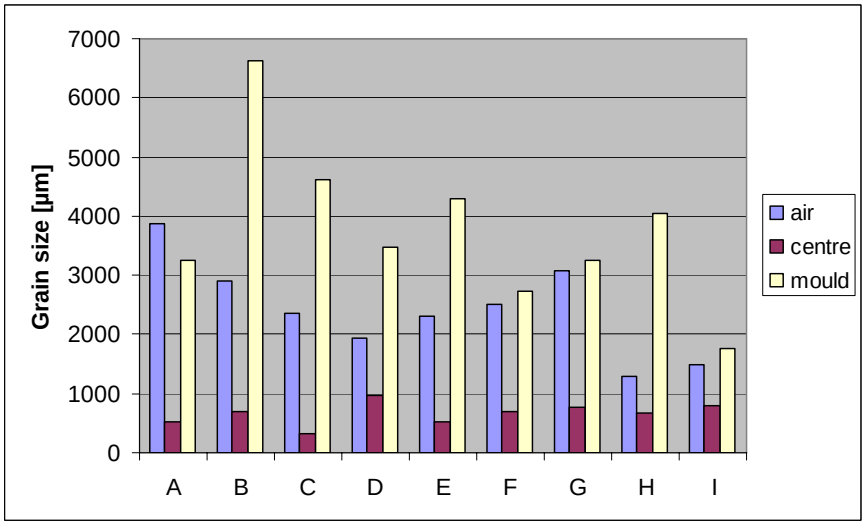

Figure 100: Grain size of different anodic areas in samples from the anode top

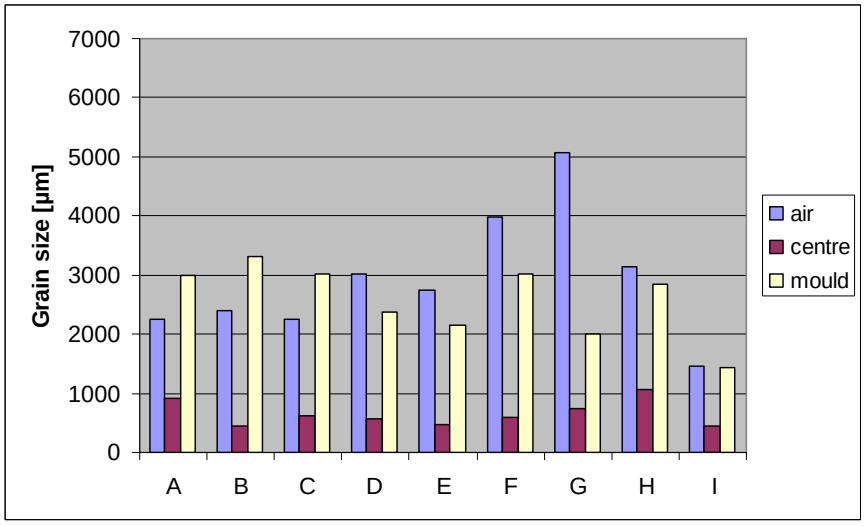

Figure 101: Grain size of different anodic areas in samples from the anode bottom

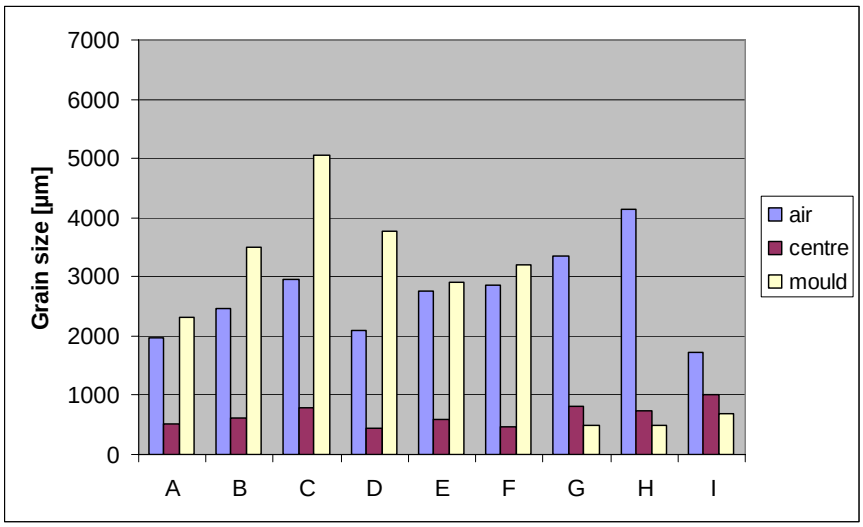

Figure 102: Grain size of different anodic areas in samples from the anode side

The different solidification conditions across the anode thickness were clearly visible from the macrostructure. In order to examine more closely the relationship between the structure and solidification time, the microstructure, namely secondary dendrite arm spacing, was also studied.

5.4.2 Microstructure of the Anodes

A dendritic microstructure was present in all samples from the air to the mould side. The dendrites consisted of relatively pure copper, the interdendritic phase was a Cu-Cu_2O eutectic, where various oxides of the accompanying elements including Ni, Sn, As, Sb, and Pb were present. No significant difference was found between the air and mould side concerning the phase type and distribution (Section 5.3.2 and Figure 103). An oxide layer with a thickness of approximately 100–1,000 µm was detected directly on the air side, which was due to contact with air during casting and solidification. However, as described in Section 5.3, this oxide layer was not analysed in the chemical analysis, as the samples had to have a flat surface for analysis and hence this outer region was removed. In some samples, pores were detected, which were visible even without a microscope.

The secondary dendrite arm spacing (DAS, λ_2) was measured across the anode thickness. The standard deviation amounted to approximately 19 and 24 µm in the outer and inner anode areas, respectively. The variation in DAS between the air and mould side (Figure 103) indicated different cooling conditions. The coarsest dendrites were found in the central region of the anode, which is the last region of the anode to solidify. This was consistent with the theory that longer solidification times lead to larger DAS, due to the ripening process.

A significant change in this DAS trend across the anode thickness was detected after implementation of the new cooling system. The more intense mould cooling and hence the anode bottom led to a more rapid solidification on the mould side and also influenced solidification of the central areas. Consequently, the largest DAS were found on the air side, and not in the central area. The measured anode DAS values, which were used for the potential measurements, are detailed in Section 5.5.

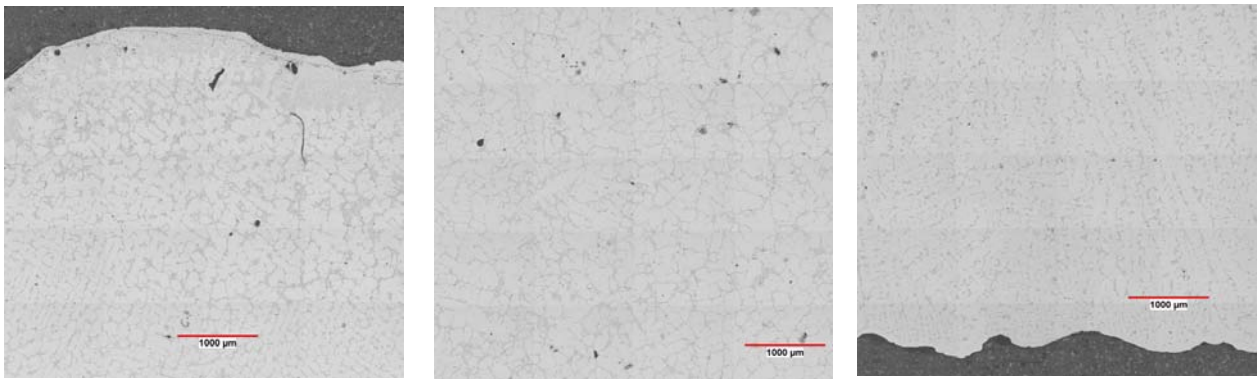

Figure 103: Microstructure on air side (left), centre (middle), and mould side (right)

Using equation 6 (Section 2.3.2.5) with the average measured DAS values for all anodes that were produced under the same cooling conditions, namely using barite, anode copper moulds, and the old cooling arrangement (85.14 µm (air side), 99.41 µm (centre), and 65.29 µm (mould side)), showed very good correlation, and hence provided values for the necessary parameters *B* and *n* (9.61 and 0.4476, respectively) to calculate DAS values from the simulation results (Figure 104 and Section 6.4). The correlation with the values of all anodes produced using barite and the old cooling system (86.31 µm (air side), 99.26 µm (centre), and 60.89 µm (mould side) resulting in $B = 6.53$ and $n = 0.5243$) is shown in Figure 105. The higher heat removal of cathode copper moulds compared to anode copper moulds and the resulting lower DAS on the mould side is visible from the different slopes of the lines in Figure 104 and Figure 105. However, the solidification conditions in the centre and on the airside are not influenced significantly by the use of anode copper or cathode copper as mould material.

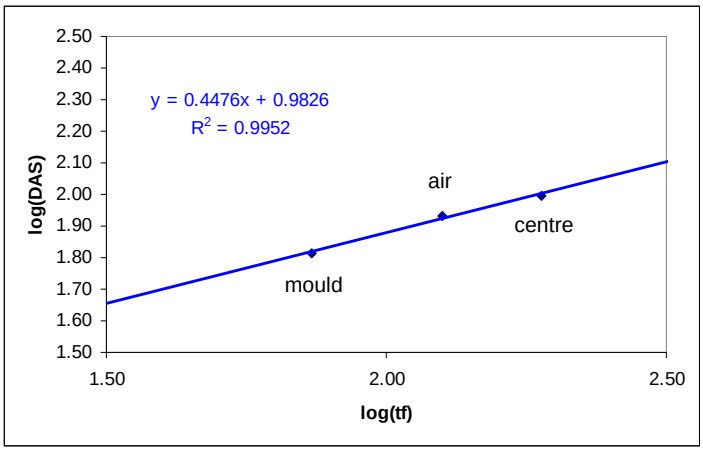

Figure 104: Relationship between the DAS and local freezing time (all anodes produced using anode copper moulds, barite, and old cooling system)

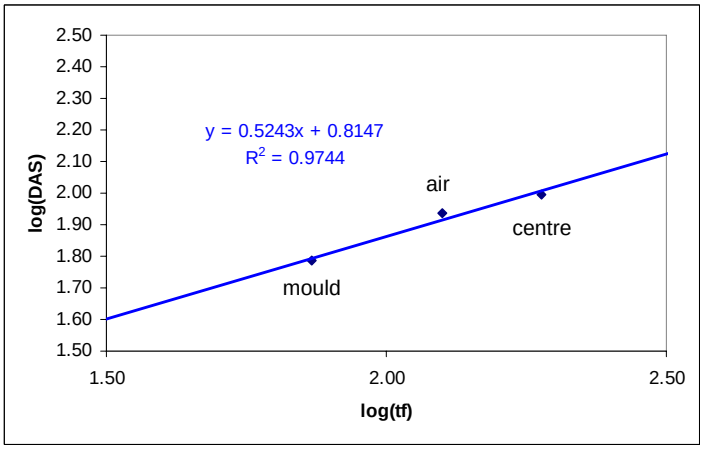

Figure 105: Relationship between the DAS and local freezing time (all anodes produced using barite and old cooling system)

As—unlike the chemical quality—the micro- and macrostructure were found to vary significantly across the anode thickness, the dissolution behaviour across the anode thickness was studied with regard to the areas with different physical qualities, namely structure. Therefore, potential measurements were performed to determine which structure is preferable for electrorefining.

5.5 Anodic Dissolution Behaviour

As the different mould temperatures and cooling conditions during anode casting did not result in definite variations in the chemical anode composition across the anode thickness (Section 5.3), the different dissolution behaviour of the air and mould side during electrorefining was considered to be caused mainly by the inhomogeneous physical quality, namely the structure and grain size (Section 5.4).

An additional indication regarding the importance of anode structure and grain size on dissolution behaviour is the current density distribution at the cathodes opposite the anode air and mould sides (Figure 106). In other investigations [5], the current density was determined on the air and mould side during the anodic crop in one cell. The produced cathodes were weighed separately and the current densities subsequently calculated [5]. The higher current density and standard deviation on the mould side for both cathodic crops are depicted in Figure 106. The relationship between the air (AS) and mould (MS) side was very similar for both cathodic crops. The results, which are representative of 10 investigations in total, are contradictory to other reports in the literature. According to the literature, there should not be any differences between the air and mould side after the first cathodic crop (1CC), as the chemical inhomogeneities are no longer present. However, a significant difference in current density distribution was also detected in the second cathodic crop (2CC). The obvious differences between the air and mould side in Figure 106 indicate that the chemical influence does not have that big influence directly on the produced cathode sheets.

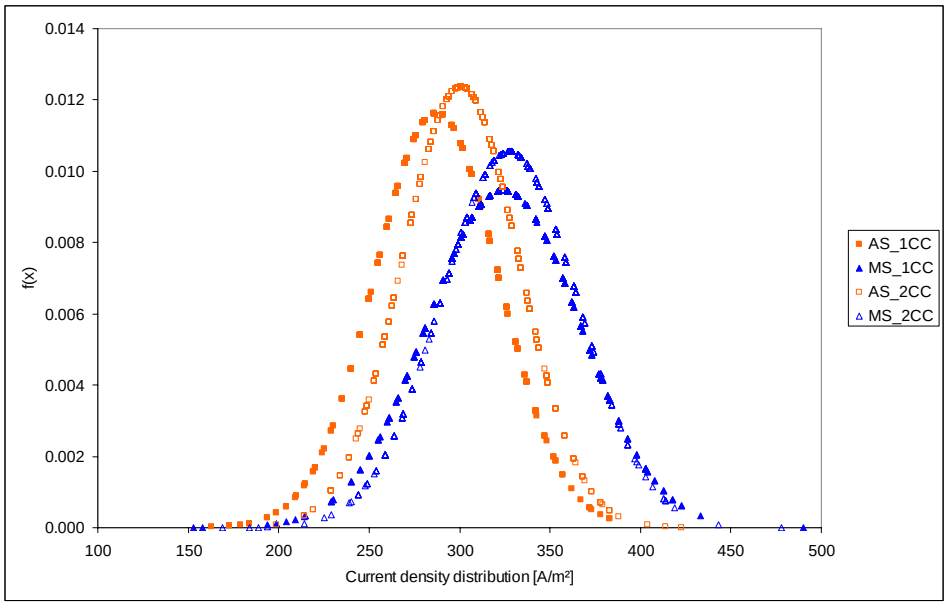

Figure 106: Current density distribution during electrorefining [119]

These findings are in good agreement with the different grain sizes detected across the anode thickness. Using the estimated dissolved anodic areas marked in Figure 86 and the corresponding grain sizes (Table 21), the deviations in the first cathodic crop can be explained by the different dissolution behaviour of areas 1 and 3, and those in the second cathodic crop by the difference in grain size within area 2 ("area 2—air" and "area 2—mould").

Potential measurements were performed to study the inhomogeneous anodic dissolution more in detail. The chemical composition of the investigated anodes is detailed in Table 23. The anodes can be chemically characterized as follows:

- Anode C: Low Cu, high O, high Ni, medium Ag
- Anode E: High Cu, high O, medium Ni, low Ag
- Anode G: Low Cu, low O, high Ni, high Ag
- Anode I: Low Cu, low O, high Ni, low Ag

Table 23: Chemical analysis (batch analysis) of the investigated anodes

Anode	**[wt.%]**								**[ppm]**				
	Cu	**Ag**	**O**	**Ni**	**Pb**	**Sn**	**As**	**Sb**	**Fe**	**Zn**	**Bi**	**Te**	**Se**
C	99.01	0.034	0.15	0.47	0.13	0.06	0.02	0.02	50	88	12	26	12
E	99.20	0.028	0.11	0.39	0.10	0.03	0.01	0.03	18	26	20	30	13
G	99.08	0.043	0.04	0.53	0.11	0.06	0.01	0.02	49	131	15	10	10
I	99.01	0.029	0.06	0.41	0.30	0.04	0.01	0.03	22	102	15	12	12

The grain sizes and secondary dendrite arm spacing (DAS) of the investigated anode samples are provided in Table 24. As not the length of the columnar crystals, but their thickness is important regarding the grain size exposed to anodic dissolution, the thickness of the columnar crystals was measured (“Col. thickness” in Table 24). These values show that the actual grain size for dissolution on the mould side is relatively fine.

Table 24: Grain size and DAS of investigated anode samples

Grain size [µm]	**C-3**	**E-3**	**G-3**	**I-3**
Air	1860	1643	1381	1240
Centre-air	466	728	624	516
Centre-mould	523	731	833	631
Mould	2561	1599	4067	3992
Col. thickness	318	-	301	417

DAS [µm]	**C-3**	**E-3**	**G-3**	**I-3**
Air	85	84	88	101
Centre-air	100	109	104	87
Centre-mould	87	106	96	77
Mould	49	45	59	58

As the chemical composition within any anode sample was found to be relatively constant across the anode thickness, the samples were chosen according to the different solidification structures (Section 4.5 and Figure 40). The dissolution experiments studied the total influence of the anode on dissolution behaviour and electrorefining, as all influences, namely the chemical and structural properties, were included.

The dissolution of anodes with a defined chemical composition and known structure was investigated. Each experiment started with the measurement of the open circuit potential for 5 minutes. This time was sufficient, as the open circuit potential reached an approximately constant value after 3 minutes at the latest. In addition, after polarization the OCP was measured for 5 minutes. The values and standard deviations of the OCP are given later in this section.

Anodic polarization scans on samples with different structures showed some differences in dissolution behaviour across the anode thickness. The dissolution behaviour can be characterized by the maximum current density at which passivation occurs (i_{max}), at the Flade potential (E_F). The difference between the OCP and the E_F is termed anode polarization. A low anode polarization, namely a less noble behaviour, is advantageous for electrochemical dissolution (as dissolution starts at the least noble phases). Hence, anodes with high current densities at low potentials would be desirable. Anodes with fine grains are reported to show a lower polarization, namely a less noble behaviour, and have a lower E_F, than anodes with coarse grains. Therefore, they dissolve preferentially at a given current density, but they also are more susceptible to passivation as a lower anode polarization is needed for the onset of passivation. A higher DAS is reported to decrease the tendency for passivation [18, 68, 79, 81, 83].

The potential measurement results, namely the anode polarization and i_{max}, were related to the anodic structure. As no definitive trends were found the overall trends are indicated by the dashed lines in the diagrams. The differences between the individual anodes may be due to their different chemical composition.

Regarding the anode polarization only the trend shown by anode G could be explained by the number of grain boundaries present, whereas anode C and I showed the opposite behaviour (Figure 107). The same behaviour was detected when the results were related to the DAS (Figure 108).

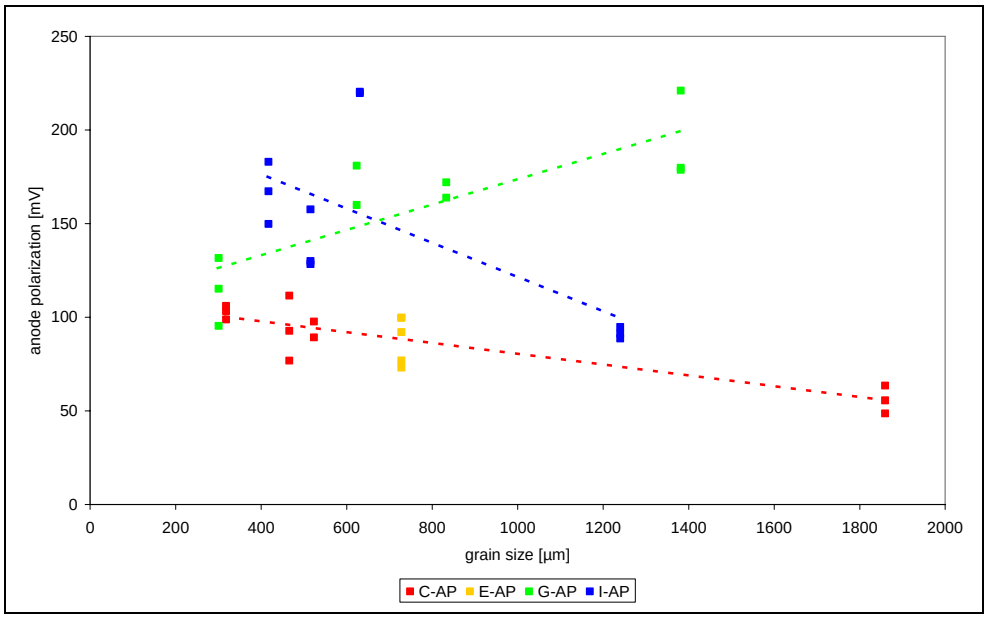

Figure 107: Anode polarization as a function of grain size

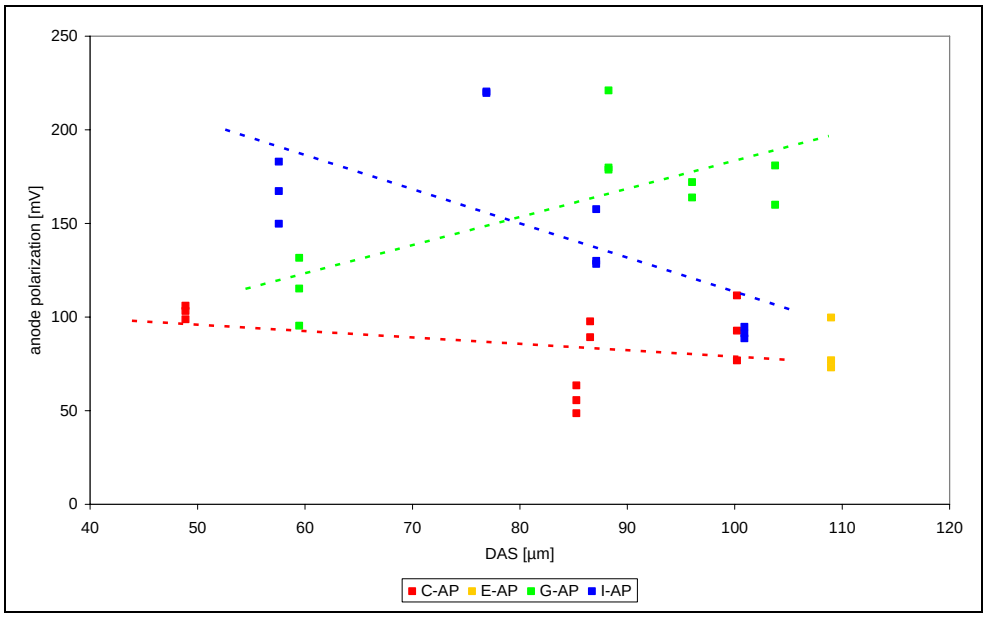

Figure 108: Anode polarization as a function of DAS

Also the correlation between the i_{max} and the grain size (Figure 109) and the DAS (Figure 110) did not show a definitive trend.

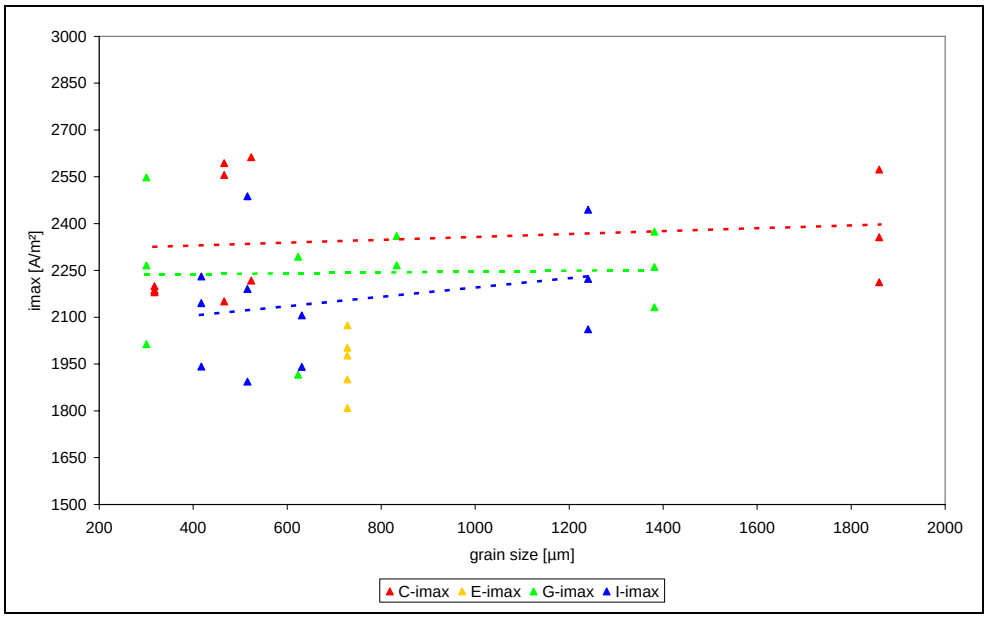

Figure 109: i_{max} as a function of grain size

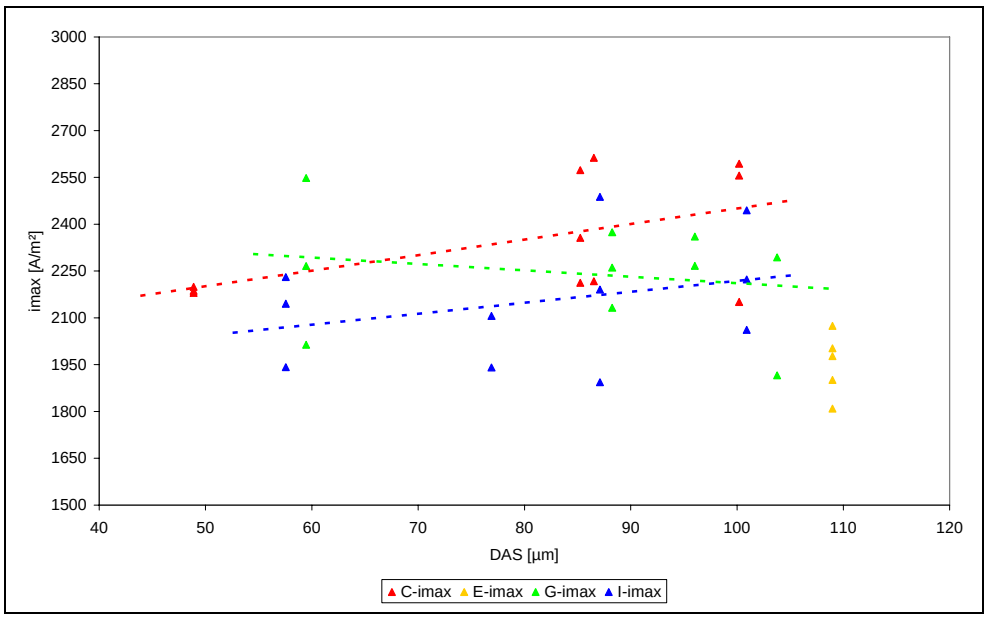

Figure 110: i_{max} as a function of DAS

Typical polarization scans, namely repeated measurements of the samples A and D from anode I, are depicted in Figure 111 and Figure 112. As can be seen from these diagrams, the samples showed different deviations between the individual measurements. Smaller deviations indicate a more homogeneous structure within the sample. The mean curves and mean values are summarized in Figure 113 and Table 25, respectively, and show an inhomogeneous dissolution behaviour across the anode thickness. The different standard deviations, which indicate different degrees of structural homogeneity in the sample, are also listed in Table 25.

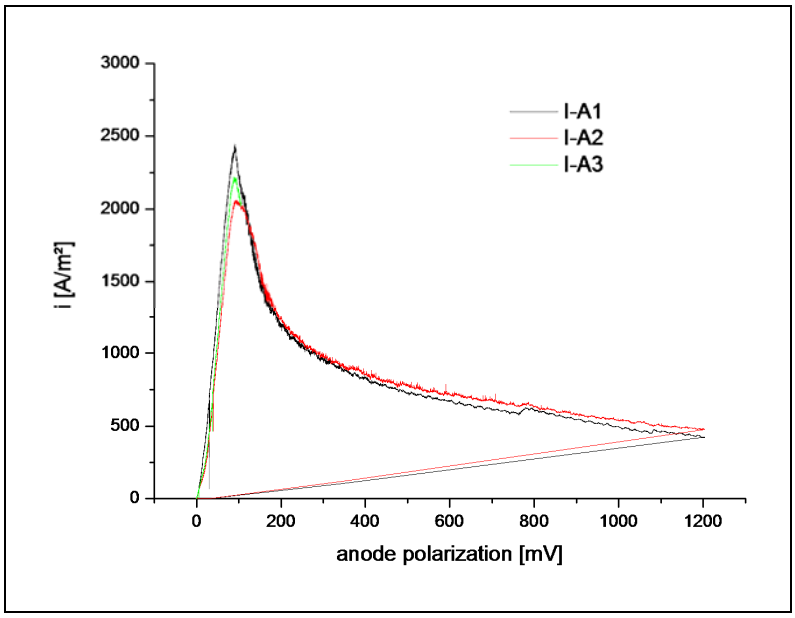

Figure 111: Anode polarization scans of sample A (anode I)

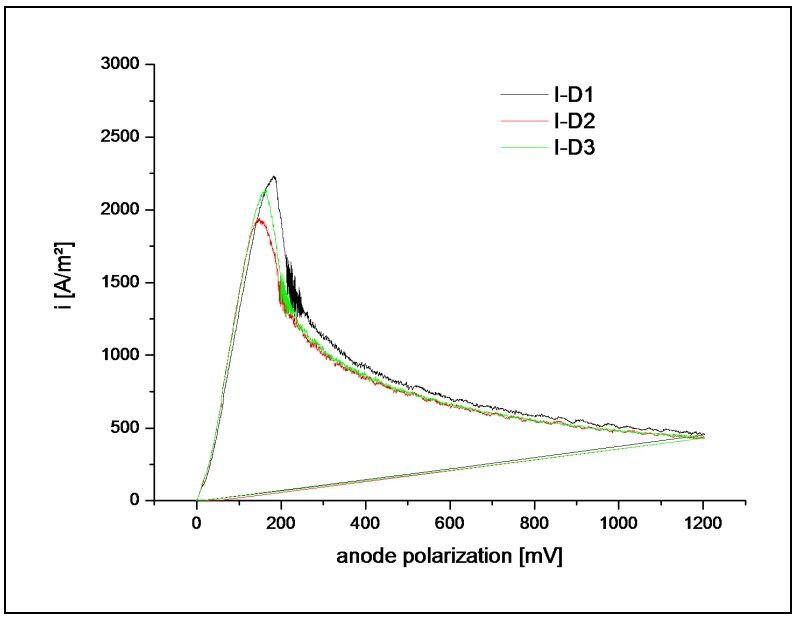

Figure 112: Anode polarization scans of sample D (anode I)

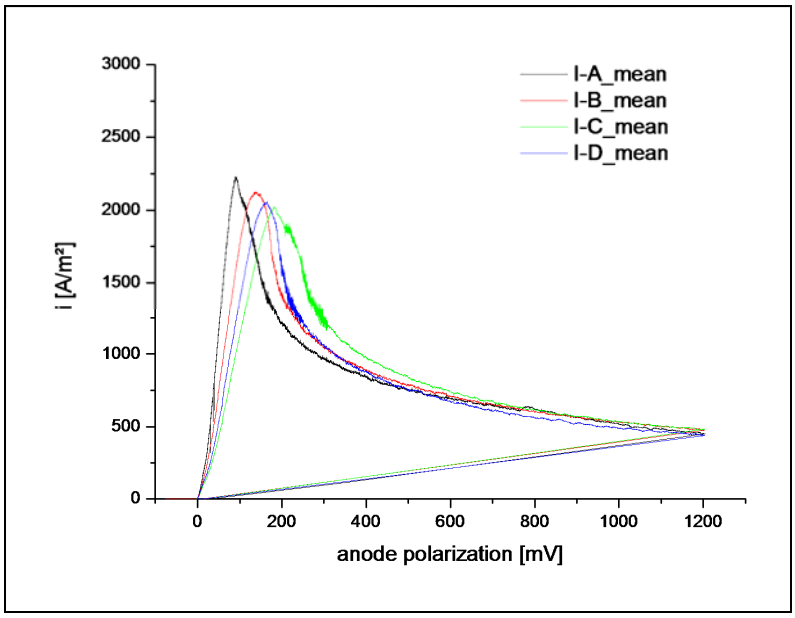

Figure 113: Mean anode polarization scans (anode I)

Table 25: Mean values and standard deviations of repeated measurements of samples across the anode thickness (anode I)

Sample	Mean OCP [mV]	Mean anode polarization [mV]	Mean i_{max} [A/m²]	StDev OCP [mV]	StDev anode polarization [mV]	StDev i_{max} [A/m²]
A	-344	92	2243	4	3	192
B	-345	139	2190	3	16	297
C	-347	220	2023	2	1	117
D	-348	167	2106	2	17	148

Also for anode G a variation in dissolution behaviour across anode thickness was found, but the trend across the anode thickness was different from anode I. The mean anode polarization scans and mean values of the samples across the anode thickness are given in Figure 114 and Table 26, respectively.

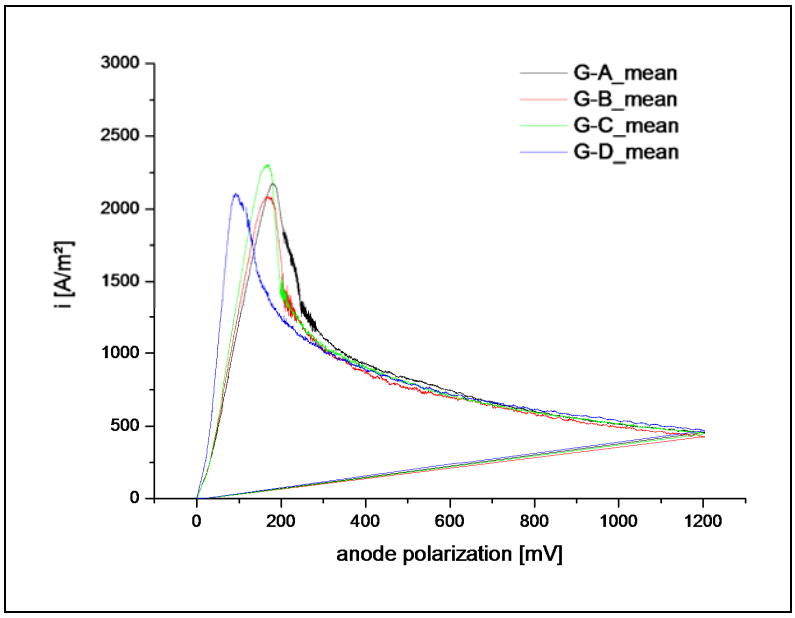

Figure 114: Mean anode polarization scans (anode G)

Table 26: Mean values and standard deviations of repeated measurements of samples across the anode thickness (anode G)

Sample	Mean OCP [mV]	Mean anode polarization [mV]	Mean i_{max} [A/m²]	StDev OCP [mV]	StDev anode polarization [mV]	StDev i_{max} [A/m²]
A	-347	193	2256	3	24	121
B	-347	170	2105	2	15	267
C	-348	168	2314	1	6	66
D	-348	114	2276	2	18	267

The differences in anodic dissolution across the anode thickness of anode C are shown in Figure 115 and Table 27. Also in this anode, a varying dissolution behaviour across the anode thickness, but also certain variations within the individual samples were found.

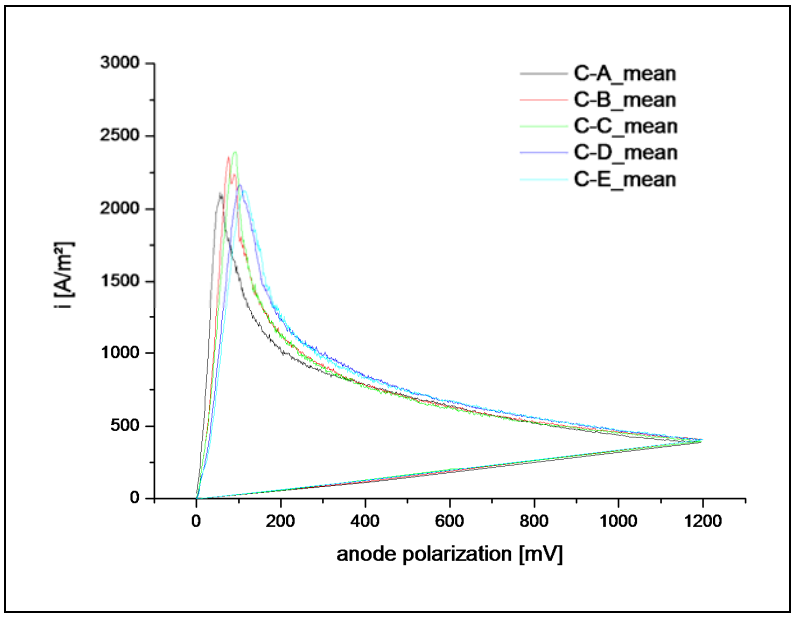

Figure 115: Mean anode polarization scans (anode C)

Table 27: Mean values and standard deviations of repeated measurements of samples across the anode thickness (anode C)

Sample	Mean OCP [mV]	Mean anode polarization [mV]	Mean i_{max} [A/m²]	StDev OCP [mV]	StDev anode polarization [mV]	StDev i_{max} [A/m²]
A	-345	56	2381	4	7	182
B	-346	94	2433	1	17	245
C	-346	93	2415	1	6	279
D	-345	103	2188	2	4	10
E	-345	112	2138	0	3	150

The extended inner globulitic area of anode E resulted in a very homogeneous dissolution behaviour, as illustrated in Figure 116 and Table 28, and showed very good reproducibility, namely smaller deviations (standard deviation) between the single measurements.

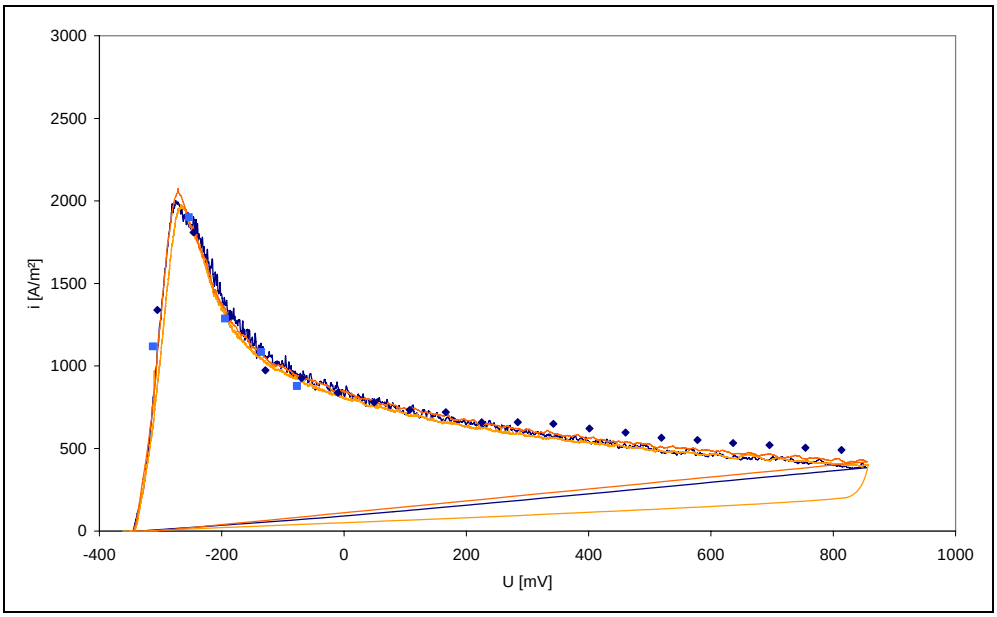

Figure 116: Anode polarization scan (anode E)—repeated measurements of the inner globulitic area

Table 28: Mean values and standard deviations of repeated measurements of samples across the anode thickness (anode E)

Sample	Mean OCP [mV]	Mean anode polarization [mV]	Mean i_{max} [A/m²]	StDev OCP [mV]	StDev anode polarization [mV]	StDev i_{max} [A/m²]
central area	-344	83	1953	1	14	101

It is evident from the mean curves (i.e., Figure 113, Figure 114, and Figure 115) that the differences in anode polarization became pronounced with higher current densities. This is of special importance with the trend to apply higher current densities during electrorefining, as the less noble part of the anode would dissolve more readily and leads to uneven anodic dissolution.

The deviations of the repeated measurements may be caused by the position of the Luggin capillary in front of the sample. As only one point of approximately 1 mm² is measured, it makes a big difference whether the Luggin capillary is located in front of the copper matrix or an inclusion, or within a grain area or on a grain boundary. Although the position of the Luggin capillary was fixed, the direct measuring point of the sample surface may have changed by the sample preparation, namely the grinding between the individual measurements of each sample. Furthermore, the measurements may have been influenced by anode slime formation on the sample.

The results of the potential measurements do not show a definitive trend regarding E_F and anode polarization with grain size and DAS, respectively. However, the experimental results confirmed that there is a variation in anodic dissolution behaviour across the anode thickness. Further investigations with a wider variation of grain size and DAS would be required to define a definitive relationship between anode structure and dissolution.

6. Simulation of Anode Casting

Although simulation and modelling are common tools in foundries and are also used for the continuous casting processes, there is no literature available regarding the simulation of anode casting. Therefore, a basic model was developed using the experimental data of the temperature measurements in order to simulate both the casting process, and create a tool to optimize mould design and cooling arrangements.

As previously described, at present the mould design optimization process is mainly performed by trial and error. The simulation should help to avoid costly mould development processes and mould prototypes. In addition, the cooling arrangement can be optimized using the model, as the cooling effect and respective cooling conditions of the anode can be estimated from the simulation results and the cooling arrangement can be altered accordingly.

The basic model is based on the temperature measurement experiments and hence on the casting process at Montanwerke Brixlegg AG, which was also used to verify the model. However, the model can be modified regarding mould geometry, cooling, and materials used, so that it can be used for any given anode casting process.

The simulation of the casting process (Figure 117), namely as the first step cooling and solidification of the anode, was performed with the MAGMASOFT® (MAGMA, Germany) and calcosoft-2D software (ESI Group, France). Calcosoft-2D was used to determine the heat transfer coefficient (HTC) between the anode and mould from the temperature measurements by inverse calculation. This HTC was then used for the simulation of anode casting with MAGMASOFT®. By correlating the calculated solidification times with the measured DAS values the constants in equation 6 (Section 2.3.2.5) were calculated (Section 5.4.2), so that the DAS values could be calculated by using a user-defined function in MAGMASOFT®. If the temperature profile in the anode is known, a more detailed simulation can be performed, namely the columnar-to-equiaxed-transition (CET) and the structure.

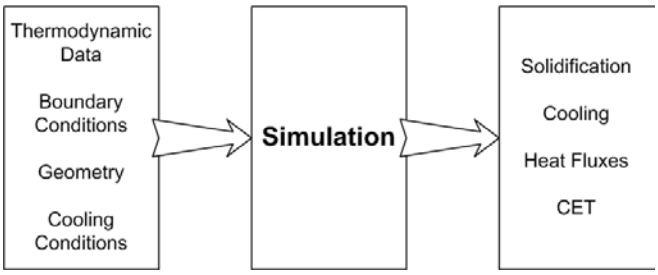

Figure 117: Schematic sequence of an anode casting simulation

The MAGMASOFT® software consists of several modules, namely Preprocessor, Enmeshment, Simulation, and Postprocessor. The geometry and the different material groups (e.g., mould, cooling, and casting) are firstly defined in the Preprocessor, and then a mesh is defined, whereby standard or user-defined settings can be used. The quality of the generated mesh can be controlled before starting the simulation in order to detect blocked cells, edge-to-edge-connections, and thin wall areas, which can cause errors in the simulation. Afterwards the parameters for the simulation, namely material data and start temperatures, HTCs between the different components of the geometry, and parameters for batch production are set and the simulation can be started. When the calculation is finished, the results can be viewed in the Postprocessor.

The calculations with MAGMASOFT® were initiated with a simplified anode and mould geometry, namely cuboid shapes. After these trials, the real geometries were used, and the parameters (i.e., material and cooling data, and HTC) were varied in order to approach the experimentally measured temperature curves determined in the anode moulds at Montanwerke Brixlegg AG.

The HTC between liquid copper and the anode mould was calculated by inverse calculation from the measured temperatures in the mould with the calcosoft-2D simulation software. Due to inhomogeneities in the overall process (i.e., differences in mould material and quality due to cracks, application and properties of mould wash, and casting temperature) the anode quality—especially the physical one—varies dramatically within one anode (Section 5.4.1), which indicates different local cooling conditions within one anode mould and anode. Hence the cooling conditions of the anode can only be estimated for those points where the temperature measurements are installed. Therefore, the simulation can only provide an overview of cooling and solidification.

Additionally, for more precise calculations, namely calculation of structure and CET, the anode copper composition also has to be taken into account. As there are certain compositional variations and hence different resulting interactions, which also influence grain nucleation and growth, a simulation of grain size and structure does not seem appropriate with the present process variations.

Similar calculations on the solidification of copper alloys during continuous casting were carried out with Calcosoft [120]. For this work, a stochastic model for grain nucleation and growth was used to model the structure based on the temperature distribution. However,

these were alloys with a defined composition. The results indicated that the different shapes of liquid pools cause different solidification structures.

The basic model for anode casting, which is described in the following sections, therefore does not contain a simulation of solidification structure, but can be used to design new anode moulds and predict the effects of a change in geometry. In a further step, it would be possible to extend the model so that it also includes the composition of the anode copper and hence a simulation of CET and grain size.

6.1 Geometry and Data for Simulation

In order to provide an overview of the situation to be modelled, the actual geometries of the anode and anode mould at Montanwerke Brixlegg AG are depicted in Figure 118 and Figure 119. The actual geometry of the casting mould and the anode mould, as well as the positions during waiting and casting are illustrated in Figure 120.

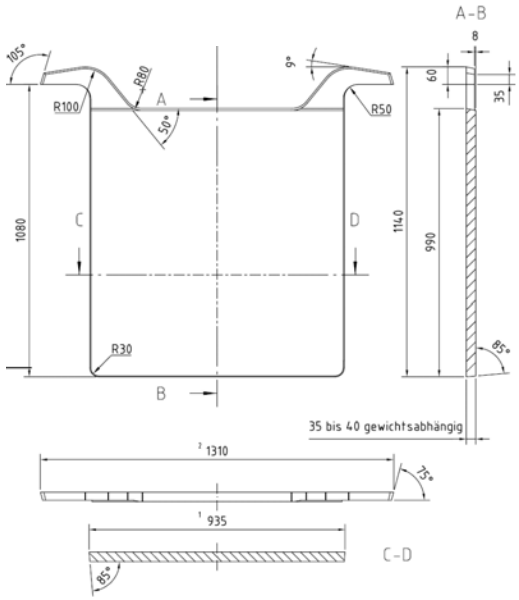

Figure 118: Anode geometry—Montanwerke Brixlegg AG

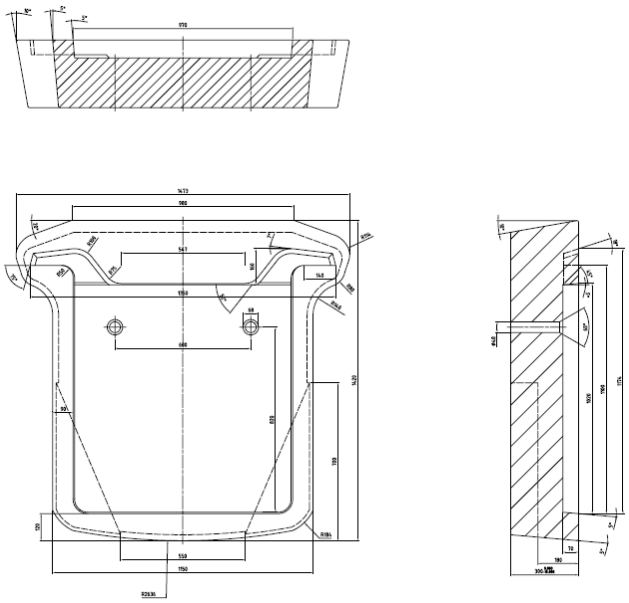

Figure 119: Anode mould geometry—Montanwerke Brixlegg AG

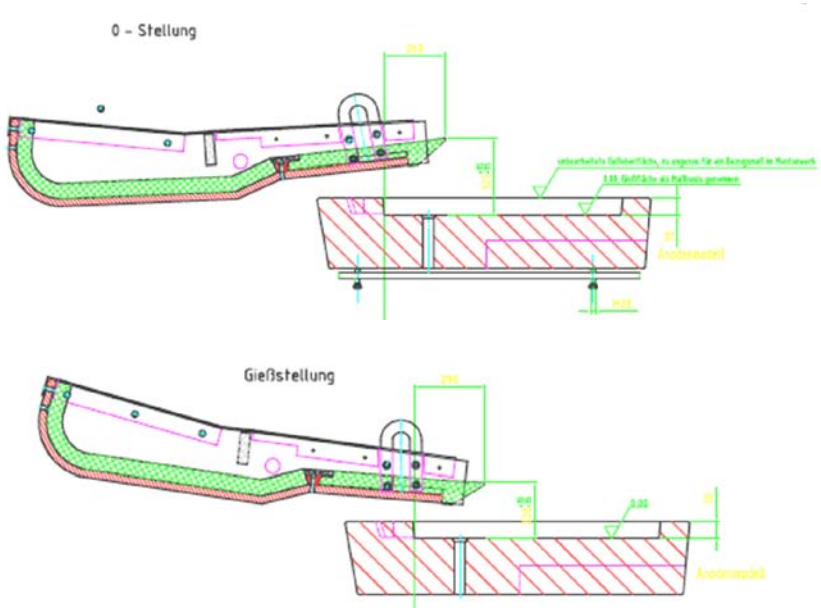

Figure 120: Casting mould in waiting position (upper picture) and casting position (lower picture)—Montanwerke Brixlegg AG

The casting wheel at Montanwerke Brixlegg AG has 14 moulds, which are made of anode copper, and barite is used as mould wash. The mould filling takes 15 s, the total time per position amounts to 21 s. The mould bottoms are cooled by water spray cooling at 6 positions (old cooling arrangement). The air side of the mould solidifies in contact with air (6 positions) and is then also cooled by water spray cooling at 2 positions (Section 5.1 and Figure 45).

The geometry for the simulation is depicted in Figure 121. In addition, the push pins were considered. In order to simulate the spray cooling on the bottom and the air side, the cooling zone was divided into air cooling (i.e., outer area) and time dependent water spray cooling (i.e., central area) (Figure 122). As the simulations using this actual geometry showed that the inlet had an influence on the cooling and temperature of the anode in the area, which is subjected to water spray cooling, even when it was defined as air (Section 6.4), the inlet was modified (i.e., shifted towards the top of the anode, Figure 123) in the following simulations to study the solidification and cooling of the anode surface more precisely.

The HTC values were selected according to the literature [88, 98, 121] (Section 2.4 and Table 29), MAGMASOFT® database, and calcosoft-2D results (Section 6.2).

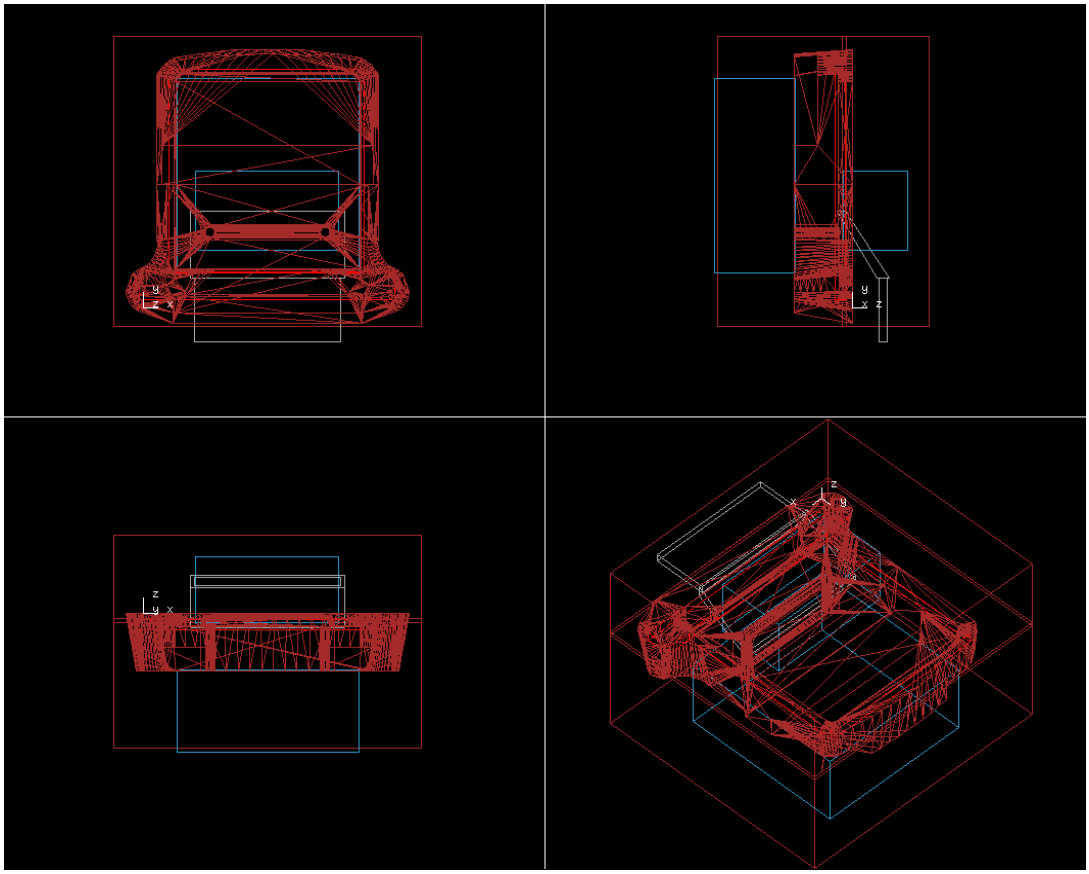

Figure 121: Actual anode and mould geometries

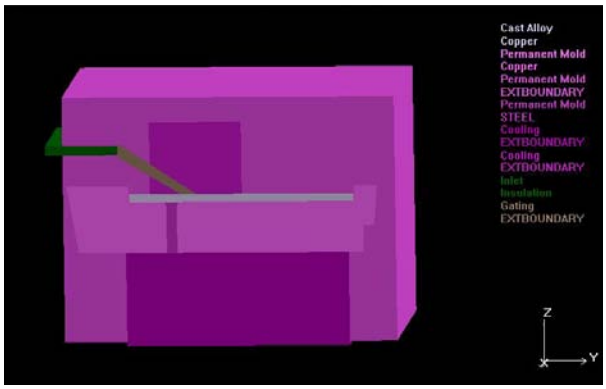

Figure 122: Actual anode and mould geometries with divided cooling zones (Dark pink: Water spray cooling area (time dependent); Light pink: Air cooling; Slicing x = 126)

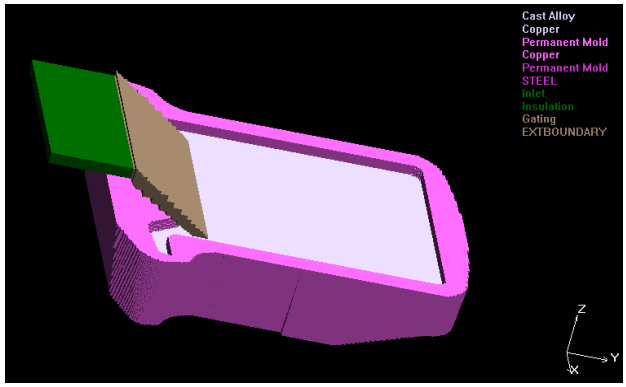

Figure 123: Anode and mould geometries with modified inlet

Table 29: HTC between the different materials

Material 1	Material 2	HTC [W/m²K]	Reference
Metal	Mould	20–800	[122]
Mould	Air	300 (constant)	[123]
Casting	Mould	700	[123]
Casting	Air	100	[123]

For the enmeshment, the "standard" option was used. In order to compare the simulation with actual anode casting, thermocouple control points were positioned in the mould at positions that corresponded to those of the thermocouples in the actual measurements.

As it was determined in preliminary calculations for 60 cycles, that the temperatures in the mould reached a constant temperature range after 10 cycles, the number of calculated cycles was reduced to 20 for the following simulations in order to save calculation time.

The MAGMASOFT® database only provides data for pure copper. The thermal conductivity was also approximated by calculation (Equation 22) [113], which resulted in values close to those for pure copper (Figure 124, green curve):

$$\lambda = \sum_i x_i \cdot \lambda_i$$ Equation 22

x_i Weight fraction of accompanying element i

λ_i Thermal conductivity of accompanying element i [W/mK]

This type of calculation is valid for electrical conductivity, which shows the same general behaviour, namely a decrease with temperature, for both pure and impure or alloyed copper. However, this is not the case for thermal conductivity: The thermal conductivity of copper alloys or impure copper increases with temperature, whereas that of pure copper decreases (Figure 125) [124]. The values were approximated accordingly, and saved as “anode Cu” in the project database. In order to compare the results for anode and cathode copper, the calculations were carried out for both materials.

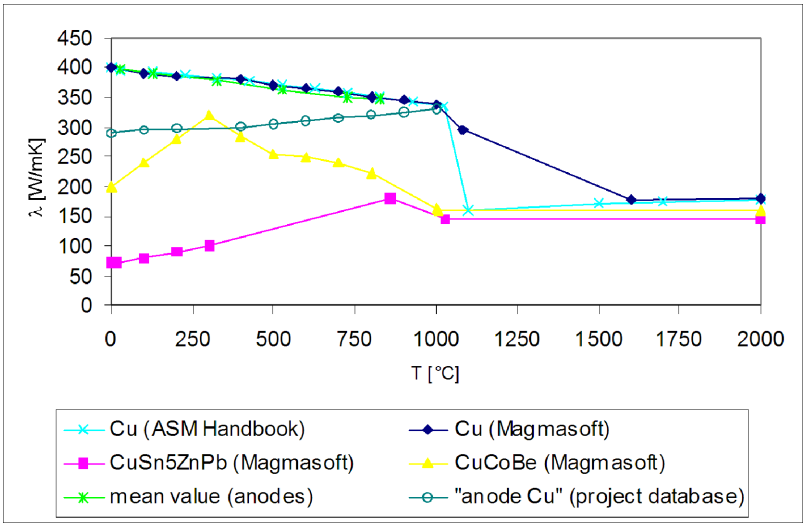

Figure 124: Thermal conductivity of pure Cu and alloyed Cu, and calculated values for anode Cu

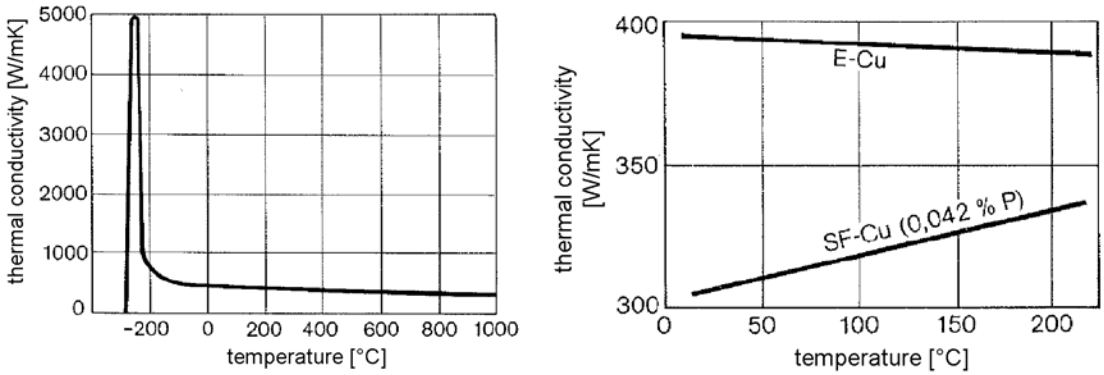

Figure 125: Thermal conductivity of pure Cu (left and E-Cu, right) and alloyed Cu (SF-Cu, right) [124]

Calculations of liquidus temperature, c_p, and solidification were carried out with the Factsage thermodynamic software (Thermfact/CRCT (Montreal, Canada) and GTT-Technologies (Aachen, Germany)). The results for c_p are illustrated in Figure 126. The general behaviour appeared to be very similar to that of pure copper. Certain differences were found between batches with relatively low and high impurity levels. However, for the first simulations average values and those for copper from the MAGMASOFT® database were used.

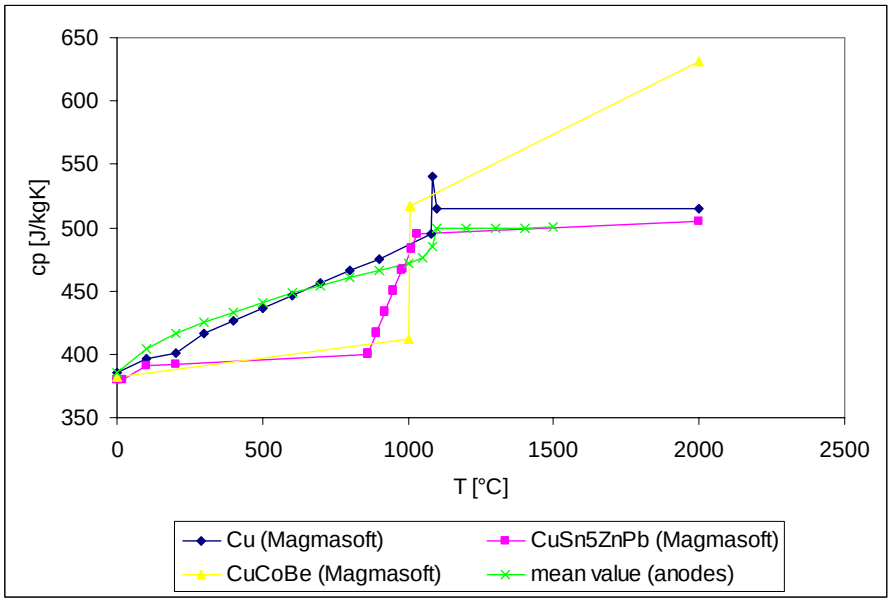

Figure 126: Specific heat capacity of pure Cu, alloyed Cu, and calculated values for anode Cu

The parameters for the calculations are provided in Table 30 and Table 31.

Table 30: Material definitions for the calculation

Component	Material group	Material	Start temperature [°C]
Anode (casting)	1_1	“anode Cu”/Cu	1,150
Lower part of mould (mould 1)	6_1	Cu	30
Upper part of mould (mould 2)	6_2	External boundary	20
Push pins (mould 3)	6_3	Steel	30
Gating	19_1	External boundary	800
Inlet	10_1	Insulation	800
Inner (water) cooling—bottom	7_1	External boundary	20
Inner (water) cooling—AS	7_2	External boundary	20
Outer (air) cooling—bottom	6_2	External boundary	20

Table 31: HTC definitions for the calculation

Component 1	Component 2	HTC	HTC [W/m²K]
Casting	Mould 1	coat_CHW	Calculated with calcosoft-2D (time dependent, Section 6.2)
Casting	Mould 2	air cooling_CHW	250
Inlet	Mould 2	air cooling_CHW	250
Casting	Mould 3	LA_steel-coat	400–620 (Temperature dependent)
Gating	Mould 2	air cooling_CHW	300
Casting	Inner (water) cooling—AS	air side-water_CHW	300–1,500 (time dependent)
Gating	Inner (water) cooling—AS	air cooling_CHW	250
Mould 2	Mould 1	air cooling_CHW	250
Mould 3	Mould 1	LA_steel-mold	1,000–2,700 (Temperature dependent)
Mould 1	Inner (water) cooling—bottom	mould-water_CHW	250–10,000 (time dependent)
Mould 2	Inner (water) cooling—bottom	mould-water_CHW	250–10,000 (time dependent)
Mould 2	Inner (water) cooling—AS	mould-water_CHW	250–10,000 (time dependent)
Mould 3	Inner (water) cooling—bottom	mould-water_CHW	250–10,000 (time dependent)

During anode casting, the cooling conditions and hence the HTC on the air side are variable with time:

- 6 positions air cooling 126 s
- 2 positions water spray cooling 42 s
- 3 positions air cooling (until removal) 63 s
- 3 positions air cooling (empty) 63 s

The HTC at the mould bottom also changes during the casting process, due to the water spray cooling (old cooling arrangement):

- 3 positions air cooling 63 s
- 6 positions water spray cooling 126 s
- 2 positions air cooling (until removal) 42 s
- 3 positions air cooling (empty) 63 s

The calculations were also carried out for the new cooling arrangement at Montanwerke Brixlegg AG, in order to study the effect of more intense cooling on the bottom. The HTC at mould bottom was defined as follows:

- 1 position air cooling 21 s
- 10 positions water spray cooling (until removal) 340 s
- 1 position water spray cooling (empty) 21 s
- 2 positions air cooling (empty) 42 s

Further calculations studied the effect of very high cooling on both the air and mould side, namely cooling conditions similar to those in the CONTILANOD® process, and a rise in casting temperature.

The following parameters were chosen for batch production and results:

- Batch production
    - 10 cycles
    - Opening parameter: 231 s
    - Closing parameter: 0 s
    - Lead time: 63 s
    - Wait time: 0 s
- Results
    - Consider casting, solid results: cycle 1 and 10
- Coating
    - Die coating: 232–252 s
    - Particles: yes
    - Quenching: no
- Filling
    - Filling time: 16 s

6.2 Calculated Temperatures in Mould and Heat Transfer Coefficient

The heat transfer coefficient (HTC) between liquid copper and anode mould was determined from the temperature measurement results by using inverse calculation (Calcosoft-2D). The range used is shown in Figure 127 (left). The temperature distribution in the mould before filling (Figure 128) was calculated from the temperature range depicted in Figure 127 (right).

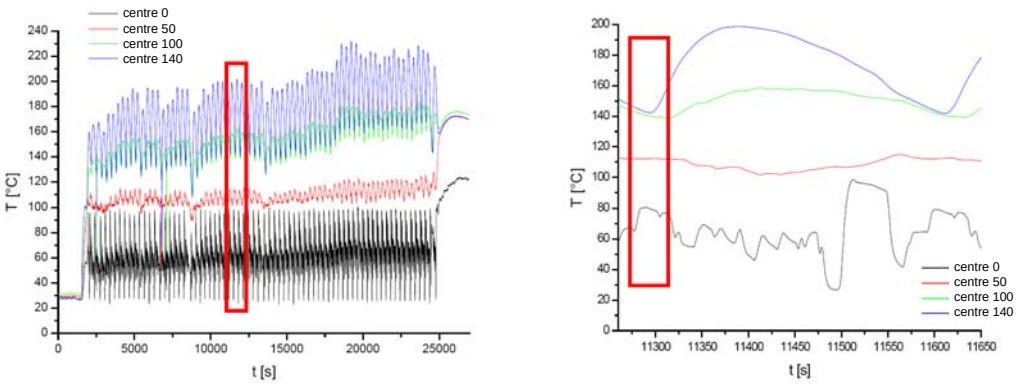

Figure 127: Used range for the inverse calculation with calcosoft-2D

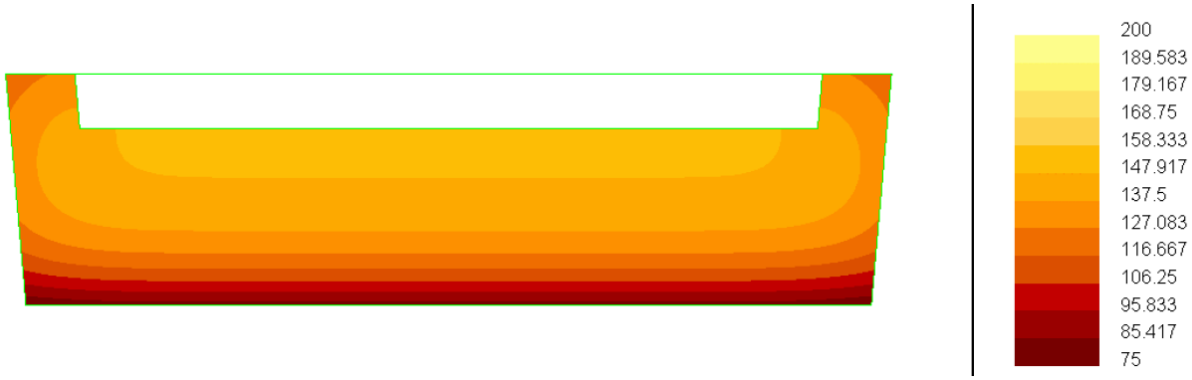

Figure 128: Temperature profile in anode mould before mould filling (left) and corresponding temperature scale [°C] (right)

The extrapolation of the minimum and maximum temperature during one cycle (Figure 129) is depicted in Figure 130 and represents an estimation of the temperature variations in the mould. This temperature difference and mould heating, respectively, was in good agreement with heat balance calculations.

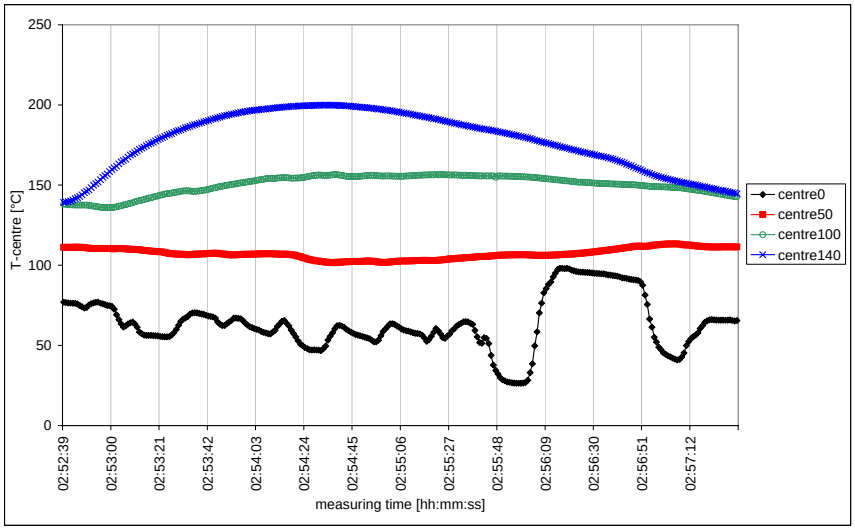

Figure 129: Temperatures during one cycle (294 s)

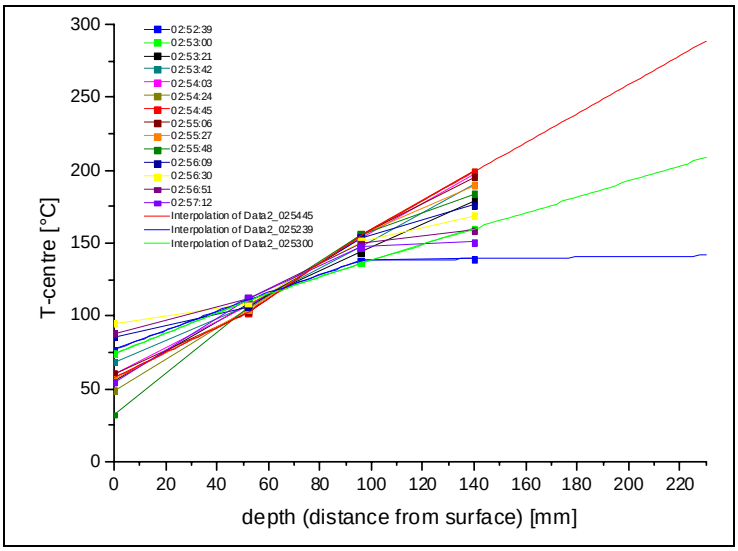

Figure 130: Extrapolated temperatures for minimum and maximum temperature of one cycle

As a first approximation the material data for cathode copper was used for the anode and anode mould. The following heat transfer was assumed for the inverse calculation:

- Sides: Heat transfer to air
- Top and bottom: Heat transfer by water spray cooling and air
- Between anode and mould: To be calculated

The temperatures of the measurement point at a depth of 140 mm were taken as the reference for the inverse calculation of the HTC. The comparison between calculated and measured temperatures is illustrated in Figure 131. A good correlation was found for the measurement points at depths of 100 and 140 mm. The behaviour of the other two thermocouples (50 mm deep and surface), which were strongly influenced by the application of cooling water could not be modelled exactly. The calculated HTC is depicted in Figure 132.

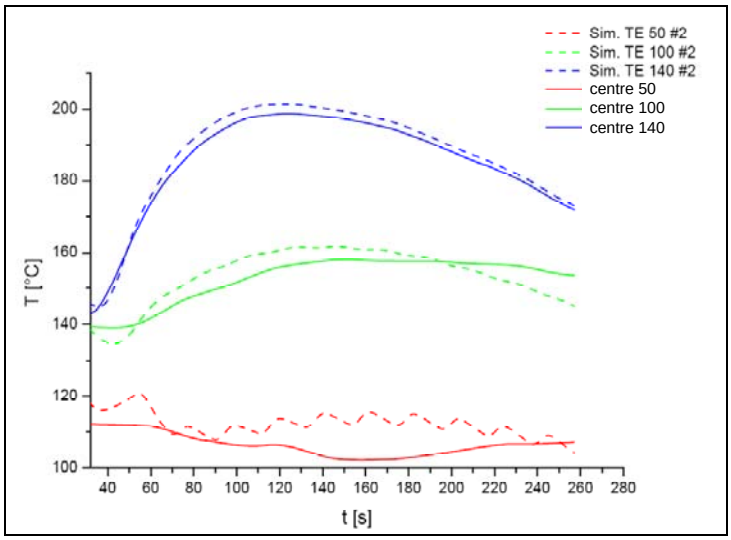

Figure 131: Comparison of calculated and actual temperatures

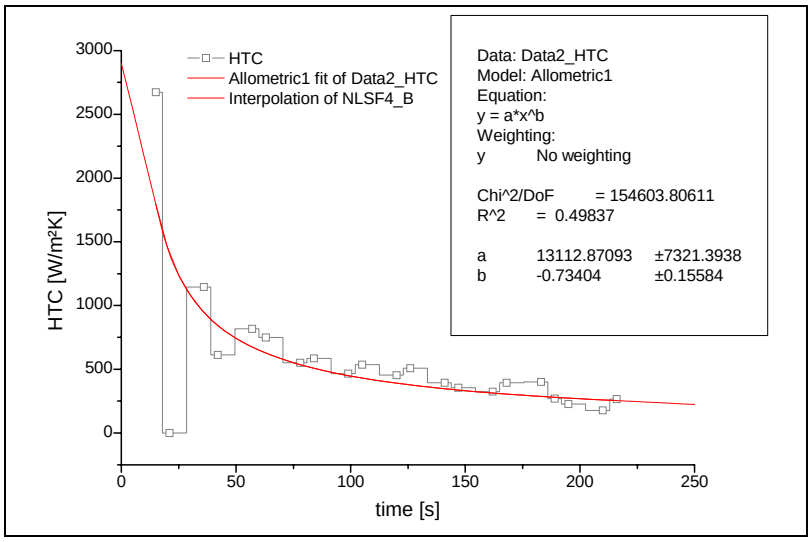

Figure 132: Calculated HTC between liquid copper and mould

The temperatures calculated with MAGMASOFT® for 20 cycles in the mould centre, using the calculated HTC between the anode and mould, are depicted in Figure 133 (left). The temperatures at the depths of 100 and 140 mm agreed very well with the actual temperatures in the mould (Figure 133, right) using the material and HTC definitions described above.

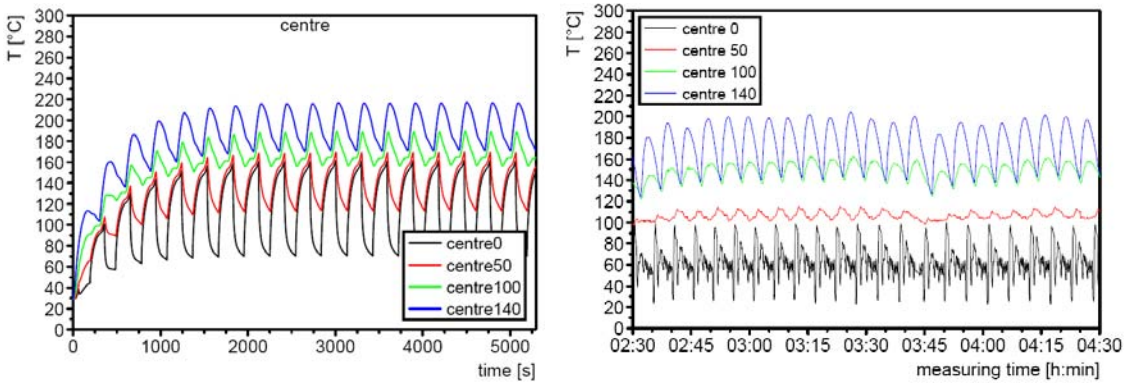

Figure 133: Calculated (left) and actual (right, new cathode Cu mould) temperature behaviour during 20 casting cycles (centre: T1–T4)

The deviations between the actual and calculated temperature curves at the measuring depth of 50 mm and the surface may result from bad contact between the thermocouple and mould during the measurements and a strong influence of the cooling water. As previously described, these two temperature measurements could not be modelled exactly with calcosoft-2D either.

The use of the user-defined anode Cu and cathode Cu as anode material resulted in only a small temperature difference, as can be seen in Figure 134. The comparison between the old and new cooling arrangements shows approximately 50 °C lower temperatures with the more intense cooling (Figure 135, left). This does not correlate with the actual measured temperatures in the mould (Figure 135, right), which are nearly the same as with the old cooling arrangement.

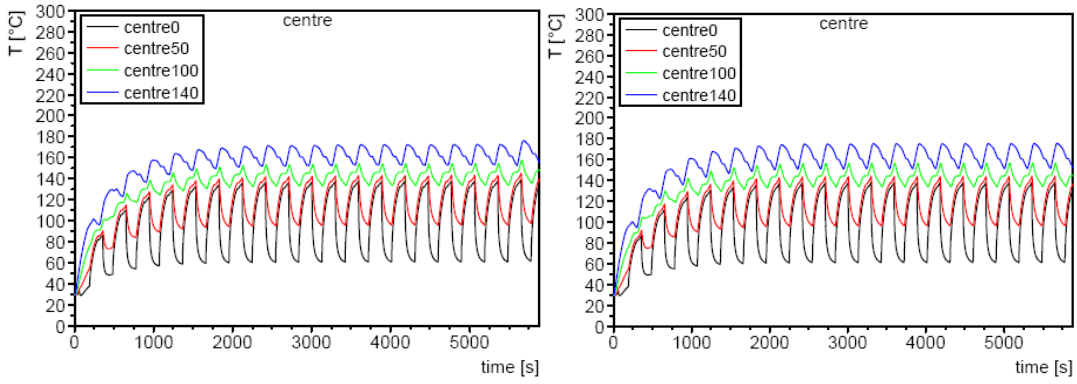

Figure 134: Calculated temperatures in mould (centre: T1–T4) with old cooling arrangement (anode defined as “anode Cu” (left) and cathode Cu (right))

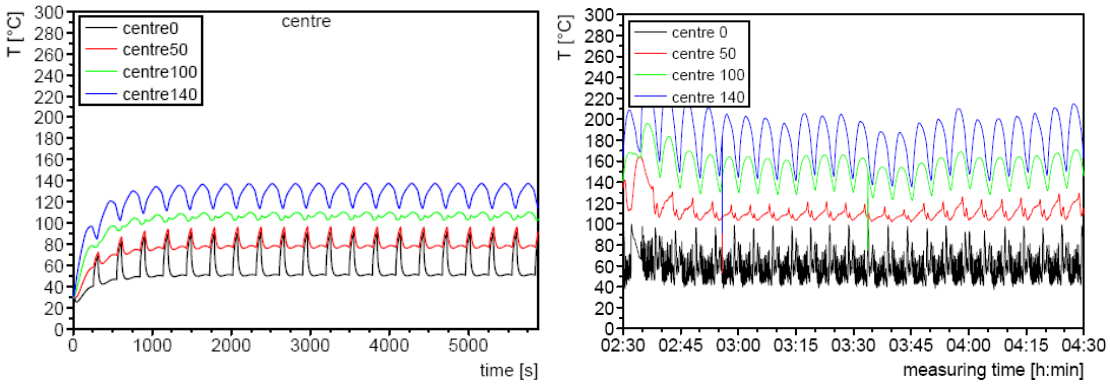

Figure 135: Temperatures in mould (centre: T1–T4) with new cooling arrangement—calculated (left, anode defined as “anode Cu”) and measured (right)

6.3 Calculated Mould Filling

The filling velocity for the real geometry is illustrated in Figure 136 and Figure 137. The turbulence during mould filling is visible. The movement of the liquid copper, namely the flow to the end of the mould and the backflow, is in good agreement with the actual movement of the liquid copper during mould filling as depicted in Figure 138. However, the basic model did not focus on mould filling in detail, but on solidification and cooling (Section 6.4).

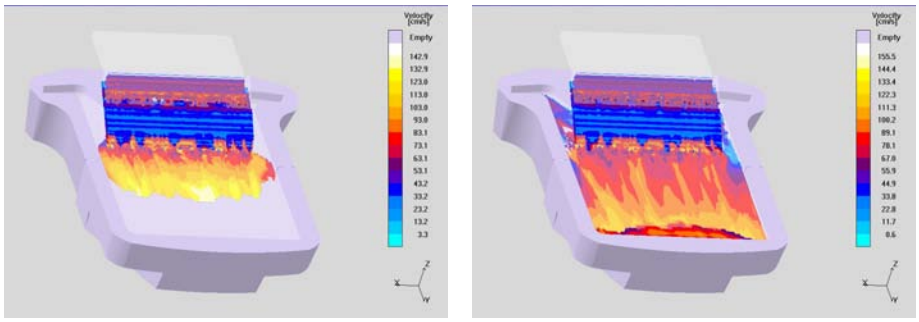

Figure 136: Calculated velocity during mould filling—(left: 40%, right: 60%)

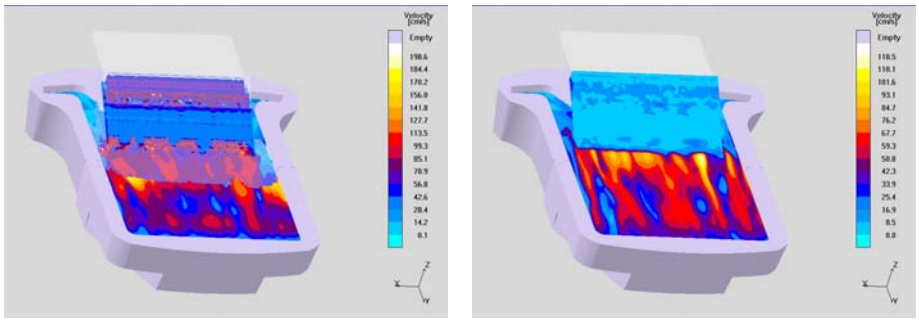

Figure 137: Calculated velocity during mould filling—(left: 80%, right: 100%)

Figure 138: Actual mould filling

The flow of the liquid copper is important, as it leads to a certain mechanical load on the mould and also has an influence on the anode quality regarding the formation of edge fins. As the flow of the liquid copper is also dependent on the design of the inlet, namely the weighing trough and its spout, the model can also be used to optimize the geometries of the casting system and mould, casting velocities, and the resulting copper flow.

6.4 Calculated Solidification

As the simulations using the actual inlet position showed that the inlet had an influence on the cooling and temperature of the anode in the area, which is subjected to water spray cooling, even when it was defined as air (Figure 139), the inlet was modified in the following simulations.

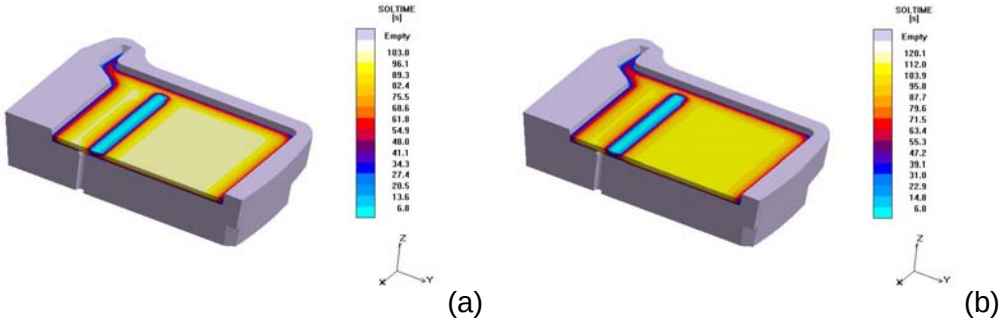

Figure 139: Calculated solidification time for cycle 1 (a) and 10 (b) (real geometry; slicing x = 126)

The calculated anode solidification times using the parameters previously described are very realistic (Figure 140). It was evident that (using the old cooling arrangement) the inner area is the last solidifying part of the anode. The solidification time on the air side is a good indicator, as it is known that the surface has to solidify within 6 positions, namely 126 s, as the water spray cooling on the air side starts at this point.

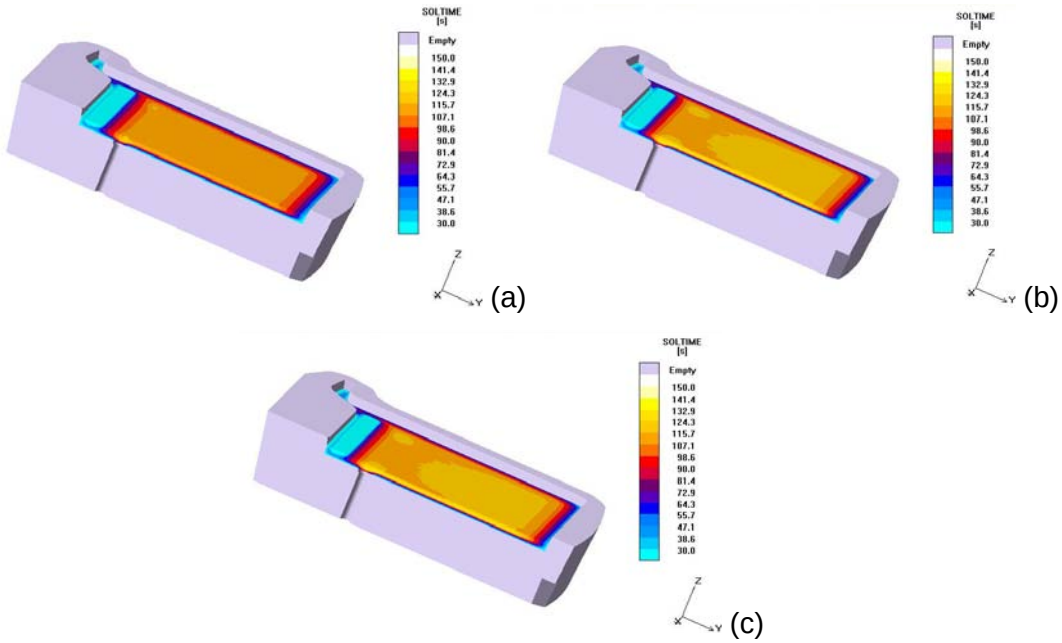

Figure 140: Calculated solidification time for cycle 1 (a), 10 (b) and 20 (c) (modified geometry; slicing x = 126; anode = “anode Cu”, old cooling arrangement)

The solidification times can be verified by considering the calculated DAS values (Figure 141). The calculated results for solidification time were used with the results from the experimental investigations (Section 5.4.2) in order to calculate the DAS values using a user defined function. As the DAS results represent the actual microstructure of the anode very accurately, it can be assumed that the solidification time on the mould side and hence the overall simulation is realistic.

The influence of the Cu material data and cooling arrangement is illustrated in Figure 141–Figure 143. The different solidification conditions within the anode are visible, and also the differences between casting in cold (cycle 1) and warm (cycle 10 and 20) moulds. The in-homogeneous solidification conditions are also visible from the temperature gradient and solid phase fraction.

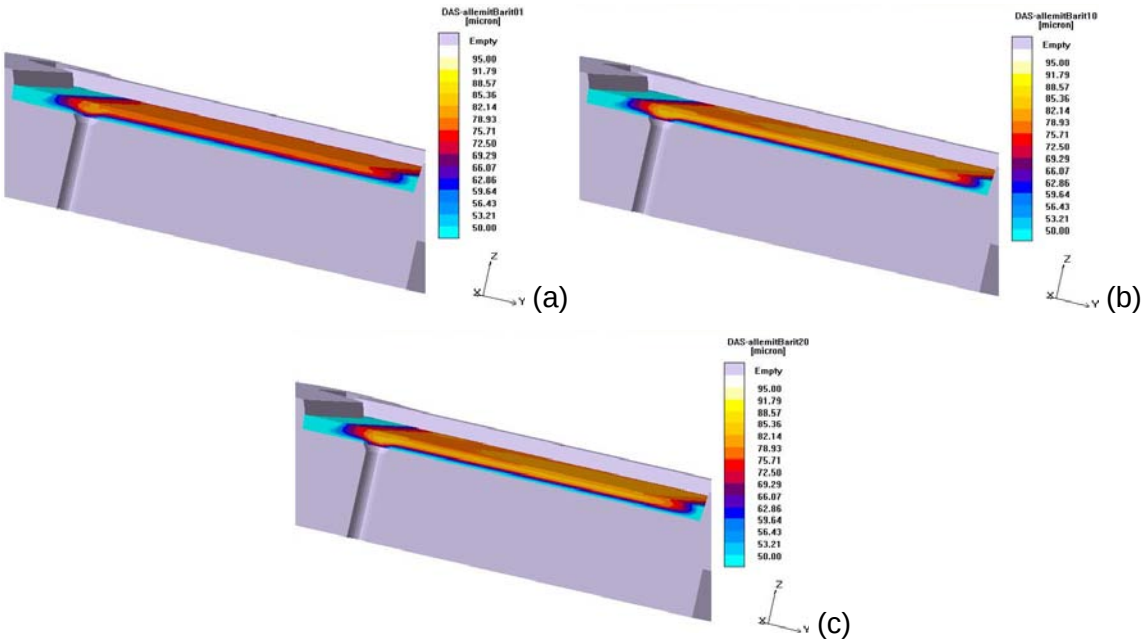

Figure 141: Calculated DAS for cycle 1 (a), 10 (b) and 20 (c) (modified geometry; slicing x = 126; anode = “anode Cu”, old cooling arrangement)

As is evident in Figure 142 and Figure 143, more intense cooling of the mould bottom does not only lead to lower mould temperatures (Section 6.2) but also results in a certain variation of the solidification time and hence the microstructure of the anode, namely the DAS values. It is also evident in Figure 142 and Figure 143 that the trend of the DAS across the anode thickness has changed. As with the old, less intense cooling the highest DAS values were found in the centre of the anode, the new cooling enhances solidification from the mould side and hence leads to faster cooling of the central areas. Consequently, with this cooling arrangement and the higher cooling, the largest DAS are found on the air side. This is consistent with the investigations of anode structure (Section 5.4.2).

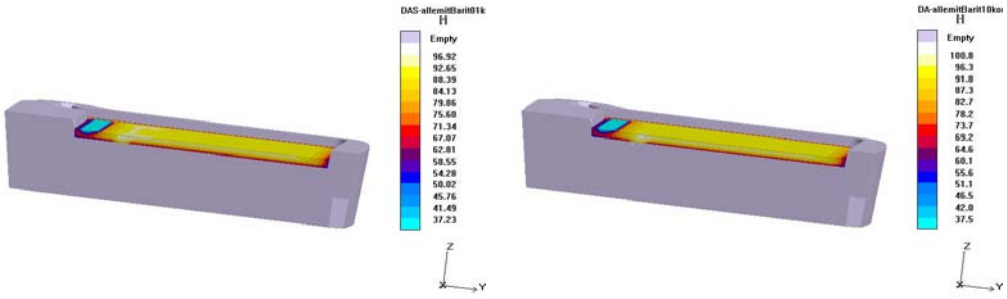

Figure 142: Calculated DAS for cycle 1 (left) and 10 (right) (modified geometry; slicing x = 126; anode = “anode Cu”, new cooling arrangement)

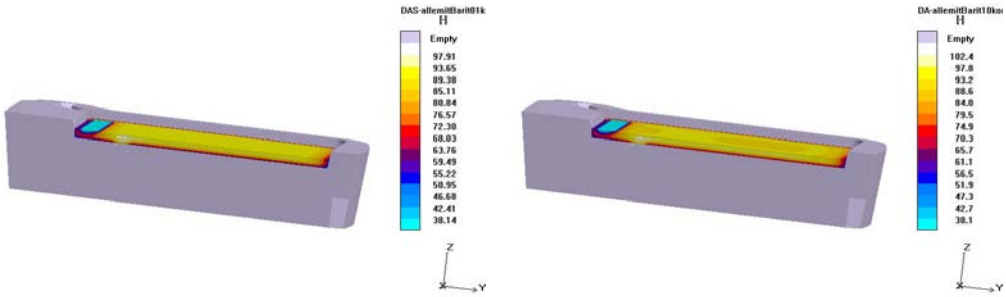

Figure 143: Calculated DAS for cycle 1 (left) and 10 (right) (modified geometry; slicing x = 126; anode = cathode Cu, new cooling arrangement)

The implementation of a very high cooling intensity on the air side as well as on the mould bottom leads to a similar trend in DAS values across the anode thickness as with the less intense cooling (old cooling arrangement), namely the largest DAS are again found in the central area of the anode. As expected, the solidification time and hence the DAS values decrease notably (Figure 144).

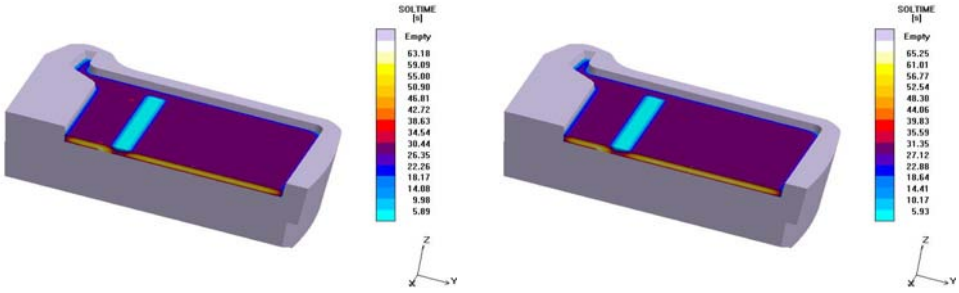

Figure 144: Calculated solidification time for cycle 1 (left) and 10 (right) (real geometry; slicing x = 126; anode= “anode Cu”, high cooling on both air and mould side)

Further simulation experiments investigated the effect of a rise in casting temperature. An increase in solidification times and hence larger DAS values were found.

The simulation results of anodic solidification are consistent with the experimental results. The basic model, which was developed, can hence be used to study effects of changes in cooling arrangement and mould design, as well as the casting system. If a definitive relationship between DAS and anodic dissolution were found, it could also be used to predict anodic dissolution behaviour to a certain extent. A further step could include the anode chemical composition, so that the columnar-to-equiaxed-transition (CET) and grain size could also be predicted, as well as the dissolution behaviour of anodes from a certain batch.

7. Summary and Conclusions

Anode casting is the link between copper pyro- and hydrometallurgy. To achieve good electrorefining performance, the anodes must have a certain chemical and physical quality. The latter is directly linked with the anode casting process. The aims of anode casting—high output and long mould lifetimes—are not consistent with the objectives of electrorefining, which include uniform dissolution, minimum anode scrap, optimum current efficiency, and high cathode quality.

The requirements for an anode regarding the chemical quality can be summarized as follows:

- For optimum electrorefining operations, the anodes should have a homogeneous chemical composition, so that the electrolysis can be adjusted properly. Gas purging in the anode furnace is recommended for a uniform chemical composition within one charge.
- The elemental distribution within one anode is important for homogeneous dissolution.
- The accompanying elements in the anode should form soluble compounds with the copper or solid solutions, as insoluble compounds lead to high Cu levels in the anode slimes or the formation of passivating layers on the anode surface.

The requirements regarding the physical quality can be summarized as follows:

- Independent of the technology used, proper control of the casting process is vital to produce high quality anodes of uniform weight that are free from casting defects.
- Anodes with a fine globulitic/equiaxed structure dissolve faster than those with coarse grains.
- Coarser globulitic/equiaxed grains are less susceptible to passivation.

The elemental distribution and the grain size can be influenced by altering the solidification conditions, for example change of cooling rate, thermal conductivity (i.e., material) of the anode moulds, and mould preheating. Faster cooling leads to finer grains and supersaturated solid solutions.

The level of non-metallic inclusions may be reduced by minimizing slag carry-over from the anode furnace as well as oxygen uptake during pouring of the liquid metal, for example using burners, which provide a reducing atmosphere. The optimization of mould wash (i.e., composition and amount) is important as adhering mould wash can cause the formation of

buds and dendrites. Preheating anode moulds may be a suitable means to reduce the number of rejects.

The following effects are related to the accompanying elements in the anode copper, and hence the chemical anode quality:

- Enhanced passivation: Ag, Se, Ni + O, Se, O, low As levels, and the presence of Pb without sufficient O for oxide formation
- Dendrite formation: low As levels
- Decreased cathode quality: Sb, Bi, (Ag, Se), and low As content
- Poor electrical conductivity of electrolyte: Ni
- Altered properties of anode slimes: Ni, As, Se, (Sn), O and oxides

These effects can be minimized either by low impurity levels and suitable relative amounts of the elements in the anode copper, which is mainly the task of fire refining, or by the appropriate chemical form of the elements and the elemental distribution, which can be influenced by the casting process and the cooling conditions.

A temperature measurement system was installed in anode moulds at Montanwerke Brixlegg AG, to determine the anode cooling and solidification conditions from the mould temperatures. To investigate the influence of the casting process on solidification, cooling conditions, and anode quality, the process parameters mould material and mould wash were varied. The casting process at Montanwerke Brixlegg AG and the corresponding anode samples were investigated in detail to establish the causes for different anode qualities and their effects on electrorefining.

Due to the use of gas purging in the anode furnace, the chemical composition within one batch of anodes, namely during the casting process, was found to be relatively constant.

Generally, a relatively constant temperature was reached after several cycles, namely several anodes cast in one mould. On some casting days an increase in casting temperature was measured towards the end of the casting process, which also led to an increase in mould temperature due to the higher liquid copper temperature. However, this increase did not occur on every casting day, and was a result of the specific furnace operations. Due to these fluctuations in casting temperature, it would be reasonable to measure the casting temperature (and anode mould temperature) continuously and then adjust the cooling accordingly.

The use of different mould materials and mould wash, as well as the different period of use of the mould, resulted in significant differences in mould temperature and hence anode cooling conditions. The rise in temperature with lifespan may have been caused by an insulating limescale, which formed on the mould bottom due to contact with the cooling water. However, these temperature variations did not seem to have an influence on chemical anode quality, as—contrarily to literature statements—a relatively uniform chemical quality across the anode thickness, as well as the phase type and distribution, was found in all investigated anodes. No definitive trends regarding elemental distribution were detected. This may be due to the relatively rapid cooling at Montanwerke Brixlegg AG. As there were no differences across the anode thickness regarding chemical quality, the inhomogeneous anodic dissolution behaviour might be caused to a great extent by structural differences across the anode thickness.

The anodes, which were produced with barite as mould wash, showed a typical cast structure. Variations in structure were detected in the different anodes. There was also a certain structural inhomogeneity within one anode, namely over the anode area, which indicated different local cooling conditions that may have been caused by uneven mould wash application as well as cracks in the mould. The variations in grain size directly on the air side, which solidifies in contact with ambient air, was probably caused by the different numbers of nuclei present. The variations in grain size close to the air side may have been caused by the Leidenfrost effect resulting in the formation of an insulating vapour film, which results in a lower heat transfer and hence reduced cooling efficiency. This could be avoided by applying atomized spray cooling or intermittent sprays, which avoid the formation of a stable vapour layer. The extension of the different solidification structures and hence the position of the central area was dependent on the cooling conditions at the air and mould side.

The cooling was found to be very important, not only regarding anode quality but also regarding mould life and casting rate. A more effective cooling on the airside, namely the avoidance of the Leidenfrost effect, and a subsequent higher heat transfer on the air side would relieve the mould underside cooling and also reduce the thermal stress of the mould. This could prolong anode mould life. Additionally, at a constant mould underside cooling the casting rate could be increased. The insulating limescale on the mould underside could be avoided by using filtrated or recycled water. Even though the water temperature of the recycled water might be higher, the insulating limescale has a much more pronounced impact on the overall cooling effect.

As dissolution occurs preferentially at the grain boundaries, the different solidification structures are reported to have different dissolution rates and tendency for passivation. Regarding electrochemical dissolution a less noble behaviour, namely fine grain, would be advantageous; regarding passivation a more noble behaviour and hence a higher anode polarization for the onset of passivation would be desirable. The inhomogeneous anode dissolution in electrorefining could be explained by structure variations, namely grain size and secondary dendrite arm spacing (DAS), over the anode area and across the thickness. Potential measurements demonstrated the different dissolution behaviours across the anode thickness. According to the experimental investigations, a homogeneous structure results in homogeneous anodic dissolution. However, no definitive correlation between the structure and the anode polarization as well as the i_{max} could be found. The investigation of a greater number of anodes with a wider range of structures would be necessary to find definitive trends for the anodic dissolution behaviour.

Regarding the measurements and investigations, it is difficult to determine the anode quality from only the temperature data, as there are many other parameters that influence the cooling and solidification, for example:

- Fluctuations in casting temperature (→ hotter moulds, different solidification)
- Uneven mould wash application: different workers, inhomogeneous density
- Moulds: Cracks, different quality and hence thermal properties, limescale

Due to these inhomogeneities in the overall process, the physical anode can vary significantly within one anode, as there are different local cooling conditions within one anode mould. Hence the cooling conditions of the anode can only be determined at those points where the temperature measurements are installed. Another parameter is the chemical composition of the anode copper, which has a certain variation range, as the nucleation of grains and also growth are linked to the impurities present.

The simulation and the basic model for anode casting, which was developed, can therefore only provide an overview of cooling and solidification. A simulation of grain size is limited by the present process variations. To perform this in a reasonable manner the following preconditions were required:

- Totally homogeneous moulds
- Totally homogenous mould wash and application
- Continuous measurement of casting and mould temperature, as well as continuous adjustment of cooling (only if the first 2 points are given, otherwise: cooling only suitable for positions with measurements but not for entire anode)

However, the calculated temperatures and solidification times together with the experimentally determined parameters to calculate DAS enable an estimation of the DAS in the anodes. Calculations with different material data and cooling arrangements demonstrated that the new cooling arrangement at the mould bottom does lead to lower mould temperatures and a significant change in the microstructure trend across the anode thickness, namely the DAS values. Due to the intense cooling from the bottom, the largest DAS were no longer found in the central, but on the air side. This was also confirmed by the experimental results and demonstrated the general validity of the basic model for the simulation of anode casting. The basic model can be used for:

- Mould design optimization
- Casting system optimization
- Cooling arrangement optimization

If a definitive relationship between DAS and anodic dissolution behaviour can be found by further investigations, also the prediction of the dissolution behaviour is possible by predicting DAS values. In order to not only predict the anodic dissolution behaviour from the cooling conditions, but predict the dissolution behaviour of each single batch, the model has to include also the chemical composition of the anode. A database of the dissolution behaviour of anodes with different chemical compositions has to be generated and linked with the model for the existing cooling conditions, so that finally the anodic dissolution behaviour of each single batch can be predicted by knowing the chemical composition.

8. References

[1] La Farga Lacambra. Internet: www.la-farga-lacambra.com (Access: 24.4.2008)

[2] Guixa O. and G. Properzi: Continuous copper rod production from 100 percent scrap. Wire Journal International, 1996, 60 - 67

[3] Guixa O. and M. Garcia: Further steps in copper scrap refining and subsequent CCR copper rod production. Internet: www.properzi.com (Access: 7.1.2008)

[4] Brocato C. M.: From Low Grade Copper Scrap to Quality Copper Rod. (2007) Internet: www.properzi.com (Access: 24.4.2008)

[5] Report - Montanwerke Brixlegg, Summer 2005. 2005

[6] Moats M., T. Robinson, W. Davenport, G. Karcas and S. Demetrio: Electrolytic Copper Refining - 2007 World Tankhouse Operating Data. Copper Cobre 2007, Volume V, Toronto, Canada: 2007, 195 - 241

[7] World Refined Copper Production and Usage Trends. Internet: www.icsg.org (Access: 24.4.2008)

[8] Definitions and Description of Copper Based Products. Internet: www.icgs.org (Access: 28.4.2008)

[9] Personal Information - Continuus Properzi. 9.5.2008

[10] International Copper Study Group - World Copper Factbook 2007. Internet: www.icsg.org (Access: 24.4.2008)

[11] GDMB: Elektrolyseverfahren in der Metalllurgie. Heft 81 der Schriftenreihe der GDMB Gesellschaft für Bergbau, Metallurgie, Rohstoff- und Umwelttechnik, 1997, 53 - 66

[12] Alarcon V. R.: Anode casting operation, process improvements and anode quality at the Ilo refinery. Converter and Fire Refining Practices, TMS, 2005, 133 - 147

[13] Personal Information - SMS Meer Kupferanlagen - Maschinen, Anlagen und Systeme. 2007

[14] Lumppio J.: Casting trough and method for casting copper anodes. WO 2005/095027 A1, 2005

[15] Personal Information - Boliden - Rönnskär Plant. 29.5.2008

[16] Robinson T., J. Quinn, W. Davenport and G. Karcas: Electrolytic copper refining - 2003 world tankhouse operating data. Copper 2003 - Cobre 2003, Vol. 5, Santiago, Chile: 2004, 3 - 66

[17] Chernomurov F. M., T. G. Kalinovskaya, F. S. Kudlai and V. N. Krivenko: Crystallization features for copper anodes when changing the design and cooling conditions for molds. Tsvetn. Met. (Non-ferrous Metals), No. 3, 1986, 23 - 25

[18] Antrekowitsch H., K. Hein, P. Paschen and D. Zavialov: Einfluss der Struktur und Elementverteilung auf das Auflösungsverhalten von Kupferanoden. Erzmetall, 52, 1999, 337 - 345

[19] Chen T. T. and J. E. Dutrizac: Mineralogical Characterization of Anode Slimes. VII. Copper Anodes and Anodes Slimes from the Chuiquicamata Division of Codelco-Chile. Canadian Metallurgical Quarterly, 30, 1991, 95 - 106

[20] Hiroshi I. and Y. Motoaki: System for continuous manufacture of copper anodes for electro-refining. DE2250792, 1973

[21] Hakakari H. and R. L. Pariani: Study of operational factors affecting copper anode quality. Proceedings of COPPER 95 -COBRE 95 International Conference, Vol.III, The Metallurgical Society of CIM, 1995, 165 - 174

[22] Swanson C.E. and M. F. Shaw: The Interface of Anode Refining with Electrorefining. Converting, Fire Refining and Casting, J.D.McCain and J.M.Floyd (editors). The Minerals, Metals and Materials Society, 1993, 269 - 284

[23] Kreuz O. and W. Hoeft: Apparatus for the production of copper anode plates. DE1956076, 1971

[24] Fire refining and anode casting. Internet: www.outotec.com (Access: 22.2.2008)

[25] Edens T. and D. Hannemann: New casting moulds for anode copper. Converter and Fire Refining Practices, TMS, 2005, 159 - 165

[26] Droste E. and others: Method for producing a mold and a device for casting anodes. WO 03/097273 A1, 2003

[27] Roberti R. A. and others: Double Cavity Mould for Anode Casting. US 4741377, 1988

[28] Filzwieser I.: The analysis and mathematical modelling of the parameters influencing cathodic deposits in copper refining electrolysis. Dissertation, Montanuniversität Leoben, Leoben, 2005

[29] Murray E. C.: Copper casting method using titanium dioxide release method. US4178981, 1978

[30] Cruz R. and others: Method of casting copper anodes using a preheated mold coating. US3867977, 1975

[31] Nyström L. and J. Lundström: Increase of converter aisle productivity at Rönnskär. Converting, Fire Refining and Casting, The Minerals, Metals and Materials Society, 1994, 311 - 322

[32] Enrico W. A. and F. Begazo: The Southern Peru Ilo Refinery, Design Features, Operation and Improvement. Aqueous Electrotechnologies: Progress in Theory and Practice, TMS, 1997, 73 - 86

[33] Jimenez O., P. Nuñez and F. Labbé: Casting process analysis, anode bulging diagnostic and solutions - Chuquicamata Smelter. Converting, Fire Refining and Casting, J. D. McCain and J. M. Floyd (editor). TMS, 1994, 215 - 225

[34] Troesch H. J. and others: Device for cooling anodes, especially copper anodes, comprises a cooling sink with cooling liquid, an insertion unit, a removal unit, a unit for

collecting anode waste products, and a unit for transporting the waste products from the sink. DE10052728, 2002

[35] Isakov V. T.: The Electrolytic Refining of Copper, 2nd edition (English translation). Technicopy Limited, Stonehouse, 1973

[36] Gauthier H., M. Manzini and E. Ghali: Effect of lead and oxygen on the passivation of copper anodes. Canadian Metallurgical Quarterly (Netherlands), 38, 1999, 22 - 32

[37] Abe S. and M. Takahashi: A Novel Method of Increasing the Dissolution activity of Unrefined Copper Anodes. The Electrorefining and Winning of Copper, Denver, Colorado: USA, 1987, 71 - 84

[38] Imamura T. and M. Katoh: Method for treatment of copper anodes to be electrorefined. DE3310818, 1983

[39] Arentzen C.: Impurity Segregation in Copper by Controlled Cooling Treatment. US4474614, 1983

[40] Habashi F.: Handbook of extractive metallurgy. Wiley-VCH, Weinheim, 1997

[41] Personal Information - Montanwerke Brixlegg AG. 2006

[42] Brugger G.: Anodenpassivierung in der Kupferraffinationselektrolyse. Diploma thesis, Montanuniversität Leoben, Leoben, 1992

[43] Schwarze M.: The CONTILANOD® process - continuous casting and cutting of copper anodes. Delft, Netherlands, November 22.-24. 2000, 2000

[44] Personal Information - SMS Meer. 2007

[45] Hazelett. Internet: www.hazelett.com (Access: 17.1.2006)

[46] Hazelett Strip-Casting Corp.: Copper Anode Casting Machines. Internet: www.hazelett.com (Access: 24.4.2006)

[47] Dion J.L., V. S. Sastri and M. Sahoo: Critical studies on determination of oxygen in copper anodes. Transactions of the American Foundrymen's Society, Vol.103, Kansas City, Missouri: USA, 1996, 47 - 53

[48] Chen T.T. and J. E. Dutrizac: A mineralogical study of the deportment of impurities during the electrorefining of secondary copper anodes. Copper 99 - Cobre 99, Phoenix, AZ: USA, 1999, 437 - 460

[49] Filzwieser A., J. Kleicker and K. Caulfield: MET KIN® - A Gas Purging System for Metallurgical Smelting Furnaces. European Metallurgical Conference 2003, Hannover, Germany: 2003, 69 - 82

[50] Forsen O. and K. Lilius: Solidification and electrolysis of copper anodes containing nickel, arsenic, antimony and bismuth. The Electrorefining and Winning of Copper, Denver, Colorado, USA: 24.-26. Feb., 1987, 47 - 69

[51] Hein K. and E. Buhrig: Kristallisation aus Schmelzen. VEB, Deutscher Verlag für Grundstoffindustrie, Leipzig, 1983

[52] Chen T.T. and J. E. Dutrizac: The Mineralogy of Copper Electrorefining. JOM, 1990, 39 - 44

[53] Buhrig E., K. Hein and H. Baum: Verteilung von Fremdelementen bei der Kristallisation von Kupfer. Metall, 33. Jg , 1979, 592 - 596

[54] Chen T. T. and J. E. Dutrizac: The deportment of selenium and tellurium during the electrorefining of copper. Minor Elements 2000: Processing and Environmental Aspects of As, Sb, Se, Te and Bi, Salt Lake City, UT, USA: Society for Mining, Metallurgy and Exploration, 2000, 199 - 212

[55] Anzinger A., J. Wallner and H. Wöbking: Über die Bedeutung des Elementes Nickel für die Kupferraffinationselektrolyse einer Sekundärhütte. Berg- und Hüttenmännische Monatshefte, 143, 1998, 82 - 85

[56] Chen T. T. and J. E. Dutrizac: Mineralogical Characterization of a Copper Anode and the Anode SLimes from the La Caridad Copper Refinery of Mexicana de Cobre. Met. and Mat. Trans. B, 36B , 2005, 229 - 240

[57] Fischer M. J.: Beitrag zur Bildung und zum Verhalten des Anodenschlammes bei der Kupferraffinationselektrolyse. Dissertation, Technische Universität Bergakademie Freiberg, Freiberg, 1998

[58] Krusmark T. F., S. K. Young and J. L. Faro: Impact of Anode Chemistry on High Current Density Operation at Magma Copper's Electrolytic Refinery. Copper 95, Vol.3, Santiago: Chile, 1995, 189 - 206

[59] Abe S. and Y. Takasawa: Prevention of Floating Slimes Precipitation in Copper Electrorefining. TMS Annual Meeting, Hoffmann J.E. and others (editors). Denver, Colorado: TMS, 1987, 87 - 98

[60] Noguchi F., H. Itoh and T. Nakamura: Effect of impurities on the quality of electrorefinined cathode copper; behavior of antimony in the anode. COPPER 95-COBRE 95, Volume III, Cooper W.C. and others (editors). The Metallurgical of CIM, 1995, 337 - 348

[61] Claessens P. L. and V. Baltazar: Behaviour of Minor Elements During Copper Electrorefining. Refining Processes in Metallurgy (Raffinationsverfahren in der Metallurgie), Hamburg: Germany, 1983, 253 - 265

[62] Noguchi F., M. Yano, T. Nakamura and Y. Ueda: Form of Antimony dissolved into Electrolyte during Copper Electrorefining. Journal of the Mining and Materials Processing, 109, 1994, 121 - 125

[63] Meyer U.: Untersuchungen über das Verhalten insbesondere von Silber und Selen bei der Kupferraffinationselektrolyse. Dissertation, TU Clausthal, Clausthal, 1993

[64] Ringel L., K. Hein and D. Schab: Untersuchungen zum elektrochemischen Verhalten von Cu-Ag-Legierungen. Neue Hütte, 19 , 1974, 193 - 197

[65] Graumann D., Ch. Fischer-Bartelk and D. Schab: Untersuchungen zum Verhalten des Silbers bei der elektrolytischen Kupferraffination. Neue Hütte, 17 , 1972, 71 - 76

[66] Ringel L.: Elektrochemische Untersuchungen an Cu-Ag-Legierungen. Dissertation, Technische Universität Bergakademie Freiberg, Freiberg, 1975

[67] Bounoughaz M., M. Manzini and E. Ghali: Behaviour of copper anodes containing oxygen, silver and selenium impurities during electro-refining. Canadian Metallurgical Quarterly, 34, 1995, 21 - 26

[68] Gumowska W. and J. Sedzimir: Influence of the Lead and Oxygen content on the Passivation of Anodes in the Process of Copper Electro-Refining. Hydrometallurgy (Netherlands), 28 , 1992, 237 - 253

[69] Lange H.-J., B. Geidel, K. Hein and H. Baum: Untersuchungen zu anodischen Reaktionen des Selens bei der elektrolytischen Kupferraffination. Freiberger Forschungshefte, B228, 1981, 123 - 142

[70] Takada Y. and A. Fuwa: Effect of Impure Elements on the structure s of Solidified Copper Anodes and Passivation Behavior During Electrorefining. Cu-O-Vb (As, Sb or Bi) System and Cu-S-Vb System. J. Min. Metall. Inst. Jpn., 104 , 1988, 177 - 181

[71] Takada Y., R. Subagja and A. Fuwa: A Study on the Relation Between Passivation Behaviour and Microstructure of Copper Anode. Cu-O-S-Vb (As, Sb or Bi) System. J. Min. Metall. Inst. Jpn., 104 , 1988, 289 - 295

[72] Plekhanov K., V. Ashikhin and V. Koryakin: Reasons for irregular anode dissolution. Copper 2003-Cobre 2003, Vol. 5, Santiago, Chile: 2003, 639 - 649

[73] Forsen O.: The behaviour of nickel and antimony in oxygen-bearing copper anodes in electrolytic refining. Dissertation, Helsinki University of Technology, Institution of Process Metallurgy, Helsinki, 1985

[74] Kurz W. and D. J. Fisher: Fundamentals of Solidification. Trans Tech Publications Ltd, Switzerland, 1998

[75] Dies K.: Kupfer und Kupferlegierungen in der Technik. Springer Verlag, Berlin/Heidelberg/New York, 1967

[76] Kondic V.: Metallurgical Principles of Founding. Edward Arnold Ltd., London, 1968

[77] Balandin G. F.: Kristallisation und Kristallstruktur in Gußstücken. VEB Deutscher Verlag für Grundstoffindustrie, Leipzig, 1974

[78] Vargas C., G. Cifuentes, O. Bustos, R. Morales and C. Rodriguez: Characterization and electrochemical behaviour of commercial copper anodes under simulated electrorefining conditions. Copper 2003 - Cobre 2003, Santiago: Chile, 2006, 327 - 338

[79] Walker W. C.: The Anatomy of a Copper Anode. Plating and Surface Finishing, 77, 1990, 16 - 17

[80] Antrekowitsch H.: Grundlagenuntersuchungen bei der Erstarrung der Nichteisenmetalle Aluminium und Kupfer im rotierenden Magnetfeld sowie Anwendungsmöglichkeiten in der Industrie. Dissertation, Montanuniversität Leoben, Leoben, 1998

[81] Ahan S.-C., S.-S. Park, Y.-H. Kim, and W.-S. Chung: A Study on the Relation between Passivation Behavior and Casting Microstructure of Copper Anode. Journal of the Korean Institute of Metals and Materials, 43 , 2005, 558 - 563

[82] Wöbking H.: Beobachtungen und Untersuchungen in der Elektrolyse Brixlegg mit besonderem Augenmerk auf die Zeit schlechter Stromausbeute (Nov/Dez 1992). 1993

[83] Chen T. T. and J. E. Dutrizac: Mineralogical Characterization of Anode Slimes from the Kidd Creek Copper Refinery. The Electrorefining and Winning of Copper, Denver, Colorado: USA, 1987, 499 - 525

[84] Wöbking H.: Anodenprobleme in der Raffinationselektrolyse der Montanwerke Brixlegg - Untersuchungen an Anoden. 1997

[85] Moreira A. L. N., J. Carvalho and M. R. O. Panao: An experimental methodology to quantify the spray cooling event at intermittent spray impact. International Journal of Heat and Mass Transfer, 28, 2007, 191 - 202

[86] Heng X. and Z. Zhou: A model for droplet evaporation near Leidenfrost point. International Journal of Heat and Mass Transfer, 2007

[87] Nikolopoulos N., A. Theodorakakos and G. Bergeles: A numerical investigation of the evaporation process of a liquid droplet impinging onto a hot substrate. International Journal of Heat and Mass Transfer, 50, 2007, 303 - 319

[88] Raudensky M. and Horsky J.: Secondary cooling in continuous casting and Leidenfrost temperature effects. Ironmaking and Steelmaking, 32 , 2005, 159 - 164

[89] Walker J: Boiling and the Leidenfrost effect. (2007) Internet: http://www.wiley.com/college/phy/halliday320005/pdf/leidenfrost_essay.pdf (Access: 23.10.2007)

[90] Harvie D.J.E. and D.F.Fletcher: A hydrodynamic and thermodynamic simulation of droplet impacts on hot surfaces, Part I: theoretical model. International Journal of Heat and Mass Transfer, 44, 2001, 2633 - 2642

[91] Viscorova R., R. Scholz, K.-H. Spitzer and J. Wendelstorf: Measurements of spray water cooling heat transfer coefficients under oxide scale formation. AISTech 2006, Cleveland, Ohio, USA: 2006, 519 - 528

[92] Huang C.-K and Van P. Carey: The effects of dissolved salts on the Leidenfrost transition. International Journal of Heat and Mass Transfer, 50, 2007, 269 - 282

[93] Harvie D. J. E. and D. F. Fletcher: A hydrodynamic and thermodynamic simulation of droplet impacts on hot surfaces, Part II: validation and application. International Journal of Heat and Mass Transfer, 44, 2001, 2643 - 2659

[94] Forster B. J.: The Law of Diminishing Returns in Roll-Cooling Strategies. (2007) Internet: www.metalproducing.com (Access: 20.2.2007)

[95] Tucker D.: A Quantitative Study into the Comparative Efficiency of Flatjet and Full Cone Nozzles when applied to the Application of Work Roll Cooling. (2008) Internet: www.lechler.de (Access: 17.4.2008)

[96] Specht E. and J. Krol: Enhancement and defined regulation of metal quenching using atomized sprays. EMC 2007, Clausthal-Zellerfeld: GDMB, 2007, 1917 - 1928

[97] Industrial Gases/Combustion: A Review of Gas Quenching from the Perspective of the Heat Transfer Coefficient. (2007) Internet: http://www.industrialheating.com (Access: 25.7.2007)

[98] Understanding Heat Transfer Coefficient. Internet: www.qats.com (Access: 18.9.2007)

[99] Lange H.-J., K. Hein and D. Schab: Anodenprozesse bei der Raffinationselektrolyse. Freiberger Forschungshefte, B195 , 1111, 29 - 49

[100] Hein K.: Theoretische Grundlagen elektrochemischer Prozesse zur Metallgewinnung.

[101] Holze R.: Leitfaden der Elektrochemie. Teubner Studienbücher Chemie, Stuttgart, Leipzig, 1998

[102] Hamann C. H. and W. Vielstich: Elektrochemie. WILEY-VCH, Weinheim, 1998

[103] Ebert H.: Elektrochemie - kurz und bündig. Vogel-Verlag, Würzburg, 1972

[104] Straschill M.: Lehrbuch der Elektrochemie. R. Oldenbourg, München, 1962

[105] Cheng X. and J. B. Hiskey: Fundamental Studies of Copper Anode Passivation during Electrorefining: Part II. Surface Morphology. Met. and Mat. Trans. B, Vol. 27B, 1996, 610 - 616

[106] Cheng X., J. B. Hiskey and T. F. Krusmark: Characterization of copper anode surface during different stages of polarization. Copper 95, Vol.3, Santiago: Chile, 1995, 225 - 240

[107] Brugger G., F. Jeglitsch, H. Wöbking and J. Wallner: Ursachen von Passivierungserscheinungen während der Kupferraffinationselektrolyse. Erzmetall, 48, 1995, 691 - 702

[108] Schmidt A.: Angewandte Elektrochemie. Verlag Chemie, Weinheim, 1976

[109] Petzow G.: Metallographisches Ätzen. Gebrüder Bornträger, Berlin-Stuttgart, 1976

[110] GDMB: Untersuchungen über das Verhalten von Zinn, Nickel, Antimon und Blei bei der Kupfer-Raffinationselektrolyse. GDMB, Heft 57 der Schriftenreihe der GDMB Gesellschaft Deutscher Metallhütten- und Bergleute, 1990

[111] Mubarok Z.: Electrochemical and Microscopic Analysis of Cathode Nodulation Behaviour in Copper Electrolytic Refining. Dissertation, Montanuniversität Leoben, Leoben, 2005

[112] Personal Information - Bank Elektronik - Intelligent Controls GmbH. 2007

[113] Hanko G.: Erfassung der Einflüsse auf die Haltbarkeit der bei den Montanwerken Brixlegg eingesetzten Anodenformen. Project Paper, Montanuniversität Leoben, Leoben, 1998

[114] Personal Information - Hazelett. 2006

[115] Brugger G., F. Jeglitsch and H. Wöbking: Charakterisierung intermetallischer Phasen im Anodenkupfer. Fortschritte in der Metallographie (Advances in Metallography), Leoben, 1995, 179 - 190

[116] Chen T. T. and J. E. Dutrizac: Mineralogical Characterization of Anode Slimes. IV. Copper-Nickel-Antimony Oxide ("Kupferglimmer") in CCR Anodes and Anodes Slimes. Canadian Metallurgical Quarterly, 28, 1989, 127 - 134

[117] Chen T. T. and J. E. Dutrizac: Mineralogical Characterization of a Copper Anode and the Anode Slimes from the La Caridad Copper Refinery of Mexicana de Cobre. Met. and Mat. Trans. B, 36B, 2005, 229 - 240

[118] VDI-Gesellschaft Verfahrenstechnik und Chemieingenieurwesen (Hrsg.): VDI-Wärmeatlas. Springer-Verlag, Berlin Heidelberg, 2006

[119] Personal Information - METTOP. 2007

[120] Eberle R.: Influence of the Fluid Flow in the Mould on the Grain Structure. Presented at the Copper Committee Meeting 2007, 2007

[121] Stewart I., J. D. Massingham and J. J. Hagers: Heat transfer coefficient effects on spray cooling. Presented 27th September at the 1995 AISE Annual Convention and Iron & Steel Exposition, Pittsburgh, Pennsylvania, 1995

[122] Liu D.R., J. J. Guo, S. P. Wu, Y. Q. Su and H. Z. Fu: Numerical prediction for columnar to equiaxed transition in solidified Ti-Al intermetallic alloy ingots by stochastic model. Materials Science and Technology, 22, 2006, 29 - 38

[123] Wu M. and A. Ludwig: A Three-Phase Model for Mixed Columnar-Equiaxed Solidification. Met. and Mat. Trans. A, 37A, 2006, 1613 - 1631

[124] Deutsches Kupferinstitut (Hrsg.): Kupfer. Saladruck Berlin, Berlin, 1982

9. List of Figures

10. List of Tables